DOE/ID/12380-18
(DE88003380)

Energy CONSERVATION

INVESTIGATION OF MATERIALS FOR INERT ELECTRODES IN ALUMINUM ELECTRODEPOSITION CELLS

By
John S. Haggerty
Donald R. Sadoway

September 14, 1987

Work Performed Under Contract No. FG07-83ID12380

For
U. S. Department of Energy
Office of Industrial Programs
Washington, D.C.

By
Massachusetts Institute of Technology
Cambridge, Massachusetts

DISCLAIMER

DISCLAIMER

Available from the National Technical Information Service, U. S. Department of Commerce, Springfield, Virginia 22161.

Price: Printed Copy A11
Microfiche A01

Codes are used for pricing all publications. The code is determined by the number of pages in the publication. Information pertaining to the pricing codes can be found in the current issues of the following publications, which are generally available in most libraries: *Energy Research Abstracts (ERA); Government Reports Announcements* and Index *(GRA* and I); *Scientific and Technical Abstract Reports (STAR);* and publication NTIS-PR-360 available from NTIS at the above address.

DOE/ID/12380-18
(DE88003380)

INVESTIGATION OF MATERIALS FOR INERT ELECTRODES IN ALUMINUM ELECTRODEPOSITION CELLS

by

John S. Haggerty
Sr. Research Scientist, Energy Laboratory

and

Donald R. Sadoway
Assoc. Professor of Materials Engineering
Department of Materials Science & Engineering

September 14, 1987

Work Performed Under Contract No. DE-FG07-83ID12380

Prepared for
U.S. Department of Energy
Idaho Operations Office, Idaho Falls, Idaho
Sponsored by the Office of the Assistant Secretary for
Conservation and Renewable Energy
Office of Industrial Programs
Washington, DC

Prepared by
Massachusetts Institute of Technology
Cambridge, Massachusetts

TABLE OF CONTENTS

Introduction

Despite its capability to produce high purity aluminum, the Hall process has always suffered from a number of significant problems. One set of problems arises from the use of consumable carbon anodes. These anodes are expensive to produce, and the cost of producing them adds significantly to the overall cost of the aluminum produced by the Hall process. In addition, vast quantities of energy are consumed in the so-called pre-bake furnaces where the raw materials are treated to form the large anode blocks. In use, it is difficult to maintain uniform anode current loading in the Hall cell since the anodes are consumed resulting in a continuous change in their shape. It is also difficult to maintain proper anode-cathode spacing during operation of the Hall cell, since the anodes are consumed. Additionally, the anode-cathode spacing is typically greater than required because of the uncertainty of the consumable anode's shape and the need to maintain a deep molten aluminum pool. Such spacing results in an inordinate consumption of electrical energy, owing to the voltage drop across the molten salt electrolyte.

Because of the problems caused by carbon anodes, substantial research has been conducted in an effort to find another anode material, particularly to find what has been referred to as an inert anode. An inert anode is defined as one that does not react with oxygen formed electrochemically at the anode, does not dissolve in the electrolyte, and is not consumed in the electrolytic reaction. Unfortunately, the research conducted to date has not resulted in the development of a fully satisfactory anode material.

Another set of problems with Hall cells arises from the use of a carbon lining. These cells are operated under conditions that cause

the molten electrolyte to freeze on the sidewall during operation, so that molten electrolyte floating on molten aluminum is contained within a shell of frozen electrolyte. This is necessary to prevent the reaction between the carbon cell lining and compounds in the molten electrolyte during operation of these Hall cells. The interface between the frozen and molten electrolyte changes, however, during operation, making it difficult to operate under uniform conditions. The necessity to maintain frozen electrolyte at the sidewalls results in a substantial heat loss and hence contributes again to the poor utilization of energy.

Still another set of problems with the Hall cell arises from the lack of a suitable cathode material. At present, carbon is used as the cathode in these cells. However, molten aluminum does not wet carbon, and therefore it is necessary to maintain an excessively deep pool of molten aluminum on the bottom of the cell. The carbon must be fully covered in order to prevent contact between the molten salt electrolyte and the carbon cathode itself in the presence of molten aluminum. Otherwise, the formation of aluminum carbides occurs and reduces the cell's productivity. The justifiable presence of the deep pool, however, gives rise to a new problem. The cell currents are extremely high, typically on the order of 100 kA to 300 kA. At these high currents the electromagnetic forces can cause the molten aluminum to develop waves of substantial physical dimension. In order to prevent the electrical shorting of the molten aluminum to the anode, it is necessary to separate the anode and cathode by a large distance. This results in an excessive voltage drop across the electrolyte and contributes to the poor energy efficiency of the cells.

Obviously, advanced materials in the form of inert anodes, sidewalls, and cathodes would contribute greatly to the effective utilization of energy in this reactor. Aluminum is one of the most

energy-intensive metals to produce, having an energy content of approximately 6 kWh/lb. When power costs were in the vicinity of 5 mils/kWh this amounted to approximately 3 cents per pound of aluminum. However, in recent years power costs have risen to the point where some producers are paying 30 mils/kWh and are facing still higher power costs in the future. Obviously, faced with such substantial power costs, aluminum producers cannot remain competitive. It is imperative that the energy content of this metal be reduced if it is to remain a viable material and our domestic producers are to retain their smelting capacity.

Objective

The objective of the research on advanced materials for energy efficient production of aluminum was to identify materials for use in Hall cells as anodes, cathodes and sidewalls. The successful completion of this research would not only serve to retrofit existing installations, making them more energy efficient, but would also permit radical redesign of the Hall cell with attendant improvements in productivity and, therefore, energy utilization.

Potential for Energy Savings

The potential for energy savings is substantial and has been well documented.* It is clear that by decreasing the inter-electrode

---

* Noel Jarrett, W.B. Frank, and Rudolf Keller, in "Advances in the Smelting of Aluminum," in Metallurgical Treatises, J.K. Tien and J.F. Elliott, editors, TMS-AIME, Warrendale PA, 1981, pp. 137-57.

spacing one will substantially decrease the energy consumption in the Hall cell itself. In addition, there are substantial energy savings accruing from the elimination of the pre-bake furnaces which in time are expected to become liabilities from the standpoint of industrial health and safety.

Results

During the first term of this project the work was divided into major efforts. The first was the growth and characterization of specimens; the second was Hall cell performance testing. Both cathode and anode materials were the subject of investigation. Preparation of specimens included growth of single crystals and synthesis of ultra high purity powders. The selection of compositions was based exclusively on the criteria as enunciated by workers in the field at that time. Special attention was paid to ferrites as they were considered to be the most promising anode materials at that time by investigators at Alcoa Laboratories where there was a major DOE sponsored research program. Indeed, MIT's role was seen by some as to study some of the more fundamental aspects of the materials science of the ferrites as Alcoa moved on to addressing the engineering issues associated with the industrial implementation of these materials. The results of this first term of work have been summarized in a document entitled, "Request for Modification of a Research Contract: 'Investigation of Materials for Inert Electrodes in Aluminum Electrodeposition Cells.'" The relevant sections of that document are reproduced here as Appendix 1. This document summarizes the activities for the first three years of the project and puts in context that work along with that which followed. For a more complete report of the first three years the reader is directed to DOE/ID/12380-13.

The activities of year four are summarized in Appendix 2, "Program Review Topics (12/18/86)." Ferrite anode corrosion rate studies represent a completion of the work begun during the first term of this project and are described in Appendix 3, "Investigation of Ferrites as Potential Inert Anodes for Hall Cells," which is the doctoral thesis of Alan McLeod, Department of Materials Science and Engineering, Massachusetts Institute of Technology. This document contains other data as well. In particular, the electrical conductivities of a set of copper-manganese ferrites were measured.

Float Zone, Pendant Drop Cryolite Experiments represent a modification of the original workplan and were undertaken because it had become apparent during the first term of the project that unsatisfactory choices of candidate materials were being made on the basis of a flawed set of selection criteria applied to an incomplete and sometimes inaccurate data base. This experiment was then constructed to determine whether the apparatus used for float zone crystal growth could be adapted to make a variety of important measurements associated with the physical chemistry of the cryolite-based melts and their interactions with candidate inert anode materials. The results are summarized in Appendix 4 in three tables. Table 1 enumerates the issues one had to come to terms with in conducting such experiments. Table 2 summarizes the experiments in which molten cryolite was suspended on a feedrod of solid cryolite. The main question was whether the evaporation of aluminum fluoride would be so fast on the time scale of the experiment that the melt chemistry would vary unacceptably. As Table 2 shows, chemical stability was maintained. However, temperature measurement was subject to error. This last point demonstrates the imprecision in noninvasive pyrometric measurements in this system. Table 3 summarizes the experiments in which the goal was to suspend molten

cryolite from a rod of alumina. The high thermal conductivity of alumina as compared to solid cryolite proved to be the undoing here. Excessive superheat was required to attain desired temperatures. This resulted in excessive vaporization from the melt with the attendant loss of stability in chemical compositional. Defocussing the laser beams failed to improve the situation to the point where the experiment could be performed reliably with the accuracy required to conduct a proper measurement of the physical chemistry of the system.

The third major topic in the fourth year was Non Consumable Anode (Data Base, Candidate Compositions). This work was driven by our perception that the basis for prior selection of candidate materials was inadequate. The results are summarized in Appendix 5 which is a reprint of an article entitled "Selection and Testing of Inert Anode Materials for Hall Cells." This was published in Light Metals 1987, and enunciates a new set of criteria for the anode problem. Consideration of these new criteria has led to the discovery of materials previously ignored for this application. Furthermore, new methods of operating the cells have become evident, as well. These are described in Appendix 6 which is the patent application derived from this work: D.R. Sadoway, J.S. Haggerty and A.D. McLeod, "Apparatus and Method for the Electrolytic Production of Aluminum," U.S. patent application, serial no. 000,657, filed January 6, 1987.

Summary

The search for inert electrodes for the Hall cell is one of the most difficult problems in all of materials science. In spite of a century of effort, no fully satisfactory materials have been found. It is the conclusion of this study that the failure to do so was due in part to the use of a set of selection criteria which were determined to be insufficient and incorrect. During the course of this research these selection criteria for the anode were questioned. What emerged was a revised set of selection criteria with the result that classes of materials previously dismissed as useless from the standpoint of this application were identified as candidate materials within newly specified operating conditions. Unfortunately, the program was terminated before these new materials and operating conditions could be tested. However, it is the opinion of the authors that if there is indeed a material that can meet the severe requirements of the Hall cell environment, then this material will be found through application of the ideas developed in the present study.

It is particularly important to appreciate how strongly cell operating conditions influence the behavior of a material that is being tested as a candidate electrode. This in part accounts for the wide variation in cell performance data for ostensibly identical materials. The corollary to this is that in the search for high performance materials for use as electrodes and sidewalls, a global approach is recommended. For example, the performance of a candidate electrode material can be dramatically altered through changes in cell bath chemistries and electrochemistries, *i.e.*, cell operating conditions. During the course of the present study it was only after the anode was viewed in the context of an element in a dynamic materials system, which in this case is the Hall cell operating under industrial conditions, that new potential solutions to the problem

were discovered.

Finally, this methodology can be extended to other materials selection problems. For example, in the production of magnesium by fused salt electrolysis of magnesium chloride, as practiced by the Dow Chemical Co., vast quantities of carbon are consumed as anodes. In trying to find an alternative material in this application, one would have to face the same set of issues described above. Fused salt electrolysis is important in the production of the alkali metals, alkaline earth metals, and the rare earth metals. This latter group is very important from the standpoint of advanced magnetic materials such as iron-neodymium-boron $Fe_{14}Nd_2B$, and as precursors to the recently identified superconducting ceramic materials, *e.g.*, $YBa_2Cu_3O_7$.

In the area of fused salt batteries, the identification of advanced materials for electrodes, separators, diaphragms, and containers would pave the way for the commercialization of this technology. Again, the selection criteria and testing methodology described above could play a major role in solving these problems. In this sense, the search for advanced materials for Hall cells can be considered a test vehicle and forms the basis for future studies directed at the problems named in this section.

List of Publications

Articles:

1. A.D. McLeod, J.S. Haggerty, and D.R. Sadoway, "Electrical Resistivities of Monocrystalline and Polycrystalline TiB_2," J. Am. Ceram. Soc., 67, 705-708 (1984).

2. A.D. McLeod, J.S. Haggerty, and D.R. Sadoway, "Inert Electrodes for Aluminum Electrolysis Cells," Energy Reduction Techniques in Metal Electrochemical Processes, R.G. Bautista and R. Wesely, editors, TMS-AIME, Warrendale PA, 1985, pp. 453-456.

3. A.D. McLeod, J.S. Haggerty, and D.R. Sadoway, "Inert Anode Materials for Hall Cells," in Light Metals 1986, R.E. Miller, editor, TMS-AIME, Warrendale PA, 1986, pp. 269-273.

4. A.D. McLeod, J.S. Haggerty, and D.R. Sadoway, "Inert Anode Materials for Hall Cells," in Proceedings of a *conversazione* on "The Production of Liquid Aluminum," E. Ozberk, D.W. Macmillan, and R.I.L. Guthrie, editors, TMS-CIM, series 25-7, No. 2, 1986, pp. 125-139.

5. A.D. McLeod, J.-M. Lihrmann, J.S. Haggerty, and D.R. Sadoway, "Selection and Testing of Inert Anode Materials for Hall Cells," in Light Metals 1987, R.D. Zabreznik, editor, TMS-AIME, Warrendale PA, 1987, pp. 357-365.

In addition to the above cited publications it is expected that there will be three publications based on the doctoral thesis of A.D. McLeod.

Patent Applications:

1. "Aluminum Reference Electrode," D.R. Sadoway, U.S. patent application, serial no. 783,776, filed October 3, 1985.

2. "Apparatus and Method for the Electrolytic Production of Aluminum," D.R. Sadoway, J.S. Haggerty and A.D. McLeod, U.S. patent application, serial no. 000,657, filed January 6, 1987.

Acknowledgements

Many people contributed to this research. Their efforts are gratefully acknowledged:

Dr. David Casey for supervising and performing the powder synthesis; as well, these students who under the auspices of MIT's Undergraduate Research Opportunities Program worked under Dr. Casey's supervision: Ray Henry, David Ming, Ken Sinanski, Jon Suber, David Volfson, and Diana Yoshimura;

Dr. Alan McLeod, who conducted Hall cell performance testing along with a variety of materials characterizations as the major part of his doctoral thesis,

Dr. Jean-Marc Lihrmann, whose survey of the literature helped to assess the status of the database on which candidate materials were being selected;

Ms. Luella Guergen, who prepared feedrods for the crystal grower;

Mr. Paul McGrath, who grew most of the single crystals.

The research program was funded by the U.S. Department of Energy, Conservation and Renewable Energy, Office of Industrial Programs, and administered through the Idaho National Engineering Laboratory.

APPENDIX 2

Summary of Activities of Year 4

APPENDIX 1

Summary of First Term's Work and its Context

I. INTRODUCTION

Although there has been a long standing interest in substituting inert electrodes for carbon electrodes in Hall aluminum cells, this replacement has not occurred because candidate materials have not realized anticipated advantages in actual use. The reasons for observed deficiencies reflect the inherent complexity of exposures encountered in the Hall cell.

This research program is designed to investigate candidate materials under conditions where materials properties, performance and failure modes can be interpreted with a level of confidence that is not possible with the poorly defined polycrystalline materials used in previous research. Two classes of candidate materials will be investigated. One is single crystal samples grown in the uniquely controllable growth conditions achievable with the MIT laser heated floating zone crystal growth apparatus. The second is ultra high purity powders synthesized from laser heated gases. Samples will be characterized in terms of parameters that reveal fundamental materials properties as well as technological parameters that reflect exposures typical of the Hall cell. Our ultimate objective is to define material compositions, critical fabrication process steps and critical operating conditions which will permit economically viable inert anodes and cathodes to be made that will exhibit adequate performance characteristics.

The specific advantages anticipated for inert anodes and cathodes differ; but each should result in reduced overvoltage, reduced thermal losses, longer cell life and improved process control. Achievement of the first two will reduce the energy needed to produce aluminum metal; the second two primarily reduce cost and improve productivity.

The consumable carbon anode represents the most important opportunity for using inert electrodes in the Hall cell. Between 420 to 550 kg of carbon is consumed per ton of Al produced. The carbon leaves the cell as a $CO-CO_2$ mixture having no practical commercial value and causing several problems attributable to bubble formation on the anode face. Largely because of the high and nonuniform rate at which carbon is consumed, it is impossible to achieve a precise location of the electrode face. A large average interelectrode distance is maintained to avoid shorting between the anode and the molten aluminum cathode. The use of an inert anode will permit the interelectrode distance to be reduced to a small fraction of present practice permitting the i^2R losses through the cell to be reduced proportionally. This and other factors should more than offset the increase in the reversible voltage for the reduction reaction.

Identification of a substitute for the carbon cathode is also important, although it does not offer the same potential for savings as the inert anode. The molten aluminum pool which acts as the cathode is supported by carbon "cathode" blocks in the present design of the Hall cell. This design also causes the interelectrode spacing to be maintained at larger than optimum distances. Because carbon is not wetted by the molten aluminum, an excessive metal pool depth is necessary to protect the carbon from the cryolite. Electromagnetic forces create standing waves and other flows in the molten aluminum pool. To avoid shorting between metal and the anode, the interelectrode spacing is increased beyond optimum. The use of a cathode that is wetted by the molten aluminum would reduce the required molten pool depth and, thus, the interelectrode spacing. As with a precisely located

inert anode, this cathode change will reduce i^2R losses in proportion to the new, reduced interelectrode spacing.

At this program's inception, it was widely believed that generally satisfactory materials had been identified for both anode and cathode applications. However, several specific issues remained troublesome for both electrodes and this program began by focussing on these topics. Failure modes of both electrodes were not defined. It appeared likely that segregation of uncontrolled impurities to grain boundaries may be responsible for widely varying life times. Also, electrical conductivities of the candidate anode materials were marginal. Our initial approach focussed on these issues by permitting definition of intrinsic electrode material properties with single crystal samples and the elimination of potential grain boundary contaminants in TiB_2 by synthesis of ultra high purity powders.

Since beginning this research program, it has become evident that the working presumptions with respect to the anode were overly optimistic. Not only did the performance of then-existing and subsequently evaluated anode materials fall short of requirements; but, the data base needed for definition of alternative materials proved inadequate. Much effort was devoted to accessing the actual data base and defining the topics that needed to be addressed before candidate materials could be selected on a rational basis. We found that solubility, contact angle, overvoltage, emf, and corrosion rate data were unreliable and sparse. This proposal outlines a program to develop these data, and using them to define suitable electrode materials by enhancing the definition of material compositions, by producing single and polycrystal candidates, and by evaluating the candidate electrode materials under appropriate conditions.

II. BACKGROUND

A. Previous Research

During the existing research program, candidate anode and cathode materials were identified based on criteria we established. These materials were synthesized as single crystals or as ultra high purity powders. Both types of materials were characterized extensively. Samples were also evaluated in a laboratory scale Hall cell to provide corrosion rate and overvoltage data under electrolysis conditions.

1. Growth and Characterization of Single Crystals

Single crystal samples were produced using MIT's CO_2 laser-heated floating-zone crystal apparatus. This facility provides MIT with a unique ability to produce high purity, controlled composition single crystals of high melting point materials needed for inert electrodes. The CO_2 laser-heated, floating-zone crystal growth process is probably the most flexible crystal growth process known in terms of the range of host compositions, dopants, and ambient atmospheres that can be considered without the restrictions typical of high temperature materials experiments or without the introduction of unwanted impurities through contact with a crucible.

The MIT laser heated crystal growth apparatus consists of a 1500 W, custom designed 2-beam CO_2 laser, beam splitting, pointing and shaping optics, and a controlled atmosphere floating zone crystal growth machine. Melts are supported by and contact only a solid "feed rod" and growing crystal having essentially the same composition as the melt. Thus, there is no contamination from a container, a major problem with very high temperature

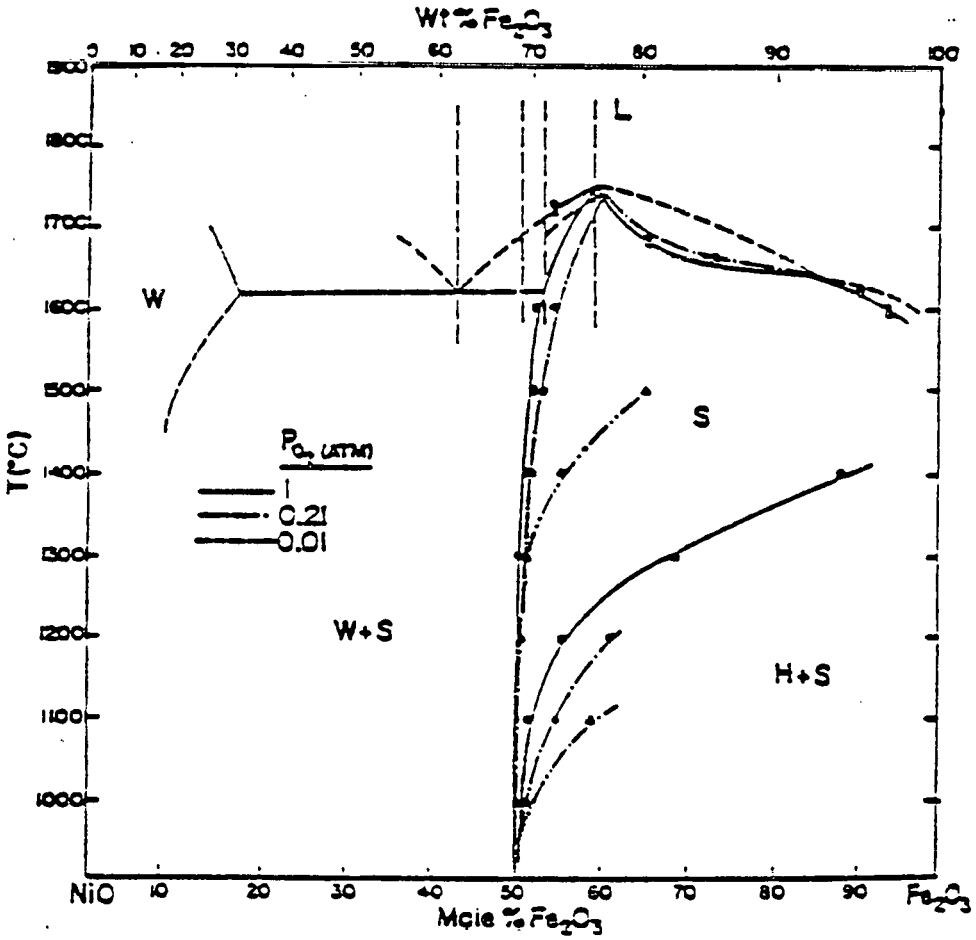

Figure 1. Phase Diagram of the $NiO-Fe_2O_3$ System showing compositions subjected to floating-zone melting.

melts. The use of the laser heat source imposes virtually no constraints on ambient atmospheres or on candidate materials that form stable melts. A laser heat source is particularly applicable to high melting point materials because it has no characteristic temperature which intrinsically limits the temperature of the melt.

Feed rods for the growth process are simple to make, permitting wide ranges of compositions to be explored. Dried powders are mixed in required proportions and isostatically pressed into rod shapes. Crystals can be grown from these low density (typically 40-55% of theoretical) unfired rods. Usually the rods are "bisk fired" under easily accessible and controllable conditions to give them improved strengths but not necessarily higher densities.

The Fe_2O_3 based compositions have been the most widely studied. Fe_2O_3 itself has an unacceptably low conductivity, but good durability. The spinel, Fe_3O_4, has high conductivity but is more soluble. The focus of materials research based on Fe_2O_3 has been to retain the high conductivity of the spinel phase while decreasing its solubility. Other low-solubility oxides such as ZnO, NiO and CoO can be substituted for FeO in Fe_3O_4 while retaining the spinel structure. At this point the formulation process becomes speculative since very few data are available on the composition dependence of the conductivity and corrosion resistance of these materials. This research program has addressed these issues by studying the behavior of pore and grain boundary free materials of various compositions in the ferrite spinel systems.

We initiated our anode research with the $NiO-Fe_2O_3$ system. Several compositions shown in Figure 1 at and near the $NiFe_2O_4$ composition have been

TABLE I

CRYSTAL GROWTH DATA

SAMPLE DESIGN-ATION	COMPOSITION (MOLE %)						GROWTH RATE (cm/hr)	COUNTER-ROTATION RATE (rpm)	LASER POWER (W)	ATM	Diam (cm)	LENGTH (cm)
	TiB_2	LaB_6	Fe_2O_3	NiO	Co_3O_4	TiO_2						
III-09	100						8	0	260	Ar	0.05	4.8
III-08	100						15	0	260	Ar	0.05	6.8
III-07	100						15	0	300	Ar	0.06	5
III-11		100					15	0	480	Ar	0.1	4
III-49			53.51	46.49			2	11	120	Air	0.5	<1
III-50			50.00	50.00			various	11	120	Air	0.5	<1
III-51			50.00	50.00			1	11	120	Air	0.5	<1
III-52			50.00	50.00			2	0	120	Air	0.5	<1
III-54			53.51	56.49			2	0	120	Air	0.5	4.4
III-56			43.00	57.00			4	0	360	Air	0.4	6
III-56a			"	"			"	"	"	"	"	5.6
III-59			59.60	40.40			2	11	360	O_2	0.5	4.5
III-59a			"	"			"	"	"	"	"	4.7
III-59b			"	"			"	"	"	"	"	10
III-59c			"	"			"	"	"	"	"	5.3
III-71			78.20		21.80		2	11	360	O_2	0.5	9
III-71a			"		"		"	"	"	"	"	8
III-72			47.50	47.50		5.0	2	11	360	O_2	0.5	1.5
III-73			47.50	47.50		5.0	2	11	360	O_2	0.5	<1
IV-01			56.62	38.38		5.0	2	11	360	O_2	0.5	4
IV-02			56.62	38.38		5.0	2	11	360	O_2	0.5	10.8
IV-03			47.50	47.50		5.0	2	11	360	O_2	0.5	9.4

produced as single crystals or oriented grain polycrystal samples by float zone melting. The crystal growth parameters used for these compositions are summarized in Table I. To ascertain the effects of TiO_2, two different spinel compositions were doped with 5 mole % TiO_2. The spinel system $CoO-Fe_2O_3$ has not been studied as extensively. The phase diagram, Figure 2, indicates a wider spinel stoichiometry range than in the $NiO-Fe_2O_3$ system; this should enable a larger variety of spinel properties to be achieved.

TiB_2 is a base material in all the inert cathode compositions proposed by industry. However, due to the difficulty of preparing crystals of TiB_2, there are very few data in the literature concerning the intrinsic properties of this material. We grew single crystals of TiB_2 and characterized them. The published results of this work clarify some of the anomalous data in the literature and establish reference values for the intrinsic resistivity. The crystal growth parameters are summarized in Table I. We have also produced single crystals of the closely related boride, LaB_6.

Mono- and polycrystalline samples were subjected to a number of characterizations to provide a basis for their evaluation as electrodes and to interpret failure modes. Many of these characterizations are destructive so they are frequently undertaken after completion of Hall cell tests. The following characterizations are done.

- X-ray Diffraction - This evaluation provides an identification of the crystalline phases present, their compositions through the lattice parameters, quantitative measures of the percentages of each phase, preferred orientations and grain sizes, if small (< 2000 Å).
- Laué Back Reflection - This X-ray technique is used primarily to define the orientation of the crystals. It also provides a measure of crystal perfection by spot splitting and indicates preferred orientation if the boules are polycrystalline.

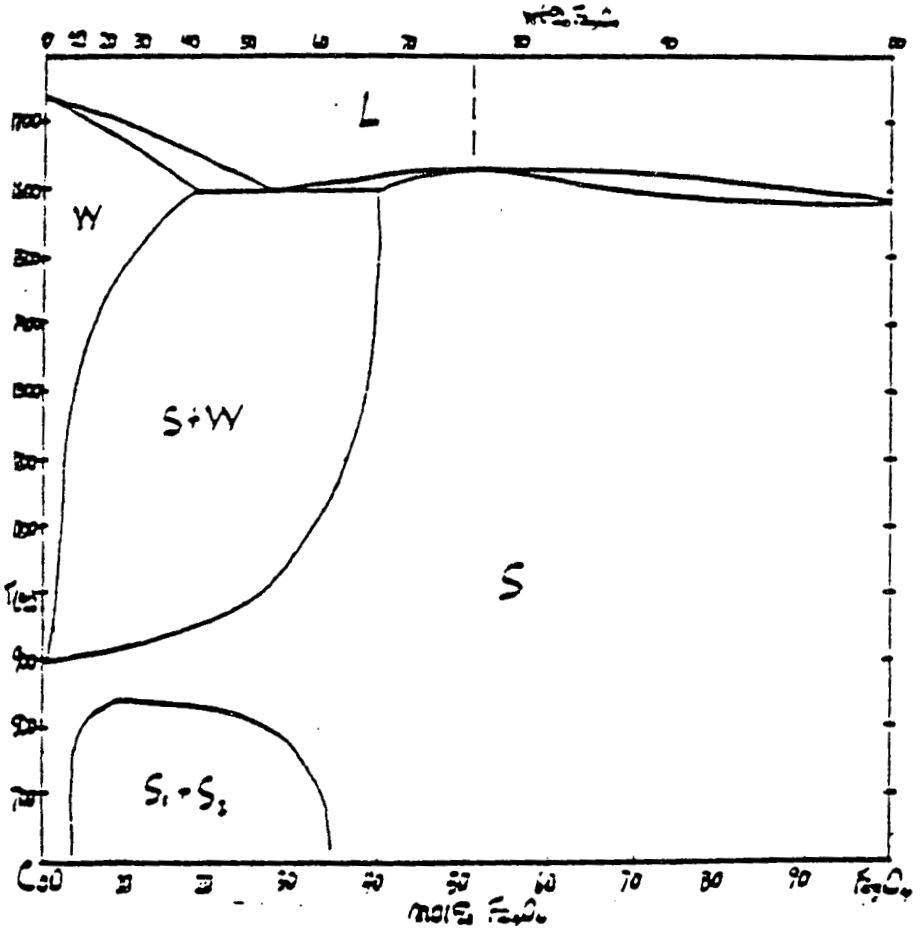

Figure 2. Phase Diagram of the CoO-Fe_2O_3 System in air showing compositions subjected to floating-zone melting.

- Microstructural Analysis - Optical and SEM microscopy is used to do quantitative phase analysis, (dimensions, volume fractions, orientations, etc.) and to detect other features such as cracks.

- Chemical Analyses - Several techniques are employed to study the chemistries. Wet chemical and X-ray fluorescence are used to determine bulk chemistries. Emission and spark source mass spectroscopy are commonly used to detect impurities. The energy dispersive X-ray analysis on the SEM and microprobe techniques are used to map compositional variations within samples.

- Mossbauer Spectroscopy - This technique is used to determine the arrangement of cations in the materials.

- Electrical Conductivity - The electrical conductivities and transport numbers are determined in candidate materials. These measurements are done as a function of temperature and prior exposure history to interpret results.

The characterizations that have been completed are summarized in Table II. The results of our characterization of TiB_2 single crystals have been published,[1] while the overvoltage measurements of monocrystalline nickel ferrite have been presented in conference[2] and will appear in print in the conference proceedings (Appendicies I and II respectively).

2. Laser Induced Synthesis of Titanium Diboride Powder

The objective of this work was to determine the applicability of the laser heated, gas phase synthesis process to the synthesis of TiB_2 powders and the definition of process variables. Candidate chemistries were selected based on computerized thermodynamic analysis, equipment was designed and constructed, and powder was synthesized.

When designing procedures that will lead to the laser syntheses of powders, one seeks certain criteria. The reactants should be volatile, preferably gaseous at ambient conditions. As many as possible of the reactants should absorb the IR radiation from the CO_2 laser. At this stage

TABLE II

COMPLETED CHARACTERIZATIONS

SAMPLE DESIGNATION	ELECTRICAL CONDUCTIVITY	OPTICAL MICROSCOPY	CHEM. ANALYSIS	SEM	X-RAY DIFFRACTION	LAUE
III-09	x	x		x		x
III-08	x					x
III-07	x		x			x
III-11	x					x
III-49		x			x	x
III-50					x	x
III-51		x				x
III-52		x PNL				
III-54		x		x		
III-56		x PNL				x
III-59		x	x			x
III-71		x PNL				
III-72						
III-73						
IV-01						
IV-02						
IV-03		x PNL				

in our program, we did not want to investigate laser induced powder production at other wavelengths emitted by different types of lasers. The chemical reaction should be thermodynamically favored (a negative free energy) and exothermic. Toxicity, corrosiveness, and explosiveness of the reactants and products are also concerns. Commercially available, relatively simple reactants are desirable.

The reactants selected during the first year of this project included titanium tetrachloride ($TiCl_4$) as the titanium source, boron trichloride (BCl_3) and diborane (B_2H_6) as the boron sources, and hydrogen (H_2) as the reductant. The reactions as presented in stoichiometrically balanced equations are:

$$TiCl_4(g) + 2BCl_3(g) + 5H_2(g) \rightarrow TiB_2(s) + 10HCl(g)$$

$$TiCl_4(g) + B_2H_6(g) \rightarrow TiB_2(s) + 4HCl(g) + H_2(g) \quad .$$

These chemical schemes involve several issues not encountered in the laser-induced synthesis of Si, SiC and Si_3N_4 powders. $TiCl_4$ and BCl_3 are corrosive; $TiCl_4$ is a liquid at ambient conditions; B_2H_6 and H_2 are explosive; B_2H_6, BCl_3, and phosgene (a contaminant in BCl_3) are toxic; and the reactions are endothermic. Conditions for transferring sufficient energy from the infrared (IR) beam of the CO_2 laser to the reactant gas mixture to induce TiB_2 formation must be experimentally determined.

We developed a thermodynamic analysis program that considers variations in the equilibrium compositions as functions of the reactant composition, the reaction temperature, and the cell pressure. Solid, liquid and gas phases were included. For the laser process, it is also necessary to determine the amount of heat required to elevate the initial reactants to the presumed reaction temperature and to transform them to the predicted equilibrium

composition at a specified pressure. This quantity is used to estimate the amount of IR radiation from the CO_2 laser which must be absorbed by the reactant gas stream and converted into thermal energy. These capabilities have been coded into a FORTRAN program called SOLGASMIX-PV.

A tuneable CO_2 laser is used in the studies of non-silicon based chemistries rather than the untuned CO_2 laser which emits only at 10.591 μ. Replacing the rear reflective mirror of a CO_2 laser with a reflective grating makes the laser tuneable, expanding the range of IR wavelengths that can be achieved and allowing some versatility in matching the absorption bands of the reactant gases to the laser output.

The power emitted from the Adkin MIRL-50 tuneable CO_2 laser varies as a function of λ. A maximum of 45 W is available at the P(20) line of the 00°1-10°0 transition. For this reason, the optimum λ for powder formation depends on the absorptivity of the reactant at a specific λ and the power available from the laser at that λ.

Before synthetic reactions were attempted in the flowing gas powder cell, potential reactant gases were studied in a static cell. Pure gases and gas mixtures were subjected to varied exposure times and power levels of the CO_2 laser to determine conditions for chemical reaction. Also, the absorptivity of gases were measured as a function of pressure and temperature.

Since the laser induced powder syntheses are thermal processes, it is important that the resulting temperature increase be defined in terms of the amount of laser power absorbed by the gas. A computational procedure was developed for calculating the induced temperature profile because the

temperature of the gas within the boundaries of the laser beam cannot be measured with physical probes.

The static cell is placed in an oven to achieve hot-wall conditions because the most promising reactant for TiB_2 synthesis is a liquid at ambient conditions; titanium tetrachloride boils at 136°C (1 atm). The reactants must be in the gas phase during the laser synthesis process; otherwise, a portion of the laser radiation would be used to supply the heat of vaporization to the liquids and the yield of product per absorbed photon would be unacceptably low.

A flowing gas delivery system was also designed and constructed for use with condensed phase reactants. The reactants must be introduced into the cell in the gaseous state and kept in this state until the reactant mixture interacts with the IR laser beam. A heated nozzle device is used to vaporize the liquid and the annular gas stream is heated to prevent condensation of the vaporized liquid before it reaches the laser beam. A diagram of the heated nozzle assembly is shown in Figure 3. Because many of the liquid reactants are corrosive, 316 stainless steel was chosen as the construction material. A gas-tight syringe pump is used to introduce the liquid reactant at a controlled rate into the heated nozzle assembly. A second channel intersects the center bore; this path is for those reactants which are gases at ambient conditions. Mixing with the vaporized liquid takes place prior to passage through the stainless steel reactant nozzle. The stainless steel reactant nozzle is a section of thin walled, stainless steel tubing inserted into a threaded, stainless steel plug.

Heat is supplied by three 50 W cartridge heaters. The thermocouples monitor the temperature distribution in the stainless steel block and provide

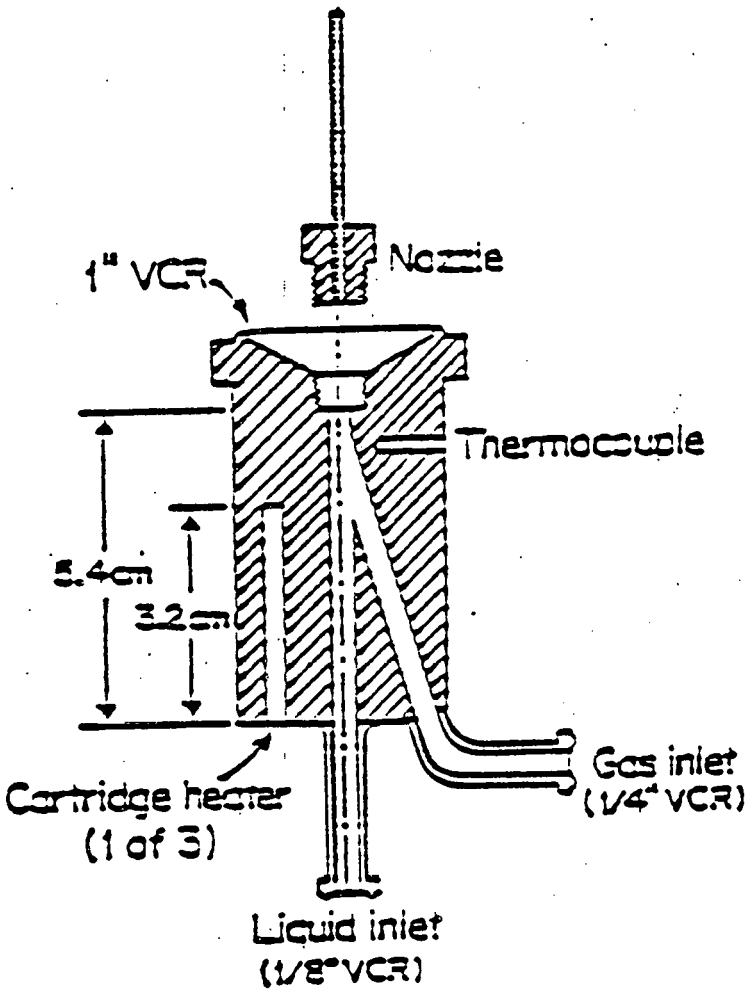

Figure 3. The heated nozzle assembly. See the text for a detailed discussion.

a control signal for a temperature control unit which controls current to the cartridge heaters.

Due to the toxic and explosive hazards associated with B_2H_6, we made a major effort to improve the safety of our laser process. Our approach has been to identify the hazards associated with each component of our system; to identify methods to minimize these individual hazards; to develop designs that provide adequate levels of safety and meet the process requirements for continuous synthesis of TiB_2. The major areas of concern are the fire hazard associated with the pyrophoric nature of diborane, the toxicity of diborane, the explosion hazard associated with a rapid release of diborane and hydrogen, the dangers associated with high power CO_2 lasers, namely the burn/fire hazard of the beam itself, and the electrocution danger from the laser power supply.

TiB_2 synthesis experiments were initiated with the BCl_3 + $TiCl_4$ reaction. One overriding factor in this decision was the less stringent safeguards required for experimentation with BCl_3 relative to those needed for B_2H_6. Our initial deduction from the literature was that BCl_3 would be the substituent that would abosrb the IR laser radiation in the reaction $TiCl_4(g) + BCl_3(g) + H_2(g) \rightarrow TiB_2(s) +$ by-products.

The interaction of BCl_3 vapor with the 10.59 μ output of the CO_2 laser was studied in the previously described static cell. The absorptivity coefficient, α, is determined from the equation, $\alpha = [1/(Pl)]\ln(I_o/I)$ in which P is the partial pressure of BCl_3, l is the cell path length, I_o is the incident laser power and I is the transmitted laser power.

Absorptivity measurements were made with BCl_3, BCl_3 plus Ar, and BCl_3 plus H_2. As the BCl_3 pressure increases, the net amount of absorbed laser

TABLE III

ABSORPTIVITY OF BCl_3

P_{BCl_3} [a]	P_{Ar}	P_H	I_o	α	ΔP
5.2t	—	—	~2W	13.1 $atm^{-1}cm^{-1}$	N.O.
"	—	50t	"	3.4	"
"	—	100	"	2.1	"
"	—	250	"	0.8	"
"	50t	—	"	2.6	1t
"	100	—	"	1.2	0.8
"	250	—	"	0.3	0.8
10t	—	—	~2W	15 $atm^{-1}cm^{-1}$	0.5t
"	—	50t	"	4.7	N.O.
"	—	100	"	3.3	"
"	—	250	"	1.6	"
"	50t	—	"	3.8	1.8t
"	100	—	"	2.3	2
"	250	—	"	1.1	N.O.
6.5t	—	—	~2W	14.6 $atm^{-1}cm^{-1}$	N.M.
"	—	—	~35W	7	1t
20t	—	—	"	5.2	6.1t
100t	—	—	"	b	24t

a. P_{BCl_3}, P_{Ar}, and P_{H_2} are the partial pressures in torr of BCl_3, Ar and H_2, respectively. I_o is the incident laser power in watts. α is the calculated absorptivity coefficient in units of $atm^{-1}cm^{-1}$. ΔP is the pressure increase in the static cell when IR radiation is absorbed. N.O. means not observed. N.M. means not measured.

b. At 100t of BCl_3, no transmitted radiation was observed.

power increases, but the calculated absorptivity decreases. The absorptivity does not follow a linear dependence on BCl_3 pressure. For a specific BCl_3 pressure, the addition of a second gas reduces the amount of absorbed laser radiation as well as the calculated absorptivity coefficient based on the BCl_3 partial pressure. Ar decreases absorptivity more than H_2. Also the pressure jump, which is indicative of a temperature rise, is more noticeable with Ar than with H_2. With a more intense beam (Table III) more laser radiation was absorbed per volume of gas but the "effective" absorptivity coefficients were lower than with the lower power beams. This is consistent with the observation made above that the inducement of a hotter gas volume by the laser radiation will result in a lower density of gas molecules within the laser beam.

The computational procedure, developed was used to estimate the temperature of BCl_3 and BCl_3 plus H_2. Figure 4 shows the calculated temperature profiles in 6.5 torr of BCl_3 exposed to a 3 W IR beam (0.19 W were absorbed per cm of path length) and to a 10 W beam (1.2 W were absorbed per cm). Due to the increased power absorption, the peak temperature at the center of the laser beam increases from 650 K to 1540 K. At 19 torr of BCl_3, 2.0 W/cm of path length is absorbed from a 40 W beam resulting in a maximum temperature of 1990 K. This trend reflects an important characteristic of the BCl_3 system, namely, that more power per unit length is absorbed at higher BCl_3 pressure while the mechanism of losing heat by thermal conductivity is not a function of pressure at pressures in excess of approximately 1 torr. A mixture of 19 torr of BCl_3 plus 20 torr of H_2 absorbs 2.1 W/cm of path length from the 40 W beam, but achieves a peak temperature of only 1000 K. The high thermal conductivity of H_2 is

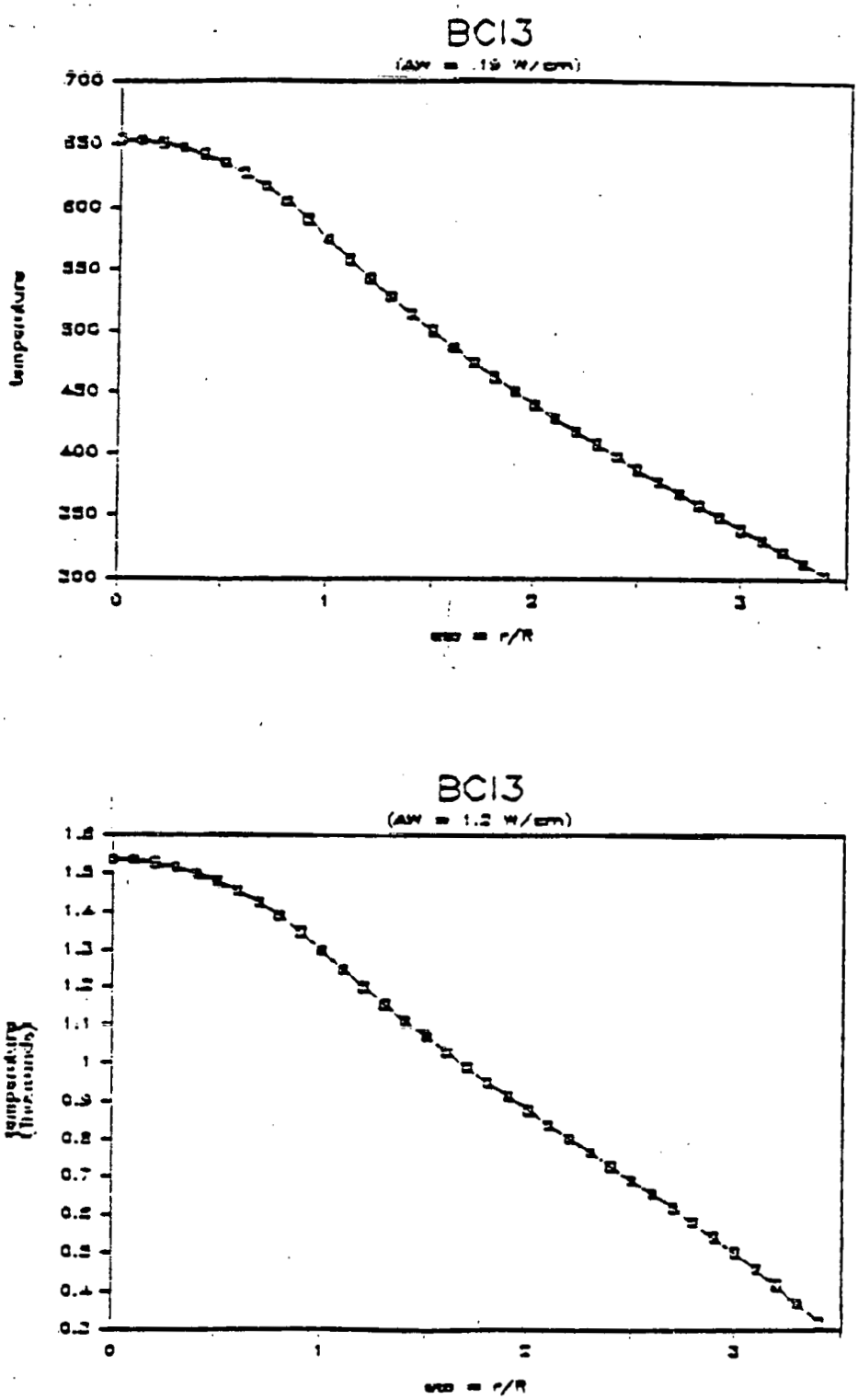

Figure 4. The calculated temperature in the static cell, due to absorption of IR laser radiation, is shown as a function of r/R. The distance from the center of the laser beam is at r and R is the radius of the laser beam. 0.19 and 1.2 W/cm were absorbed by 6.5 torr of BCl_3 for incident laser powers of 3 and 10 W, respectively.

responsible for the reduced temperature. These calculated temperatures are high enough to cause the formation of TiB_2 powder.

The static cell apparatus has been used to define the range of processing conditions that induce a chemical reaction. A mixture of 10 torr of $TiCl_4$, 20 torr of H_2 and 20 torr of BCl_3 absorbed 24 W of laser radiation, but no powder was formed. Changing the gas composition to 10 torr of $TiCl_4$, 50 torr of H_2 and 100 torr of BCl_3 resulted in all the laser radiation being absorbed (~ 35 W) within the 10.2 cm long static cell. A luminescent emission was observed but no powder formed. At 10 torr of $TiCl_4$, 100 torr of H_2 and 240 torr of BCl_3, 1 second laser pulses produced luminescent flashes and white film was detected on the front cell window. Longer pulses of laser radiation caused fracturing of the front KCl window. HeNe light scattering indicates that powder was located throughout the static cell, but the location of the powder formation could not be determined. When the window film was exposed to air, it changed appearance, apparently lifting off from the window surface. It has not been determined if a chemical or morphological change took place.

We have successfully synthesized TiB_2 powder under flowing gas conditions and have completed initial characterization of powders made with both varied process conditions and alternative chemistries. These accomplishments satisfy a major milestone for MIT's Grant DE-FG07-83ID-12380 entitled "Investigation of Materials for Inert Electrodes in Aluminum Electro Deposition Cells."

Flowing gas titanium diboride synthesis experiments have been based on two alternative chemistries. These are:

$$TiCl_4 + 2BCl_3 + 5H_2 \rightarrow TiB_2 + 10HCl$$

and

$$TiCl_4 + B_2H_6 \rightarrow TiB_2 + 4HCl + H_2.$$

These chemistries required resolution of several new issues with respect to the laser heat powder synthesis process that were not encountered with SiH_4 based chemistries. These include condensible reactants, endothermic reactions, low absorptivities and potentially competing reaction pathways to products other than TiB_2.

Powders were made under flowing gas conditions using both chemistries. Characterizations revealed that the B_2H_6 boron source yielded TiB_2 and the BCl_3 source produced $TiCl_3$ powder. We anticipate that process conditions which cause higher reaction temperatures will produce TiB_2 powder from BCl_3. The reactions were carried out under varied flow rates and pressures. Wide ranges of process variables produced stable reactions; it is therefore anticipated that process variables can be manipulated to optimize the properties of the resulting powders.

Powders have been characterized by X-ray diffraction, surface area analysis (BET), transmission electron microscopy (TEM) and chemical analysis (atomic absorption). X-ray diffraction indicates whether the powders are crystalline and is used to identify the crystalline phases and their grain sizes. Only TiB_2 diffraction patterns were observed in the powders formed from B_2H_6 and the grain size was determined to be 120 to 140 Å. BET analysis of these powders indicates a surface area of 47.5 m^2/gr; assuming a powder density of 4.5 gr/cm^3, this corresponds to a spherical equivalent diameter of 280 Å. TEM analysis of the B_2H_6 originating powders indicated a particle size ranging from 300 to 500 Å, a crystalline diffraction pattern corresponding to TiB_2 and no necks between contacting particles. The

physical dimensions indicated by X-ray, BET and TEM analysis are in agreement with one another. They show that the powders are polycrystalline with a grain size of approximately 1/3 the particle size. The TEM micrographs also show that the powder has a uniform particle size and contains no hard agglomerates. Atomic absorption analysis give a bulk composition of 23 mole % Ti and 77 mole % B. This composition is boron rich, corresponding to the gas mix used in the powder synthesis.

3. Hall Cell Performance Testing

A laboratory-scale electrolysis cell has been designed and built to test the Hall cell behavior of candidate anode materials. The cell can both conduct the electrolysis of alumina in cryolite and perform scientific corrosion tests, the latter owing to the invention at MIT of what appears to be a stable, drift-free aluminum reference electrode.

The cell has three electrodes: a test anode, a counter-electrode or cathode, and an aluminum reference electrode. The electrolyte is held in a crucible of either alumina or pyrolytic boron nitride, depending upon the degree of melt saturation with respect to Al_2O_3. An HBN grade boron nitride cylinder holds the test specimen and contains the reference electrode and a thermocouple well. A concentric cylinder of Mo foil serves as the cathode. The whole electrode assembly is lowered into the premelted electrolyte. There is an argon atmosphere in the cell. Specimens are tested at current densities of up to 1 A/cm^2. A current interrupter is used to measure potentials between electrodes. When combined with the stable reference electrode, this apparatus measures overpotentials during electrolysis. The traditional weight loss measurements are also made, and samples are subjected

to microstructural analysis. To date, several anode compositions have been studied including traditional graphite and compositions from the nickel ferrite system. A comparison of overvoltage measurements with the literature validates the test procedure and demonstrates the stability of the reference electrode.

The capability of doing scientific corrosion testing is the result of the reference electrode invented at MIT. The stability of this electrode is derived from the physical placement of the electrolyte, molten aluminum, and refractory metal lead wire in such a way as to avoid shorting and mixed potentials. SrF_2 or BaF_2 in the amount of 30 wt.% is added to cryolite making the melt sufficiently dense to cause the liquid aluminum pool to float on top of the electrolyte. In this way it is possible to ensure that the W or TiB_2 lead touches only the aluminum and not the salt. Thus, a truly reversible and stable interface is established between the aluminum pool and the melt which is chemically but not electrically isolated from the electrolyte by means of a porous boron nitride plug. The resistance of the plug, once it is saturated with electrolyte, is about 20 Ω. Another improvement over conventional reference electrode designs is the placement of the reference tip at the edge of the current path in the test cell. In this way the reference does not disturb the current streamlines, and allows consistency in the means of overvoltage measurement between different sample geometries. The electrolyte is contained in an alumina or pyrolytic boron nitride crucible which in turn is contained inside an air-tight alumina tube to maintain at all times an inert atmosphere above the test cell. Al_2O_3 additions can be made without opening the cell to the atmosphere. This

atmosphere control ensures that the electrolyte composition will not change during testing as well as between different runs.

4. Summary and Conclusions

Our research has produced important results in several topical areas needed to define inert anode and cathode materials for the Hall-Héroult cell. This research has also shown that needed background data are sparse and inaccurate, a combination that is, at best, misleading. The methodology for making and evaluating candidate materials has been developed. The basis for selecting candidate materials is seriously deficient.

Candidate materials have been surveyed and likely compositions for both anode and cathode applications have been defined. Single crystals of anode and cathode candidate materials have been grown and characterized. The cathode compositions were TiB_2 and LaB_6; anode candidates were based on Ni and Co ferrites. Both single crystal and multiphase, oriented grain anode samples were produced. Characterizations include crystallographic, metallographic, chemical, electrical and dissolution kinetics analyses. The high temperature electrical conductivity of single crystal TiB_2 was measured for the first time to provide a measure of intrinsic property values which differ from those of polycrystalline samples.

Several topics have been addressed with respect to the synthesis of ultra high purity TiB_2 powders. Candidate chemistries have been reviewed in terms of criteria important to the laser heated gas phase powder synthesis process. Safety equipment and procedures were a major topic because of the hazards represented by candidate gases. The chemistries selected are based on $TiCl_3$, BCl_3, B_2H_6 and Ti-isopropoxide. A computerized thermodynamic

analysis has been revised substantially to facilitate its usage and to provide graphic outputs of predicted concentrations of reaction products. Hot-wall static and flowing gas reactor cells have been developed. The static cell has been analyzed further to provide more accurate measures of the optical absorptivity and induced temperature rise in the reactant gas. The flowing gas cell and heater assembly has also been analyzed to insure complete and uniform volatilization of liquid reactants. Experiments of several types have been undertaken; these include absorptivity measurements, volatilization rate studies, peak gas temperature measurements, synthesis runs in a cold-wall, static cell and flowing gas synthesis runs with a heated nozzle. TiB_2 powders have been made under controlled and predicted process conditions. The powders appear suitable for fabrication into test samples.

A laboratory scale Hall cell was designed, constructed and made operational. The cell incorporates several novel design features that improve the quality of the scientific observations. Current densities, electrolyte composition, and other operating parameters span the range of industrial practice.

A potentially patentable aluminum reference electrode for the Hall cell was developed. The existence of a stable reference electrode permits for the first time potentiodynamic polarization studies to quantify corrosion rates measured in cryolite melts. Also, the reference electrode is being incorporated into a system for real-time monitoring of the electrolyte composition.

The results of this research have been disseminated widely throughout the technical community. This has been done by presentations both on and off campus, as well as by publications in the technical literature.

The research program is fully developed following the proposed approach. The proposed methodology for investigating candidate electrode materials under conditions where materials properties, performance and failure modes can be interpreted with a unique level of confidence is obviously correct given the inherent complexity of the Hall-Héroult cell.

It has become apparent that many of the presumptions made at the time the proposal was written are in fact not correct. The data base for making materials selection is completely inadequate. We have outlined the topics that require further study. Only with those data will it be possible to make materials selections on a rational rather than happenstance basis.

VII. REFERENCES

1. K. E. Spear and M. S. Wan, "Thermochemical Caluclations on the LPCVD of Si_3N_4 and SiO_2", Solid State Technology, 63-68, July (1980).

   C. F. Wan and K. E. Spears, "Experimental and Thermodynamic Analysis of the CVD of Nb_3Ge", in Proceedings of the Eighth International Conference of Chemical Vapor Deposition 1981; Editors J. M. Blocher, G. E. Vuillard and G. Wahl; The Electrochemical Society, Pennington, NJ, 54-65, (1981).

2. T. M. Besmann and K. E. Spear, "Analysis of the Chemical Vapor Deposition of Titanium Diboride", J. Electrochem. Soc., 124, 786-790 (1977).

3. T. J. Yurick and K. E. Spear, "Thermodynamics of TiB_2 from Ti-B-N Studies", in Thermodynamics of Nuclear Materials 1979, Vol. I., International Atomic Energy Agency, Vienna, 73-90, (1980).

4. R. E. Scruby, J. R. Lacher and J. D. Park, "The Infrared Spectrum of Boron Trichloride", J. Chem. Phys. 19, 386-387 (1951).

5. P. L. Houston, A. V. Nowak and J. I. Steinfeld, "Infrared Double Resonance in Boron Trichloride", J. Chem. Phys. 58, 3373-3380 (1973).

6. D. R. Sadoway, Aluminum Reference Electrode, U.S. patent application, Ser. No. 783776, October 3, 1985.

7. Yu. K. Delimarsky and B. F. Markov, Electrochemistry of Fused Salts, Sigma Press, Washington, 1961, pp. 133-137.

APPENDIX 2

Summary of Activities of Year 4

PROGRAM REVIEW TOPICS (12/18/86)

- Staffing
- Ferrite Anode (Corrosion Rate Studies)
  - Compositions
  - Crystal Growth
  - Crystal Characterizations
    - Metallographic
    - X-ray
    - Electrical Conductivity
  - Hall Cell
    - Computerized Operation & Data Acquisition
    - Anode Experiments
- Float Zone, Pendant Drop Cryolite Experiment
  - Cryolite on Cryolite
  - Cryolite on Al_2O_3
- Non Consumable Anode (Data Base, Candidate Compositions)
  - Definition of Selection Criteria
  - Data Survey
  - Candidate Materials
- Publications, Presentations, Visits
- Work Plan

APPENDIX 3

"Investigation of Ferrites as Potential Inert Anodes for Hall Cells,"
Alan D. McLeod, PhD thesis, Massachusetts Institute of Technology, 1987

INVESTIGATION OF FERRITES AS POTENTIAL INERT ANODES FOR HALL CELLS

by

Alan David McLeod

B.A.Sc., University of Toronto (1978)

M.A.Sc., University of Toronto (1983)

Toronto, Canada

Submitted to the
Department of Materials Science and Engineering
in partial fulfillment of the requirements
for the degree of

DOCTOR OF PHILOSOPHY

at the

Massachusetts Institute of Technology
Cambridge, Massachusetts

September, 1987

Signature of Author_____
Dept. of Mat. Sci. and Eng., Aug. 7, 1987

Certified by_____
D.R. Sadoway, Assoc. Prof. of Materials Engineering, Thesis Supervisor

Accepted by_____
J.B. Vander Sande, Chairman, Dept. Grad. Comm.

Abstract

The suitability of ferrites as inert anode materials in Hall cells was investigated using copper - manganese ferrites as a test system. Single crystal specimens were prepared so that testing took place upon equilibrated samples not affected by preparation. Electrical conductivities were measured in the temperature range 900 to 1450°C under an atmosphere of oxygen and were found to be less than 10 $(\Omega cm)^{-1}$ at the Hall cell operating temperature, 960°C. The importance of the effect of oxygen pressure upon intrinsic properties was demonstrated. In a bench - scale Hall cell ferrite specimens were tested as anodes. They corroded at unacceptably high rates, and the corrosion products were co - deposited with aluminum. In situ measurements of cell potential were made as a function of current density. The use of a stable reference electrode enabled electrochemical measurements such as anodic overvoltage and a variety of transient techniques.

Table of Contents

List of Figures

List of Tables

Acknowledgements

The author would like to thank his thesis supervisor, Prof. D.R. Sadoway, for his constant guidance and support throughout this work. He would also like to thank his wife, Bev Worthington, for showing patience while waiting to return to Canada. Thanks are due to Ms. Luella Gergen for the feed rod preparation work and to Mr. Guenter Arndt for his machining. Thanks also go to Prof. H.L. Tuller for his help in designing the conductivity experiment, and to Dr. J.S. Haggerty for his help and guidance in growing the ferrite crystals. Discussions with Dr. E.W. Dewing and Mr. W. Haupin helped in designing the Hall cell experiment. Thanks go to Dr. D. Townsend for supplying bath ratio and alumina content analysis techniques. The author also thanks Prof. R.E. Spjut and Prof. Y.-M. Chiang for their helpful comments and for serving on his thesis committee. Finally, the author would like to acknowledge the support of the U.S. Dept. of Energy, Office of Industrial Programs, through Grant No. DE-FG07-83ID12380.

1. Introduction

Aluminum is produced primarily by the Hall - Héroult process. In this high temperature molten salt electrowinning process, direct current is passed between a carbon anode and a molten aluminum cathode. The passage of this current through the electrolyte supplies sufficient Joule heating to maintain the temperature of the bath at around 960°C. The aluminum cathode, also referred to as a pad, can be between 14 and 40 cm in thickness. The pad to anode spacing in a well run cell lies between 4 and 6 cm. Industrial electrolytes consist mainly of cryolite, Na_3AlF_6, with additions of AlF_3, Al_2O_3 refined from bauxite by the Bayer process, and various concentrations of CaF_2, MgF_2 or LiF. Current densities lie between 0.7 and 1.2 A/cm^2 with a cell voltage in the range of 4.5 to 6 V and a current efficiency of about 91%. The overall cell reaction for the production of aluminum as given below has a reversible potential of 1.20 V at 960°C.

$$2Al_2O_3 + 3C = 4Al + 3CO_2 \qquad \varepsilon^\circ = 1.20\ V \qquad (1)$$

The components of a typical operating cell voltage are given in Table 1 (1,2).

Aluminum production requires about 15 kW-hr/kg in the form of electrical energy. At present production levels this quantity represents about 2.5% of the total electrical energy produced in the United States (3). An increase in the energy efficiency of the process from its present value of about 40% would result in a significant energy savings as well as a lower cost product. One way to lower the energy consumption would be to lower the cell voltage. An examination of Table 1 shows that the components of the cell voltage that could be lowered are the electrode resistances,

the electrolyte resistance (resulting in the so-called "IR drop") and the anodic overpotential. The most feasible way to lower the electrolyte resistance would be to decrease the anode to pad spacing. Electromagnetically - induced standing waves on the pad and the uneven wear of the anode are the principle reasons for the present non - optimal spacing. A cathode wettable by liquid aluminum would solve the standing wave problem since a thick pad would no longer be needed. A dimensionally stable anode, not consumed in the electrolytic process, would compliment the use of the wettable cathode allowing a decrease in spacing to possibly as little as 1.5 cm. This could result in a savings of about 1.2 V from the overall cell voltage.

	(V)
Busbar to Anode	0.1
Busbar to Anode Interface	0.05
Carbon Anode	0.33
Anode Overvoltage	0.48
Electrolyte Resistance	1.76
Reaction (1)	1.20
Cathode Overvoltage	0.05
Carbon Lining	0.33
Busbar to Lining Interface	0.06
Busbar to Lining	0.3
Total	4.66

Table 1 Components of Cell Voltage

Carbon anode consumption results in problems other than dimensional stability. The cost of the materials and energy

needed to fabricate anodes accounts for at least 7% of the total cost of the process. Cell design is restricted since the prebaked anodes must be replaced every 21 days. The release of sulfur containing, as well as carcinogenic, gases from the burnt anode material necessitates gas collecting and scrubbing apparatus above the potlines. The carbon is also a source of impurities such as Fe, Si, V and Ni which will co - deposit with aluminum.

The quantity of patents (4) granted since the pioneering work of Belyaev (5,6) indicates that the search for an inert anode has been actively going on for at least 50 years. When the present investigation was undertaken, it was uniformly felt that an inert anode would meet the following design criteria, listed in the order of their importance :

1) Low solubility in the electrolyte.
2) Low resistance.
3) Sufficient mechanical strength.
4) Ease of fabrication.
5) Low cost.
6) Facilitate stable electrical connections.

While the search for an inert anode has involved the testing of many different materials, no single design has been accepted by the industry.

Of the metals that have been tested only the noble metals such as Pt or Au are nearly inert. Belyaev found that Cu displayed some resistance to corrosion due to the formation of a layer of copper oxide on the metal surface. Unfortunately this layer would spall off, exposing fresh metal surfaces for corrosion.

Oxides were also selected for testing in various anode designs by first considering their solubility. The oxides

that are known to have solubilities of less than 1% in cryolite are ZnO, NiO, Co_3O_4, Cr_2O_3, Fe_2O_3, and SnO_2 (7). The next step taken was to design anode formulations so as to meet the second criterion, minimum resistance, as listed above. For this reason, mixtures based upon SnO_2 (Swiss Aluminum Ltd. (8,9), Sumitomo Chem. Co. Ltd. (10), Great Lakes Carbon Corp. (11)), Cr_2O_3 (Sumitomo (12)) and Fe_2O_3 (Sumitomo (13), Swiss Aluminum (14), Diamond Shamrock (15), Aluminum Co. of America (16), Great Lakes Carbon (17)) have received a great deal of attention. Other lower conductivity oxide bases such as Y_2O_3 (Diamond Shamrock (18)) and the oxygen ion conductors, stabilized ZrO_2 and doped CeO_2 (Swiss Aluminum (19,20)) have also been investigated. The most successful inert anode designs, at the time the present investigation was begun, were based upon Fe_2O_3. The development, by ALCOA (21), of a cermet anode design based upon this oxide will be used to show how all of the above design criteria were met.

Hematite, Fe_2O_3, has an unacceptably low conductivity of about 0.1 $(\Omega cm)^{-1}$ at 1000°C (22). Higher conductivities can be obtained from oxide solid solutions or compounds with the spinel structure based upon Fe_2O_3, hereafter referred to as "ferrites". Magnetite, Fe_3O_4, the ferrite with the highest conductivity of about 200 $(\Omega cm)^{-1}$ at 1000°C (23), is only stable for $P_{O_2} \leq 10^{-5.5}$ atm at 1000°C. Other ferrites that are stable at high P_{O_2}, having intermediate conductivities, can be formed using the above low solubility oxides such as zinc, nickel, and cobalt ferrites. Nickel ferrite, $NiFe_2O_4$, was the choice for further investigation. It was quickly found that this ferrite still did not have a sufficiently high conductivity, was prone to brittle mechanical failure, and was difficult to fabricate. The addition of a metal phase, either Fe, Ni, or Cu, to form a cermet material was found to dramatically improve the conductivity and mechanical properties. Intensive trial and error - type

testing was carried out until it was found that a cermet containing Cu gave the best results (24). A typical anode material would consist of a certain amount of porosity, a matrix of $NiFe_2O_4$, a monoxide (Ni,Fe)O phase, unreacted NiO and Fe_2O_3, and discrete copper particles. The final design criterion, stable electrical connections, was met by using a contact welding process carried out under a reducing atmosphere.

When the present investigation was started, a cermet using a Ni metal phase was considered the state of the art. However the design failed in ways that were difficult to interpret. As a consequence of using polyphase materials under conditions that were not always well defined, test results could not be easily duplicated. Furthermore, the effects of testing metastable phases under high oxygen pressures and temperatures were not fully appreciated. For these reasons, the extent to which the oxide phase contributed to the corrosion resistance of the tested material could not be determined. The initial goal of the present investigation was to determine how to improve the behavior of the ferrite phase through changes in composition. The experimental program involved the testing of nickel, cobalt, and a series of copper - manganese ferrites. In order to eliminate the variation in performance due to the variation in processing of the specimens, single phase, single crystal specimens, prepared by floating zone melting, were tested under conditions where the spinel phase would be at thermodynamic equilibrium. Electrical conductivity measurements were made at 1 atm. oxygen pressure for temperatures between 900 and 1450°C. In situ electrochemical measurements as well as results from pre - and post - test examination were all combined to portray the corrosion behavior of these specimens used as anodes in a bench - scale Hall cell.

While the testing of ferrites was being carried out, some attention was given to the design criteria, given on page 12, initially used to select ferrites. It was felt that selection could be improved by defining the requirements of an inert anode material rather than those of an inert anode. This necessitated considering an inert anode material in the context of its severe environment. This consists of immersion in a molten salt electrolyte, made mainly from cryolite with some dissolved alumina, near unit activity, at 960°C. While current is being passed at 1 A/cm^2 current density, oxygen gas is evolving on the anode at pressures above one atmosphere. The electrolyte also contains dissolved aluminum and the anode material may also occasionally contact the molten aluminum pad. So, the first materials selection criterion became :

1) The material must resist chemical attack and/or electrochemical dissolution in the Hall cell environment.

The second criterion became :

2) The material must have a sufficiently high electrical conductivity at 960°C and P_{O_2} = 1 atm so that it will not make an excessive contribution to the voltage drop across the anode assembly.

The design and construction of the anode largely determines how well a material meets the second criterion. For example, a thin layer of material would cause a small voltage drop even if the material did not have a relatively high conductivity. The remaining design criteria, nos. 3 to 6 on page 12, could be applied to a material that passed the above two materials selection criteria.

The testing of ferrite anodes in this study led to the

conclusion that even though they satisfied the materials selection criteria given above, they were not suitable for use as anodes. While the samples "resisted" chemical and electrochemical attack, they still corroded at rates that would not provide long term dimensional stability. More importantly, the corrosion products co - deposited with aluminum, yielding an impure metal product. Another materials selection criterion was enunciated, taking co - deposition into account, since all oxides will dissolve to some degree. This criterion is the most selective and therefore should be considered before criteria 1 and 2 from above :

0) The material should not co - deposit with Al.

An oxide like Fe_2O_3 would not pass this criterion since its reversible decomposition potential is higher, i.e. less negative, than that of Al_2O_3. However, an oxide with a more negative decomposition potential could still pass the materials selection criteria even if it had a high solubility. The material would saturate the electrolyte, after which irreversible corrosion would be halted, allowing the electrowinning cell to continue making pure aluminum.

One conclusion of this study was that ferrites should not be used in anode formulation. This was not appreciated at the time systems were selected for study. Nevertheless, this investigation has yielded some results that have contributed towards an understanding of how the composition of a material affects its properties and its behavior in a given environment.

2. Selection of Materials for Laboratory Investigation

While the system chosen for investigation should have industrial relevance it should also be convenient in terms of preparation and the interpretation of measurements. Six criteria were used to select a system for investigation :

[1] Compositions should be based upon ferrites having the cubic spinel structure.

[2] These ferrites should exhibit a sufficiently wide range of stoichiometry under conditions of thermodynamic equilibrium at 1000°C and P_{O_2} = 1 atm. While it is possible and quite common for solid state measurements to be made upon oxides in metastable crystallographic arrangements, the operating temperature of the Hall cell is probably too high to prevent the transformation to equilibrium states in a short time. It would then be difficult to separate the effects of electrode - melt interaction and thermodynamically driven phase formation.

[3] Small changes in composition or dopant level may cause dramatic changes in electrical conductivity without causing noticeable differences in electrode behavior. On the other hand small concentrations of certain oxides may cause electrocatalytic effects on electrodes. Where possible, the effects due to such minor additions should be avoided until bulk interactions are better understood.

[4] The compositions should be amenable to the application of floating zone crystal growth techniques. This implies that the composition should form a stable, low vapor pressure melt under an atmosphere of O_2 even with a 50 to 100° superheat. The vaporization should not be so excessive as to disrupt the liquid zone. If a second phase

forms as a result of crystal growth then this phase should be easily dissolved by further heat treatment of the crystal.

[5] The literature must contain sufficient information concerning the thermodynamic, structural, and electrical properties of the selected system. More specifically, enough information must be available in order that the second and fourth criteria can be satisfied without extra investigation. The literature must indicate that the electrical conductivity at 1000°C must be n - type and high enough to allow the material to conduct significant currents without Joule heating. An arbitrary lower conductivity limit of about 0.1 $(\Omega cm)^{-1}$ can be used. The cation distribution should be sufficiently well understood so as to allow the formulation of a model for conductivity.

[6] The compositions should contain varying amounts of the Fe^{2+} cation. This ion has a direct affect upon conductivity and may have an interesting influence upon electrode behavior. Also, if possible, the compositions could contain varying amounts of CuO as this oxide may provide a measure of corrosion resistance to ferrites.

The phase stability of various ferrites was examined using the Phase Diagrams for Ceramists compilation (25) as well as the review by Sticher and Schmalzried (26). Diagrams for ferrites having the general formula $Me_xFe_{3-x}O_4$ were examined for the stability of a spinel phase at 1000°C and P_{O_2} = 1 atm. Ferrites formed with Me = Cr, V, Ti, Mo, La, Nb, Ta, Al, Fe, Ca, Sn, and Zr are not stable. Ferrites of Co, Ni, Cu, Mg, Mn, Li, and possibly Ba and Zn do form stable spinels under these conditions. The Mg, Li, and Ba ferrites may have high solubilities in molten cryclite due to the high solubilities of MgO, Li_2O, and BaO (7). Zinc ferrite was eliminated as well since little is known

concerning the phase stability of this ferrite. This left the cobalt, nickel, copper, and manganese ferrites.

While cobalt and nickel ferrites were successfully grown as part of the anode study this work concentrated upon crystal compositions grown from the manganese ferrite and copper - manganese ferrite systems. It was found that the only single phase nickel ferrite composition that could be grown was at 60 mole% Fe_2O_3, the congruent melting point of the spinel in the NiO - Fe_2O_3 system (27). Compositions on either side of this congruent point would lead to multiphase materials. As well, the stoichiometric range of $NiFe_2O_4$, the ferrite stable at 1000°C, is very narrow (28). The CoO - Fe_2O_3 system is not as well known as the nickel ferrite system. However, it is probable that the stoichiometric range for $Co_xFe_{3-x}O_4$ does not widen significantly until P_{O_2} is lowered below 10^{-2} for temperatures above 1000°C (26). Crystal growth from the liquid would be difficult in the copper ferrite system due to the lack of a either a congruent melting point or a flat liquidus (29).

The relevant Fe_2O_3 - Mn_2O_3 phase diagrams in air are shown in Figures 1 and 2. Both were measured using X - ray phase identification of quenched samples. The diagram by Wickham (31) agrees well with the classical diagram of Muan and Somiya (30) except for the exact boundary shape of some regions. Other phase diagrams have been given for lower oxygen pressures (32,33). Generally the phase boundaries move to lower temperatures as the P_{O_2} is lowered. The flat liquidus of this system allows the crystal growth of a wide range of spinel compositions even at 1 atm. O_2. As will be

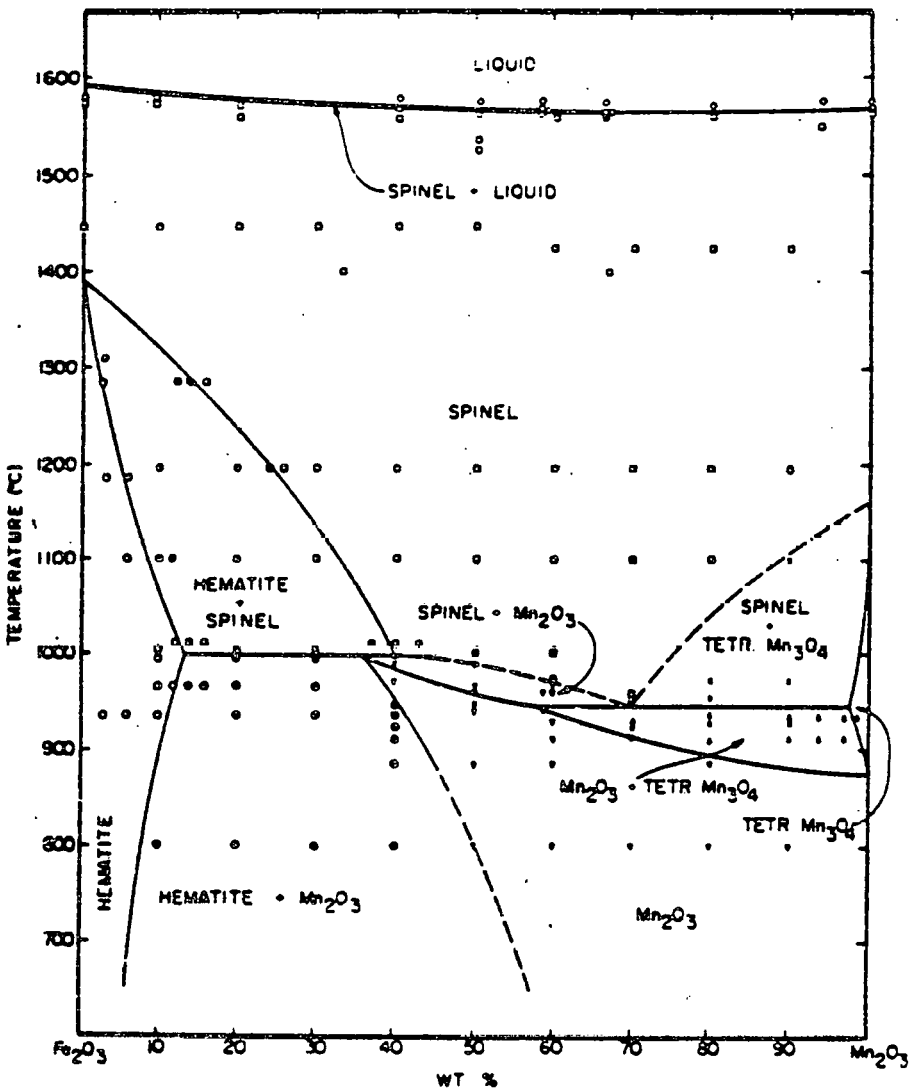

Figure 1 Fe_2O_3 - Mn_2O_3 Phase Diagram in Air According to Muan and Somiya (30)

discussed in section 4 this system has been widely used for crystal growth using various techniques.

While no useful phase diagrams for the CuO - Fe_2O_3 - Mn_2O_3 system exist, the work that is available (34,35) indicates that the addition of CuO to manganese ferrites extends the spinel region to lower temperatures. It is

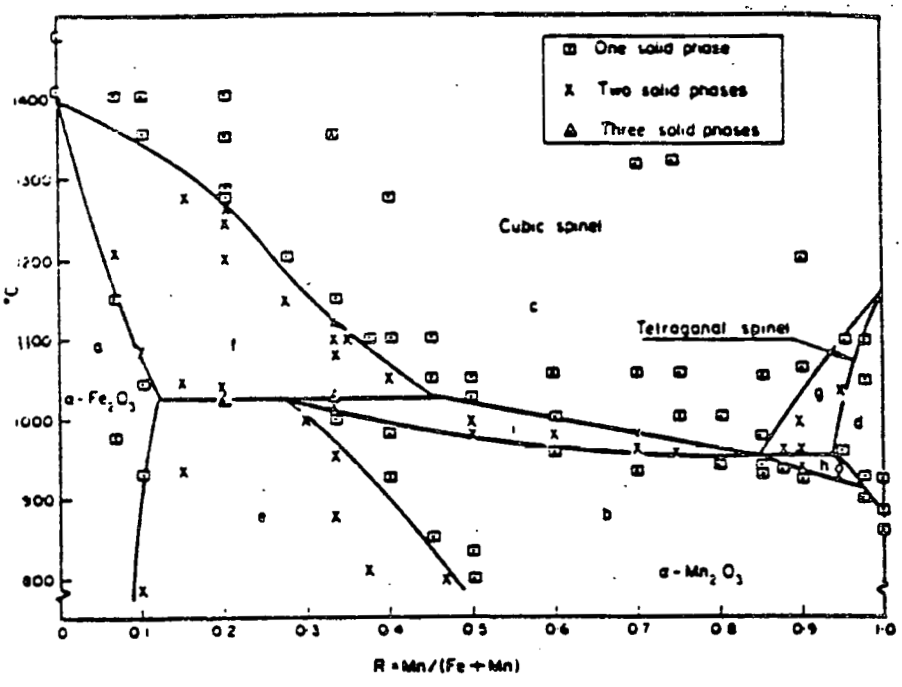

Figure 2 Fe_2O_3 - Mn_2O_3 Phase Diagram in Air According to Wickham (31)

possible then, that the presence of CuO could increase the compositional range of spinel solutions at 1000°C. This system yields compositions of the type $Cu_xMn_yFe_{3-x-y}O_4$. Even though it would be possible to form a number of spinel compositions of this type using the NiO - CoO - Fe_2O_3 systemwith x+y near 1, little is known about this system and it is likely that the conduction process would be p - type for x+y slightly greater than 1. As will be discussed in sections 3.6 and 3.7 the conduction of the copper - manganese ferrites remains n - type for nearly all values of x+y. As well, this system has been subject to a certain number of investigations concerned with magnetic properties as result of its square hysteresis loop properties. (36,37). The proposed compositions are listed in Table 2. The Mn : Fe ratio is kept constant within a series while Cu is added. Composition IIIa corresponds to the eutectoid composition as

	I	II	III
a	$Mn_{0.6}Fe_{2.4}O_4$	$Mn_{1.2}Fe_{1.8}O_4$	$Mn_{2.1}Fe_{0.9}O_4$
b	$Cu_{0.2}Mn_{0.6}Fe_{2.2}O_4$	$Cu_{0.2}Mn_{1.1}Fe_{1.7}O_4$	$Cu_{0.2}Mn_{2.0}Fe_{0.8}O_4$
c	$Cu_{0.5}Mn_{0.5}Fe_{2.0}O_4$	$Cu_{0.5}Mn_{1.0}Fe_{1.5}O_4$	$Cu_{0.5}Mn_{1.7}Fe_{0.8}O_4$

Table 2 Proposed Compositions

shown in Figure 1 at 70 wt% Mn_2O_3 in Fe_2O_3. Composition IIa corresponds to 40 wt% Mn_2O_3 and Ia to 20 wt%. The available literature concerning the structure and electrical conductivity of the copper - manganese ferrite system will be reviewed in the next section after a short review of the fundamental models used for spinels.

3. Relevant Properties of Manganese and Copper - Manganese Ferrites from the Literature

3.1 Spinel Structure

Several reviews on the structure and properties of ferrites are available, including the one by Smit and Wijn (38) and that by van Hook (39). The unit cell of a spinel ferrite consists of 8 $MeFe_2O_4$ molecules. The 32 oxygen anions are arranged in a face - centered close packed lattice. This lattice contains 64 tetrahedral (or "A") interstitial sites, only 8 of which are occupied by metal cations, and 32 octahedral (or "B") sites, half of which are occupied. In a "normal" spinel the Me^{2+} ions are located on the tetrahedral sites only :

$$Me^{2+}[Fe_2^{3+}]O_4 \qquad (2)$$

In a completely "inverse" spinel the Me^{2+} cations are all located on octahedral sites :

$$Fe^{3+}[Me^{2+}Fe^{3+}]O_4 \qquad (3)$$

Many ferrites including manganese ferrites are neither completely normal nor inverse and can have cations distributed over both types of sites. Since the cation distribution cannot be determined by chemical analysis alone other techniques such as X-ray diffraction, neutron diffraction, saturation magnetization, or Mössbauer spectroscopy must be used. The distribution can also be inferred from measurements of thermodynamic or electrical properties.

The situation for the ferrite $Cu_xMn_yFe_{3-x-y}O_4$, is inherently complex as all of the valence states: Cu^+, Cu^{2+},

Mn^{2+}, Mn^{3+}, Mn^{4+}, Fe^{2+}, and Fe^{3+} can exist in the structure at concentrations dependent upon x and y, as well as the temperature, oxygen pressure, and thermal history.

3.2 Electrical Conductivity in Ferrites

Electrical conductivity in these materials can be described using the small polaron hopping model as reviewed by Parker (40) and Bosman and van Daal (41). Simply put, small polaron hopping describes the movement of electrons between Fe^{2+} and Fe^{3+} ions on the octahedral sites. The conductivity, σ, of a n - type conductor is described by :

$$\sigma = ne\mu \tag{4}$$

where n is the concentration of charge carriers, often assumed to be equal to the concentration of Fe_B^{2+} ions. The mobility of the carriers is represented by μ, with e as the charge on an electron. For the hopping mechanism :

$$\mu = \frac{ed^2w}{kT}\exp\left[\frac{-\varepsilon}{kT}\right] \tag{5}$$

where d is the hopping distance, w, the frequency of lattice vibrations, k, the Boltzman constant, and ε, the activation energy for conduction. Combining equations (4) and (5) yields :

$$\sigma = \frac{ne^2d^2w}{kT}\exp\left[\frac{-\varepsilon}{kT}\right] \tag{6}$$

$$\text{or} \quad \sigma = \frac{\sigma_o}{T}\exp\left[\frac{-\varepsilon}{kT}\right] \tag{7}$$

A plot of $\ln(\sigma T)$ vs. T^{-1} will yield $-\varepsilon/k$ for the slope and

$\ln(\sigma_o)$ for the intercept. This model was first applied by Jonker (42) in his classical paper on the semiconducting properties of $Co_xFe_{3-x}O_4$ for $0.9 \leq x \leq 1.3$. He assumed that d was the distance between octahedral sites :

$$d = \frac{1}{4}\sqrt{2}a \qquad (8)$$

and used a value of 6.5×10^{12} sec^{-1} for w. The model has since been successfully applied to numerous other ferrites including nickel ferrite (43).

3.3 Lattice Parameter and Phase Transition

The measurement of crystal lattice parameter using X - ray diffraction often has been used for spinel phase identification as well as aiding in the interpretation of the effects of composition, temperature, and P_{O_2} upon structure. In 1938 Motoro (44) found complete miscibility between Fe_3O_4 and Mn_3O_4 at 1200°C. This miscibility is of interest because Fe_3O_4 is cubic while Mn_3O_4 has a tetragonal lattice. Montoro found tetragonal lattices for $x \geq 2$ in $Mn_xFe_{3-x}O_4$. Finch et al. (45) found similar results to those of van Hook and Keith (46). They found that their samples, sintered in air at 1200°C, would be cubic at high temperatures and undergo the tetragonal transformation upon cooling to room T. Both papers report that the tetragonal lattice is found for $x > 1.8$ and Finch et al. conclude that the transformation takes place when the stoichiometric concentration of Mn^{3+} on the B sites exceeds 1.2. The Mn^{3+} ion is identified as a Jahn - Teller ion (47) that will distort the lattice when present on an octahedral site at a certain concentration. Brabers (48) also found a tetragonal lattice for $x > 1.9$ for quenched metastable cubic samples that were re - heated to 200 to 300°C. He interpreted this

behavior by assuming that the reaction :

$$Mn_B^{2+} + Fe_B^{3+} == Mn_B^{3+} + Fe_B^{2+} \qquad (9)$$

goes to the right at lower temperatures, inducing the phase transition. However, Hucl et al. (49), using Mössbauer spectroscopy, did not find any Fe_B^{2+} in tetragonal samples with x = 1.9 and 2.0. They concluded that the cause of the phase transition was not known.

Of greater interest to this study was the behavior of the structure for $x < 2$. A few measurements for x = 1, $MnFe_2O_4$, have been reported : 8.517 A for a sample annealed in air for 24 hr at 1400°C and then quenched (50); 8.505 A, annealed in air for 3 hr at 1100°C (51); 8.510 A, annealed at P_{O_2} = 0.8 at 1300°C and quenched (52). Bergstein (53) reports lattice parameters for $0.52 < x < 1.987$ for samples sintered in air. For samples quenched from 1210 to 1310°C and for $0.52 \leq x < 1$ the lattice parameter, a (in A), could be represented by $a = 8.38 + 0.14x$. A discontinuity is seen at x = 1. For $x > 1$ the lattice parameters for quenched samples increased at slower rates. The measurements made at high temperature confirm this behavior. For measurements made at 1210°C, $a = 8.520 + 0.091x$ for $0.52 \leq x < 1$, and $a = 8.581 + 0.030x$ for $1 < x < 1.987$. For measurements made at 1250°C, $a = 8.551 + 0.064x$ for $0.52 \leq x < 1$, and $a = 8.605 + 0.011x$ for $1 < x < 1.987$. These results could be interpreted for $x < 1$ as being caused by the linear substitution of Mn^{2+} (ionic radius, r = 0.91 A) for Fe^{3+} (r = 0.67 A) on A sites, while Fe^{2+} is being replaced by Fe^{3+} and some amount of Mn^{3+} on the B sites. For $x > 1$, Mn^{3+} (r = 0.70 A) substitutes for Fe^{3+} (r = 0.67 A) since the A sites are nearly filled with Mn^{2+}. The differences in the slopes is a direct result of the differences in the ionic radii. This kind of dependence of the lattice parameter upon x for $x < 2$ has also been observed by Wickham (31),

Brabers (54) and Bakare et al. (55). Brabers' results were $a = 8.39 + 0.13x$ for $0 < x < 1$, and $a = 8.52 + 0.04x$ for $1 < x < 1.9$, for samples annealed above 1250°C at $P_{O_2} \leq 0.1$ and quenched. In good agreement with Brabers and Bergstein, Bakare et al. report $a = 8.385 + 0.122x$ (± 0.005) for $0 \leq x \leq 1$.

Tanaka (56) has measured the effects of P_{O_2} and sintering temperature upon the values of the lattice parameter and γ for $Mn_xFe_{3-x}O_{4+\gamma}$ with $0.80 \leq x \leq 0.95$. He found a maximum value of the lattice parameter for when $\gamma = 0$, usually near $P_{O_2} = 0.01$. For lower values of P_{O_2}, γ was less than zero indicating the formation of anionic vacancies, causing a small decrease in the lattice parameter. For higher values of the P_{O_2}, γ was positive, and the lattice parameter decreased at a higher rate with the increase in P_{O_2} as a result of the formation of cationic vacancies. From an analysis of Tanaka's results, $a = 8.392 + 0.122x$ for a sintering temperature of 1300°C, and $a = 8.409 + 0.105x$ for 1350°C and $0.80 \leq x \leq 0.95$, at $P_{O_2} = 1$.

Some work has been carried out on the effect of CuO additions upon the lattice parameter of manganese ferrites. Andriyevskiy et al. (57) report the lattice parameter relationship $a = 8.4585 - 0.0645x$ (± 0.002 A) for $Cu_xMn_{1-x}Fe_2O_4$ samples annealed at 1200°C. Zinovik et al. (58) report $a = 8.511 - 0.122x$ for this formula and $a = 8.537 - 0.148x$ for $Cu_xMn_{3-3x}Fe_{2x}O_4$ samples fired above 1000°C. Muthukumarasamy et al. (59) report $a = 8.498 - 0.108x$ for $Cu_xMn_{1-x}Fe_2O_4$ samples annealed at 1200°C in air. While these authors do not attempt to interpret these results, probably due to the complexity of this system, a possible source for the lattice shrinkage may be the replacement of Mn^{2+} ($r = 0.91$ A) by Cu^{2+} ($r = 0.80$ A).

It can be seen that while the measurement of lattice

parameter may lend support to certain cation distributions, it is in itself not sufficient. Several other techniques have been applied to gain a better measure of the cation distribution.

3.4 Cation Distribution of Manganese Ferrites

As a result of the complexity of manganese ferrites no single technique is capable of completely determining the distribution. Usually the results from a number of investigations must be combined with several assumptions to arrive at the complete picture. The determination of the distribution is complicated by its dependence upon composition, temperature, P_{O_2}, and thermal history. This section reviews the more useful studies available in the literature. Some results have been listed in Table 3.

Before the work of Hastings and Corliss (50), $MnFe_2O_4$ was assumed to be completely inverse. Applying neutron diffraction to a sample annealed for 24 hr at 1400°C in air and quenched, they found the manganese content on A sites to be 0.81. Further analysis, and assuming that Mn^{2+} prefers A sites with Mn^{3+} and vacancies preferring B sites, Harrison et al. (60) arrived at the tabulated distribution. Krupicka and Zaveta (61) found a similar distribution using saturation magnetization measurements. Continuing the work of (61), Broz et al. (62) found it necessary to have Mn_B^{4+} in order to account for the magnetic moments measured upon the samples listed in Table 3. It is interesting to note that the concentration of Fe_B^{2+} increases at the expense of Fe_B^{3+} as the Mn content increases. They explain the apparently contradictory increase of ε, the activation energy for conduction, with increasing Mn by using the model of Mn^{4+} - Fe^{2+} pair formation first proposed by Eschenfelder (63).

Reference	Sample(s)	Preparation	Technique(s)	$Mn_a^{2+}Fe_{1-a}^{3+}[Mn_b^{2+}Mn_c^{3+}Mn_d^{4+}Fe_e^{2+}\square_f Fe_{2-b-c-d-e-f}^{3+}]O_{4+\gamma}^{2-}$ a	b	c	d	e	f	γ
(60) Harrison et al	$MnFe_2O_4$	24 hrs, 1400°C, air, water quench	neutron diffraction	0.79	0	0.18	0	0.11	0.04	
(61) Krupicka and Zaveta	$MnFe_2O_4$	1200 - 1400°C, air	saturation magnetization, elec. cond.	0.8	0	0.2	0	0.2		0
(62) Broz et al	$Mn_{1+x}Fe_{2-x}O_{4+\gamma}$ $0 \le x \le 0.96$	1200 - 1400°C, air	magnetic moment	0.8 + 0.18x	0	0.2	0.82x	0.2 + 0.64x		0
(65) Butler and Buessem	$MnFe_2O_4$	1200 - 1330°C, various P_{O_2}'s	saturation magnetization $P_{O_2}=1$ for: 1200°C	0.77	0	0.23	0	0.23		n.m.
			1250°C	0.84	0	0.16	0	0.16		"
			1330°C	0.94	0	0.06	0	0.06		"
(68) Simsa	$Mn_xFe_{3-x}O_{4+\gamma}$ $0 \le x < 2.5$	crystals	Seebeck coeff. for: x=0.95	0.79	0	0.16	ass.0	0.19		0.01
(52) Yamanaka	$MnFe_2O_4$	1400°C	anomalous X - ray dispersion	0.79	0	0.21	ass.0	0.15	0.02	
(76) Marais et al	$Mn_xFe_{3-x}O_{4+\gamma}$ $1.2 \le x \le 1.6$	1200°C, P_{O_2} reduced to keep $0.02 \le \gamma \le 0.03$	Mössbauer, magnetic after effect for: x=1.2	0.84	0.10	0.26	0	0		0.032
			x=1.4	0.82	0.13	0.46	0	0		0.024
			x=1.6	0.81	0.15	0.64	0	0		0.020
(78) Peltcn et al	$Mn_xFe_{3-x}O_4$ $0 \le x \le 3$		thermodynamic model for; x=1 at 900°C	0.31	0.57	0.15	ass.0	0.06		
				also Fe_A^{2+} = 0.03						
(79) Dorris	$Mn_xFe_{3-x}O_4$ $0 \le x \le 3$	1300°C, 3 hr, P_{O_2} reduced for $x \le 1$, air for $x > 1$	Mössbauer, Seebeck, thermo. model for: 1000°C x=1	0.69	0.14	0.11	0.07	0.27	n.m.	
			1300°C x=1	0.54	0.20	0.13	0.11	0.36	"	
				also Fe_A^{2+} = 0.03						

Table 3 Some Cation Distributions Proposed for Manganese Ferrites (ass.=assumed, n.m.=not measured)

Once paired with Mn^{4+}, the Fe^{2+} ion requires an additional activation energy in order for it to contribute to the conduction process. Yamzin et al. (64) applied neutron diffraction to crystals of $Mn_xFe_{3-x}O_4$ for $0.43 \leq x \leq 1.58$ grown using the Verneuil technique. They measured the compositional dependence of the inversion degree and oxygen parameter ("a" and "γ" in Table 3). For $0.43 \leq x \leq 0.53$, "a" = 0. At x = 0.84 "a" jumps to 0.78 in agreement with previous results, and then steadily rises to 0.92 for x = 1.58.

The work by Butler and Buessem (65) on $MnFe_2O_4$ was probably the first systematic study of the effect of sintering temperature and P_{O_2} upon the cation distribution. They arrived at the distribution given in Table 3 by measuring the magnetization at low temperature and assuming that Mn^{3+} - Fe^{2+} are the stable pairs on the B lattice. However, Lotgering (66), after making conductivity measurements upon various manganese ferrites concluded that reaction (9) goes to the left rather than the right as previously assumed. Conductivity was a result of "thermally generated" Fe_B^{2+} ions.

Debate at this stage was centered around explaining apparently contradictory results. Neutron diffraction and magnetic measurements indicated relatively high concentrations of Fe_B^{2+} even at at x = 1 in $Mn_xFe_{3-x}O_4$. While Seebeck coefficient measurements indicated n - type conduction up to values of x well beyond 1, conductivity measurements could not support such high concentrations of Fe^{2+}. In retrospect, it can be seen that two other considerations clouded the issue.

The first consideration is the possible temperature dependence of the equilibrium of reaction (9). The direction of the reaction could very well shift from left to

right with increasing temperature. Also, the reaction involves the movement of an electron without any necessary movement of ions. While ionic position can be "frozen" by quenching from high temperature, electron movement from one localized position to another could probably not be prevented. Nearly all studies are made upon quenched samples with the assumption that they represent the configuration of the material at its sintering temperature.

The second consideration is the effect of oxygen pressure as shown by the following reaction :

$$Fe_B^{2+} + \frac{1}{4}O_2 == Fe_B^{3+} + \frac{1}{2}O_O^{2-} + \frac{3}{8}\square_B \qquad (10)$$

As discussed in the previous section, preparation of manganese ferrites must take place with the P_{O_2} below about 0.01 atm if the formation of cationic vacancies is to be avoided. While some investigators take this into account, others prepare samples in air or under argon, for example. This variation of the P_{O_2} used during preparation adds to the difficulty of comparing experimental results. The importance of these considerations became better recognized as the debate over the cation distribution continued.

Simsa (67) explains Lotgering's results by considering that reaction (9) goes to the right and Mn^{3+} - Fe^{2+} pairs form. The stabilization provided by the pair formation is a result of Fe_B^{2+} countering the tendency of Mn_B^{3+} to distort the crystal lattice. The stabilization energy, about 0.30 eV, must be supplied in order to allow the paired up Fe_B^{2+} to supply an electron for conduction. To support this thecry Simsa (68) measured the Seebeck coefficient for various manganese ferrites. For the composition listed in Table 3 the "free" Fe_B^{2+} that can contribute towards conduction is actually 0.03.

Applying the Mössbauer technique in a magnetic field to $MnFe_2O_4$, Sawatzky et al. (69) confirmed the neutron diffraction results of Hastings and Corliss (50). Not all of the early Mössbauer work was in such agreement. Bunget (70) explains differences as being a result of the influence of preparation on the amount of Fe^{2+}. In particular he points out the influence of cooling rate and the amount of oxygen excess or deficiency. In another study, Sawatzky et al. (71) did not find any Fe_B^{2+} in $MnFe_2O_4$ at 7K. Still using a similar technique, Hucl et al. (49) did not find any Fe_B^{2+} in $Mn_{1.0}Fe_{1.1}O_4$ or Mn_2FeO_4.

Brabers and Dekker (72) used yet another technique, infra - red spectroscopy, to support the idea that reaction (9) goes to the left, giving Mn_B^{2+} rather than Mn_B^{3+}. In applying Mössbauer and X - ray anomalous dispersion to $MnFe_2O_4$ in order to study the effects of sintering temperature and P_{O_2}, Yamanaka (52) found that the reaction goes to the right. Using his results, a cation distribution has been calculated and included in Table 3. It is in good agreement with previous measurements. The work of Jirak and Vratislav (73) in applying neutron diffraction to $MnFe_2O_4$ has been reviewed and developed by Simsa (74). Measurements were made upon crystals grown by Brabers (75) using the floating zone technique. The samples were held in "sealed vessels" and measurements were made in the range 330 to 1170°C. It should be noted that the ferrite will not be thermodynamically stable for much of this range regardless of the P_{O_2}. They found a relationship for the temperature dependence of y, the concentration of Mn_B, by using K_{11}, the equilibrium constant for the reaction :

$$Mn_A + Fe_B == Mn_B + Fe_A \qquad (11)$$

$$K_{11} = \frac{y^2}{(1-y)(2-y)} = \exp\left[-\frac{3900 - 4100y}{kT}\right] \qquad (12)$$

It is curious that the equilibrium constant, K_{11}, would depend on the concentration of one of the components of that equilibrium. Contrary to the results of Marais et al. (76), Rotter et al. (77) found only Mn^{3+} on the B sites in ferrites with x = 0.95, 1.0, and 1.4. They applied NMR spectroscopy to the float - zone crystals of Brabers which had been annealed so as to ensure a 3:4 stoichiometry.

More recently, the concept of ionic equilibria has been applied to model the Mn_3O_4 - Fe_3O_4 system. Pelton et al. (78) have modelled the cation distribution by using the following free energies of reaction :

$$Fe_A^{2+} + Fe_B^{3+} == Fe_B^{2+} + Fe_A^{3+} \qquad \Delta G_{13} = 0 \quad (kJ) \qquad (13)$$

$$Mn_A^{2+} + Mn_B^{3+} == Mn_B^{2+} + Mn_A^{3+} \qquad \Delta G_{14} = 83.6 \qquad (14)$$

$$Fe_A^{2+} + Mn_B^{3+} == Fe_B^{2+} + Mn_A^{3+} \qquad \Delta G_{15} = 83.6 \qquad (15)$$

$$Fe_B^{3+} + Mn_B^{2+} == Fe_B^{2+} + Mn_B^{3+} \qquad \Delta G_9 = 154.2 - 0.96T \quad (9)$$

Their ΔG for reaction (9) indicates that the reaction will go to the right at higher temperatures. Solving for the relative ionic concentrations using an iterative method yields the distribution shown in Figure 3. The distribution as given in Table 3 for x = 1 is not in agreement with other measurements. Dorris (79) has used a more involved thermodynamic model for cation distribution to account for his Seebeck coefficient and Mössbauer measurements. He chose six thermodynamic parameters so that the equilibrium constants of the following reactions could be calculated.

"Cation Distribution" : $Mn_A^{2+} + Fe_B^{3+} == Mn_B^{2+} + Fe_A^{3+}$ (16)

$-RT\ln(K_{16}) = \alpha + 2\beta b$ with $\alpha = 53.0$, and $2\beta = -60.0$ (kJ/mole) (17)

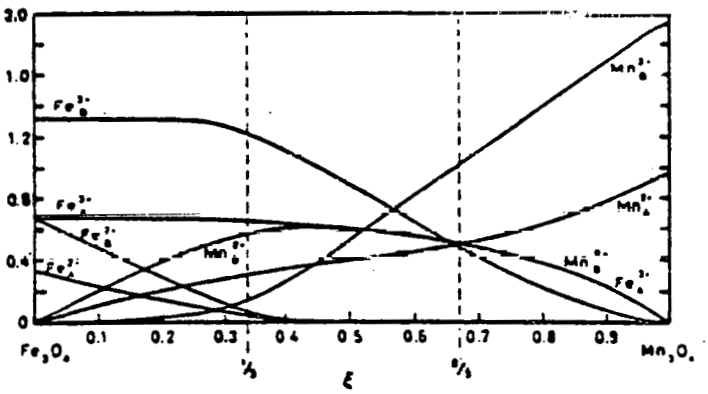

Figure 3 Proposed Cation Distribution in the Fe_3O_4 - Mn_3O_4 System at 900°C (78)

$$\text{"Disproportionation"} : \quad 2Mn_B^{3+} \rightleftharpoons Mn_B^{2+} + Mn_B^{4+} \qquad (18)$$

$$\Delta G_{18} = 16.98 - 11.47 \times 10^{-3} T \quad (kJ/mole) \qquad (19)$$

$$\text{"Redox"} : \quad Mn_B^{2+} + Fe_B^{3+} \rightleftharpoons Mn_B^{3+} + Fe_B^{2+} \qquad (9)$$

$$\Delta G_9 = 14.39 + 3.57 \times 10^{-3} T \quad (kJ/mole) \qquad (20)$$

The form of equation (17), which is similar to equation (12), derived by Jirak and Vratislav (73), was derived using statistical thermodynamics by O'Neill and Navrotsky (80). The concentration parameter, b, represents the concentration of Fe_A^{3+}. The resulting distributions are shown in Figure 4. The distributions for x = 1 are given in Table 3 for comparison. It is interesting to note the high

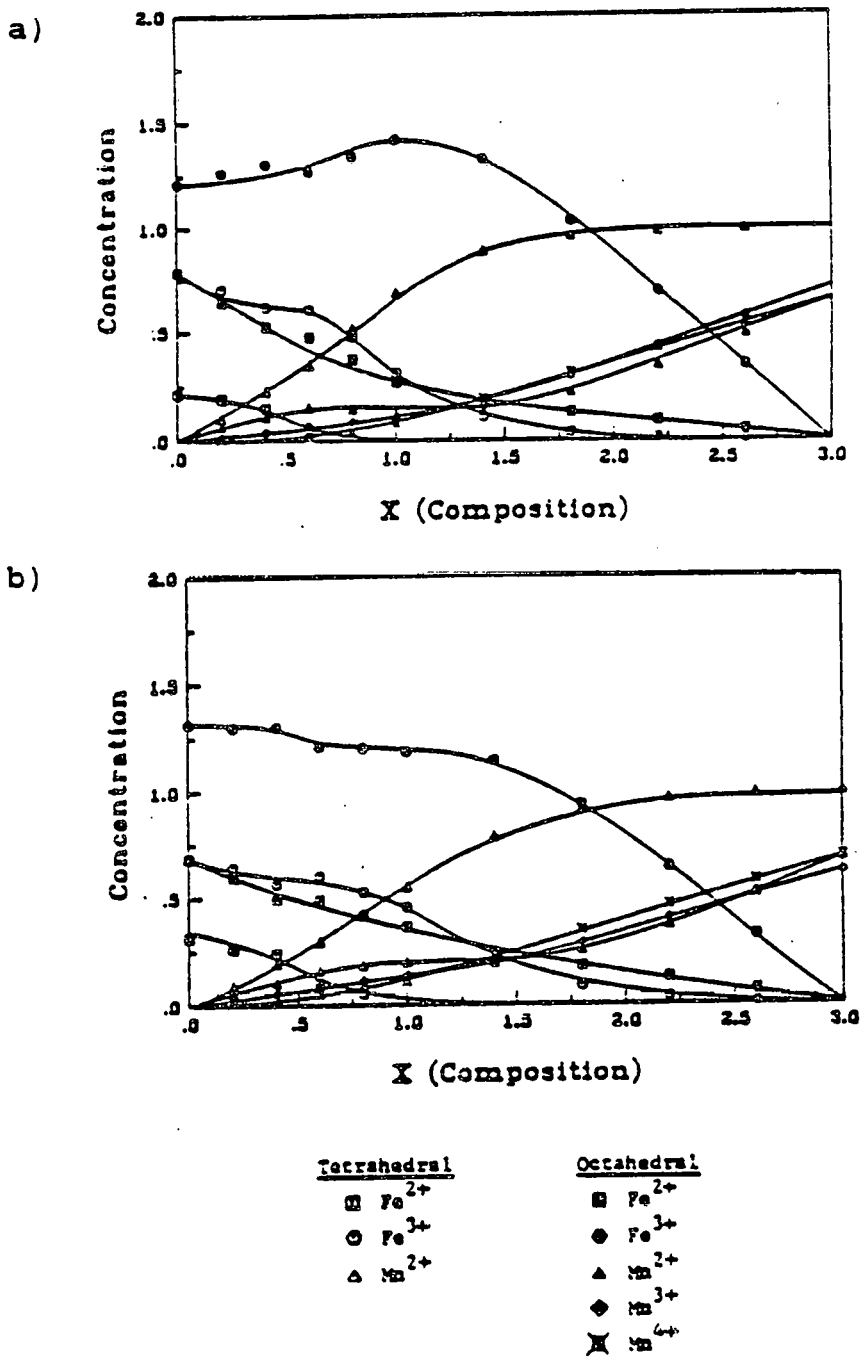

Figure 4 Proposed Cation Distribution in the Fe_3O_4 - Mn_3O_4 System at a) 1000, and b) 1300°C (79)

concentration of Fe_B^{2+} even though the model indicates that reaction (9) will go to the left at all temperatures. Dorris indicates that Mn_B^{4+} must be present in order to account for his Seebeck coefficient measurements. Since

taking into account the effect of reaction (10) would only result in a more complicated model and the introduction of more variables, it can be understood why neither Pelton et al. nor Dorris consider the effect of P_{O_2}. This assumption would be more valid had Dorris used the same P_{O_2} in preparing all samples and carried out analyses so as to determine the exact stoichiometry of his samples.

The literature indicates the difficulties that have been encountered in trying to determine the cation distribution of manganese ferrites. The addition of CuO to the spinel can only further complicate the picture as the next section will show.

3.5 Cation Distribution of Cu - Mn Ferrites

Bunget et al. (81) interpreted their Mössbauer results by Cu^{2+} substituting for Mn_A^{2+}. Errors in the paper and the lack of sample preparation details decreases the usefulness of this work. Cervinka and Simsa (82) proposed the following distribution for $Cu_{0.5}Mn_{0.5}Fe_2O_4$ sintered at 1200°C for P_{O_2} = 0.25 and quenched :

$$Cu^{+}_{0.08}Mn^{2+}_{0.41}Fe^{3+}_{0.51}\left[Cu^{2+}_{0.43}Mn^{3+}_{0.08}Fe^{2+}_{0.08}Fe^{3+}_{1.41}\right]O^{2-}_{3.997} \qquad (21)$$

With evidence provided by X - ray diffraction and saturation magnetization measurements, the above distribution was arrived at by assuming that Cu^{+}, Mn^{2+}, and Fe^{3+} prefer A sites and that Cu^{2+}, Mn^{3+}, Fe^{2+}, and Fe^{3+} prefer B sites (ie. Fe^{3+} can go to either site). Tsitsenovskaya and Tarasyuk (83) applied neutron diffraction to a similar sample prepared under identical conditions, and after making the same assumptions found the distribution :

$$Cu^{+}_{0.04}Mn^{2+}_{0.33}Fe^{2+}_{0.02}Fe^{3+}_{0.61}\left[Cu^{2+}_{0.46}Mn^{3+}_{0.17}Fe^{2+}_{0.21}Fe^{3+}_{1.16}\right]O^{2-}_{4} \qquad (22)$$

The agreement between the formulae (21) and (22) is good considering the difference in techniques used. Rezlescu and Cuciureanu (84) studied the effects of sintering temperature and P_{O_2} on the Curie temperature of copper - manganese ferrites. They concluded that Cu^{+} prefers A sites above 950°C. Increasing P_{O_2} caused the reaction below to go the right.

$$Cu^{+}_{A} + Mn^{3+}_{B} == Cu^{2+}_{B} + Mn^{2+}_{A} \qquad (23)$$

Tsirkunova (85) applied neutron diffraction at room temperature to samples of $Cu_{0.5}Mn_xFe_{2.5-x}O_4$ with

$0 \leq x \leq 1.5$, prepared at 1200°C under a P_{O_2} of about 1 atm. The distribution of the samples is given as the values of a, b, h, and i for the formula :

$$Cu_a^{+}Fe_h^{3+}Fe_{b-h}^{2+}Mn_{1-a-b}^{2+}\left[Cu_{0.5-a}^{2+}Fe_i^{2+}Fe_{2.5-x-b-i}^{3+}Mn_{x+a+b-1}^{3+}\right]O_4^{2-} \quad (24)$$

x	a	b	h	i	lattice parameter (A)
0	0.19	0.81	0.69	0.15	8.41
0.3	0.04	0.70	0.51	0	8.44
0.5	0.04	0.63	0.54	0.04	8.45
0.6	0.01	0.54	0.51	0	8.45
0.8	0.04	0.46	0.46	0.04	8.46
1.5	0.01	0.50	0.49	0	8.46

The values of a and b are a result of the neutron diffraction study. The values of h and i are taken from a Mössbauer study performed on the same samples by Belogurov et al. (86). The measured values of h and i agree well with the values that were calculated by Tsirkunova based upon the same cation site preference assumptions made by Simsa (82). These results indicate that reaction (23) will go completely to the right with an addition of Mn greater than 0.3. For $x \geq 0.3$ the Cu distribution is not changed. The Mn_A^{2+} concentration reaches a maximum of about 0.5 for x near 0.7.

Narayanasamy and Häggström (87) measured the Mössbauer spectra of $Cu_xMn_{1-x}Fe_2O_4$ for $0.2 \leq x \leq 1$ at 4.2K in an external magnetic field. The samples were annealed at 1200°C for 6 hr in air and then slow cooled. The distribution of formula (25) is given below.

$$Fe_a^{3+}Cu_b^{2+}Mn_{1-a-b}^{2+}\left[Fe_{2-a-c}^{3+}Fe_c^{2+}Cu_{x-b}^{2+}Mn_d^{3+}Mn_{a+b-d-x}^{2+}\right]O_4^{2-} \quad (25)$$

x	a	b	c	d
0.2	0.46	0	0.10	0.10
0.4	0.50	0.09	0.04	0.04
0.6	0.54	0.13	0	0
0.8	0.62	0.18	0	0
1.0	0.78	0.22	0	0

The authors assume that the concentration of Fe_B^{2+} and Mn_B^{3+} will be the same and that the Cu_A : Cu_B ration is independent of x, retaining the value it has at x = 1. They also acknowledge the possibility of having a small amount of Cu_A^+.

3.6 Electrical Conductivity of Mn Ferrites

The experimental techniques mentioned in the previous two sections are more direct methods of measuring cation distribution. However, since electrical and magnetic properties depend directly upon the distribution they can be used for model confirmation. The electrical property of most concern in the following section is the electrical conductivity.

Belov et al. (88) grew crystals of $MnFe_2O_4$ using the Verneuil technique. They do not report any further heat treatment for these crystals so it is not known what the P_{O_2} conditions were. They measured conductivity up to 650°C. A plot of $\ln(\sigma)$ vs. T^{-1} indicated a discontinuity at T_c, the Curie temperature, and a slope of 0.44 eV for $T > T_c$. A later paper by Belov et al. (89) reports the similar preparation of crystals of $Mn_xFe_{3-x}O_4$ with x = 0.84 and 1.16. The activation energies were 0.18 for x = 0.84 and 0.59 eV for x = 1.16. Zaveta et al. (90) did apply a heat treatment to the x = 1.16 crystal. After annealing in air at 800°C, ξ = 0.29 eV, and for an identical treatment in

vacuum ε = 0.04 eV. The authors discuss their results in terms of the effect of P_{O_2} upon Fe_B^{2+} concentrations without getting into any detail. Krupicka and Zaveta (61) prepared polycrystalline $MnFe_2O_{4+\gamma}$ samples with various values of γ by firing in air at different temperatures in the range of 1200°C to 1400°C. The measurement of conductivity at temperatures below 25°C allows them to report the values of ε for different stoichiometries. The activation energy, ε, rose from a value of 0.07 eV for γ = 0 to a value of 0.36 eV at γ = 0.24. While both (90) and (61) present a definite indication of the impact of P_{O_2} and the resulting stoichiometry upon conductivity, most subsequent work disregards this effect. While careful preparation can be used to maintain a 3 : 4 stoichiometry, the majority of authors disregard the effect that a low P_{O_2} can have upon the concentration of Fe_B^{2+}. In the main, the conductivity, and in particular ε, are seen to depend upon composition with the implicit assumption being made that preparation can have little effect.

Funatogawa et al. (91) report conductivity measurements without discussion in the range 100 to 280K for samples of $Mn_xFe_{3-x}O_4$ with $0.1 \leq x \leq 1.14$ whose preparation and characterization are not known. ε decreased from 0.06 eV for x = 0.1 to 0.04 eV for x near 0.9. At x = 1.14, ε jumps to a value of 0.19 eV. The intercept of the $\ln(\sigma)$ vs. T^{-1} plot, $\ln(\sigma_o)$, decreases from 7.8 at x = 0.1 to 2.1 at x = 1.14, for σ in $(\Omega cm)^{-1}$. While not particularly useful in itself, this paper is the first of a number of papers that report similar behavior for ε as a function of x.

Probably the most quoted of these is the paper by Lotgering (66). He reports conductivity and Seebeck coefficient measurements upon samples of $Mn_xFe_{3-x}O_{4+\gamma}$ for $0.8 \leq x \leq 1.8$. A number of these samples were single crystals grown by Kooy and Couwenburg (92) using the

floating zone technique. All samples were given a heat treatment at temperatures above 1300°C in order to ensure that $|\delta| < 0.003$. While exact details are not given, samples with x less than about 1 were annealed under CO_2. Samples with x greater than about 1.6 were annealed in air, and samples with $1 < x < 1.6$ were annealed with $P_{O_2} = 0.01$. The activation energy was obtained from plots of $\ln(\sigma T)$ vs. T^{-1}, using conductivity data obtained in the 150 to 500K range using a 4 - point technique. For $x < 1$ the ε vs. x dependence is similar to that reported by Funatogowa. At $x = 1$ the activation energy jumps by about 0.30 eV to about 0.32 eV and continues to increase to about 0.50 eV at $x = 1.8$. The room temperature conductivity also drops by about 3 orders of magnitude for $x > 1$. The Seebeck coefficient, while it is negative for all x values, also shows a discontinuity at $x = 1$. Lotgering explains his results by considering that reaction (9) goes to the left, having a positive enthalpy of reaction of 0.30 eV. Once the Mn^{2+} ions have replaced all of the Fe^{2+} ions at $x = 1$, an additional energy of 0.30 eV must by supplied in order to create a Fe_B^{2+} ion. Using this concept of "thermally generated" Fe_B^{2+}, Lotgering explains how the conductivity can remain n - type even though reaction (9) goes to the left. The weakness of Lotgering's study lies in the fact that the seemingly high Fe_B^{2+} content for $x < 1$ is probably a result of the low P_{O_2} used for annealing these samples rather than a low Mn concentration. The discontinuity at $x = 1$ is in part due to a change in sintering atmosphere instead of just a change in the mechanism of Fe_B^{2+} generation.

Rosenberg et al. (93) confirmed and continued Lotgering's study by making measurements for $2 \leq x \leq 3$. They showed that ε continued up to about 0.65 eV for $x = 2.8$. The Seebeck coefficient continued to be negative. These authors did not state the atmosphere used for sample preparation.

Simsa (68) measured the Seebeck coefficient for manganese ferrite crystal samples, $Mn_xFe_{3-x}O_{4+\gamma}$, with $0 \leq x \leq 2.5$ prepared by Gerber et al. (94). Without being specific, Simsa states that the atmosphere for measurement and preparation was adjusted to have a low enough P_{O_2} so as to maintain a 3 : 4 stoichiometry. The measured activation energies, which follow Lotgering's measurements, and the negative values of γ as reported in (94) support the conclusion that a reducing atmosphere was used. Simsa interprets his results, measured from 20 to 600°C, by considering that reaction (9) goes to the right as opposed to the left as assumed by Lotgering. He explains the decrease in σ as x increases by considering the formation of stabilized Fe^{2+} - Mn^{3+} pairs. If no remaining "free" Fe_B^{2+} is present, an additional 0.30 eV must be supplied in order to allow the paired Fe_B^{2+} to contribute to the conductivity. While Simsa's model may by more attractive than Lotgering's, his work is also weakened by the lack of consideration for the effect of P_{O_2}.

Brabers (75) also made measurements of Seebeck coefficient and conductivity upon single crystals grown using the Bridgman or floating zone technique in an unspecified atmosphere. Conductivity measurements made for $0.5 \leq x \leq 1.60$ in the 20 to 150°C range gave ε values in agreement with Lotgering's data. In a later paper (95) on crystals with $0.8 \leq x \leq 3$ measurements are reported in the range 20 to 600°C. Brabers found a discontinuity in the measured coefficients and resistivities at around 300°C. He found that for samples that had been heated beyond 300° that ε, from $\ln(\sigma T)$ vs. T^{-1} plots, increased by an amount of 0.15 to 0.30 eV over the values for unheated samples. He reports only for heated samples with $1 \leq x \leq 2$ that ε is nearly constant at around 0.65 eV. Brabers does not appear to consider the explanation that for temperatures above 300°C

ionic motion is possible. The sample is in a metastable state in terms of its phase composition and ionic equilibrium with O_2. Heating the sample above 300°C allows it to begin to equilibrate, causing changes in cation distribution and stoichiometry.

This effect was further demonstrated by Rezlescu et al. (96) who studied the time variation of conductivity for a number of ferrites. A sample of $MnFe_2O_4$ was prepared by quenching in air a sample that had been heated in air for 4 hr at 1300°C. The conductivity decreased by 4.3% after 7 days at 25°C, and decreased by 15% after only 5 hr at 200°C. Simsa (97,98), after noting the same behavior as did Brabers, explains the effect using a complicated model incorporating the effects of multiple level electron donors and ionic diffusion. It is interesting to note that in the discussion section of another paper (99), Simsa denies the possibility that chemical decomposition of the samples could cause the effects seen, even though no X - ray or metallographic examinations were made upon heated samples.

The recent work by Dorris (79) is one of the few studies that attempts to measure the electrical properties of manganese ferrites for conditions under which the sample is at thermodynamic equilibrium. He measured the temperature dependence of the Seebeck coefficient and electrical conductivity for polycrystalline $Mn_xFe_{3-x}O_4$ samples with $0 \leq x \leq 3$. For $x \leq 1$ measurements were made in the range $600 \leq T \leq 1350$°C and for $x > 1$ in the range $1000 \leq T \leq 1500$°C. For $x \geq 1.4$ measurements were made in air. For $x \leq 1.0$, Dorris states, without being specific, that the P_{O_2} was reduced using CO/CO_2 gas mixtures in order to keep the sample as a single phase spinel. According to Pelton et al. (78), the P_{O_2} would have to be as low as around 10^{-12} in order to maintain a stable spinel for temperatures approaching 600°C. Dorris states, without reporting any

measurements, that he could vary the P_{O_2} across the stability range without noticing any change in the electrical properties. This is possible if the P_{O_2} was not varied across a wide range as it could not be at the relatively low temperatures used. As discussed in section 3.3, Tanaka (56) showed that the P_{O_2} would have to be increased beyond about 10^{-2} at high temperatures before cationic vacancies would form. Below this P_{O_2}, anionic vacancies, vacancies in the O lattice, form. A reaction like that given below might not have a strong effect upon electrical properties.

$$\frac{1}{2}O_O^{2-} + Mn_B^{3+} = Mn_A^{2+} + \frac{1}{2}\square_O + \frac{1}{4}O_2 \qquad (26)$$

As will be discussed later, this problem of P_{O_2} dependence bears further study. Since Dorris used reduced P_{O_2}'s for $x < 1$, it is not surprising that his activation energies follow to some extent the same trends as that shown by the other studies discussed above. The discontinuity shown at $x = 1$ is not as extreme as the low temperature studies. His results are listed in Table 4. The activation energies are take from plots of $\ln(\sigma T)$ vs. T^{-1}. Conductivity values were all corrected for sample porosity.

x	ε (eV)	σ at 1400°C $(\Omega cm)^{-1}$
0.2	0.120	125
0.4	0.167	86
0.6	0.309	57
0.8	0.390	28
1.0	0.470	24
1.4	0.679	27
1.8	0.717	25
2.2	0.795	30
2.6	0.779	23
3.0	0.788	39

Table 4 Results of Electrical Conductivity Measurements for $Mn_xFe_{3-x}O_4$ (79).

3.7 Electrical Conductivity of Cu - Mn Ferrites

While few papers on the effect upon electrical properties of adding CuO to manganese ferrites are available, some general trends are indicated. Rosenberg et al. (100) prepared samples of $Cu_xMn_{1-x}Fe_2O_4$ with $0.14 \leq x \leq 0.97$ by sintering at 1200°C under an unspecified atmosphere. For temperatures above T_c, they report $\varepsilon = 0.5$ and $\log(\sigma) = -5.5$ at 300K for $x = 0.14$, and $\varepsilon = 0.53$ with $\log(\sigma) = -6.0$ at 300K for $x = 0.28$. They report a negative Seebeck coefficient for all values of x. Simsa and Andrejev (101) prepared two crystals and several polycrystalline samples of $Cu_{0.5}Mn_xFe_{2.5-x}O_4$ with $0 \leq x < 1$. In their measurements for $-200 \leq T \leq 600$°C they found that $\ln(\sigma)$ vs. T^{-1} plots were not linear for the polycrystalline samples. Nonetheless they were able to observe a discontinuous rise in ε for $x > 0.3$. They conclude that all of the Fe_B^{2+} has been trapped into $Fe^{2+} - Mn^{3+}$ pairs by the time x reaches 0.3.

Rezlescu and Cuciureanu (84) measured the conductivity of $Cu_xMn_{1-x}Fe_2O_4$ samples for $x = 0.35$, 0.55, and 0.8. From the $\ln(\sigma)$ vs. T^{-1} plots they found that for $T > T_c$ (ie. paramagnetic behavior), for samples annealed in air at 1200°C for 4 hr and quenched, $\varepsilon = 0.273$ eV and $\log(\sigma) = -2.6$ at 298K for $x = 0.35$, and $\varepsilon = 0.301$ eV with $\log(\sigma) = -2.7$ at 298K for $x = 0.55$. For these same compositions, annealed at 1000°C under pure O_2 for 2 hr and then quenched, $\varepsilon = 0.704$ eV with $\log(\sigma) = -5.4$ at 298K for $x = 0.35$, and $\varepsilon = 0.734$ eV with $\log(\sigma) = -5.0$ at 298K for $x = 0.55$. These results demonstrate that changing preparation can have a more dramatic effect upon conductivity than changing composition. The result that conductivity decreases with the addition of CuO to manganese ferrites has also been confirmed by Wu et al. (102). They found that the addition of 5% Cu_2O to

$MnFe_2O_4$ decreased the room temperature conductivity by a factor of 10.

3.8 Summary

In the only other review of any significance on the cation distribution of ferrites in the Cu - Mn - Fe - O system, Tsirkunova (103) concludes that there is no agreement in the literature on the cation distribution and that more work needs to be done. The literature survey contained herein confirms his viewpoint and also points out a few considerations that have not been fully appreciated in previous studies.

These considerations revolve about the concept of ionic equilibration. Most measurements are made at low temperature upon metastable samples. While the atomic position may be "frozen in" by quenching to room temperature, electron movement can still change the cation distribution. Also, if these quenched samples are heated beyond about 250°C, ionic movement can take place as the ionic equilibria begin to assert themselves. At the very least, this heating will result in the precipitation of other phases. The first important conclusion resulting from this literature survey is that measurements made upon metastable samples can not represent the properties of equilibrated structures.

Samples also reach an equilibrium with the surrounding pressure of O_2 at higher temperatures. The survey shows that, for example, the activation energy for conduction, ε, probably has a stronger dependence upon P_{O_2} than upon composition, especially for samples with a high iron content. The second conclusion then, is that the effect of

P_{O_2} must either be accounted for, or eliminated, when trying to interpret experimental measurements. Giving consideration to these two conclusions will minimize the effects that preparation will have upon the structure being investigated. It is difficult to determine the effects of preparation when the intrinsic properties are not yet understood.

In this study, the electrical conductivity of essentially single crystal ferrite samples was measured under an atmosphere of O_2 at temperatures where it can be assured that complete equilibration will be reached. While the few measurements reported here represent only a small fraction of the work required to exactly define the structure, this study is useful in that it demonstrates the kind of experimental considerations that must be applied in order to arrive at consistent structural models.

4. Crystal Growth

4.1 Literature

Manganese ferrite crystals have been grown using a variety of techniques (104). The Verneuil or flame fusion technique involves the injection of oxide powder into a hydrogen/oxygen flame. The condensing oxide is collected on a boule in a heated furnace. Generally this technique produces small, poor quality ferrite crystals. Another problem is the uncertainty in the value of the P_{O_2} in the flame. The Bridgman or Bridgman - Stockbarger technique produces better quality crystals. A long crucible containing the oxide is pulled through a steep temperature gradient. While container contamination can be a problem, the atmosphere and temperature are closely controlled. The method is capable of growing large crystals of controlled dimensions. In the Czochralski method, the crystal is pulled from a crucible - contained melt under controlled atmosphere and temperature. In the floating zone method a liquid zone is held between the growing crystal and a sintered polycrystalline feed rod. Various heat sources, including induction, arc, arc image, electron beam, gas flame and lasers can be used. This method has the advantage of the lack of container - melt interaction. While atmosphere control is possible, temperature control is more difficult. A disadvantage of growing crystals from the melt is a result of the evaporation of one or more high vapor pressure components of the melt. Crystals can be grown at lower temperatures through the use of flux - based methods. Crystals grow from saturated fluxed solutions upon cooling or evaporation. Fine quality, but small and often dendritic crystals can be grown.

The flame fusion technique was used by Scott (105) to grow a wide variety of oxides and ferrites including manganese ferrite. Burger and Hanke (106) report on the inclusion of α-Fe_2O_3 layers in flame - grown crystals of $MnFe_2O_4$. These layers, found in a zone of 0.5 to 1.5 mm depth from the surface, formed along the octahedral planes of the matrix spinel. Vichr (107) used the Verneuil and Bridgman techniques to grow crystals of $Mn_xFe_{3-x}O_4$ with $0.37 \leq x \leq 2.5$ and $Cu_xMn_yFe_{3-x-y}O_4$ with $0.113 \leq x \leq 1.00$ and $0.25 \leq y \leq 0.887$. The Bridgman technique yielded the better quality crystals and a significant loss of Cu was noted from the use of the Verneuil technique. Bridgman growth was also applied to various manganese ferrites by Gerber et al. (94) and Penoyer and Shafer (107). Solid state diffusion techniques have been applied to grow $MnFe_2O_4$ crystals by Paulus and Hamelin (108) and Zyryanov (109). Monforte et al. (110) pulled manganese ferrite crystals from a melt formed in a frozen skull contained in a water - cooled copper induction coil. Massau and Broyer (111) also employed the Czochralski technique to pull manganese ferrite crystals from melts contained in a rhodium crucible. The results showed that it was difficult to maintain dimensional uniformity.

The first report of the use of the floating zone technique to produce manganese ferrite crystals was probably that of Kooy and Couwenberg (92). They used the focused image of a carbon arc from a cinema projection lamp as a heat source to grow $Mn_xFe_{3-x}O_4$ with $0.9 \leq x \leq 1.2$ under various oxygen pressures. Growth rates were usually 6 cm/hr and up to 20 cm/hr with rotations of between 60 and 120 rpm. Crystals of iron, nickel, and manganese ferrites to a few cm in length were grown by Poplawsky (112,113) using the floating zone technique. A focussed arc image was used as the heat source. The problem of a lack of dimensional uniformity may have been a result of the use of a large

volume melt and about a 3 times difference between the feed and crystal diameters. Brabers (114), using a setup similar to that of Kooy and Couwenberg, except that the heat source was a xenon lamp, grew manganese ferrite crystals weighing up to 5 g.

4.2 Results of Present Study

In the electronics industry, ferrite crystals of considerable size and purity are manufactured using Bridgman techniques. These crystals are used in tape and video recording heads and have applications in microwave devices. In this investigation, since high purity, atmospheric equilibration, and experimental convenience are important, the floating zone technique was used. For possibly the first time, a laser, in this case a 1.5 kW CO_2 laser, was used as the heat source. The apparatus, designed and constructed by J.S. Haggerty (115), provided large, high purity crystals, and allowed accurate dimensional control during growth. The quality of these crystals is mainly due to the ability of the apparatus to aim the lasar beams accurately and control their power.

Crystals were pulled at a rate of 2 cm/hr with rotation. For most samples the polycrystalline feed rod was fed in from above and the crystal pulled out below. However, those samples with the highest CuO content (Ic, IIc, and IIIc in Table 2) showed considerable melt instability as a result of the evaporation of this oxide. It was found that pulling in the opposite direction produced a more stable liquid zone for these compositions. Growth was carried out under a static atmosphere of O_2 with a beam power under 200 watts.

Feed rods were prepared by first mixing reagent grade

oxides in distilled water according to the proportions given in Table 2. After mixing for at least 24 hr, the water was evaporated and the oxide mixture packed into latex tubing. After pressing in an isopress, the green rods were fired in O_2 in a Pt boat at 1200°C for at least 20 hr. Rods of sufficient quality were used as feed rods for crystal growth.

The crystals produced were 0.4 to 0.5 cm in diameter by about 10 cm in length. Previous Laué back reflection studies on cobalt and nickel ferrite crystals, grown before the copper - manganese series, indicated the lack of a preferred growth orientation. It was also found that the use of X - ray diffraction could not lead to a useful means of phase detection and quantification because of overlapping patterns and the resulting low sensitivity of the technique. The most useful means of checking phase composition and crystallinity was metallographic examination. Crystal pieces were cut using a diamond saw, mounted in bakelite, ground on fresh SiC papers to 600 grit, and then polished using successively finer grades of diamond powder. The resulting examination indicated that all samples were single phase. The high iron samples : Ia, Ib, and Ic, each had a small quantity of the Fe_2O_3 layers, like those observed by Burger and Hanke (106), in a zone a short distance from the surface. These layers probably form as the crystals cool after growth. Their morphology resembles that of the Fe_2O_3 precipitates that grow in normal polycrystalline samples as observed by Yamaguchi and Kimura (116) in zinc ferrites. Crystals Ia, Ic, and IIb proved to consist of a few large grains that grew in a direction parallel to the growth axis. These grain boundaries should not have any effect upon conductivity measurement as current will be passed in a direction parallel to the growth axis as well. Crystal IIIc proved to contain a number of pores of a size easily discernible without the microscope. The reverse growth

direction used for this crystal probably allowed the entrapment of bubbles formed in the liquid zone during growth.

Using the piconometric technique, the densities of 1 to 2 g sized crystal pieces were measured after these air quenched samples had been annealed at 1400°C in O_2 for 15 hr. These same pieces were then sent to Luvac Inc. (Boylston, MA) for chemical analysis for Cu, Mn, Fe, and O. The accuracy of the metal analyses, carried out using plasma emission spectroscopy, is to ±0.1 wt%. The oxygen analyses, carried out using inert gas fusion, was less accurate at ±0.5 wt%. The results of these analyses are listed in Appendix I. The calculated sample stoichiometries, measured densities, and calculated lattice parameters are listed in Table 5. The stoichiometry is listed for the formula : $Cu_xMn_y\square_zFe_{3-x-y-z}O_{4.000}$. As indicated in the literature, it is more reasonable to expect cationic vacancies rather than an oxygen excess.

Sample	x	y	z	δ (g/cm^3)	a (Å)
Ia	0	0.464	0.25	5.014	8.316
Ib	0.116	0.490	0.185	5.066	8.346
Ic	0.183	0.542	0.17	5.019	8.389
IIa	0	1.189	0.24	4.924	8.366
IIb	0.004	1.133	0.20	4.977	8.369
IIc	0.163	1.189	0.13	4.997	8.415
IIIa	0	2.030	0.14	4.878	8.458
IIIb	0.084	1.932	0.11	4.861	8.493
IIIc	0.141	1.896	0.11	(4.795)	(8.542)

Table 5 Stoichiometry and Density of Crystal Samples for the Formula : $Cu_xMn_y\square_zFe_{3-x-y-z}O_{4.000}$.

The lattice parameter was calculated using :

$$a = 10^8 \left[\frac{8MW}{N_o \delta}\right]^{\frac{1}{3}} \qquad (27)$$

where MW is the molecular weight of the sample, and N_o the Avogadros number. The accuracy of x and y in Table 5 is ±0.004 with z only being accurate to ±0.05. The values for IIIc are in brackets as the sample had contained porosity not accounted for in the density measurement.

Table 5 shows that the samples lost more than half of the CuO from the original formulations given in Table 2. This was a result of the vapor pressure of the copper oxide being higher than that for the oxides of iron and manganese. This result ties in with the observation of liquid zone instability for the high CuO samples. The densities and vacancy content are discussed in the next section.

4.3 Lattice Parameters and Oxygen Excess

Unfortunately, most authors report stoichiometry results in terms of an oxygen excess rather than a cationic vacancy concentration. They report γ in the formula $Mn_xFe_{3-x}O_{4+\gamma}$. In order to be able to compare the present results with those in the literature, the stoichiometry has been re-calculated in Table 6. The accuracy of the calculated values of γ is ±0.07. The majority of the values of γ reported in the literature are four to five times lower than those reported in Table 6. Bergstein (117) has difficulty explaining a complicated dependence of γ upon x for $Mn_xFe_{3-x}O_{4+\gamma}$ samples annealed between 1200 and 1310°C in air. Showing three peaks in the experimental curves, γ varied between 0.03 and -0.02 for $0.5 \leq x \leq 2.0$.

Sample	x	y	γ
Ia	0	0.506	0.37
Ib	0.123	0.522	0.26
Ic	0.194	0.575	0.24
IIa	0	1.292	0.35
IIb	0.004	1.213	0.28
IIc	0.171	1.245	0.19
IIIa	0	2.126	0.19
IIIb	0.087	2.007	0.16
IIIc	0.146	1.965	0.15

Table 6 Stoichiometry of Crystal Samples for $Cu_xMn_yFe_{3-x-y}O_{4.000+\gamma}$.

He reports a better behaved dependence of γ upon x for $Cu_{0.5}Mn_xFe_{2.5-x}O_{4+\gamma}$ samples annealed at 1200°C (118). At P_{O_2} = 1, γ is near 0 for x > 0.5 and then increases to near 0.09 as x approaches 0. Wickham (31), who reported the phase diagram given in Figure 2, measured γ for samples of $Mn_xFe_{3-x}O_{4+\gamma}$ annealed in air. The values of γ decreased as the temperature increased. At 1400°C γ decreased smoothly from 0.09 at x = 0 to 0 at x = 0.45. For x > 0.45, γ remained near zero. Tanaka (56) reports γ = 0.03 for a sample with x = 0.8, annealed at 1300°C at P_{O_2} = 1. Oleinikov et al. (119) also report values of γ that decreased as temperature increases. Their values are more in keeping with those given in Table 6. At 1200°C for P_{O_2} = 1, γ decreases from 0.5 at x = 0.25 to 0.08 at x = 1, from where it decreases at a slower rate to about 0.05 at x = 1.9. They indicate that a hematite phase will precipitate when γ approaches 0.5. This is reasonable since the formula $Mn_xFe_{3-x}O_{4.5}$ is equivalent to $Mn_xFe_{2-x}O_3$. Their results indicate that the closer the spinel is to the hematitie precipitation phase boundary, as shown in Figures 1 and 2, the higher will be the value of γ. As seen from Table 6, composition Ia, the composition closest to the phase

boundary at 1400°C, has the highest value for γ of 0.37. The other samples have decreasing values of γ with increasing Mn content. The phase boundary also moves to lower temperatures for higher concentrations of Mn. The agreement of the results in Table 6 with those of Oleinikov et al. encourages the adoption of their qualitative interpretation. However, the higher magnitude of the present results as compared to the others discussed above cannot be explained without a greater knowledge of the analytical techniques used in these investigations and a knowledge of the exact nature of the heat treatment given to their polycrystalline samples.

The decrease in γ with increasing manganese content is in agreement with the literature. This can be explained by considering the cationic vacancy formation reaction :

$$Fe_B^{2+} + \frac{1}{4}O_2 == Fe_B^{3+} + \frac{1}{2}O_O^{2-} + \frac{3}{8}\square_B \qquad (10)$$

Increasing manganese content decreases the concentration of Fe_B^{2+}, which forces the concentration of $\square_B$ to decrease. It appears that Mn_A^{2+} is not as easily oxidized as Fe_B^{2+}. The replacement of Fe_B^{2+} by Cu_B^{2+} would also serve to lower the vacancy concentration in a similar way. The temperature dependence of reaction (10), as observed in the literature, could be explained by assuming that while the reaction is exothermic, it results in a net decrease in entropy. Since a gas is involved only on the left side of the reaction, a negative value for ΔS_{10} is reasonable. In this way reaction (10) would go more to the left at higher temperatures, as observed.

As can be seen by considering the lattice parameters reported in section 3.3, the values reported in Table 5 are low by about 0.15 Å. If the oxygen excess is ignored, the values of 8.492 for Ia, 8.534 for IIa, and 8.552 Å for IIIa

are calculated. These results are in better agreement with the literature. The low values for the lattice parameters reported in Table 5 are consequently a result of the low molecular weights used in equation (27). The increase in lattice parameter with increasing manganese content confirms the expectations predicted by the literature survey.

4.4 Summary

The floating zone crystal growth technique used in this study generated copper - manganese ferrite crystals of high chemical purity and homogeneity. The chemical equilibration of the samples with O_2 is ensured by the mixing of the liquid zone during growth. The use of these samples for conductivity measurement, as discussed in the next section, provided measurements not affected by porosity, grain growth, and grain boundary resistance. However, the growth of crystals from the liquid is not without its drawbacks. As can be seen from a comparison of Tables 2 and 5 the technique caused significant compositional changes during growth due to selective evaporation of melt components. The choice of compositions was limited by the need of a congruent melting point or a flat liquidus. Finally, grown crystals contained a large amount of built - in stresses due to their rapid cooling from the liquid. These stresses must be relieved by annealing in order to increase the resistance of the sample to brittle cracking.

The results discussed above indicate an unusually high vacancy concentration in the analyzed crystals. As much of the literature reports measurements for polycrystalline samples annealed in air at temperatures lower than 1400°C, comparison is difficult. More investigation is required to confirm the presented results and form a consistent model.

5. Electrical Conductivity Measurements

5.1 Experimental Apparatus and Automation

Measurements of electrical conductivity in the 900 to 1450°C temperature range were made for samples Ia to IIIb under a pressure of one atmosphere of flowing oxygen. This P_{O_2} was used as it is the pressure of oxygen that the material will be subject to while being tested as an anode in a Hall cell. Measurements were not made upon sample IIIc due to its porosity. The standard four point DC technique, similar to that applied by Tuller et al. (120) was used. Care was taken to ensure that the sample had equilibrated with the atmosphere at the temperature of measurement before recording data. An IBM PC-AT computer was used to automate the measurements, which took as long as five or six days per sample to complete.

Crystal pieces, about 2.5 cm in length, were cut from the samples using a diamond saw. The saw was also used to cut notches about 0.5 cm from either end of the piece. Pt wires, wrapped around the sample, and kept in place by the notches, were used as the two voltage measurement contacts. The separation of these contacts and the sample diameter were measured using micrometer calipers. These dimensions and their estimated accuracy are given along with the conductivity measurements in appendix III. Pt disks, four millimeters in diameter, were put on the ends of the sample, and held in place with Pt paste. The current contacts to these disks were made using a Pt - Pt/13% Rh thermocouple at either end of the sample. These two thermocouples were also used to help position the sample so that the temperature difference between the ends was less than two degrees. While this design should allow the measurement of the

Seebeck coefficient, it was found that such measurements were scattered and of low accuracy, probably as a result of the low ΔT used. Such measurements are better suited to a system that either allows for sample movement or that has a controlled temperature gradient.

A furnace with elements of SiC was designed and built with an 8 cm long temperature zone, constant in temperature to within 2°. A Eurotherm (Eurotherm Corp., Reston, VA) solid state temperature control system was used to control the furnace. The control system had a remote setpoint option that allowed the computer to set the temperature. The computer also controlled a KEPCO (KEPCO, Inc., Flushing, NY) DC power supply that was used to apply a voltage to the sample. An analog to digital system, DT 2805, manufactured by Data Translation (Data Translation, Inc., Marlborough, MA), was used as the interface between the computer and the experiment. Sample current was calculated from the measured voltage drop across a calibrated resistor. The controlling program, listed in appendix II, was written using the Asyst programming language (Macmillan Software Co., New York, NY). A brief description of the algorithm will serve to describe the operation of the experiment.

First of all, the sample was heated to 1400°C at a rate of 200 K/hr, and annealed at this temperature for 4 hr. Temperature was then increased to the first temperature of measurement, 1450°C. The system waited until the sample temperature was constant and then waited a further 20 min at that temperature. Measurements of sample resistance were made every 10 min. One hundred current - voltage points were taken in a few seconds during a voltage step sweep, that swept from 0 to a maximum of 0.1 V between the voltage probes. The slope, the sample resistance, and the intercept were calculated by linear regression. The intercept was always less than 1 mV. An automatic check was made for

sample polarization. If detected, the maximum sample voltage would be decreased by 10%. Visual inspection of the current - voltage plots confirmed that no polarization occurred for maximum sample voltages of less than 0.1 V. Resistance measurements were made until the sample resistance was constant. Constant resistance was defined as the agreement of three successive resistances to within the experimental deviation of the values, typically 0.2%. Once constant, the current - voltage values were recorded along with the data shown in appendix III for that particular temperature. The program would then repeat the process described above for the next lower temperature until the lower temperature boundary, usually 900°C, was reached. The process was then repeated in the direction of increasing temperature so that the reproducibility of the results could be tested. When the measurements were completed, the sample was cooled to room temperature at a rate of no more than 200 K/hr.

5.2 Results

The data from the experiment described above were then imported into a spreadsheet program. The data, and the results of the spreadsheet calculations are given in appendix III. The columns listed from left to right, are the temperature, the average from the left and right thermocouples; the sample resistance in Ω; the error in the sample resistance; and then the intercept of the current - voltage data and its error. The "R" following this data, not to be confused with the sample resistance, is the goodness of fit coefficient from the linear regression of the current - voltage data. This value was in the range of 0.9999 to 0.99999, indicating a good fit. The time indicated in the next column of data is the time required to

reach a constant resistance. The following columns contain calculated values: T^{-1}; the conductivity, σ, in $(\Omega cm)^{-1}$; and the error in σ. This error was calculated taking account the error in the sample resistance and its dimensions. However, the error given on the activation energy, -k times the slope of the $\ln(\sigma T)$ vs. T^{-1} data, was a result of the linear regression analysis only. The calculation of the slope used both the heating and cooling data. The goodness of fit coefficient lay between 0.99 and 0.999.

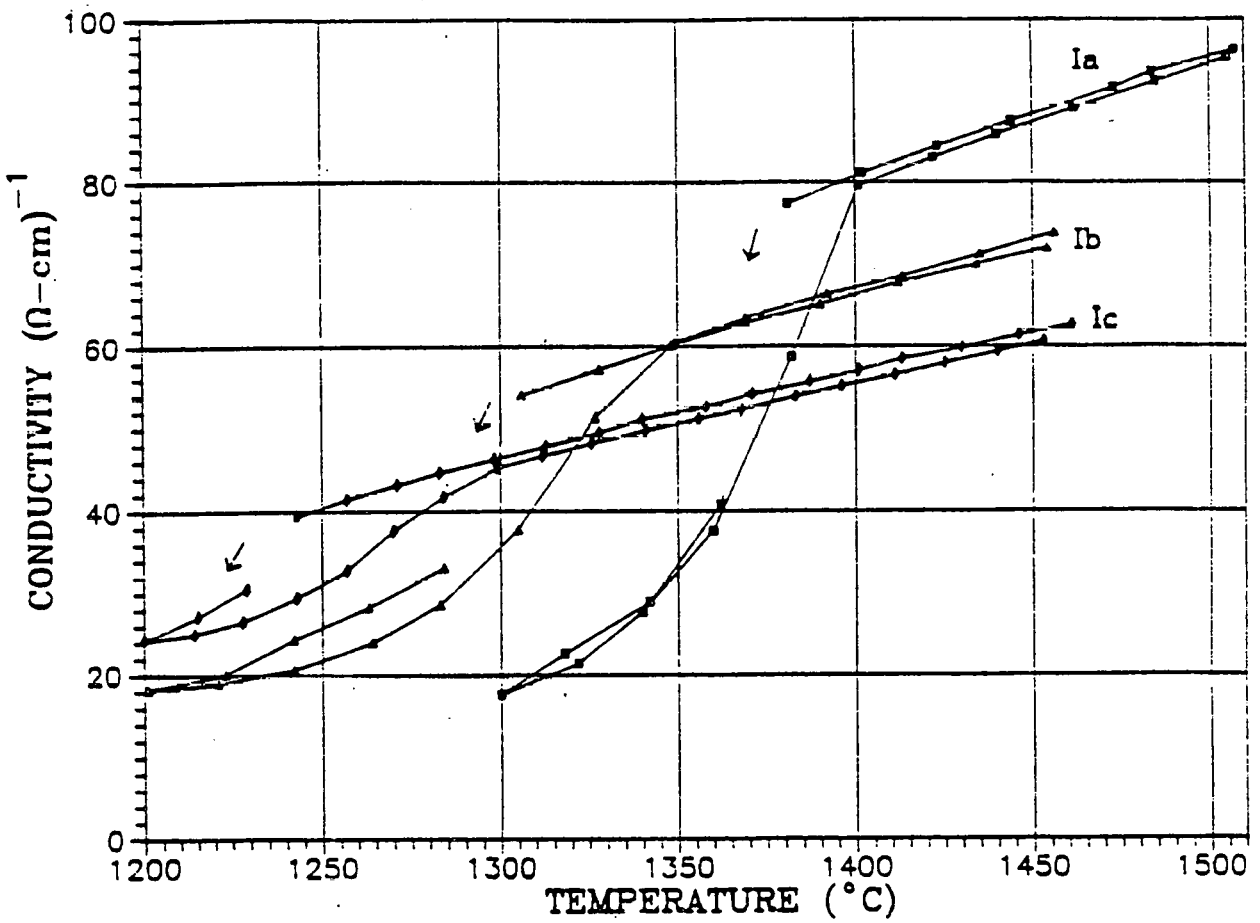

Figure 5 Electrical Conductivity as a Function of Temperature for Crystals Ia, Ib, and Ic

The results have been plotted in Figures 5 to 12. Figure 8 is a summary of the conductivity vs. temperature data presented in Figures 5 to 7. Figure 12 is a summary of the $\ln(\sigma T)$ vs. T^{-1} plots shown in Figures 9 to 11.

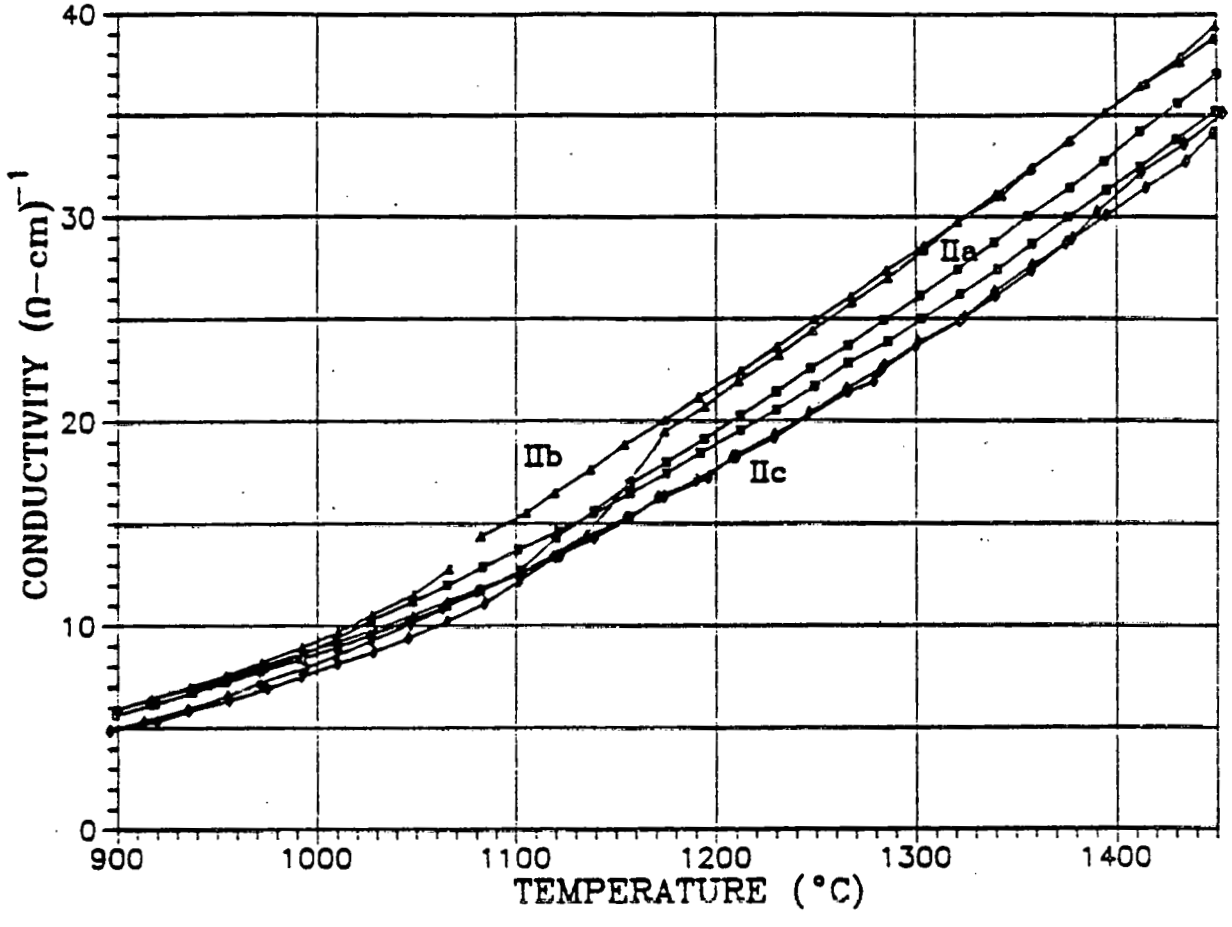

Figure 6 Electrical Conductivity as a Function of Temperature for Crystals IIa, IIb, and IIc

Both Figures 5 and 6 show a discontinuity in the measured temperature dependence of the conductivity. Not only does the conductivity show a marked decrease at this discontinuity, but the amount of hysteresis between the heating and cooling sections has increased. This

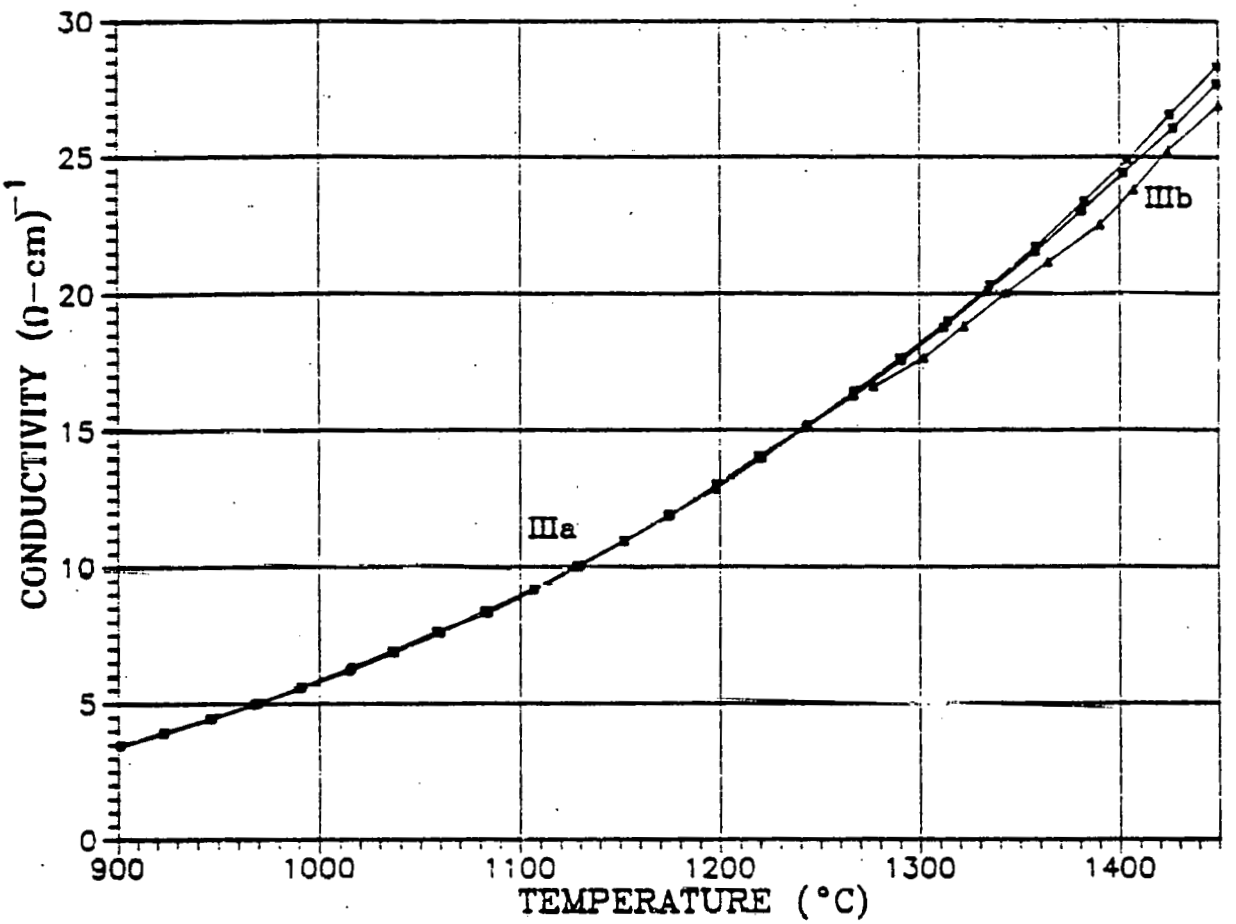

Figure 7 Electrical Conductivity as a Function of Temperature for Crystals IIIa and IIIb

discontinuity was interpreted as being the result of the onset of Fe_2O_3 precipitation. This hematite phase has a low conductivity, and will precipitate in fine layers throughout the sample, thus causing a decrease in conductivity. Yamaguchi (116) has studied the kinetics of Fe_2O_3 precipitation from spinels and has concluded that the precipitation is nucleation controlled rather than growth rate controlled. The consequence of nucleation control is that upon decreasing the temperature, undercooling is observed before precipitation begins. This would result in hysteresis in the conductivity data. Another set of

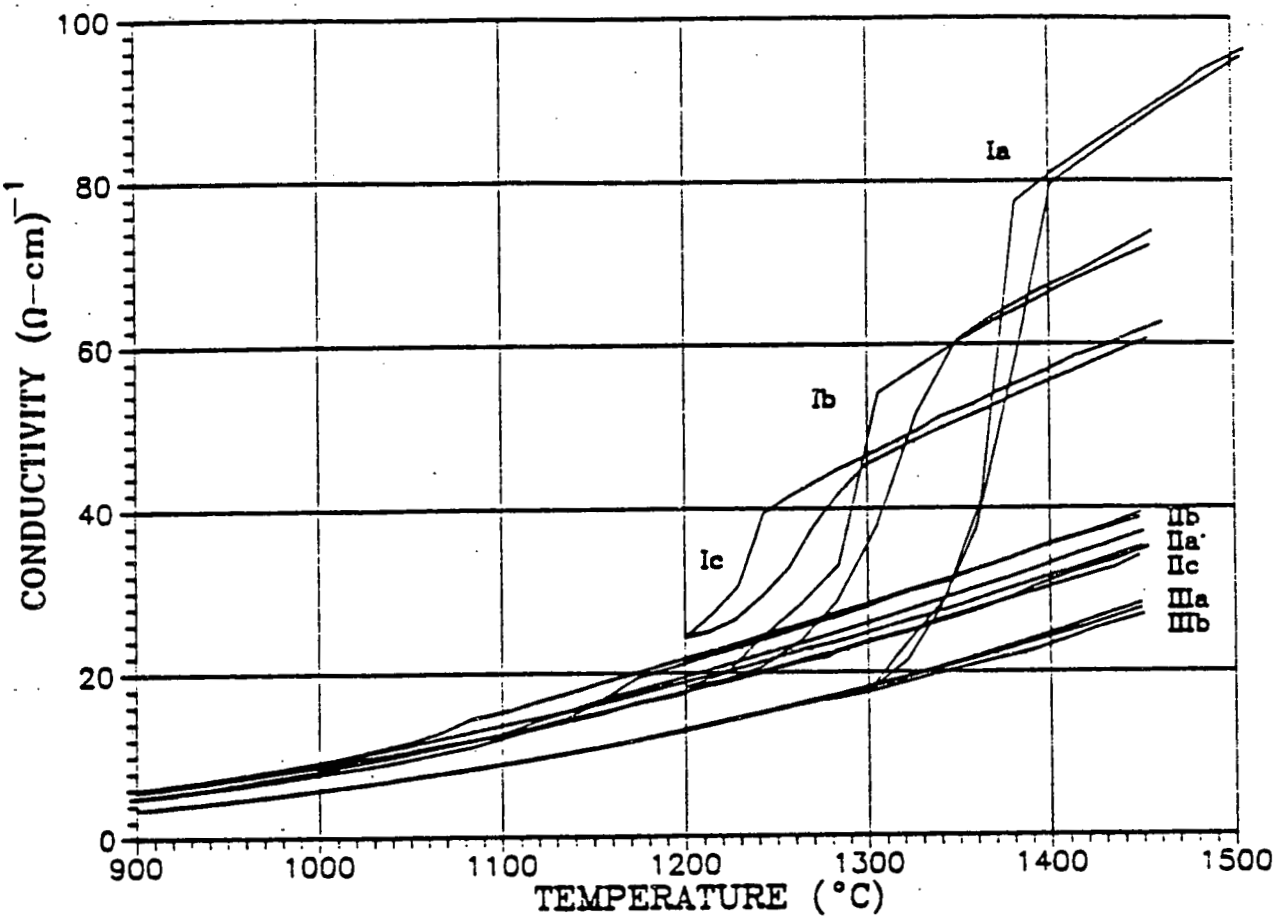

Figure 8 Electrical Conductivity as a Function of Temperature for all Crystals

conductivity measurements was made for sample Ia for temperatures spanning the region of hysteresis. For this experiment, the system waited 4 hrs at each temperature before taking measurements. The nucleation control model was confirmed by these measurements as the area of the hysteresis region did not decrease a great deal. Because of the undercooling, the actual reversible temperature for the onset of Fe_2O_3 precipitation is that temperature where, upon heating, the Fe_2O_3 precipitates disappear. These temperatures, where observed, have been listed in Table 7 in the next section. The temperature of transformation becomes

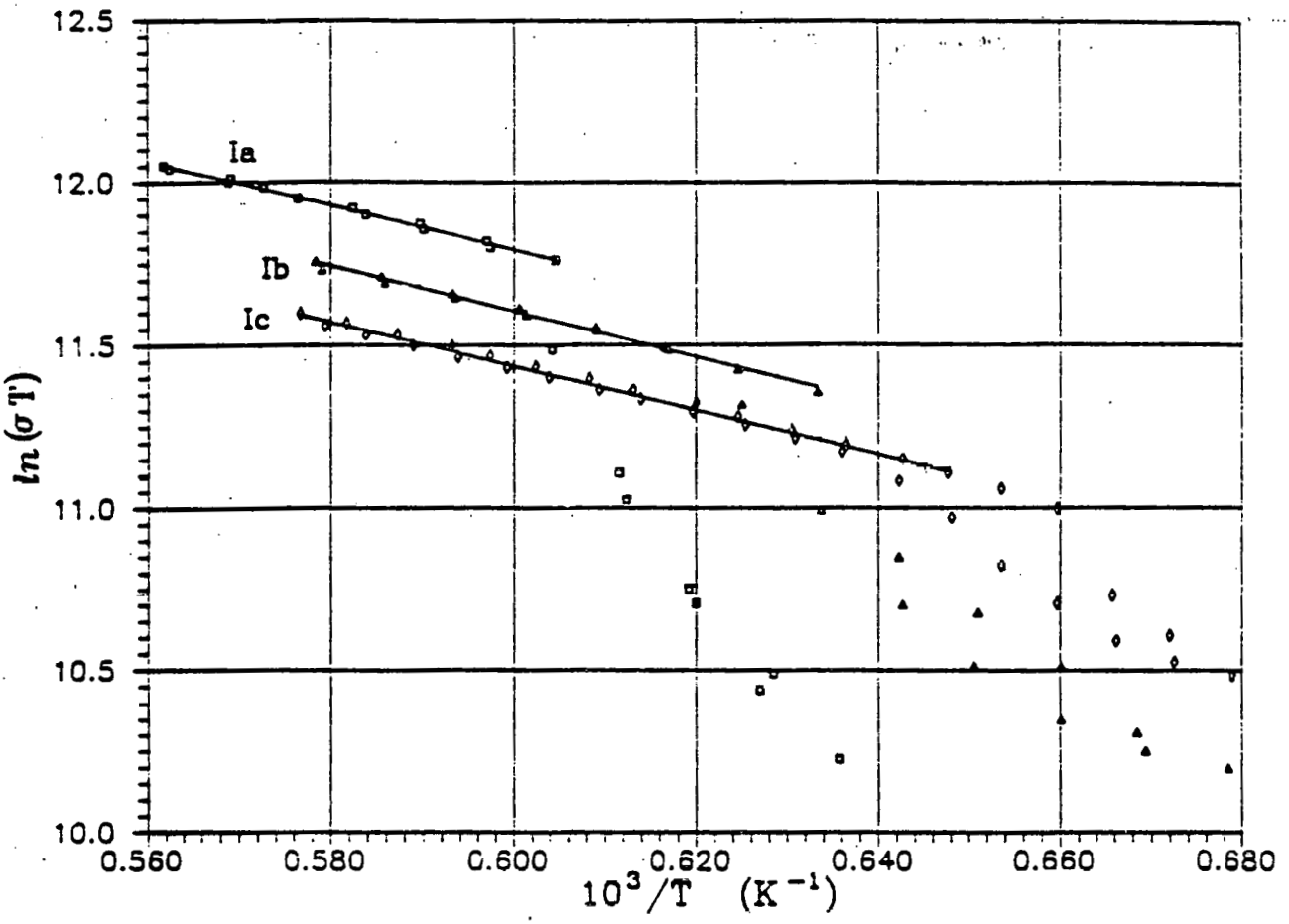

Figure 9 Ln(σT) vs. T^{-1} for Crystals Ia, Ib, and Ic

more difficult to observe at lower temperatures as the hysteresis spreads out along the curve in the direction of the temperature axis, and the conductivity change is not as great.

5.3 Discussion

The results of the conductivity measurements are summarized in Table 7.

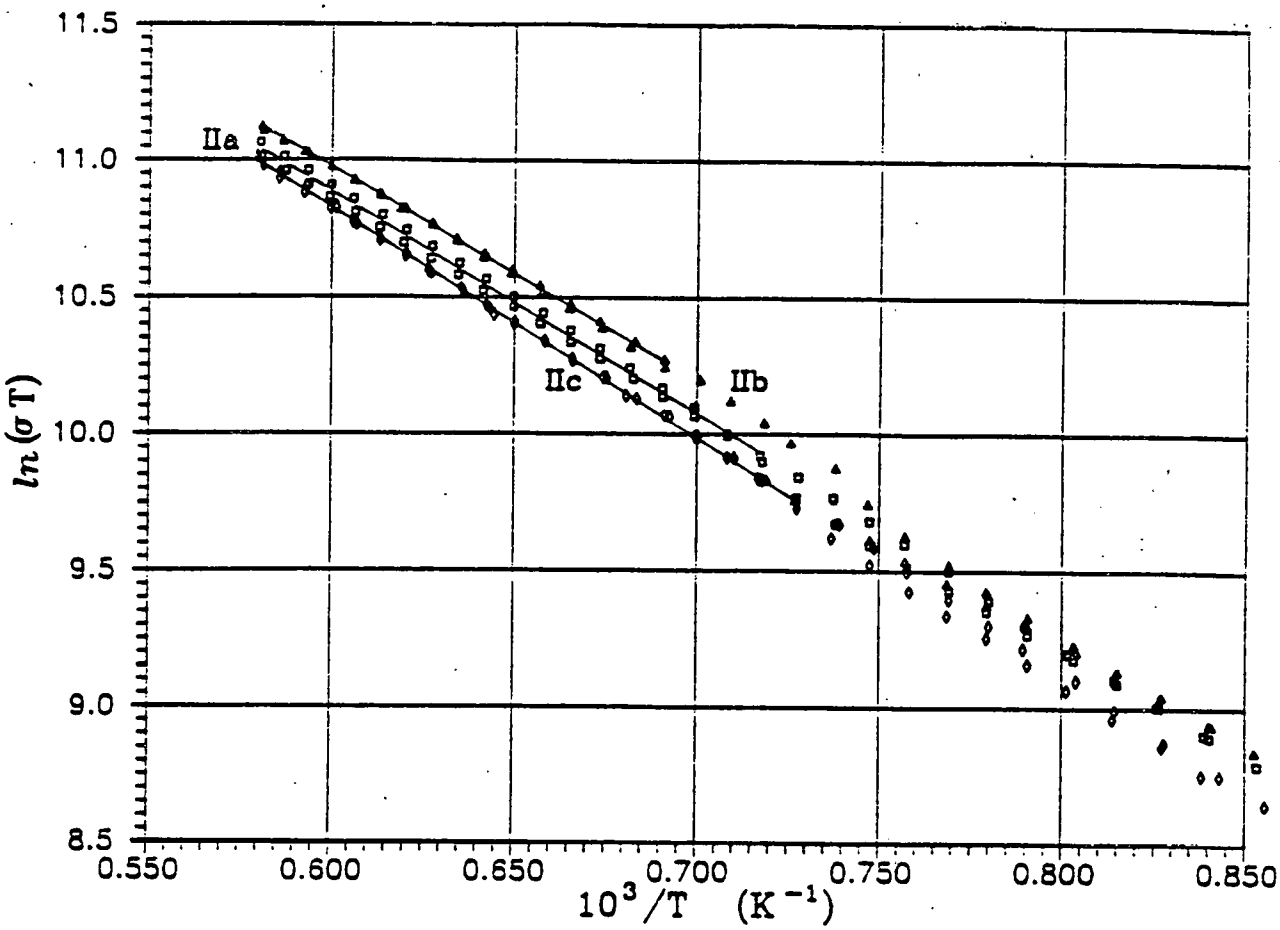

Figure 10 Ln(σT) vs. T^{-1} for Crystals IIa, IIb, and IIc

Sample	log(σ) at 25°C	σ at 1400°C (Ωcm)$^{-1}$	ε (eV)	T_f (°C)
Ia	-4.17	80.2	0.58 ± 0.01	1390 ± 10
Ib	-5.81	66.4	0.60 ± 0.01	1325 ± 20
Ic	-5.60	56.1	0.58 ± 0.01	1280 ± 20
IIa	-7.44	32.4	0.698 ± 0.008	~1120
IIb	-7.00	35.5	0.669 ± 0.004	~1170
IIc	-7.83	30.6	0.724 ± 0.003	~1100
IIIa	-8.74	24.2	0.782 ± 0.002	(not
IIIb	-8.86	23.4	0.79 ± 0.01	observed)

Table 7 Summary of Electrical Conductivity Results Measured Under 1 atm. Oxygen for Temperatures of Up to 1450°C

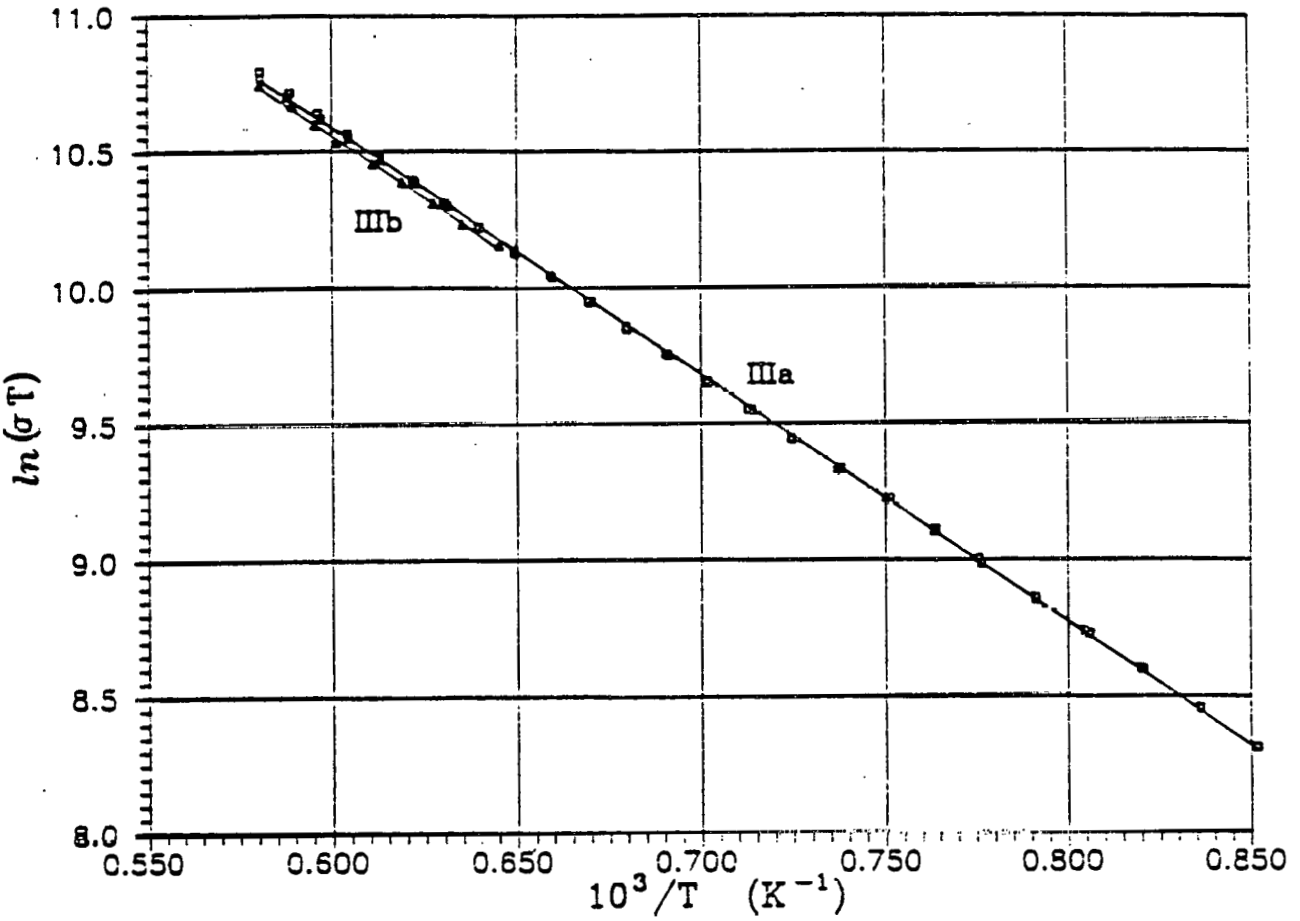

Figure 11 Ln(σT) vs. T^{-1} for Crystals IIIa and IIIb

The values of log(σ) at 25°C have been extrapolated and the values of σ at 1400°C interpolated from the best fit ln(σT) vs. T^{-1} lines. ε is the activation energy for conduction, as seen in equation 7, and T_f is the estimated reversible temperature for the precipitation of Fe_2O_3.

The values of T_f are significantly higher than the temperatures given for the phase boundaries shown in Figures 1 and 2. There are two reasons for this. The first is that the phase diagrams given in Figures 1 and 2 were measured in air, and it is known that the phase boundaries move to

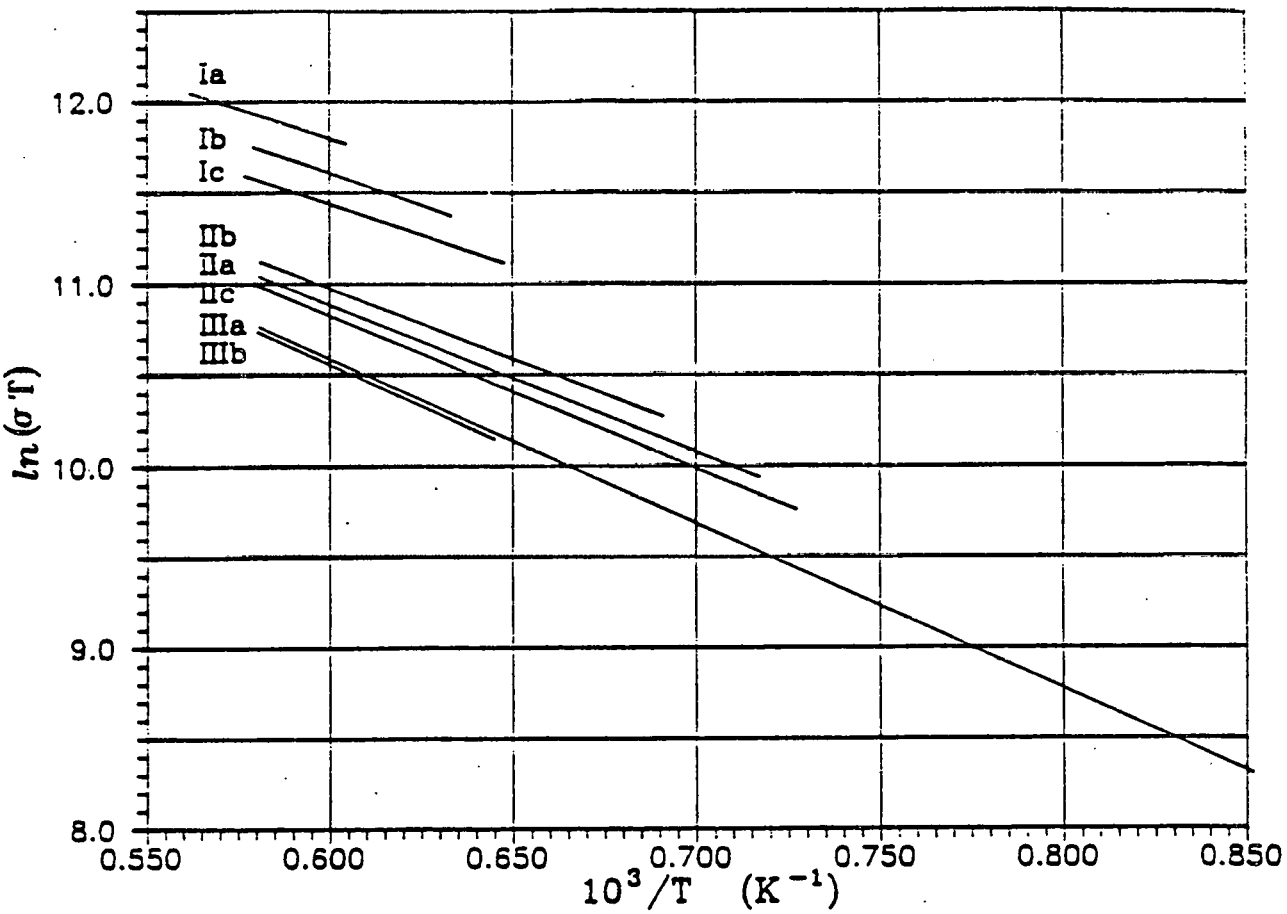

Figure 12 Ln(σT) vs. T^{-1} for all Crystals

higher temperatures with increasing P_{O_2}. The second reason is that the conductivity measurements are more sensitive to the presence to Fe_2O_3 than X - ray diffraction spectra would be. Conductivity measurements can also separate the reversible precipitation temperature from the undercooled precipitation temperature. Also, quenched samples may not be representative, since precipitation is relatively slow.

Activation energies were plotted for comparison in Figure 13. The combined results of Funatogawa et al. (91), Lotgering (66), and Rosenberg et al. (93), representing the most accepted values, are described by the solid curve.

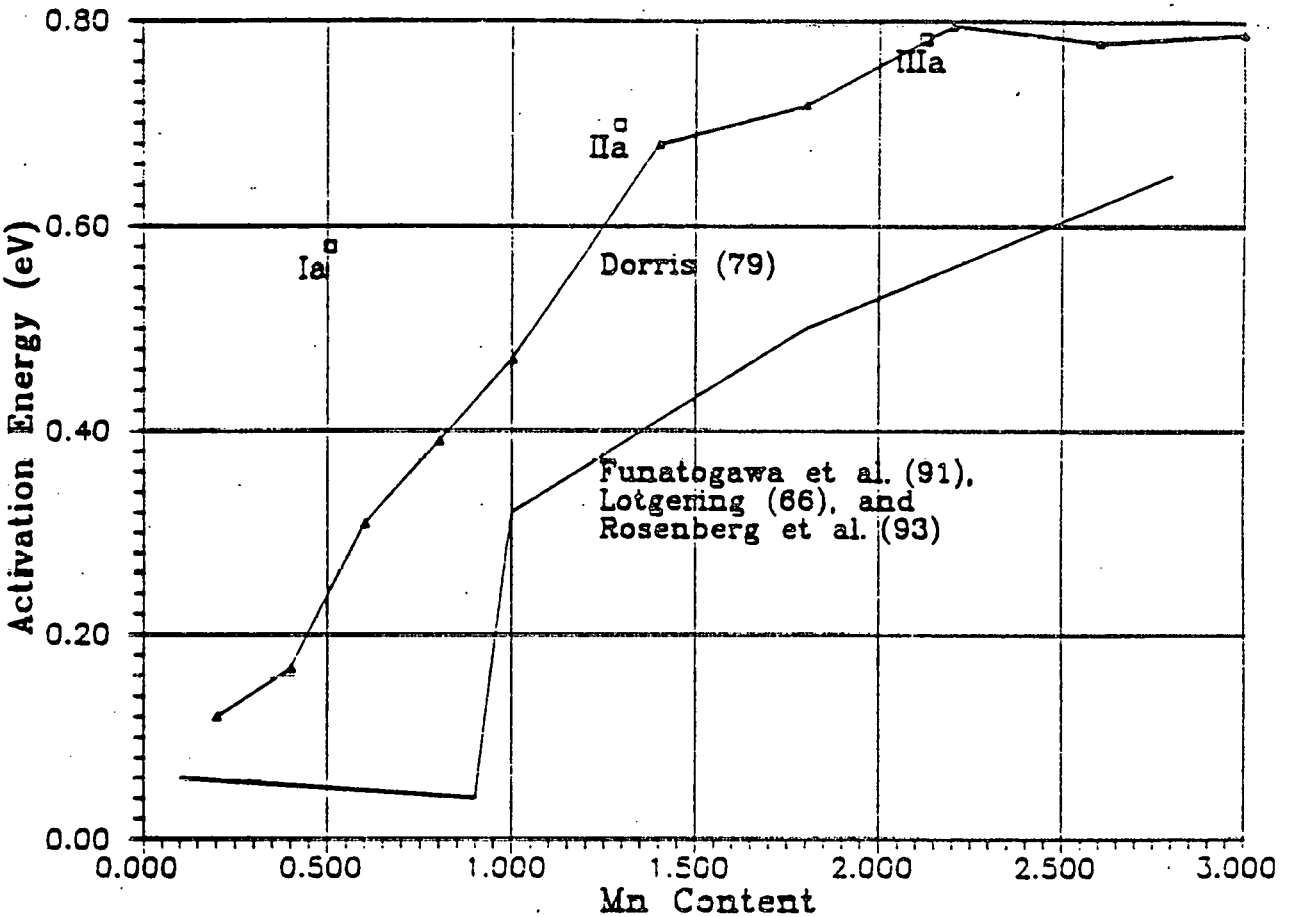

Figure 13 Activation Energies for Electrical Conductivity in Manganese Ferrites

These measurements were made at low temperatures upon metastable samples prepared under reducing conditions. The results of Dorris (79) were taken from measurements made upon stable samples at high temperatures. The measurements were made by Dorris under reducing atmospheres for $x \leq 1.0$, and in air for $x \geq 1.4$. The results for samples Ia, IIa, and IIIa were taken from high temperature measurements, all made at $P_{O_2} = 1$. The effect of the oxygen pressure of preparation is greatest for those samples with $x \leq 1.0$. Measurements made upon metastable samples have yielded activation energies lower than those measured from the

conductivity measurements taken at high temperature.

Previous observations have been confirmed by the measurements presented in this section. Low temperature measurements made upon metastable samples cannot represent the high temperature intrinsic properties. The effects of preparation, particularly the P_{O_2}, cannot be ignored as it will have a direct influence upon the electrical properties. The effect of P_{O_2} is probably strongest when the pressures are high enough to cause the formation of cationic vacancies. The formation of oxygen vacancies, at lower P_{O_2}'s, may not have such a strong effect upon the electrical properties.

The conductivity data indicated that a plot of $\ln(\sigma T)$ vs. T^{-1} is linear in the single phase spinel region. While this linearity seemed to confirm the small polaron hopping model briefly discussed in section 3.2, equation (6) could not be used to calculate reasonable values for n, the concentration of Fe_B^{2+}. The only conclusion made, based on the present study, is that while the mobility does appear to be an activated process, the small polaron model does not provide an adequate description. The application of a more extensive model should await the acquisition of a larger data base. In particular, more measurements need to be made at higher oxygen pressures, say for $P_{O_2} \geq 10^{-2}$, in order that the effect of cation vacancies can be studied.

5.4 Summary

The conductivity measurements have demonstrated the effect that a relatively high P_{O_2} can have upon the electrical properties of manganese ferrites, particularly those with high iron contents. The inapplicabilty of the

small polaron model ruled out any attempts to determine the cation distribution quantitatively. The decreasing conductivity with increasing Mn content indicated a decreasing Fe_B^{2+} concentration. However, the conductivity remained high even when the Mn concentration exceeded the Fe concentration by a factor of two. Either the Fe_B^{2+} concentration remained high or the conductivity mechanism changed. This question has not been answered in the literature and requires more investigation. The addition of the small amount of CuO to samples IIa and IIIa did not greatly affect the conductivity other than to cause a small decrease. Unfortunately the Fe : Mn ratio did not remain constant in samples Ia to Ic as a result of evaporation losses during crystal growth. The decrease in conductivity could then be a result of either increasing Cu or increasing Mn content.

The results discussed above demonstrated the sensitivity of electrical conductivity to the appearance of a second phase in this system. This suggests that the experimental technique discussed above could also be used in phase diagram determination studies. The technique would be applicable at temperatures above about 1100°C, where the kinetics of precipitation are sufficiently rapid. The precipitating phase must also have an identifiably different conductivity from that of the parent phase. The results show that the samples Ia through IIc will not be stable at 960°C, the temperature of operation of the bench - scale Hall cell. The samples that were chosen for electrochemical testing were IIIa and IIIc. Sample IIIc was chosen so as to demonstrate the effect that an amount of dissolved CuO may have on the anodic behavior of the sample.

6. Bench - Scale Hall Cell Testing

6.1 Previous Work

The overall cell reaction for an aluminum electrowinning cell operated with an inert anode would be :

$$2Al_2O_3 == 4Al + 3O_2 \qquad \varepsilon^\circ = 2.20\ V \qquad (28)$$

Aluminum would collect on the cathode as before. Oxygen gas would be the reaction product on the inert anode. Lacking the reducing power of carbon, the reversible cell potential has increased by a volt. Optimistically, in spite of the higher reaction voltage, the voltage of an operating cell will be lower as a result of more efficient cell design. This design would, in part, result from the use of a dimensionally - stable anode. The intensity of the search by the aluminum industry for a practical inert anode material has been reflected more by the number of patents issued (4), rather than in the few papers that have been published. It was only recently, once it was found that most "inert" materials would react with the electrolyte, that the problem has become one of scientific interest as well. One of the greatest barriers to solving this problem has been the difficulty in reproducing the results that have been communicated. Part of the reason for this difficulty must be attributed to the problems associated with carrying out research upon the particular molten salt system used to dissolve alumina. The other source of difficulty was the variation in experimental techniques employed in testing candidate materials. One of the objectives of the present study was to try to identify those aspects of the testing of anode materials that are the most critical.

Gold is probably the only anode material that is completely inert. Platinum, which appears inert, does become etched and and somewhat brittle after extended use. The reasons for this are not known. As the present study will demonstrate, it is useful to compare the behavior of candidate materials to the behavior of completely inert materials. Unfortunately, very little has been published about the anodic behavior of Pt, and even less published for Au. Thonstad (121) measured the overvoltage for the evolution of O_2 on Pt using the traditionally designed aluminum reference electrode with the aluminum on the bottom. Oxygen was bubbled over the Pt wire anode. The electrolyte consisted of Greenland cryolite saturated with alumina at 1000°C. The overvoltage was 0.17 V at a current density of 1 A/cm^2. Voltage decay measurements indicated that the reversible decomposition voltage for the cell was 2.205 V. Thonstad does not describe either the exact means of overvoltage measurement, or the means of IR voltage compensation. The "IR voltage" was that component of the voltage drop resulting from the resistance of the electrolyte that was included in the potential measured between the reference electrode and the anode. Zhang and Qiu (122) report overvoltage measurements in agreement with those of Thonstad measured using "modified continuous impulse" and voltage sweep techniques. Dewing and Van der Kouwe (123) report chronopotentiometric results for Au and Pt anodes. This work was of limited use to the present study as the authors did not apply current densities of less than 10 A/cm^2.

Unfortunately, the use of Au or Pt would not be practical on an industrial scale. Interest has revolved around other metals, notably upon copper, and oxides such as those based upon SnO_2 or Fe_2O_3. In 1937, Belyaev and Studentsov (5) tested as anodes in a bench - scale Hall cell, oxides of Fe, Sn, Co, Ni, Zn, Cu, and Cr. The oxides

Fe_3O_4, SnO_2, Co_3O_4, and NiO were the most stable. Seeking an improvement in conductivity, Belyaev (6) then tested ferrites of Zn, Ni, Ca, Mg, Al, Sn, Cr, and Co. The ferrites of Sn, Ni, and Zn led to the production of the metal with the lowest impurity concentrations. In what probably was the first paper of its kind, Liu and Thonstad (124) reported the overvoltages for oxygen evolution upon anodes based upon SnO_2. The composition used : 2% Sb_2O_3, 2% (by wt.) CuO in SnO_2, was thought to be, at the time, a leading inert anode candidate. It was found later that while the Sn content of the aluminum produced was low when this anode was used, it was high enough to cause tearing problems during the production of aluminum sheet and foil. The testing cell was very similar in design to the cell used in the present study except that it employed a traditional Al reference electrode. The authors reported the effect upon the overvoltage of various surface - level doping agents. They noted a significant current at voltages less than 2.2 V. This current was interpreted as being a result of the anodic oxidation of dissolved Al rather than as a result of the corrosion of SnO_2. Russell (125) reported polarization measurements made upon SnO_2 and various ferrites. He gave corrosion rates without stating how they were measured. Other experimental results in this paper are suspect due to the lack of pre - electrolysis purification of the electrolytes used. In a later paper, Russell (126) reported the activity of oxide films formed upon metal and cermet anode materials. Horinouchi et al. (127) reported the results of in situ electrolysis of various low solubility oxides for times of up to 40 hr. They noted corrosion of all oxide anodes without giving any further discussion. While the paper reported the results of what must have been a large study, it was noticeably lacking in detail.

Recently, investigators from ALCOA Laboratories reported

some of the results they obtained from their recent five - year effort on inert anode materials. They claimed success for a cermet material which consisted mainly of a nickel ferrite matrix that supported up to 17% of a fine discrete Cu metal phase. The oxidation of the copper at the anode surface seems to allow the formation of a passivating layer that prevents further corrosion. The mechanism of passivation is not yet well understood. Ray (21) has discussed the selection process for the composition used. DeYoung (128) has measured the dissolution rates of various oxides using a rotating disk technique. Tarcy (129) reported upon the corrosion and passivation of cermets. Ray (130) has reported the effects of bath additives and cell operating parameters upon the behavior of dimensionally stable anodes. Investigators at Pacific Northwest Laboratory have continued the development of the copper - containing cermet material. Windisch and Marschman (131) have reported a study of the passivation of copper and the cermet material.

A study of the techniques used in industry to investigate the anodic behavior of candidate inert anode materials led to the cell design and testing procedure described in the next section. While the cell was smaller and the equipment less sophisticated than that available in the industry, the experimental techniques to be described have produced useful results under carefully controlled conditions upon fully characterized, single phase specimens.

6.2 Experimental Apparatus and Control

The bench-scale Hall cell is shown in Figure 14.

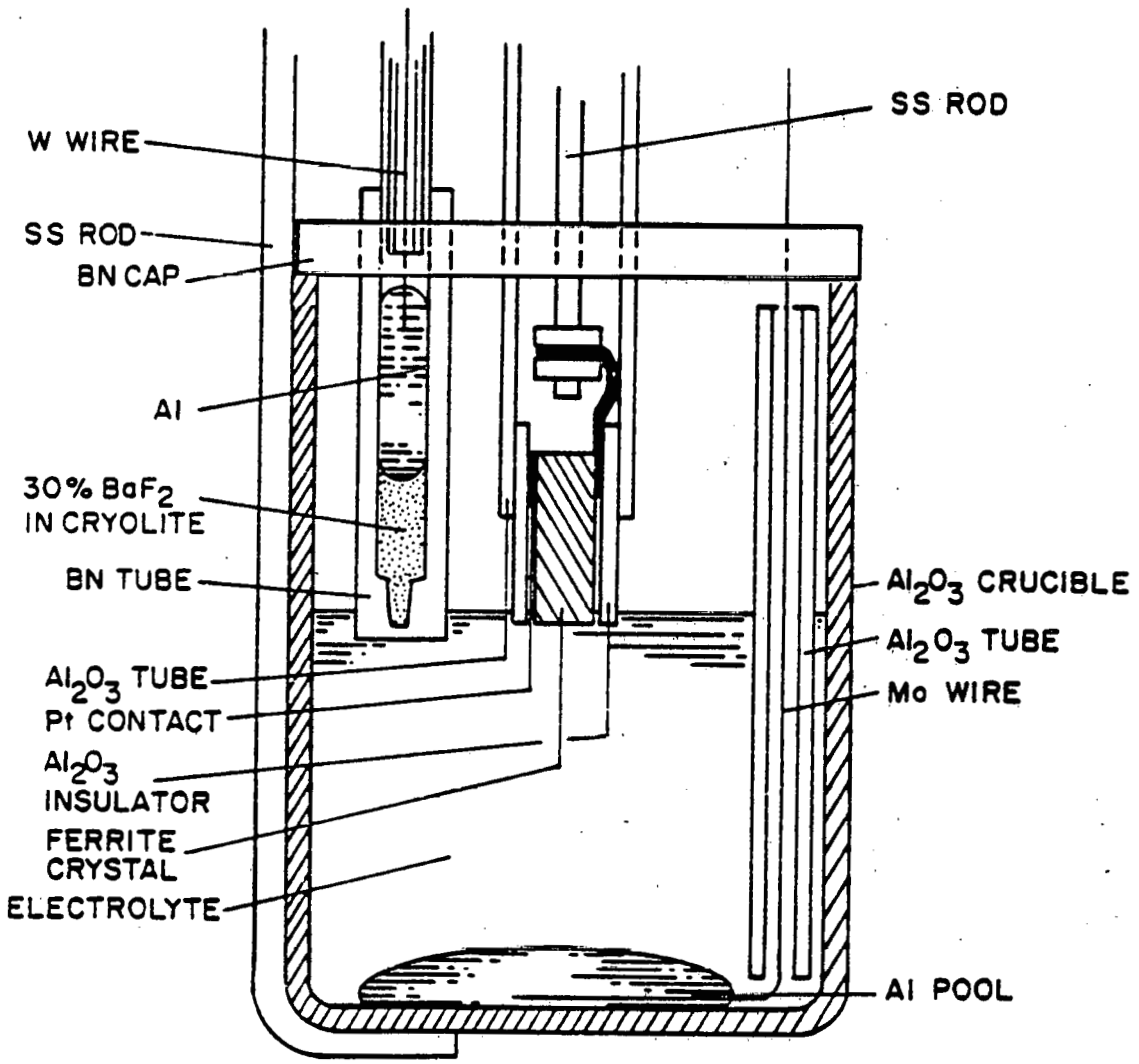

Figure 14 Bench - Scale Al_2O_3 Electrowinning Cell

A section of test specimen of about 2 cm in length was cut from the crystal with a diamond saw. This section was mounted in an alumina tube with an electrical connection provided by Pt paste and Pt foil. The mounting design minimized the distance between the electrical connection and

the electrolyte and insulated the sides of the sample from significant current flow. The mounted sample, attached to a stainless steel rod, was immersed only a few millimeters in the melt. Electrical connection to the molten Al pool cathode was provided by a molybdenum wire. The approximately 150 ml of electrolyte was contained in an alumina crucible which was covered with a BN cap to help minimize evaporation losses.

The aluminum reference electrode (132) was contained in a grade HBN boron nitride tube which was immersed in the melt next to the test sample. The addition of 30%, by weight, of BaF_2 to cryolite allowed the Al to float on this reference solution, thus ensuring that no contact could be made between the tungsten lead wire and the salt. This eliminated the common problem of mixed and non-stable reference potentials. The bottom of the BN tube was drilled to within 1 mm of the bottom. This layer of BN acted as a porous plug - type membrane between the reference solution and the electrolyte. The level of the reference solution was maintained above that of the electrolyte so that any flow of salt would occur out of the reference. This ensured that the composition of the reference solution remained constant. The potential between the reference electrode and the cathode, which contained only junction and membrane potentials when the cell was at rest, remained constant at 0.06 V during the experiments.

The reference solution was pre - electrolyzed in order to remove electroactive impurities. The cell used for the purification of the reference solution employed a graphite crucible as the anode. The molten aluminum cathode was held in an alumina riser tube, 1 cm in dia., which was immersed in the melt to a depth of approximately 1.5 cm. Electrical contact to the aluminum was made by tungsten wire. Pre - electrolysis was carried out by applying 3 V for

several hours. This electrolysis moved any electroactive impurities into the aluminum cathode, thus ensuring that the reference interface was Al/Al^{3+} only. It is doubtful that the positive effect of reference solution pre - electrolysis upon the stability of the electrode has ever been fully appreciated.

Not shown in Figure 14 are the thermocouple and gas inlet tubes which were held just above the melt. The cell was contained within another alumina tube which allowed maintenance of a dry atmosphere of argon over the cell. Heating was done by an electrical resistance furnace. The top fitting was designed to permit rapid removal and replacement of anodes.

The electrolyte was formulated to contain 5% CaF_2, 7% Al_2O_3, and have a bath ratio (BR) of 1.15 in order to resemble industrial compositions. The bath ratio is defined as the weight ratio of NaF to AlF_3 in the electrolyte. The cryolite ratio (CR), defined as the mole ratio of these two compounds, is twice the bath ratio. Greenland cryolite and reagent grade CaF_2 and Al_2O_3 were used. The AlF_3 was supplied by ALCOA. Impurity levels and water contents were taken into account during formulation. The resulting mixture was 79.39%, by weight, cryolite; 10.28% AlF_3; 3.75% CaF_2; and 6.58% Al_2O_3 before melting. The total weight of salt added to the cell was 297 g, and 78.7 g of Al were added for the cathode. After electrolysis, the melt was analyzed for $\%Al_2O_3$ and BR using the $AlCl_3$ and pyrotitration methods, respectively. The Al_2O_3 content increased to a value of 11% while the BR stayed at 1.11 ± 0.02. Quenched melt samples were seen to contain fine crystals of Al_2O_3. This supersaturation accounted for the high measured concentration. On the basis of these measurements it was decided that AlF_3 and Al_2O_3 additions need not be made during this set of experiments.

Once the electrolyte was molten and the temperature was stable at 960°C, pre - electrolysis was carried out using a Pt anode with a surface area of 1.6 cm^2. At an applied voltage of 3.00 V a current density of about 1 A/cm^2 was observed. The current density decreased as the impurity concentration decreased. Electrolyte purity was measured by applying voltage sweeps at a rate of 20 mV/s in order to determine the residual current, defined as the current density at a voltage slightly less than that required for Al_2O_3 reduction. A clean melt would show a residual current density of less than 20 mA/cm^2. Generally pre - electrolysis took less than 3 hr.

The test anodes were immersed in the melt after the completion of pre - electrolysis and after some measurements were made upon Pt. The test specimen was lowered into the hot zone over a time of about 2 hr so that thermal shock was avoided. The measurements were made using the instrumentation diagrammed in Figure 15.

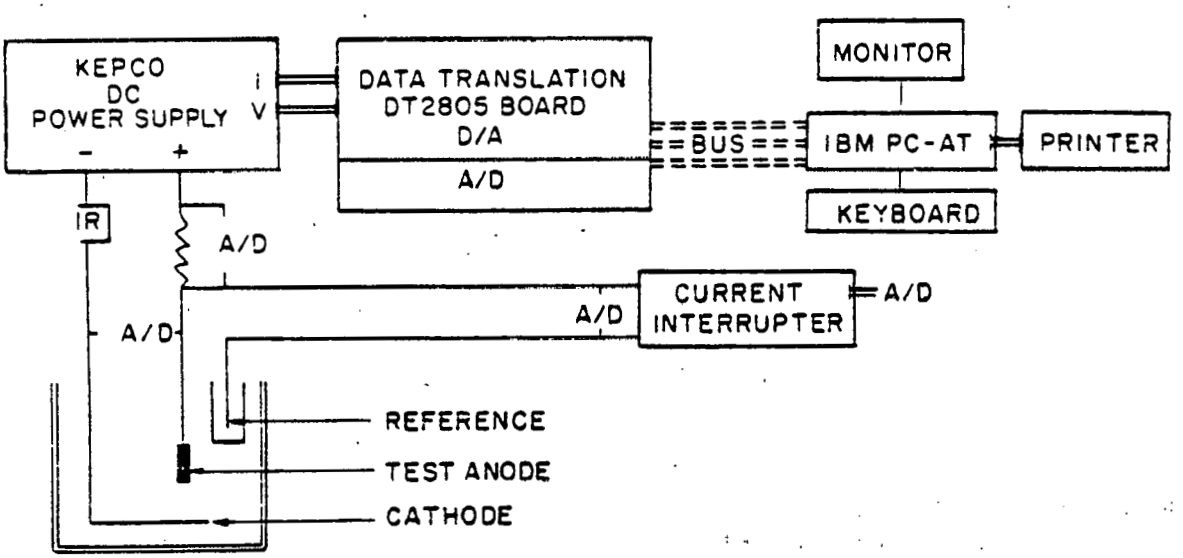

Figure 15 Computer Controlled Electrochemical Testing Instrumentation

The current interrupter (ESC Model 810-02, modified, The Electrosynthesis Co., Inc., E. Amherst, N.Y.) was used to measure that portion of the IR drop that was included in the measured anode to reference potential. The overvoltage was calculated by subtracting this IR drop and the zero current emf from the anode to reference potential. The zero current emf was obtained from the extrapolation of the anode to reference voltage to open circuit, i.e., $i = 0$, and usually measured 2.16 V. This potential contains a component of magnitude -0.06 V, the result of membrane and thermal emf's. All potentials were measured using the DT2805 analog to digital board. The output channels of the board were used to control the DC power supply in either voltage or current control modes. The board in turn, was controlled by the computer using the program listed in appendix IV. This system was capable of making a variety of electrochemical measurements as well as just applying potentiostatic or galvanostatic electrolysis. Any mathematically describable transient could be applied to the cell. The program listed was capable of conducting voltage sweeps, galvanostatic pulses, and making potential or current step steady state measurements. The program also displayed and stored the data. The acquisition rate of the system was limited by the DT2805 board to a maximum rate of a point every 0.2 ms. The response time of the DC supply was less than 0.2 ms. This system was equivalent in operation to the combination of a potentiostat/galvanostat, a signal programmer, a current interrupter, a digital storage oscilloscope, and a chart recorder. Not only did the computer based system have the advantage of lower cost, but it was capable of supplying higher currents beyond the capabilities of most potentiostats. Also, unlike most potentiostats, both sides of the output of the DC supply were isolated from ground, eliminating any ground loop problems.

6.3 Results of Electrochemical Measurements

6.3.1 Tests I to III

The results reported in section 6.3 were measured in five different experiments. Some measurements were made upon Au, Pt, and a cobalt ferrite crystal designated C1 in three different experiments. These results have been discussed in greater detail elsewhere (133,134). Some results are shown in Figure 16 as curves of cell voltage vs. current density. The current on the Au and Pt anodes did not increase until a cell potential of 2.2 V was reached. This is the decomposition potential for Al_2O_3 in a saturated solution at 960°C. However the current on the cobalt ferrite sample was significant at potentials less than 2.2 V. This effect was also found on the manganese ferrite samples whose results are reported in the next two sections. The Figure also demonstrated the difficulty in obtaining consistent results, even with identical anodes. One of the problems was being able to define the electrode area. Changes in melt level, and the ability of the melt to creep up the sides of the electrode contributed to the problem. Measurements also depended upon the melt purity and technique used. All of the results shown in Figure 16 were made with melts purified by pre - electrolysis, using the voltage - step steady state technique.

While these initial trials helped to establish a working cell design, two problems existed with the experimental technique used. An immersion time of 1.5 hr for the ferrite test anodes was found to be too short to show observable corrosion. Later work, discussed in section 6.3.3, carried out on the manganese ferrites after a repair of the current

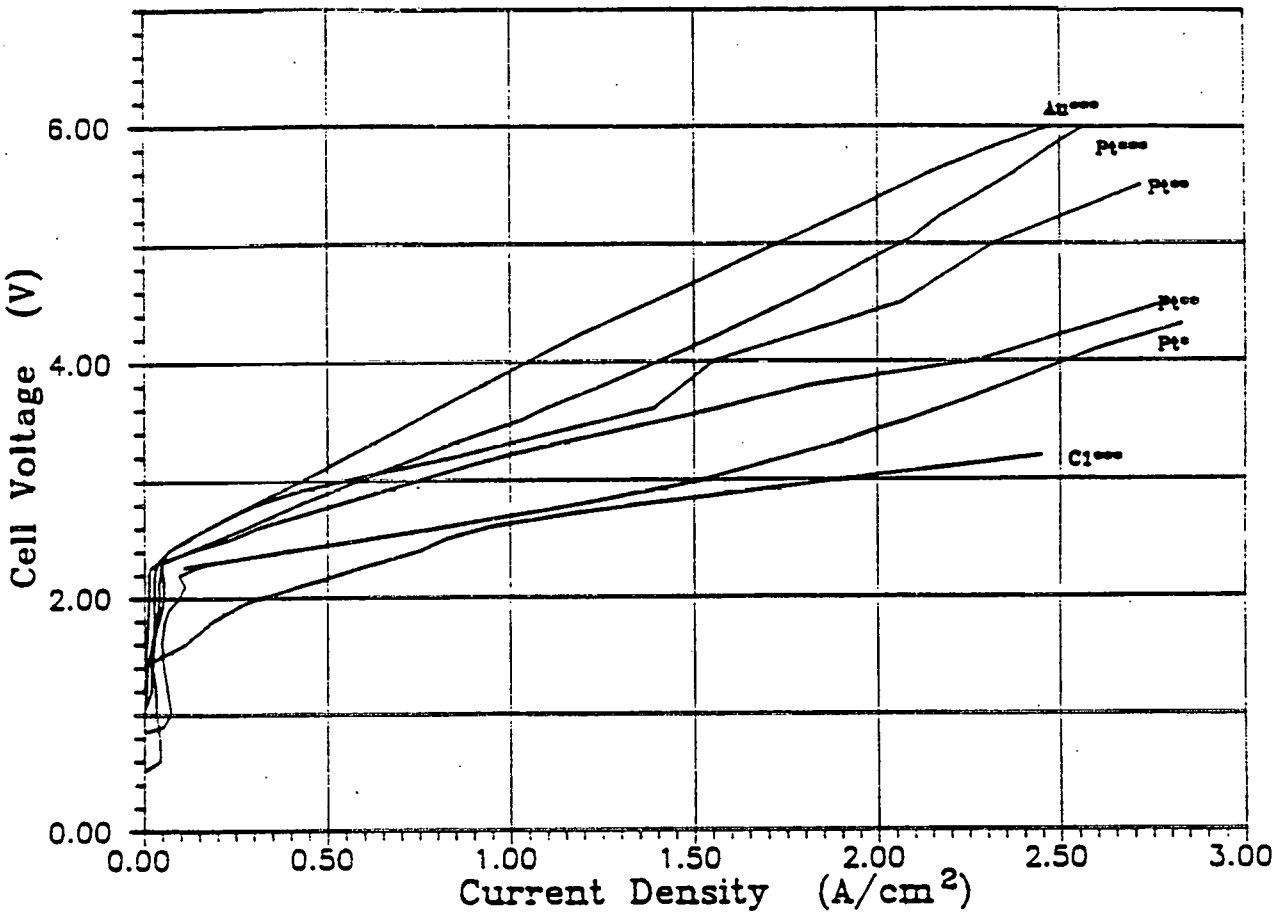

Figure 16 Cell Voltage vs. Current Density for Various Anodes for Tests I to III

interrupter, showed that previous IR measurements may have been too high. These problems decreased the usefulness of the results measured in tests I to III. However some useful results were obtained from a scanning electron microscopic examination of the electrolyzed cobalt ferrite specimens. A sample of composition 25 wt% CoO in Fe_2O_3, after electrolysis at 3.0 V and 1 A/cm^2 for 1 hr, showed the formation of an interface layer 8 μm in thickness. A sample of identical composition electrolyzed at 2.0 V for 1 hr had a layer 25 to 30 μm in thickness. The current increased from 0.20 to 0.29 A/cm^2 during electrolysis for this sample.

It is possible that a higher rate of oxygen evolution impeded the formation of the layer. Elemental profiles showed the interface layer was an alumina - rich oxide solution containing a small amount of fluoride. A diffusion profile out of the sample was observed for Co and Fe. Alumina was forced to diffuse into the sample because the activity of alumina in the melt was 1. Post - test chemical analyses of the electrolyte and metal did not show a high enough increase in the Fe and Co concentration to allow the calculation of an accurate corrosion rate.

6.3.2 Test IV : Sample IIIa

Improved test methods resulting from the experience gained in earlier experiments allowed the extraction of the maximum amount of consistent information from tests IV and V. Cell voltage results are given for various anodes in Figure 17. These curves were measured using the current - step steady state technique. In this technique the current was increased by 0.02 to 0.03 A/cm^2 increments. The system waited for around 5 s at each step, took 100 points in 1 s, and then stored the mean value of these measurements. This digital averaging technique effectively filtered out much of the fluctuations in the measured voltage caused by bubble evolution or electrolyte flow at the anode. This noise level was as high as ±0.5 V at current densities greater than 1 A/cm^2.

Curves are given for the anodes: graphite (Gr), Pt in a pre - electrolyzed melt (Pt), Pt after the 750 min electrolysis of IIIa (Pt'), and the ferrite IIIa after its electrolysis (IIIa). The residual current, defined as the current density at voltages less than 2.2 V, on Pt' was at least 8 times higher than that for the clean melt.

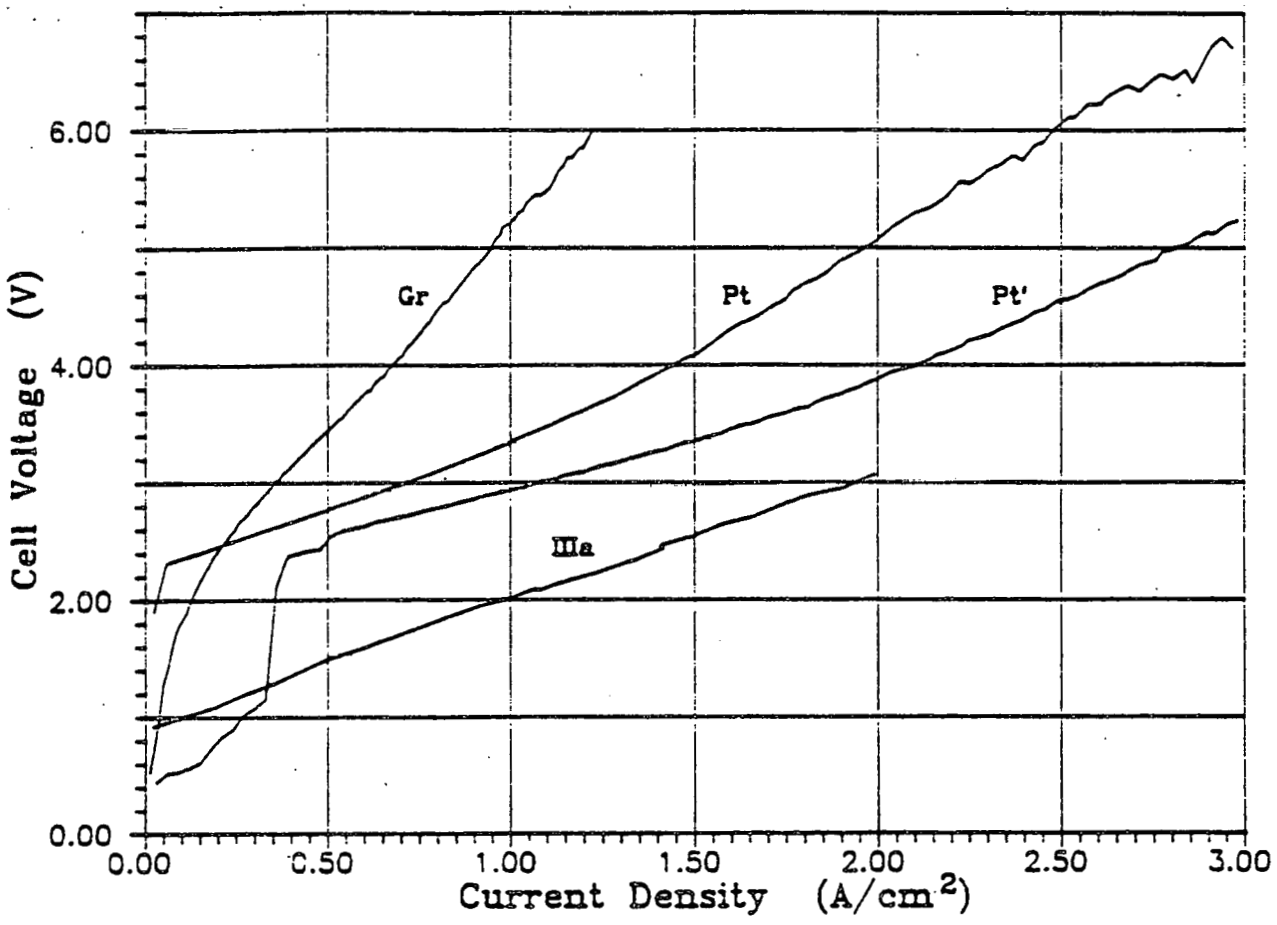

Figure 17 Cell Voltage vs. Current Density for Various Anodes for Test IV (Pt' is for immersion of Pt anode after electrolysis of IIIa)

The higher residual on Pt' was a result of the electrolysis of the impurities added to the electrolyte as a consequence of the corrosion of IIIa. Current began to pass on IIIa at potentials as low as 0.9 V vs. the Al cathode. The high residual on IIIa was a result of a combination of corrosion current and the electrolysis of these corrosion products. An examination of the relevant decomposition potentials helped to explain why the electrolysis of sample IIIa began at 0.9 V. These potentials were calculated using reaction 29 and equation 30 :

$$MeO_{\frac{n}{2}} \Longrightarrow Me + \frac{n}{4}O_2 \qquad (29)$$

$$\varepsilon^{\circ}_{29} = -\frac{\Delta G^{\circ}_{29}}{zF} \qquad (30)$$

ΔG°_{29} was calculated assuming unit activities for all three of the components at 1300 K. The ΔG values were taken from Barin and Knacke (135,136). Unit activity was a reasonable assumption for oxygen gas. The activity of the metal oxide will only be one when it has saturated the electrolyte. While few solubility data are available, values of 0.003 to 0.2 wt% have been reported for Fe_2O_3 in cryolite (see page 365, ref.7). Therefore it would not take a great deal of oxide to saturate the electrolyte. Reducing the Me activity by dissolution into Al could decrease the potential by as much as 0.2 V for an activity of 10^{-2} or by 0.5 V for an activity of 10^{-4}. Such low activities for Fe and Mn in Al were not expected since the Al used in the pad already contained some Fe before use, and the solubilities of Fe and Mn are less than 1 wt% at 960°C. The relevant oxide decomposition potentials are :

Oxide	$-\varepsilon^{\circ}_{29}$ (V)
CuO	0.21
Cu_2O	0.38
Fe_2O_3	0.84
FeO	0.99
Mn_2O_3	1.07
MnO	1.49
Al_2O_3	2.17

Table 8 Relevant Oxide Decomposition Potentials Calculated at 1300 K

For sample IIIa the lowest of the potentials is that for Fe_2O_3 at 0.84 V. Since IIIa had been electrolyzed in the melt for 12.5 hr prior to the measurements shown in Figure 17, it was not unreasonable to assume that sufficient Fe_2O_3 had dissolved into the electrolyte so as to approach saturation. So the overall cell reaction on IIIa, as well as upon Pt', at potentials around 0.9 V would be the decomposition of Fe_2O_3. As the cell potential was increased the electrolysis of dissolved manganese oxides would commence, followed by the electrolysis of Al_2O_3. Results to be discussed later will confirm this explanation. In particular, chronopotentiometric measurements performed upon Pt' have confirmed that the electrolysis of Fe_2O_3 began at the reversible potential given in Table 8.

It was noted that due to the smaller area of IIIa, assumed to be 0.23 cm^2, that the error on the current density for this sample was larger than that for the Pt anode. As a result of the tendency of the anode to round out as a result of corrosion and the creeping of the electrolyte, the actual electrolyzed surface area was probably as much as a factor of 2 higher.

The overvoltage results shown in Figure 18 were measured at the same time as the results in Figure 17 using the same technique. These results were higher than the other results discussed in section 6.1, especially at higher current densities. Since the overvoltage for oxygen evolution has not yet been established it was not possible to say what measurements were in error. However, the simple calculation that will be presented in the next section confirmed that this is the overvoltage that is being measured. It was possible that since measurements were made at steady state, an additional polarization potential, related to gas bubble

evolution, was included in the overvoltage.

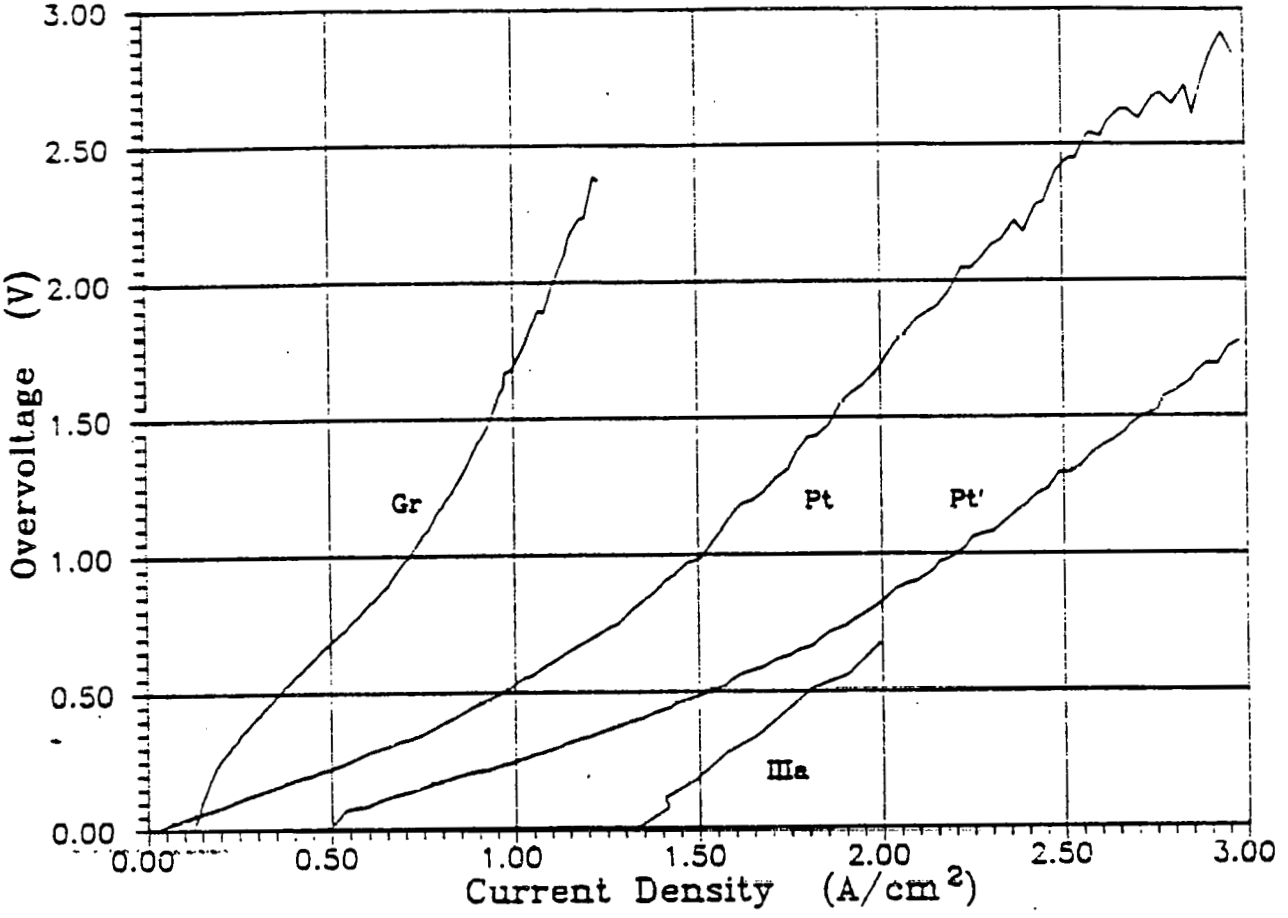

Figure 18 Overvoltage vs. Current Density for Various Anodes for Test IV

The effect of melt impurities was also observed using the voltage sweep technique. The curves in Figure 19 are for a melt purified by pre - electrolysis. The remaining peaks below the decomposition potential for Al_2O_3 indicated that the melt was not completely free of impurities, as can be expected. The highest potential peak was probably for Si^{4+}, while the lowest may be for Fe^{2+}. The middle peak could not be identified. Chemical analyses indicated that

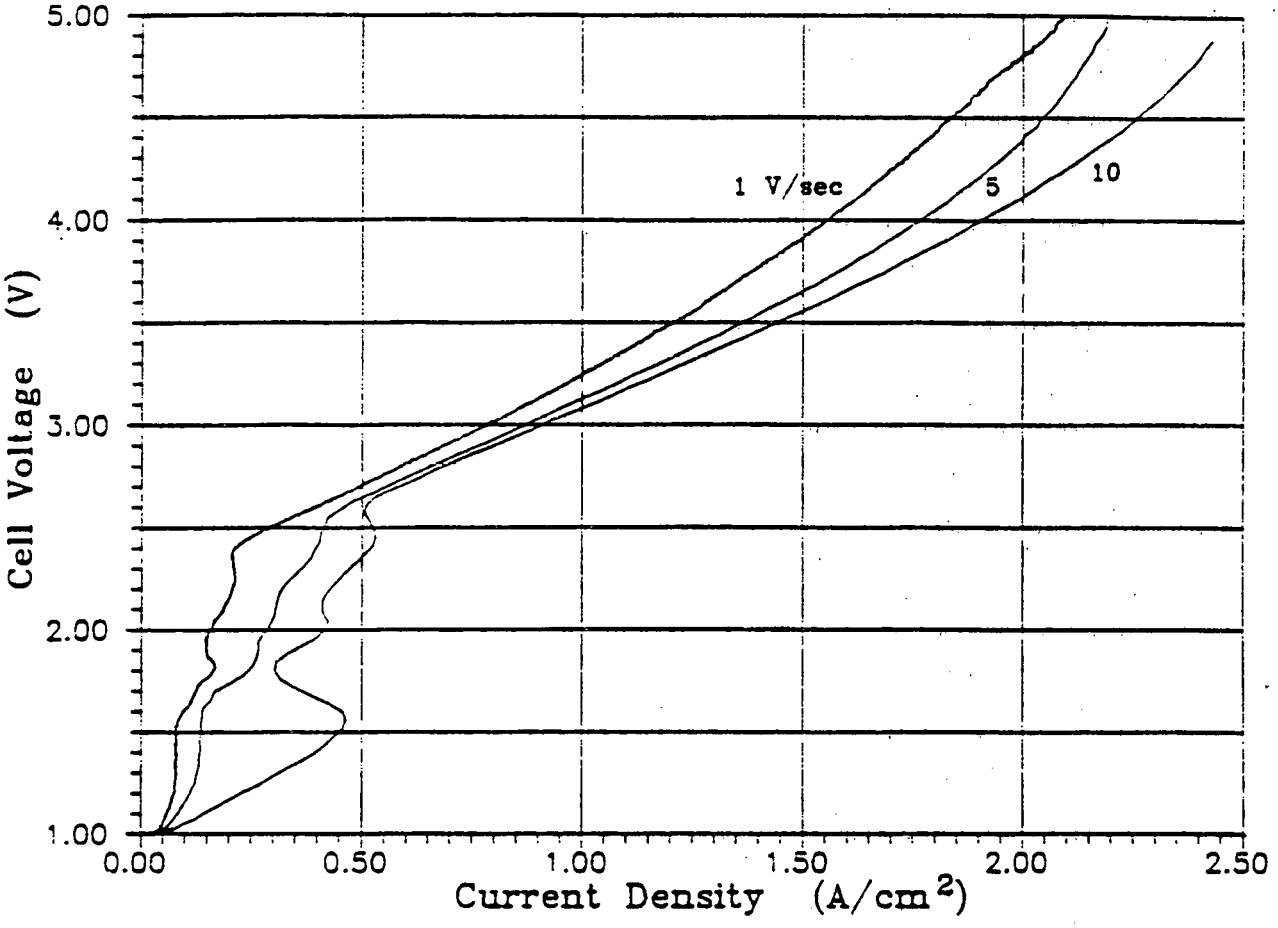

Figure 19 Voltage Sweeps on Pt for a Pre - Electrolyzed Electrolyte for Test IV

these impurities are already present in the cryolite added to the cell. Pre - electrolysis reduced the electrolyte concentration of these impurities to a level dependent upon the potential applied to the cell during the pre - electrolysis. The sweeps shown in Figure 20 indicated that the impurity level was much higher after the electrolysis of IIIa. The large peak shown started at a potential of 0.83 V, and thus confirmed the electrolysis of Fe_2O_3. While the peak height was proportional to the square root of the sweep rate, no other quantitative results were obtained from these measurements. Even though the rapid sweeps should have

avoided gas polarization effects the reproducibility of the peak height was poor.

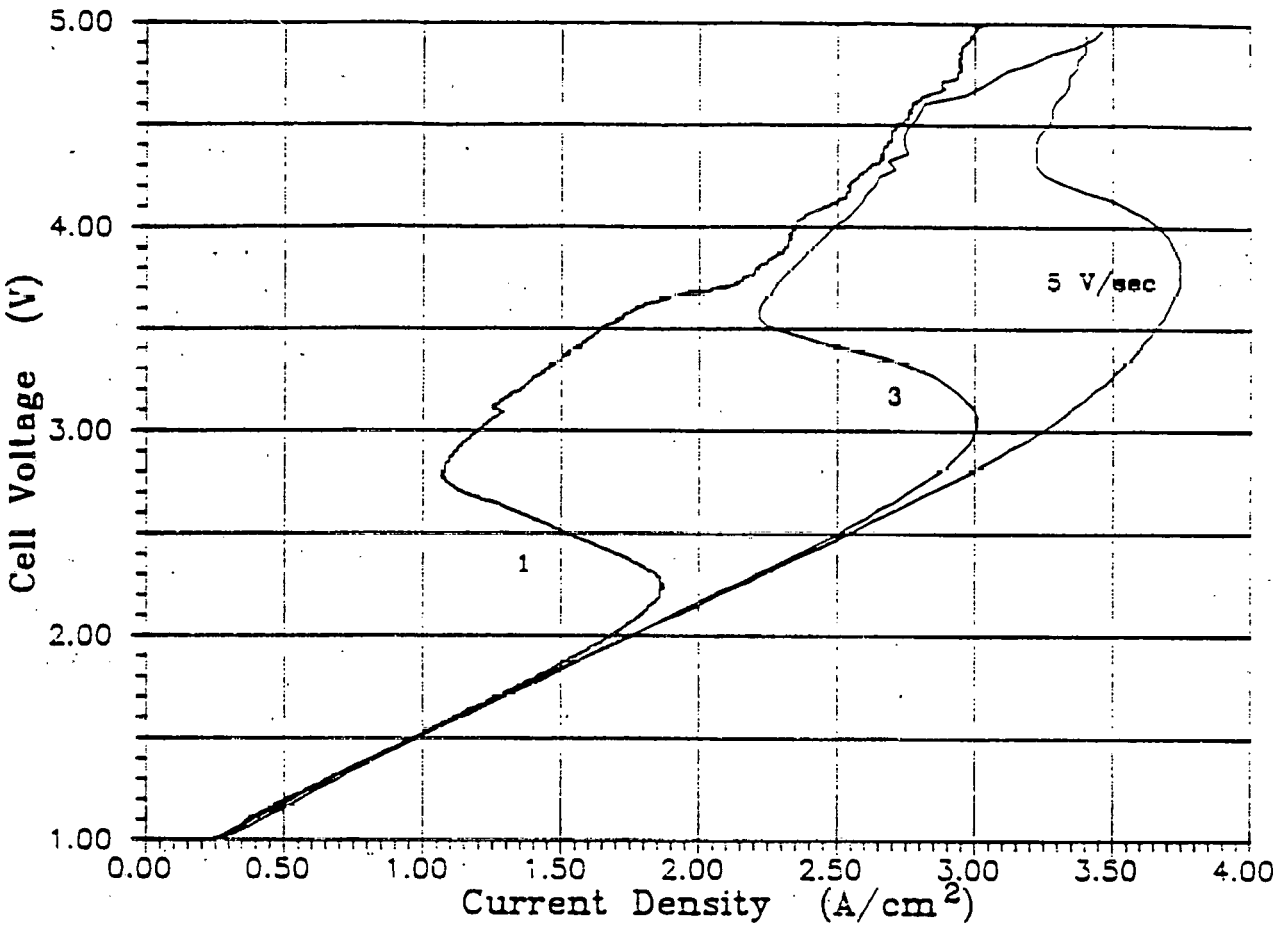

Figure 20 Voltage Sweeps on Pt' for Test IV

The anode to reference potential measured during the electrolysis of sample IIIa is shown in Figure 21. Bubble evolution was the cause of the fluctuations of this potential around 3.0 V. Since the average potential did not drift noticeably it was concluded that the reference electrode was well behaved, and that the test specimen did not corrode to such an extent so as to impede the current flow.

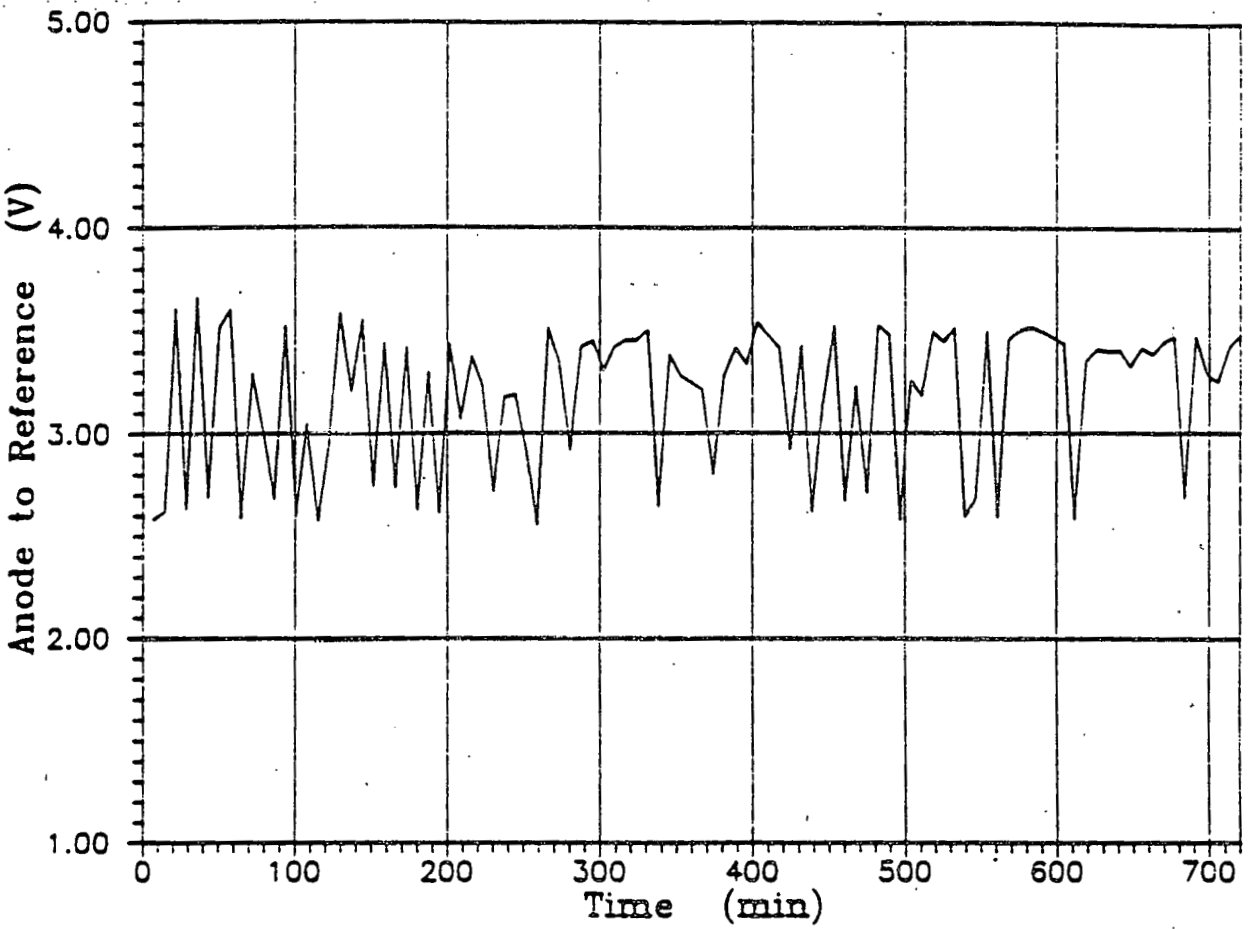

Figure 21 Anode to Reference Potential During the Electrolysis of IIIa During Test IV

In the chronopotentiometric technique, a constant current pulse was applied to the cell and the response of the anode to reference potential measured. This technique was useful for two reasons. First of all, the IR potential was disregarded because it was constant. This meant that the response of the anode to reference potential was due to a change in anodic overvoltage only. The second reason is that this response occurred before enough current was passed so as to allow the formation of a significant amount of gas at the anode. As has been shown, the release of a gas bubble caused discontinuities in measured potentials. The

chronopotentiometric curves given in Figure 22 demonstrated

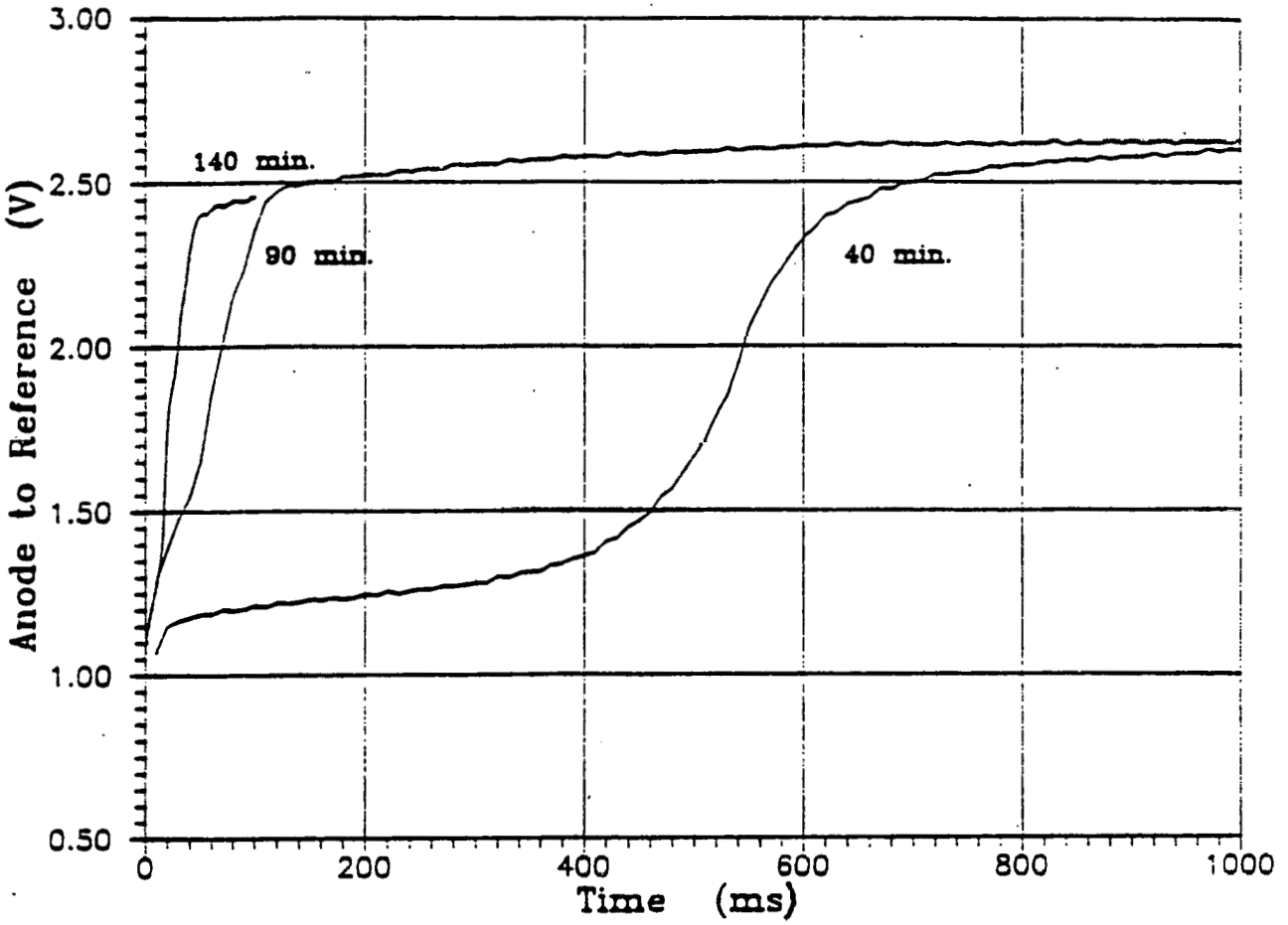

Figure 22 Chronopotentiometric Curves for 1 A/cm^2 Applied at Various Pre - Electrolysis Times During Test IV

the effect of pre - electrolysis upon the total impurity content of the electrolyte. A point of inflection occurred at the transition time, τ, at potentials above 2.2 V when the electrolysis of Al_2O_3 began. For times less than τ, impurities were being electrolyzed. Figure 22 shows that τ decreased as the concentration of electrolyte impurities was lowered by pre - electrolysis. Chronopotentiograms are

given in Figure 23 for Pt in a purified electrolyte. Since

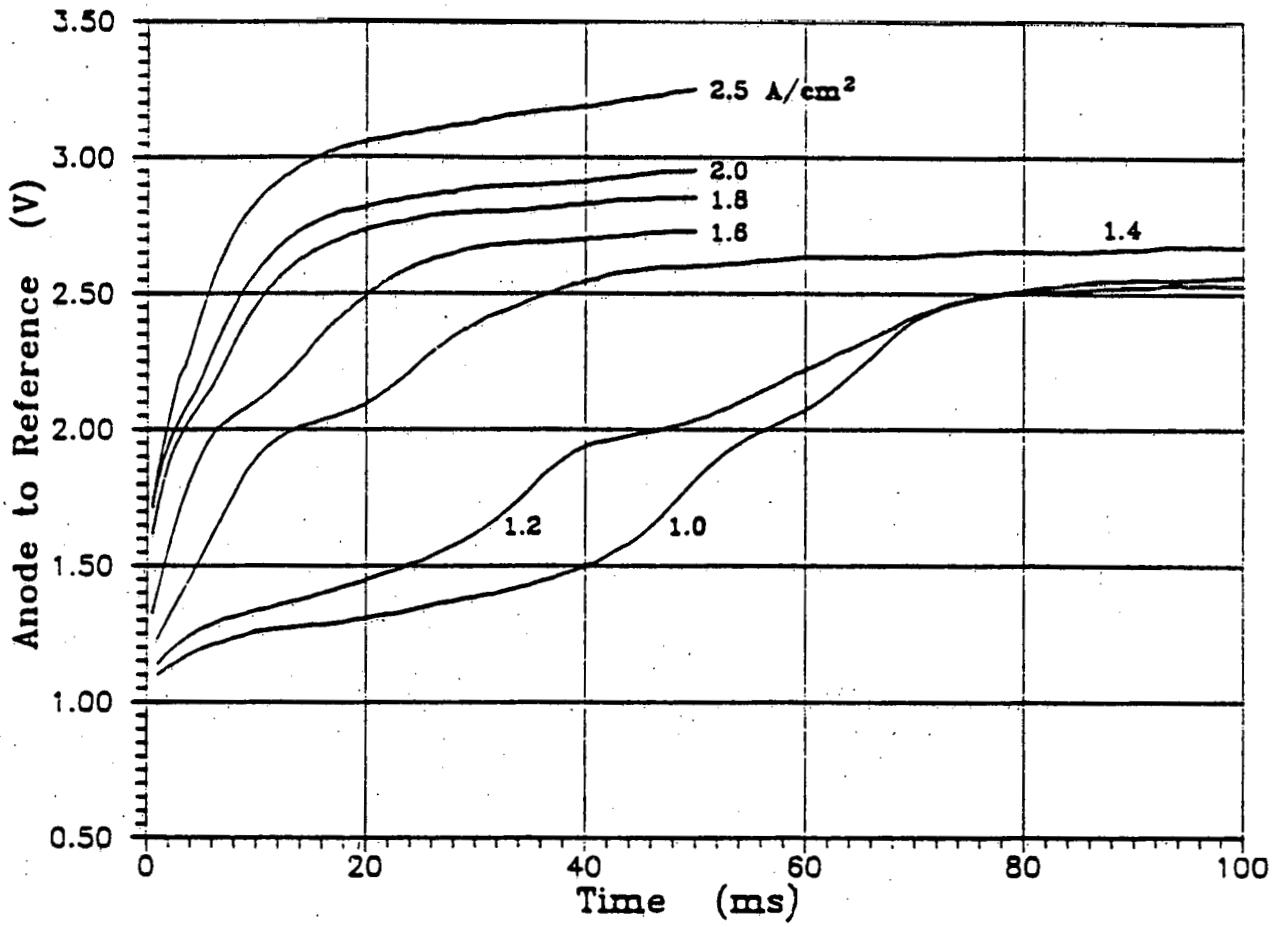

Figure 23 Chronopotentiometric Curves on Pt for a Pre - Electrolyzed Melt for Test IV

the impurity concentration was low in this electrolyte, the electrode reaction was diffusion controlled. The transition time, τ, represented the time it took for the impurity concentration, C, to reach zero at the electrolyte surface. The solution of this diffusion problem (see page 124-5, ref.137, for example) results in Sand's equation given below:

$$i\tau^{1/2} = \frac{nFD^{1/2}\pi^{1/2}C^{o1/2}}{2} \qquad (31)$$

where i is the current density, n the number of electrons exchanged, F the Faraday constant, D the diffusion coefficient, and C^o the bulk concentration. For the results in Figure 23, $i\tau^{1/2} = 0.20 \pm 0.05$ ($As^{1/2}/cm^2$). A value of 2×10^{-5} (cm^2/s) (see page 181-2, ref.7) was used for D. This is the diffusion coefficient for Al_2O_3 in cryolite and was used to approximate the coefficient for the impurity. For the anodic reaction of O^{2-}, n = 2. The concentration of O^{2-} from the impurity oxide, C^o, is then calculated to be about 3×10^{-4} ($mole/cm^3$). For comparison, the concentration of O^{2-} from Al_2O_3 was 6×10^{-3} ($mole/cm^3$). The calculated concentration of impurity was high, but reasonable considering the assumptions made.

Chronopotentiograms were also taken on IIIa for current densities of up to 8 A/cm^2. A constant voltage was reached in less than 0.1 s and no steps were observed. It appeared that none of the three possible anodic reactions were diffusion limited at these current densities. As will be discussed in section 6.5, the reaction mechanism on oxides can be complex, adding to the difficulty in interpreting measurements.

Chronopotentiograms obtained on Pt', the Pt anode immersed after the IIIa electrolysis, are shown in Figure 24. The transition times were longer due to the higher impurity concentration in this electrolyte. For this system $i\tau^{1/2}$ was not constant, but was a linear function of current density : $i\tau^{1/2} = 1.059 + 1.151i$. The coefficient of fit was 0.986 for this equation. According to the text by Macdonald (page 141, ref.137), this linearity was the result of a chemical reaction being coupled to the charge transfer reaction, the so called "CE" mechanism. This coupled reaction was the decomposition reaction of the impurity

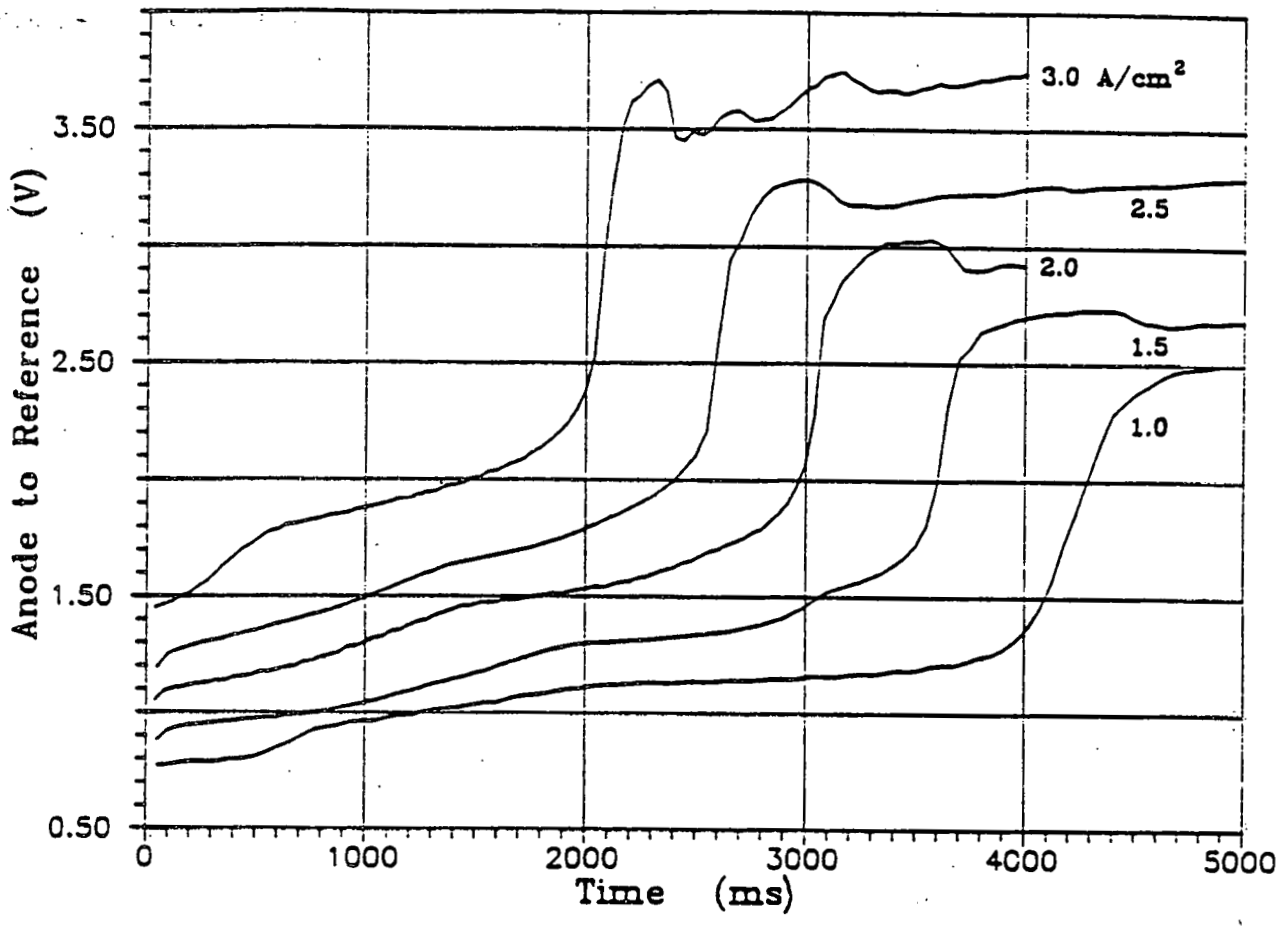

Figure 24 Chronopotentiometric Curves on Pt' After the Electrolysis of IIIa for Test IV

containing complex to produce the O^{2-} ion that was discharged on the anode. Possible reactions will be discussed in section 6.5. In this case the intercept, 1.059, equals the right hand side of equation 31. A similar calculation to that given above yielded the concentration of 1.4×10^{-3} (mole/cm^3). While the absolute values of the concentrations calculated using equation 31 were not that accurate, their ratio was more representative of the physical situation. This ratio implied that the impurity concentration after the electrolysis of IIIa was 5 times higher than before the electrolysis of IIIa. So the

chronopotentiometric measurements have confirmed the impurity concentration increase qualitatively indicated by the steady state cell voltage measurements shown in Figure 17.

The curves shown in Figure 24 also yielded important information concerning the major impurity species electrolyzed before Al_2O_3. The potential of the plateau before the transition point, ε_p, was linear with respect to current. The relationship, $\varepsilon_p = 0.83 + 0.34i$, fit the data to ± 0.01 V with a goodness of fit coefficient of 0.9998. The extrapolated potential at i = 0 was the reversible decomposition potential, ε°, for the electrolysis of the impurity. This voltage was identical to the decomposition potential of Fe_2O_3 given in Table 8. This confirmed the hypothesis given earlier, that the electrolysis of IIIa resulted in a concentration of Fe_2O_3 near saturation in the electrolyte. Plateaus for the decomposition of Mn_2O_3 and MnO were not seen, possibly because the concentrations of these oxides were not as near to saturation as was the concentration of Fe_2O_3. The only measurement available indicated that the solubility of Mn_3O_4 was just over 1 wt% (see page 365, ref.7). A concentration below saturation increased the already higher decomposition potential, so that it was nearer to that of Al_2O_3.

6.3.3 Test V : Sample IIIc

The composition of IIIc was similar to that of IIIa except that IIIc contained an amount of CuO. It was shown that this amount of CuO should have little effect upon the electrical properties of this high manganese ferrite. However, some electrochemical studies (129,131) have indicated that the presence of Cu metal leads, in some way,

to a passivation of the anode. This sample was tested in order to confirm the behavior of IIIa and to see if this amount of CuO provided any passivation. The results on IIIc will not be discussed in as much detail, except to indicate where the results confirm the behavior discussed in the previous section.

The cell voltage vs. current density results for the anodes used in test V are given in Figure 25.

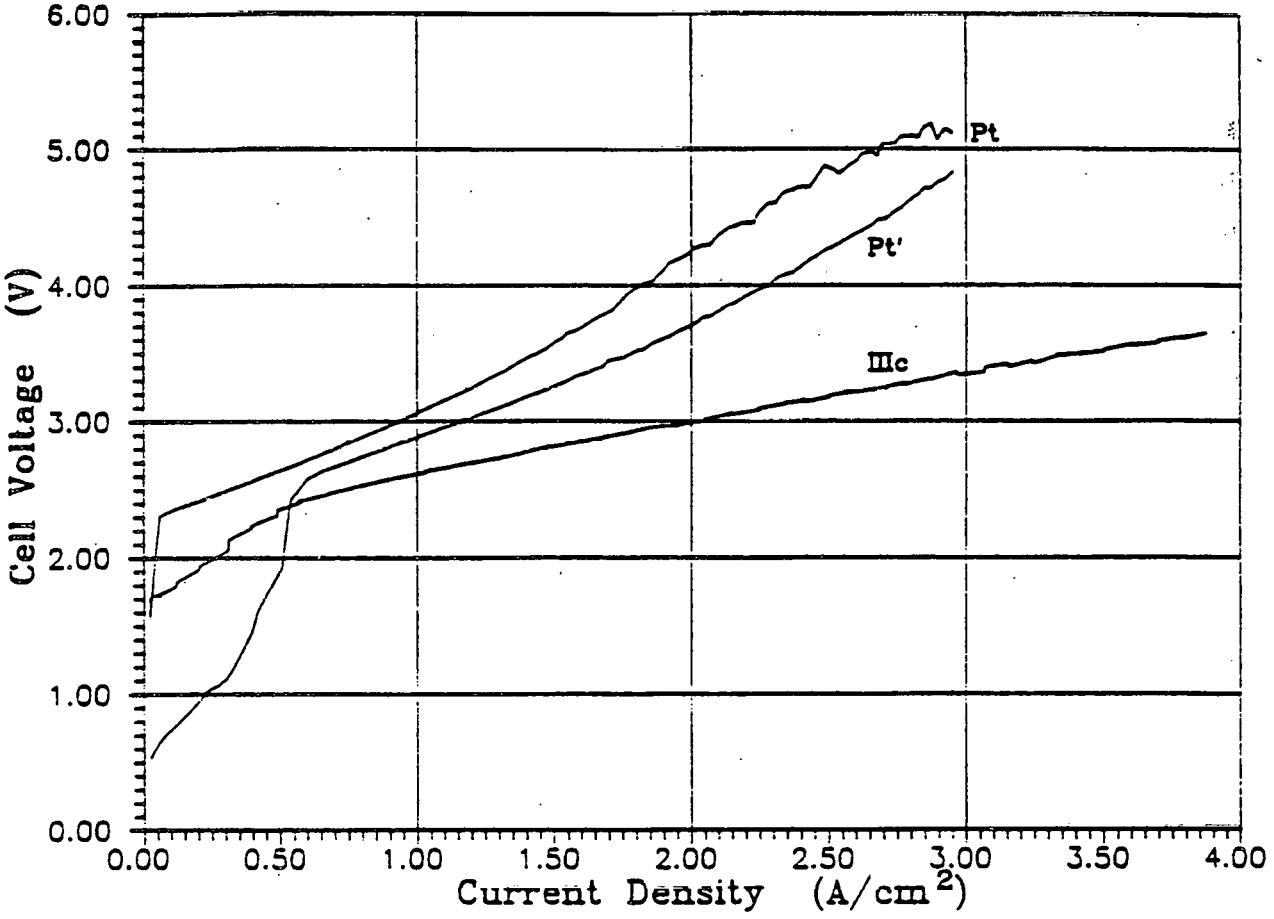

Figure 25 Cell Voltage vs. Current Density for Various Anodes for Test V

The curve for Pt was measured after 3 hr of pre-electrolysis, and the Pt' data were taken after the 14 hr electrolysis of sample IIIc at about 1 A/cm^2 and 3.3 V. Sample IIIc was assumed to have an area of 0.2 cm^2. Unlike the steady state results measured for IIIa, shown in Figure 17, the data for IIIc were measured before electrolysis. For this reason, the residual current was significantly lower even when the uncertainty in the electrode area was taken into account. This was a result of the lack of impurities in the electrolyte just after the immersion of IIIc. The residual current observed on IIIc was a combination of corrosion current and the electrolysis of remaining melt impurities. The high residual for Pt', whose curve had a similar shape to the Pt' anode in Figure 17, confirmed that the IIIc anode did corrode during electrolysis, resulting in a higher impurity content in the melt.

The voltage sweeps shown in Figure 26 confirmed previously observed behavior. The sweep on IIIc was taken after its 13 hr electrolysis. Again, the presence of a concentration of Fe_2O_3 near saturation, generated by the corrosion of IIIc, has led to a reversible potential near 0.9 V for the electrolysis of IIIc.

Figure 27 shows the overvoltage results for Pt, Pt', and IIIc measured before electrolysis. These data were taken at the same time as the data shown in Figure 25. The dashed lines represent the results of a calculation of overvoltage that was in good agreement with measured values. This overvoltage was calculated by first considering the components of the total cell voltage, ε_{cell}:

$$\varepsilon_{cell} = \varepsilon^{\circ} + \varepsilon_c + \varepsilon_a + IR \qquad (32)$$

The cell resistance, R, consisted mainly of electrolyte

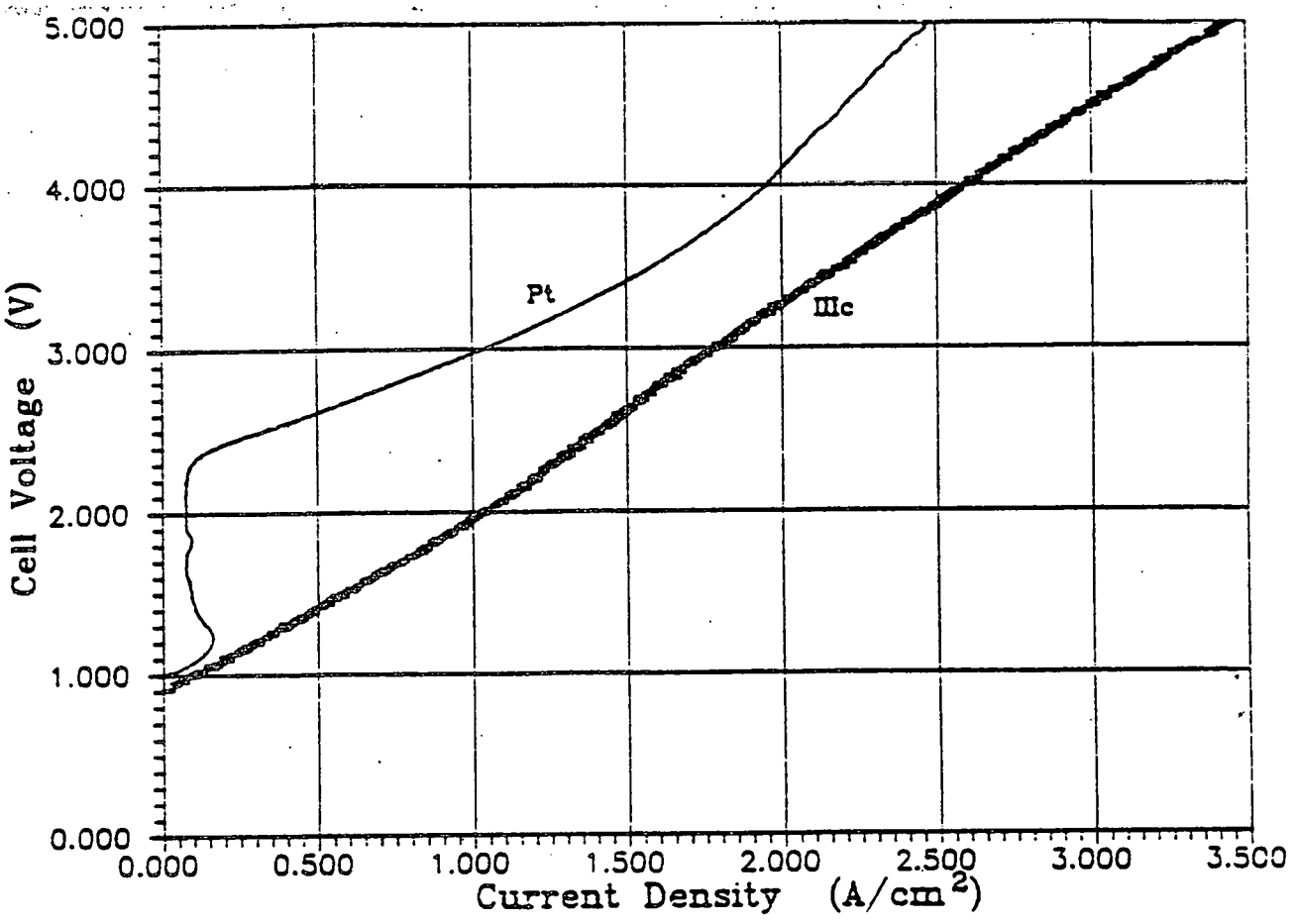

Figure 26 Voltage Sweeps on Pt and IIIc at 1 V/s for Test V

resistance since 3/16" dia. stainless steel rods were used for current leads and high surface area connections were used at all contact points between the anode and cathode. The Pt anode to Al cathode resistance was measured to be 0.234 Ω by an AC impedance bridge. The current, I, equals iA, where A is the electrode area. ε°, the reversible reaction potential, was measured to be 2.27 V, using the curve for Pt in Figure 25. The overvoltage for the cathode, ε_c, was neglected since this overvoltage was small as compared to ε_a and the electrode area for the cathode is

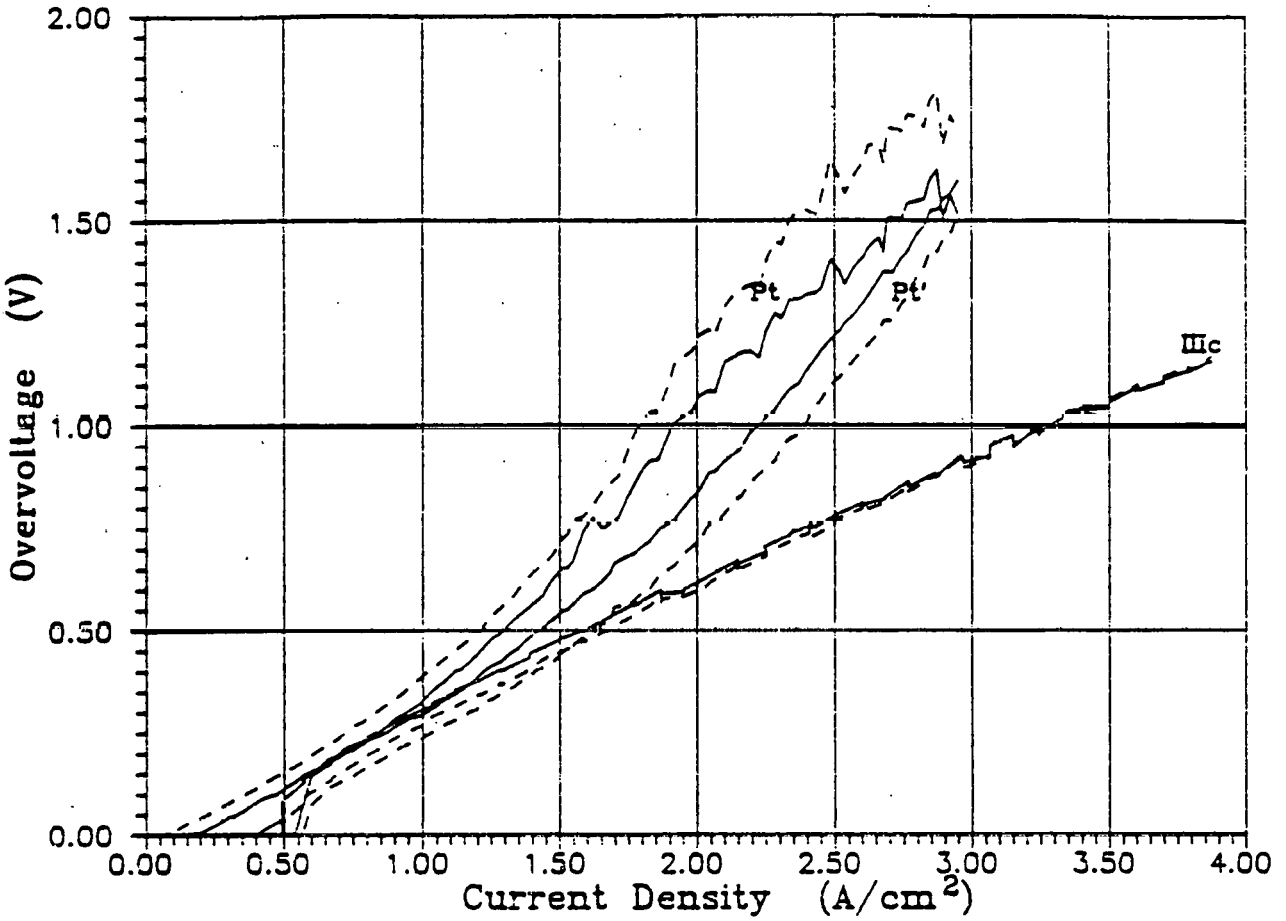

Figure 27 Overvoltage vs. Current Density for Various Anodes for Test V

much larger than the area for the anode. This led to equation 33 :

$$\varepsilon_a = \varepsilon_{cell} - 2.27 - iA(0.234) \qquad (33)$$

Equation 33 was used to calculate the dashed curves given in Figure 27 from the data given in Figure 25. The good agreement supported the view that the potentials given in Figure 27 were indeed anodic overvoltages. The agreement for IIIa data was also good. Since the equation could not predict the overvoltage results of tests I to III in a

similar manner, these earlier results must remain doubtful. Unfortunately, so little is known about the overvoltage of O_2 evolution and how it is affected by measurement technique that the results given here cannot be confirmed.

Chronopotentiometric curves taken using a Pt anode in a melt pre - electrolyzed for 3 hr are given in Figure 28.

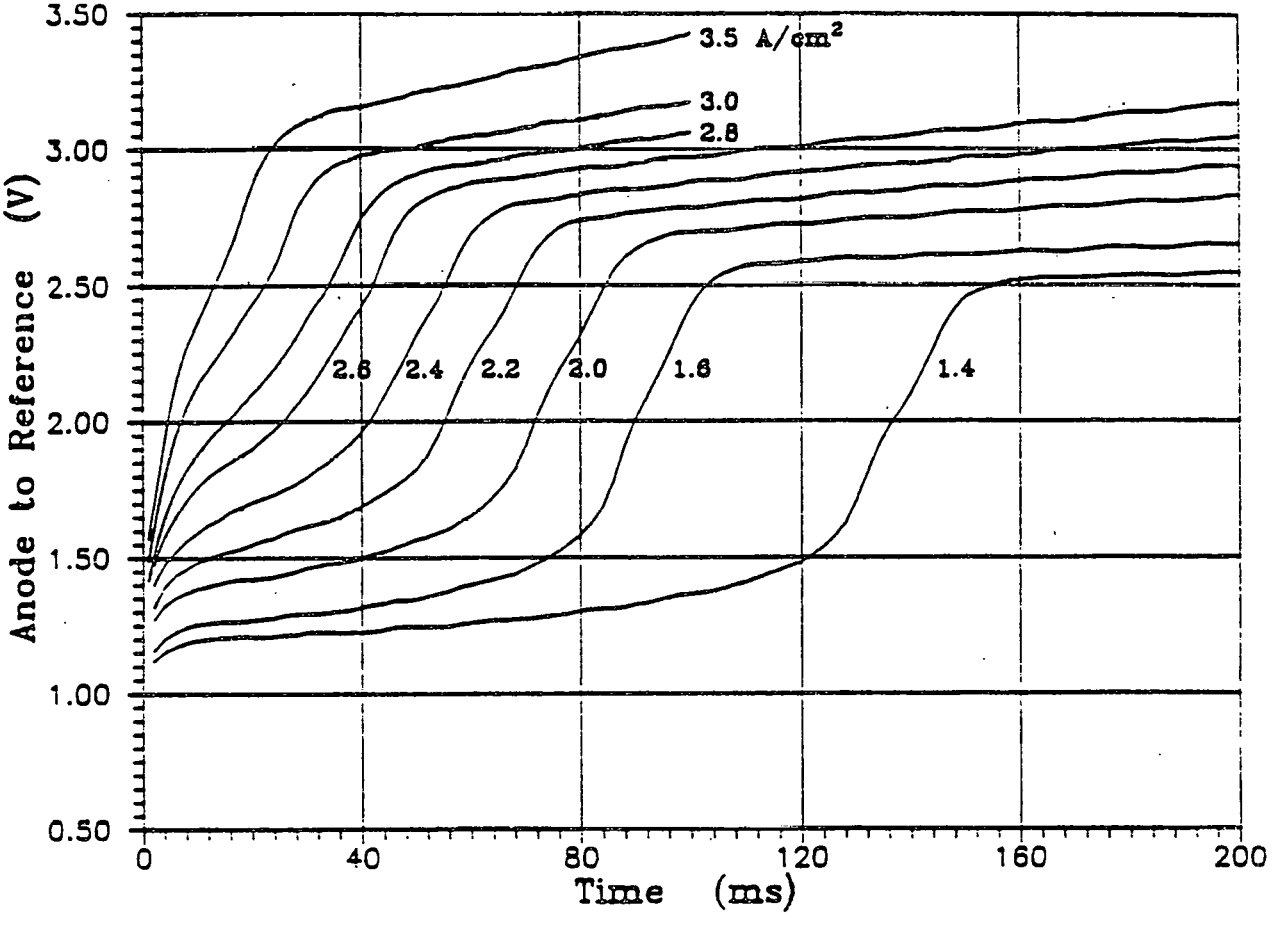

Figure 28 Chronopotentiometric Curves on Pt for a Pre - Electrolyzed Melt for Test V

For these results $i\tau^{1/2}$ was constant at 0.53 ± 0.03 ($As^{1/2}/cm^2$). This led to a concentration somewhat higher than that calculated in Test IV.

6.4 Bath and Metal Analyses

Chemical analyses were carried out by Luvac Inc for Si, Mn, Fe, and Cu in pre - and post - test samples of melt and metal. The results are listed below in Table 9.

ELECTROLYTE

Element	Before Electrolysis	After	
		IIIa	IIIc
Si	0.035	0.002	0.005
Mn	<0.002	0.024	0.015
Fe	0.023	0.016	0.015
Cu	0.002	0.011	0.005

METAL

Element	Before Electrolysis		After	
	IIIa	IIIc	IIIa	IIIc
Si	0.036	0.023	0.13	0.10
Mn	0.003	0.002	0.084	0.095
Fe	0.115	0.056	0.16	0.081
Cu	-	<0.001	-	0.007

Table 9 Pre - and Post - Test Chemical Analyses of Electrolyte and Metal in Weight %

The analyses of Si demonstrated the effect of pre - electrolysis. The Si content of the metal increased while the electrolyte concentration decreased. The Fe content of the electrolyte decreased. This was a result of the reduction, by pre - electrolysis, of the electrolyte concentration followed by a concentration increase resulting from the ferrite electrolysis. This Fe content was

equivalent to a Fe_2O_3 content of 0.022 wt%. DeYoung (128) reports a Fe_2O_3 solubility of 0.13 wt% for a bath ratio of 1.1, and an alumina content of 6.5 % at 960°C. For the present study, a higher alumina content of 11 % would probably result in a lower Fe_2O_3 solubility. It was also possible that the Fe_2O_3 content was below saturation. The slight difference this might cause in the calculation of ΔG_{29} was compensated for by the Fe content in the metal being below saturation as well.

The most accurate calculation of the corrosion rate used the Mn analyses as they were near zero before electrolysis. However, it was realized that error in the calculation could be introduced as a result of the evaporation of the metal fluorides from the molten electrolyte. The corrosion rate calculated here was then the lowest possible value. Using the initial salt and metal weights, the amount of Mn corroded from the ferrite to the salt and metal was calculated to be 0.132 g for IIIa and 0.115 g for IIIc. This was the result of the corrosion of 0.263 g of IIIa oxide, and 0.248 g IIIc oxide. Using the crystal densities given in Table 5, this was calculated to be equivalent to 2.4 mm of IIIa, and 4.1 mm of IIIc. These lengths compared well with the observed lengths of crystal corroded. Calculated wear rates were 94 ($mg/hrcm^2$) for IIIa, and 95 for IIIc, or in other units : 0.94 (kg/hrm^2) for IIIa, and 0.95 for IIIc. The close agreement of the wear rates indicated that the amount of CuO in IIIc did not provide any significant resistance to corrosion. It was also observed that these corrosion rates were so high as to preclude the use of these materials as dimensionally stable anodes.

6.5 Anodic Reaction Mechanism

The results detailed above indicated that the ferrite samples did corrode during electrolysis. Some of the corrosion products were electrolyzed into the metal while the remainder stayed in the electrolyte. The anodic reaction was complex, since four reactions could be taking place in conjunction, depending upon the applied potential. These reactions were the electrochemical corrosion of the ferrite, the chemical dissolution of the ferrite, the electrolysis of dissolved corrosion products, and the electrolysis of Al_2O_3. The chemical dissolution of the ferrite would be independent of potential. While no definite indication of electrochemical corrosion could be inferred from the results, the possibility could not be eliminated. The results shown in Figure 25 for IIIc showed that if electrochemical corrosion took place, it did so at potentials above those required for the electrolysis of dissolved corrosion products. The electrolysis of corrosion products began at potentials as low as 0.83 V with the electrolysis of dissolved Fe_2O_3. The electrolysis of other dissolved oxides took place at higher potentials, followed by the electrolysis of dissolved alumina at potentials higher than 2.2 V. While the results did not indicate any specific mechanism for any of these reactions, certain possibilities can be discussed. It was possible to show that the observed behavior of the anode was reasonable considering what was is known about the chemistry of the electrolyte.

It has been postulated (7), and some evidence exists to support the theory, that the major ionic species in a molten Al_2O_3 - Na_3AlF_6 solution are : Na^+, F^-, $AlOF_x^{1-x}$, and AlF_y^{3-y}, with $3 \leq x \leq 5$ and $4 \leq y \leq 6$. Thonstad (121) has postulated the following anodic reaction mechanism for the evolution of

O_2 on Pt :

$$AlOF_x^{1-x} \Longrightarrow AlF_x^{3-x} + O^{2-} \quad (34)$$

$$O^{2-} \rightleftharpoons O(ad) + 2e^- \quad (35)$$

$$O^{2-} + O(ad) \rightleftharpoons O_2(ad) + 2e^- \quad (36)$$

$$O_2(ad) \Longrightarrow O_2(g) \quad (37)$$

Reaction 34 was fast and the reaction rate was controlled by either 35 or 36. Thermodynamic analyses (134) showed that oxides that will co - deposit with Al do not form stable fluorides in preference to AlF_3. So these oxides probably formed an oxy - flouride complex. This complex could be formed by either chemical dissolution or electrochemical corrosion :

$$MO_{\frac{n}{2}} + xF^- \rightleftharpoons MOF_x^{n-2-x} + \frac{n-2}{2}O^{2-} \quad (38)$$

$$MO_{\frac{n}{2}} + xF^- \rightleftharpoons MOF_x^{n-2-x} + \frac{n-2}{4}O_2(g) + (n-2)e^- \quad (39)$$

For n = 2 a complex like $M_2OF_x^{2n-2-x}$ could form instead. The discharge of the metal - containing complex would follow a reaction scheme like 34 to 37. The combined chemical reaction found using the chronopotentiometric technique on Pt, discussed in section 6.3.2, would be the equivalent of reaction 34 :

$$MOF_x^{n-2-x} \rightleftharpoons MF_x^{n-x} + O^{2-} \quad (40)$$

The electrochemical reactions following reaction 40 would be identical to 35 and 36. It was seen that any metal oxide could undergo this anodic reaction. Since no completely

insoluble oxide is known, the important question becomes one of electrochemical stability. Once the oxide is in solution, following reaction 38 or 39, for example, the subsequent discharge by reactions 40, etc. can only take place if the oxide is less electrochemically stable than Al_2O_3, as are the oxides of Fe, Mn, and Cu. In fact, nearly all of the oxides of interest to the aluminum industry as inert anode materials will co - deposit with Al. However, as discussed in reference 134, a few oxides do exist which will not co - deposit. It is expected that these are the materials that will be used to solve the inert anode problem.

6.6 Summary

An experimental apparatus and procedure was developed to test different anode materials in a bench - scale Hall cell. The cell incorporated a novel reference electrode design that could be more widely applied to thermodynamic emf studies as well as to further overvoltage measurements. The replacement of the alumina crucible with a boron nitride crucible could allow testing for longer electrolysis times with lower Al_2O_3 concentrations in the bath. The steady state technique was used to measure overvoltage, and provided a measure of the melt contamination level, as well as the reversible cell potential. The chronopotentiometric or galvanostatic pulse technique was used to confirm relative melt contamination levels, reversible potentials, and yielded some information on the anodic reaction mechanism. While the voltage sweep technique showed some usefulness, few measurements were taken due to a lack of reproducibility. If test times could be extended by using a BN crucible, since it was found that an alumina crucible would last less than 50 hr, then greater care could be taken

during measurement. For example, a wait of several minutes after each voltage sweep would allow the electrolyte to eliminate concentration gradients by convective stirring. A number of measurements with identical sweep rates could be taken and then averaged. Unfortunately, the melt composition will probably change as more current is passed, especially if a significant impurity concentration is present.

The experiments described in this section provided an awareness of the important issues that must be considered when testing anode materials. Testing took place in a dry atmosphere under conditions where evaporation losses were minimized. The behavior of a completely inert anode such as Au or Pt was established in a melt purified as much as possible using pre - electrolysis with the same anode. Completely inert anodes provided a comparative basis for the study of the behavior of non - inert materials. A stable reference electrode provided a means of isolating the anode behavior from the behavior of the rest of the cell. The iR drop was measured using a current interrupter, since this potential was a significant part of the measured anode to reference voltage. The problem of noise resulting from gas evolution on the anode was taken into account. At longer times, digital averaging was used to eliminate much of the noise effect. Other measurements were made at short enough times so that a significant amount of gas was not generated. Such transient techniques precluded the use of a current interrupter. This encouraged the use of galvanostatic techniques, where the iR drop is constant as well. Testing times were long enough so that a measurable amount of corrosion took place during electrolysis. Test times would have to be even longer than the 13 hr periods used in this study if the test specimens either passivated or had a very low solubility.

Some problems can not be solved using better experimental techniques and must instead await the results of many more successful investigations. The data base concerning inert anode testing was found to be small and inconsistent. The complex, and not well understood bath chemistry, made the interpretation of results difficult. The high temperature, and corrosive nature of the electrolyte restricted cell design and did not allow physical observation of the cell during operation. The tendency of the melt to creep gave rise to significant uncertainties in electrode areas, particularly those used for the ferrite anodes.

Not only has the present study laid down, for the first time certain experimental techniques that should be followed when testing possible inert anode materials, but it has also obtained a number of useful results concerning the anodic behavior of manganese ferrites. The most important result, that the ferrite corrodes, was indicated by electrochemical measurement and confirmed by post - test sample examination and salt and metal analyses. A wear rate was calculated using the Mn accumulation. The electrochemical measurements showed that the Fe_2O_3 concentration in the melt approached saturation as a result of the electrolysis of the ferrite. The presence of Fe_2O_3 in the melt lowered the reversible potential of the cell to near the reversible decomposition potential of Fe_2O_3, 0.84 V. The small amount of CuO in sample IIIc did not reduce the wear rate of the sample. If the oxide components of an inert anode just dissolved up to the saturation limit without any further losses, corrosion could be halted. The present study proved that the electroactive impurities generated by anode corrosion and/or dissolution did not remain in the melt but co - deposited with aluminum. In this way corrosion continued for as long as the anode was in the melt. Two possible routes to an inert anode remain. The first is the use of some means of

passivation that can operate at temperatures around 1000°C, where most kinetic barriers are usually ineffective. The second route is through the use of oxides that will not co - deposit with aluminum. The use of such oxides has not yet been considered since their solubilities are high enough to alter bath chemistry. However, these oxides exist (134), and their use bears further study.

7. Conclusions

In this study care was taken to ensure that testing was carried out upon samples equilibrated with their environment. Single crystal specimens were prepared and annealed so that each had the same preparation. The intrinsic property of electrical conductivity was measured over the temperature range of spinel phase stability at 1 atmosphere of oxygen. Samples that were single phase spinels at 960°C and P_{O_2} = 1 were selected for bench - scale Hall cell testing. The result of this attention to phase equilibria is that results were interpreted in terms of intrinsic properties, not influenced by sample preparation. The study has led to a number of useful conclusions both in terms of inert anode development and materials science.

Those conclusions that are of interest to the further development of inert anodes are :

[1] Spinel ferrites that are stable at 960°C and P_{O_2} = 1 atm will not have conductivities higher than 10 $(\Omega cm)^{-1}$ under these conditions. Metastable ferrites will precipitate a low conductivity Fe_2O_3 phase. This limit was seen from measurements made upon the manganese ferrites used in this study and is known to apply to other ferrites as well. This places severe restrictions upon the design of a cell utilizing an all - oxide anode. This anode would have to be 100 times thinner than a carbon anode in order not to increase the bulk anode voltage drop. A practical anode that utilizes a ferrite matrix would have to be made more conductive by the addition of a second metal phase to form a cermet.

[2] This study has shown that the ferrite phase of an anode will corrode and that the corrosion products will co -

deposit with aluminum. The wear rate found for the manganese ferrites tested in this study indicated that these materials would not make useful anodes. In fact, all ferrites are unacceptable materials for use in inert anode formulation. This conclusion led to the creation of a revised set of materials selection criteria. In this set, the criterion of co - deposition has primary importance, replacing the old design criterion of low solubility.

[3] The solution to the inert anode problem lies either in some means of passivation protection for the ferrite, or in the use of oxides that will not co - deposit with aluminum. The new materials selection criteria have identified a new group of candidate materials for future testing.

A number of conclusions are more of scientific interest :

[4] The electrical conductivity measurements reported in this study are unique in that they are measured upon stable samples all at 1 atmosphere of oxygen. The attention paid to sample equilibration has resulted in the conclusion that the activation energy for conduction of high iron containing ferrites has a strong dependence upon higher values of the P_{O_2}. It is likely that much of the variation in the activation energies reported in the literature was a result of a variation in the P_{O_2} used for preparation rather than just a change in composition.

[5] Electrical conductivity of the manganese ferrites decreased with increasing manganese content. While the measurements confirmed that the mobility was an activated process, the small polaron hopping model was not followed.

[6] The anodic reaction mechanism of a ferrite anode was

complex, thus adding to the difficulty of interpreting measurements. However, based on the results of this study, the corrosion mechanism of the ferrites consisted of a slow chemical dissolution step, followed by a more rapid decomposition reaction of the metal oxide - containing complex ion. The O^{2-} ion thus released was electrolyzed to form oxygen gas at the anode, and the metal ion co - deposited at the cathode. It was not possible to identify the rate controlling step, although it does not appear to be diffusion, even at relatively high current densities.

A number of accomplishments resulting from the bench - scale Hall cell testing experiments are also given :

[7] Very little work has been reported on the behavior of oxide anodes in an electrolyte as corrosive as molten cryolite. This study pointed out important experimental considerations that must be followed in order that results be reproducible and open to interpretation. The electrochemical techniques most useful to the study of possible inert anodes were identified and applied. The experiments demonstrated the means by which <u>in situ</u> measurements of anodic corrosion could be made. Previous studies of candidate materials relied exclusively on pre - and post - test sample examination and chemical analyses.

[8] The use of stable reference electrode allowed the measurement of the steady state overvoltage for oxygen evolution on various anodes. Very few measurements of this type are available.

[9] The cell design, measuring instrumentation, and experimental procedure would be applicable to any electrochemical investigation. This system provides an advantageous alternative to traditional potentiostat - based systems.

8. Recommendations for Further Study

A number of research opportunities in both anode development and materials science can be outlined. If ferrites are to be used as anodes, the passivation mechanism must be confirmed. Cell testing must be carried out in the manner outlined in this study. Polycrystalline samples with a higher CuO content could be prepared by traditional ceramic techniques. Samples containing Cu metal should also be obtained. A BN crucible would be an asset to further cell testing as longer test times will be needed and lower Al_2O_3 contents could be used. The use of a BN crucible would probably necessitate the occasional addition of Al_2O_3 to the electrolyte. An electrode that passivates will show an initially high residual current that will drop to zero as complete surface passivation occurs. The composition and stability of this surface layer is of interest. If complete passivation does not occur, then the use of ferrites must be abandoned in favor of oxides that do not co - deposit. Such materials have been identified (134). The use of these oxides will result in different bath chemistries due to their high solubilities. Further investigation into the bath chemistry would be needed in order to demonstrate the ability of the electrolyte to still produce high purity aluminum.

The conductivity apparatus and procedure developed in this study could be applied to many different materials. A need exists for measurements made upon stable materials under controlled atmosphere. The P_{O_2} dependence of the conductivity of high iron containing ferrites is also of interest. The effect of P_{O_2} upon activation energy must be confirmed, and further measurements are required for the application of suggested models. The apparatus could be

used to make Seebeck coefficient measurements if a sacrifice of some automation could be tolerated. It may be necessary to use more complicated mobility models in order to interpret results. The use of a technique such as Mössbauer spectroscopy in a magnetic field could be used in conjunction with the electrical property measurements in order to arrive at a cation distribution. The literature survey showed that the conductivity mechanism and cation distribution of manganese ferrites remains a puzzle.

9. Appendices

I Crystal Sample Analyses

Luvak Inc.
722 Main Street
Boylston, MA 01505
Tel. (617) 869-6401

Analytical Report No. 0-1765

REQUESTED BY Massachusetts Institute of Technology
Cambridge, MA 02139

ATTENTION Alan McLeod
Room 8-111

Invoice Date: 12/22/86

Invoice Number	Customer's Order Number	Customer's Requisition Number	Date Received
006329	GF-R-694424	544350	12/10/86

DESCRIPTION

3 Samples, Manganese Ferrite, analzyed for Iron, Manganese and Oxygen content.

6 Samples, Manganese Ferrite, analyzed for Iron, Manganese, Oxygen and Copper content.

RESULTS

SAMPLE IDENTIFICATION	IRON %	MANGANESE %	OXYGEN %
Sample # Ia	58.6	11.7	29.4
IIa	39.9	29.7	29.1
IIIa	20.9	50.0	28.7

SAMPLE IDENTIFICATION	IRON %	MANGANESE %	OXYGEN %	COPPER %
Sample # Ib	55.9	12.2	29.0	3.33
Ic	53.3	13.5	29.0	5.27
IIb	42.9	28.7	29.5	.12
IIc	37.9	29.3	28.7	4.65
IIIb	21.6	47.1	28.4	2.37
IIIc	21.1	45.9	28.2	3.94

LUVAK INC.
By

II Conductivity Program Listing

```
INTEGER SCALAR IT
INTEGER SCALAR RAT
INTEGER SCALAR RATE
INTEGER SCALAR S.TIME
INTEGER SCALAR A.TIME
INTEGER SCALAR W.TIME
INTEGER SCALAR STATUS
INTEGER SCALAR V.DC.MAX
INTEGER SCALAR TICKS
INTEGER SCALAR NEW.T
INTEGER SCALAR LOW.T
INTEGER SCALAR HIGH.T
INTEGER SCALAR SINT.T
INTEGER SCALAR ZZ
INTEGER SCALAR STP
INTEGER SCALAR DIRECT
INTEGER SCALAR N.PTS
INTEGER SCALAR START.POINT
INTEGER SCALAR N.SBK
INTEGER SCALAR SKIP
INTEGER DIM[ 100 ] ARRAY XS
INTEGER DIM[ 100 ] ARRAY YS
REAL SCALAR A0
REAL SCALAR A1
REAL SCALAR A2
REAL SCALAR A3
REAL SCALAR A4
REAL SCALAR F.SET
REAL SCALAR MV
REAL SCALAR V.SAMP.MAX
REAL SCALAR LENGTH
REAL SCALAR AREA
REAL SCALAR EX
REAL SCALAR EY
REAL SCALAR EX2
REAL SCALAR EY2
REAL SCALAR EXY
REAL SCALAR M
REAL SCALAR B
REAL SCALAR S2
REAL SCALAR ERR.M
REAL SCALAR ERR.B
REAL SCALAR R
REAL SCALAR DELTA.T
REAL SCALAR LR.VOLT
REAL SCALAR DROOP
REAL DIM[ 30 ] ARRAY X
REAL DIM[ 30 ] ARRAY Y
REAL DIM[ 120 ] ARRAY WAIT
REAL DIM[ 180 ] ARRAY SBK.SAMP
REAL DIM[ 61 , 7 ] ARRAY DATA
REAL DIM[ 61 , 4 ] ARRAY SBK
60 STRING SAMPLE.NAME
30 STRING X.LABEL
```

```
30 STRING Y.LABEL
\
0 0 A/D.TEMPLATE COLD.JUNCTION
1 1 A/D.TEMPLATE LEFT.THERM
2 2 A/D.TEMPLATE RIGHT.THERM
3 3 A/D.TEMPLATE CURRENT
4 4 A/D.TEMPLATE VOLTAGE
5 5 A/D.TEMPLATE DC.OUTPUT
6 6 A/D.TEMPLATE DIVIDER.OUTPUT
7 7 A/D.TEMPLATE LR.POT
\
0 0 D/A.TEMPLATE F.CONTROL
1 1 D/A.TEMPLATE DC.CONTROL
\
COLD.JUNCTION 3 A/D.GAIN
LEFT.THERM 3 A/D.GAIN
RIGHT.THERM 3 A/D.GAIN
CURRENT 2 A/D.GAIN
VOLTAGE 1 A/D.GAIN
DC.OUTPUT 1 A/D.GAIN
DIVIDER.OUTPUT 2 A/D.GAIN
LR.POT 3 A/D.GAIN
\
GRAPHICS.DISPLAY
0 0.1 VUPORT.ORIG
1.8 0.85 VUPORT.SIZE
VUPORT ISEE
23 3 24 79 WINDOW BOTLN
NORMAL.DISPLAY (DEF)
\
: IMPRESS
   STP 1 = IF EXIT THEN
   NORMAL.DISPLAY SCREEN.CLEAR HOME
   INVERSE.ON 0 1 GOTO.XY 25 SPACES ." STATUS" 25 SPACES "DATE "TYPE 8 SPACES
      5 "TIME "LEFT "TYPE 3 SPACES
   0 24 GOTO.XY 80 SPACES INVERSE.OFF
   0 3 GOTO.XY ." TEMPERATURES IN DEGREES C :" 20 SPACES ." DESIRED ="
   CR CR ." SETPOINT =       , ACTUAL:  LEFT =" 9 SPACES ." RIGHT ="
      9 SPACES ." AVERAGE ="
   CR ." LEFT MINUS RIGHT =" 7 SPACES ." ,  POTENTIAL DIFFERENCE =" 9 SPACES
      ." (mV), COEFF. ="
   CR CR ." HEATING RATE =" 5 SPACES ." (DEG/HR),  SETTLING TIME =    (MIN)"
   CR ." MAXIMUM SAMPLE VOLTAGE =" 8 SPACES ." (V)"
   CR CR DATA [ 1 , 1 ] 0 = IF CR CR CR CR ELSE
      ." DATA TAKEN AT" 7 SPACES ." DEGREES C:"
      CR CR ." RESISTANCE =" 9 SPACES ." +/-" 7 SPACES ." (OHM),  COND. ="
        9 SPACES ." (OHM-CM)-1"
      CR ." INTERCEPT =" 8 SPACES ." +/-" 8 SPACES ." (VOLT), GOODNESS OF FIT,
      ." R =" 9 SPACES ." IN     (MIN)"
      CR ." SEEBECK COEFF. =" 9 SPACES ." +/-" 9 SPACES ." USING" 5 SPACES
         ." POINTS" THEN
   CR 29 SPACES ." ====================="
   64 18 GOTO.XY ." DATA SETS STORED"
;
: LABEL.AXES
   NORMAL.COORDS
   0.55 0.05 POSITION HORIZONTAL 0 LABEL.DIR X.LABEL CENTERED.LABEL
   0.02 0.74 POSITION VERTICAL 270 LABEL.DIR Y.LABEL CENTEREL.LABEL
```

```
   0 LABEL.DIR WORLD.COORDS
;
: CONV.T
   273.15 + 1. SWAP / 1000. *
;
: CONV.R
   1. SWAP / LENGTH * AREA / LN
;
: PROMPT
   INTEN.OFF
   0 23 GOTO.XY 80 SPACES
   0 23 GOTO.XY ." NEW VALUE = " #INPUT
   INTEN.ON
;
: CHANGES
   0 23 GOTO.XY
   0 STP = IF ." FREEZE; " ELSE ." THAW  ; " THEN
   ." CONTINUE; CHANGE: MAX. SAMP. VOLTAGE, HEATING RATE, OR SETTLING TIME"
   INTEN.ON 0 23 GOTO.XY 0 STP = IF ." F" ELSE ." T" THEN
   8 23 GOTO.XY ." C" 26 23 GOTO.XY ." M"
   46 23 GOTO.XY ." H" 63 23 GOTO.XY ." S"
   KEY CASE
      70 OF 1 STP := ENDOF
      84 OF 0 STP := ENDOF
      77 OF PROMPT V.SAMP.MAX := 6 4 FIX.FORMAT 25 9 GOTO.XY V.SAMP.MAX . ENDOF
      72 OF PROMPT RATE := 3 0 FIX.FORMAT 15 8 GOTO.XY RATE . ENDOF
      83 OF PROMPT S.TIME := 2 0 FIX.FORMAT 46 8 GOTO.XY S.TIME . ENDOF
      67 OF ENDOF
   ENDCASE
   0 23 GOTO.XY 80 SPACES
   1 STP = IF 30 23 GOTO.XY ." DISPLAY FROZEN" THEN
   INTEN.OFF
;
: TEST
   ?KEY IF KEY 124 = IF CHANGES THEN THEN
;
: SEC.DELAY
   1 + 1 DO
      1000 MSEC.DELAY
      TEST
   LOOP
;
: PLOT.1
   STP 1 = IF EXIT THEN
   GRAPHICS.DISPLAY
   ISEE
   " +" SYMBOL
   X 1000. * Y XY.AUTO.PLOT
   " mA" X.LABEL ":= " V" Y.LABEL ":= LABEL.AXES
   SOLID
   X [ 1 ] 1000. * X [ 1 ] M * B + POSITION
   X [ 30 ] 1000. * X [ 30 ] M * B + DRAW.TO
   8 4 FIX.FORMAT
   BOTLN HOME ." SLOPE = " M . ."  +/-" ERR.M . ."  (OHMS)"
   7 6 FIX.FORMAT CR
   BOTLN ." GOODNESS OF FIT = " R .
   (DEF)
;
```

```
: PLOT.2
   STP 1 = IF EXIT THEN
   GRAPHICS.DISPLAY
   ISEE
   HORIZONTAL LINEAR 0 TICKS 1 - 10 * WORLD.SET
   WAIT [ 1 ] A0 := WAIT [ 1 ] A1 :=
   TICKS 2 DO
      A0 WAIT [ I ] MIN A0 :=
      A1 WAIT [ I ] MAX A1 :=
   LOOP
   VERTICAL LINEAR A0 3. * A1 - 2. / A1 3. * A0 - 2. / WORLD.SET
   WORLD.COORDS
   XY.AXIS.PLOT
   " TIME (MIN)" X.LABEL ":= " OHMS" Y.LABEL ":= LABEL.AXES
   AXMIN AYMIN POSITION
   " +" SOLID&SYMBOL
   TICKS 1 DO
      I 1 - 10 * WAIT [ I ] DRAW.TO
   LOOP
   7 4 FIX.FORMAT
   BOTLN HOME ." LATEST RESISTANCE ERROR =" ERR.M .
   (DEF)
;
: PLOT.3
   STP 1 = IF EXIT THEN
   GRAPHICS.DISPLAY
   ISEE
   0 IT :=
   BEGIN
      IT 1 + IT :=
      IT 62 = IF IT 62 = ELSE 0 DATA [ IT , 2 ] = THEN
   UNTIL
   IT 1 - IT :=
   TICKS 2 < IF DATA [ 1 , 1 ] ELSE NEW.T THEN DUP A0 := A1 :=
   TICKS 2 < IF DATA [ 1 , 2 ] ELSE WAIT [ TICKS 1 - ] THEN DUP A2 := A3 :=
   IT 1 + 1 DO
      DATA [ I , 1 ] A0 > IF DATA [ I , 1 ] A0 := THEN
      DATA [ I , 1 ] A1 < IF DATA [ I , 1 ] A1 := THEN
      DATA [ I , 2 ] A2 > IF DATA [ I , 2 ] A2 := THEN
      DATA [ I , 2 ] A3 < IF DATA [ I , 2 ] A3 := THEN
   LOOP
   HORIZONTAL LINEAR A0 CONV.T A1 CONV.T WORLD.SET
   VERTICAL LINEAR A2 CONV.R A3 CONV.R WORLD.SET
   WORLD.COORDS
   XY.AXIS.PLOT
   " (10)3/T" X.LABEL ":= " LN(COND)" Y.LABEL ":= LABEL.AXES
   " +" SOLID&SYMBOL
   DATA [ 1 , 1 ] CONV.T DATA [ 1 , 2 ] CONV.R POSITION
   IT 1 + 2 DO
      DATA [ I , 1 ] CONV.T DATA [ I , 2 ] CONV.R DRAW.TO
   LOOP
   " +" SYMBOL
   TICKS 1 > IF NEW.T CONV.T WAIT [ TICKS 1 - ] CONV.R DRAW.TO THEN
   TICKS 1 > IF BOTLN CR ." LATEST DATA IS SHOWN AS SINGLE POINT." THEN
   (DEF)
;
: BLANK.1
   0 18 GOTO.XY 40 SPACES
```

```
;
: BLANK.2
   0 22 GOTO.XY 20 SPACES
;
: BLANK.3
   25 22 GOTO.XY 60 SPACES
;
: OTH.UPDATE
   STP 1 = IF EXIT THEN
   INTEN.ON
   3 0 FIX.FORMAT 15 8 GOTO.XY RATE .
   2 0 FIX.FORMAT 46 8 GOTO.XY S.TIME .
   6 4 FIX.FORMAT 25 9 GOTO.XY V.SAMP.MAX .
   INTEN.OFF
;
: DATA.UPDATE
   STP 1 = IF EXIT THEN
   0 IT :=
   BEGIN
      1 IT + IT :=
      IT 62 = IF IT 62 = ELSE 0 DATA [ IT , 2 ] = THEN
   UNTIL
   IT 1 - IT :=
   IT 0 = IF 57 18 GOTO.XY 0 . EXIT THEN
   5 0 FIX.FORMAT 14 11 GOTO.XY DATA [ IT , 1 ] .
   7 4 FIX.FORMAT 13 13 GOTO.XY DATA [ IT , 2 ] .
   5 4 FIX.FORMAT 25 13 GOTO.XY DATA [ IT , 3 ] .
   6 3 FIX.FORMAT 48 13 GOTO.XY LENGTH DATA [ IT , 2 ] / AREA / .
   6 5 FIX.FORMAT 12 14 GOTO.XY DATA [ IT , 4 ] .
   23 14 GOTO.XY DATA [ IT , 5 ] .
   7 6 FIX.FORMAT 59 14 GOTO.XY DATA [ IT , 6 ] .
   3 0 FIX.FORMAT 70 14 GOTO.XY DATA [ IT , 7 ] FIX .
   7 5 FIX.FORMAT 17 15 GOTO.XY SBK [ IT , 2 ] .
   29 15 GOTO.XY SBK [ IT , 3 ] .
   3 0 FIX.FORMAT 43 15 GOTO.XY SBK [ IT , 4 ] FIX .
   60 18 GOTO.XY IT .
;
: SHOW.STATUS
   STP 1 = IF EXIT THEN
   STATUS CASE
      0 OF BLANK.1 BLANK.2 BLANK.3 0 22 GOTO.XY ." RAISING TZMPERATURE" ENDOF
      1 OF BLANK.2 0 22 GOTO.XY ." AT TEMPERATURE" ENDOF
      2 OF BLANK.1 0 18 GOTO.XY ." WAITING     MINUTES" ZZ 1 = IF 18 18 GOTO.XY
           ."   " THEN 3 0 FIX.FORMAT 8 18 GOTO.XY ZZ . ENDOF
      3 OF BLANK.1 0 18 GOTO.XY ." MEASURING RESISTANCE" ENDOF
      4 OF BLANK.3 25 22 GOTO.XY ." SAMPLE POLARIZED" ENDOF
      5 OF BLANK.3 25 22 GOTO.XY ." CONSTANT RESISTANCE" ENDOF
      6 OF BLANK.1 BLANK.2 BLANK.3 0 22 GOTO.XY ." LOWERING TEMPERATURE" ENDOF
      7 OF BLANK.3 ENDOF
      8 OF BLANK.1 0 18 GOTO.XY ." SAVING DATA" ENDOF
      9 OF BLANK.1 0 18 GOTO.XY ." SAVING I - V" ENDOF
      10 OF BLANK.1 0 18 GOTO.XY ." SAVING R - t" ENDOF
      11 OF BLANK.1 0 18 GOTO.XY ." TESTING RANGE OF DC SUPPLY" ENDOF
   ENDCASE
;
: CLUMSY
   BEGIN
      4 2 "TIME "SUB " 00" "=
```

```
   UNTIL
;
: CONVERT.TYPE.R
   1000. * MV :=
   MV 0 < IF 1 RAT := EXIT THEN
   MV 3400. <= IF
      0 A0 :=
      1.6251434E-1 A1 :=
      -2.0454379E-5 A2 :=
      2.5404935E-9 A3 :=
      -1.1767904E-13 A4 := ELSE
   MV 11160. <= IF
      4.5509556E1 A0 :=
      1.1284875E-1 A1 :=
      -2.8603978E-6 A2 :=
      8.5173702E-11 A3 :=
      -1.1440038E-15 A4 := ELSE
   MV 16020. <= IF
      -4.1134459E0 A0 :=
      1.2738464E-1 A1 :=
      -4.3132296E-6 A2 :=
      1.3863582E-10 A3 :=
      -1.5283798E-15 A4 := ELSE
   MV 19530. <= IF
      1.4180146E2 A0 :=
      9.0181346E-2 A1 :=
      -7.4068329E-7 A2 :=
      -1.4487255E-11 A3 :=
      9.4290495E-16 A4 := ELSE
   2 RAT := EXIT THEN THEN THEN THEN 0 RAT :=
   A0 MV A1 * + MV 2 ** A2 * + MV 3 ** A3 * + MV 4 ** A4 * +
;
: ROOM.T
   COLD.JUNCTION A/D.IN -20. 20. A/D.SCALE 0.5 /
;
: LEFT.T
   5 "TIME "LEFT " 23:59" "= IF CLUMSY THEN
   101 1 DO
      LEFT.THERM A/D.IN XS [ I ] :=
      5 MSEC.DELAY
   LOOP
   XS MEAN -20. 20. A/D.SCALE CONVERT.TYPE.R ROOM.T +
;
: RIGHT.T
   5 "TIME "LEFT " 23:59" "= IF CLUMSY THEN
   101 1 DO
      RIGHT.THERM A/D.IN XS [ I ] :=
      LR.POT A/D.IN YS [ I ] :=
      5 MSEC.DELAY
   LOOP
   YS MEAN -20. 20. A/D.SCALE LR.VOLT :=
   XS MEAN -20. 20. A/D.SCALE CONVERT.TYPE.R ROOM.T +
;
: SAMP.T
   LEFT.T RIGHT.T + 2. /
;
: T.UPDATE
   STP 1 = IF 1 SEC.DELAY EXIT THEN
```

```
   INVERSE.ON 72 1 GOTO.XY 5 "TIME "LEFT "TYPE
   INVERSE.OFF INTEN.ON
   4 0 FIX.FORMAT 57 3 GOTO.XY NEW.T .
   5 0 FIX.FORMAT 11 5 GOTO.XY F.SET .
   6 1 FIX.FORMAT 34 5 GOTO.XY LEFT.T EX := EX .
   50 5 GOTO.XY RIGHT.T EY := EY .
   5 0 FIX.FORMAT 68 5 GOTO.XY EX EY + 2. / .
   6 2 FIX.FORMAT 19 6 GOTO.XY EX EY - .
   7 3 FIX.FORMAT 51 6 GOTO.XY LR.VOLT .
   N.SBK 0 = IF 1 N.SBK := THEN
   EX EY - 0 <> IF 5 3 FIX.FORMAT 74 6 GOTO.XY LR.VOLT EX EY - / DUP
      SBK.SAMP [ N.SBK ] := . N.SBK 180 = IF 0 N.SBK := THEN
      N.SBK 1 + N.SBK := THEN
   INTEN.OFF
;
: ALL.UPDATE
   T.UPDATE
   OTH.UPDATE
   DATA.UPDATE
   SHOW.STATUS
;
: DATA.SAVE.INIT
   FILE.TEMPLATE
      3 COMMENTS
      REAL DIM[ 61 , 7 ] SUBFILE
   END
   " DATA.AST" DEFER> FILE.CREATE
   FILE.TEMPLATE
      3 COMMENTS
      REAL DIM[ 61 , 4 ] SUBFILE
   END
   " SBK.AST" DEFER> FILE.CREATE
;
: DATA.SAVE
   8 STATUS := SHOW.STATUS
   " DATA.AST" DEFER> FILE.OPEN
   SAMPLE.NAME 1 >COMMENT
   5 "TIME "LEFT "  ON " "CAT "DATE "CAT 2 >COMMENT
   " T (C), R (OHM), ERR.R, B (V), ERR.B, R, t (MIN)" 3 >COMMENT
   DATA ARRAY>FILE
   FILE.CLOSE
;
: SBK.SAVE
   " SBK.AST" DEFER> FILE.OPEN
   SAMPLE.NAME 1 >COMMENT
   5 "TIME "LEFT "  ON " "CAT "DATE "CAT 2 >COMMENT
   " T (C), SEEBECK COEFFICIENT IN V, ERROR ON SEEBECK, #POINTS" 3 >COMMENT
   SBK ARRAY>FILE
   FILE.CLOSE
;
: WAIT.SAVE
   10 STATUS := SHOW.STATUS
   FILE.TEMPLATE
      3 COMMENTS
      REAL DIM[ 120 ] SUBFILE
   END
   I 9 > IF 2 0 FIX.FORMAT ELSE 1 0 FIX.FORMAT THEN
   " WAIT" I "." "CAT " .AST" "CAT DEFER> FILE.CREATE
```

```
   " WAIT" I "." "CAT " .AST" "CAT DEFER> FILE.OPEN
   SAMPLE.NAME 1 >COMMENT
   5 "TIME "LEFT "  ON " "CAT "DATE "CAT 2 >COMMENT
   " OHMS VS TIME, 10 MIN PER POINT AT " 6 1 FIX.FORMAT DATA [ I , 1 ] "."
      "CAT "  DEGREES C" "CAT 3 >COMMENT
   WAIT ARRAY>FILE
   FILE.CLOSE
;
: IV.SAVE
   9 STATUS := SHOW.STATUS
   FILE.TEMPLATE
      4 COMMENTS
      REAL DIM[ 30 ] SUBFILE
      2 TIMES
   END
   I 9 > IF 2 0 FIX.FORMAT ELSE 1 0 FIX.FORMAT THEN
   " IV" I "." "CAT " .AST" "CAT DEFER> FILE.CREATE
   " IV" I "." "CAT " .AST" "CAT DEFER> FILE.OPEN
   SAMPLE.NAME 1 >COMMENT
   5 "TIME "LEFT "  ON " "CAT "DATE "CAT 2 >COMMENT
   " FIRST ARRAY CURRENT IN A, SECOND VOLTS" 3 >COMMENT
   " TAKEN AT " 6 1 FIX.FORMAT DATA [ I , 1 ] "." "CAT "  DEGREES C AFTER "
      "CAT DATA [ I , 7 ] "." "CAT "  MINUTES." "CAT 4 >COMMENT
   1 SUBFILE X ARRAY>FILE
   2 SUBFILE Y ARRAY>FILE
   FILE.CLOSE
;
: T.OUT
   F.SET 1590. > IF 1590. F.SET := THEN
   F.CONTROL F.SET 0.3903222 / FIX D/A.OUT
;
: T.UP
   F.SET 1. + F.SET := T.OUT
;
: T.DOWN
   F.SET 1. - F.SET := T.OUT
;
: CHECK.T
   NEW.T SAMP.T - EX :=
   EX ABS 2. <= IF EXIT THEN
   0 DIRECT = IF EX -2. < IF T.DOWN ELSE T.UP THEN EXIT THEN
   0. DROOP = IF EX -3. < IF 1 DIRECT = IF T.DOWN THEN
      ELSE -1 DIRECT = IF T.UP THEN THEN EXIT THEN
   0. DROOP > IF EX 3. > IF T.UP THEN EXIT THEN
   0. DROOP < IF EX -3. < IF T.DOWN THEN EXIT THEN
;
: Z
   ZZ :=
   ZZ 0 = IF EXIT THEN
   2 STATUS :=
   ZZ 1 + 1 DO
      IMPRESS ALL.UPDATE 9 SEC.DELAY
      5 "TIME "LEFT " 23:59" "= IF CLUMSY THEN
      TICKS 1 > IF PLOT.1 10 SEC.DELAY ELSE T.UPDATE 9 SEC.DELAY THEN
      TICKS 3 > IF PLOT.2 10 SEC.DELAY ELSE TICKS 1 > IF IMPRESS
         ALL.UPDATE ELSE T.UPDATE THEN 9 SEC.DELAY THEN
      DATA [ 2 , 2 ] 0 > IF PLOT.3 10 SEC.DELAY ELSE TICKS 3 > IF IMPRESS
        ALL.UPDATE ELSE T.UPDATE THEN 9 SEC.DELAY THEN
```

```
      DATA [ 2 , 2 ] 0 > IF IMPRESS ALL.UPDATE ELSE T.UPDATE THEN 9 SEC.DELAY
      T.UPDATE 2 SEC.DELAY
      CHECK.T
      ZZ 1 - ZZ :=
   LOOP
;
: T.SET
   NEW.T :=
   NEW.T SAMP.T - ABS 2. < IF 1 STATUS := SHOW.STATUS EXIT THEN
   NEW.T SAMP.T > IF 1 DIRECT := 0 STATUS := SHOW.STATUS
      ELSE -1 DIRECT := 6 STATUS := SHOW.STATUS THEN
   4000 SYNC.PERIOD
   SYNCHRONIZE
   BEGIN
      5 "TIME "LEFT " 23:59" "= IF CLUMSY 4000 SYNC.PERIOD SYNCHRONIZE THEN
      RATE 900. / DIRECT * F.SET + F.SET := T.OUT
      T.UPDATE
      SYNCHRONIZE TEST
      NEW.T SAMP.T - ABS 20. <
   UNTIL
   0. DROOP :=
   1 I = IF S.TIME Z THEN
   SAMP.T NEW.T - ABS 5. < IF 1 STATUS := SHOW.STATUS EXIT THEN
   BEGIN
      NEW.T SAMP.T - DROOP :=
      DROOP ABS 0.2 * DROOP + F.SET + F.SET := T.OUT
      S.TIME Z
      SAMP.T NEW.T - ABS 5. <
   UNTIL
   0 DIRECT :=
   1 STATUS := SHOW.STATUS
   5 SEC.DELAY
;
: RATS
   RAT 0 = IF EXIT THEN
   INTEN.ON BLINK.TOGGLE
   3 20 GOTO.XY ." PROBLEM"
   BLINK.TOGGLE
   12 20 GOTO.XY
   RAT CASE
      1 OF ." NEGATIVE OFF SCALE ON THERMOCOUPLE." ENDOF
      2 OF ." POSITIVE OFF SCALE ON THERMOCOUPLE." ENDOF
      3 OF ." NOT ENOUGH POWER TO FURNACE." ENDOF
      4 OF ." DIVIDER OUTPUT TOO LOW." ENDOF
      5 OF ." DIVIDER OUTPUT TOO HIGH." ENDOF
      6 OF ." MORE THAN 20 HR WAIT FOR CONSTANT RESISTANCE." ENDOF
   ENDCASE
   3 22 GOTO.XY ." PRESS <RETURN> TO CONTINUE AFTER FIXING."
   "INPUT
   INTEN.OFF CHANGES
   RAT 6 = IF 1 TICKS := THEN
   RAT 3 = IF SAMP.T F.SET := NEW.T T.SET THEN
   0 20 GOTO.XY 80 SPACES
   0 22 GOTO.XY 80 SPACES
   0 RAT :=
;
: LR
   0 EX := 0 EY := 0 EX2 := 0 EY2 := 0 EXY := 0 A1 :=
```

```
   31 1 DO
      X [ I ] EX + EX :=
      Y [ I ] EY + EY :=
      X [ I ] X [ I ] * EX2 + EX2 :=
      Y [ I ] Y [ I ] * EY2 + EY2 :=
      X [ I ] Y [ I ] * EXY + EXY :=
   LOOP
   EX2 30. * EX EX * - A0 :=
   EXY 30. * EX EY * - A0 / M :=
   EX2 EY * EX EXY * - A0 / B :=
   31 1 DO
      Y [ I ] X [ I ] M * B + - 2 ** A1 + A1 :=
   LOOP
   A1 28. / S2 :=
   S2 30. * A0 / SQRT ERR.M :=
   S2 EX2 * A0 / SQRT ERR.B :=
   EXY 30. * EX EY * - EY2 30. * EY EY * - A0 * SQRT / R :=
;
: REPLACE
   SBK.SAMP [ 180 N.SBK - ] SBK.SAMP [ IT ] :=
   N.SBK 1 + N.SBK :=
   IT 1 - IT :=
;
: FILTER
   SBK.SAMP MEAN A0 :=
   0 N.SBK :=
   1 IT :=
   BEGIN
      SBK.SAMP [ IT ] A0 / 2. > IF REPLACE THEN
      IT 1 + IT :=
      IT N.SBK + 180 >
   UNTIL
   1 IT :=
   BEGIN
      SBK.SAMP [ IT ] A0 / 0.5 < IF REPLACE THEN
      IT 1 + IT :=
      IT N.SBK + 180 >
   UNTIL
   N.SBK 170 > IF 0 M := 0 S2 := EXIT THEN
   0 A0 :=
   181 N.SBK - 1 DO
      A0 SBK.SAMP [ I ] + A0 :=
   LOOP
   A0 180. N.SBK - / M :=
   0 A0 :=
   181 N.SBK - 1 DO
      SBK.SAMP [ I ] M - 2 ** A0 + A0 :=
   LOOP
   A0 178. N.SBK - / S2 :=
;
: FEEL
   5 "TIME "LEFT " 23:59" "= IF CLUMSY THEN
   0 IT :=
   BEGIN
      IT 5 + IT :=
      IT 4095 > IF 4 RAT := DC.CONTROL 0 D/A.OUT RATS 5 IT := THEN
      DC.CONTROL IT D/A.CUT
      10 MSEC.DELAY
```

```
      VOLTAGE A/D.IN -1.0 1.0 A/D.SCALE V.SAMP.MAX >=
   UNTIL
   DC.CONTROL 0 D/A.OUT
   IT 5 - V.DC.MAX :=
   V.DC.MAX 60 < IF 5 RAT := RATS MYSELF THEN
;
: RES
   5 "TIME "LEFT " 23:59" "= IF CLUMSY THEN
   V.DC.MAX 30. / MV :=
   31 1 DO
      DC.CONTROL MV I * FIX D/A.OUT
      500 MSEC.DELAY TEST
      101 1 DO
         CURRENT A/D.IN XS [ I ] :=
         VOLTAGE A/D.IN YS [ I ] :=
         5 MSEC.DELAY
      LOOP
      XS MEAN -0.10 0.10 A/D.SCALE 0.2037 / X [ I ] :=
      YS MEAN -1.0 1.0 A/D.SCALE Y [ I ] :=
   LOOP
   DC.CONTROL 0 D/A.OUT
   XS MEAN 4093 > IF V.SAMP.MAX 0.9 * V.SAMP.MAX := 1 Z FEEL 1 Z MYSELF THEN
;
: RESIST
   BEGIN
      11 STATUS := SHOW.STATUS FEEL RATS 1 Z
      3 STATUS := SHOW.STATUS RES LR 4 STATUS :=
      4 1 DO
         Y [ 31 I - ] X [ 31 I - ] M * B + - S2 SQRT < IF 3 STATUS := THEN
      LOOP
      4 STATUS = IF
         Y [ 30 ] Y [ 28 ] - X [ 30 ] X [ 28 ] - / M - ERR.M > IF
            V.SAMP.MAX 0.9 * V.SAMP.MAX := SHOW.STATUS OTH.UPDATE ELSE
            3 STATUS := THEN THEN
      3 STATUS =
   UNTIL
   7 STATUS := SHOW.STATUS 3 STATUS := SHOW.STATUS
;
: RESISTANCE
   1 TICKS :=
   BEGIN
      SAMP.T RATS DUP DATA [ I , 1 ] := SBK [ I , 1 ] :=
      RESIST
      M WAIT [ TICKS ] :=
      TICKS 1 + TICKS :=
      TICKS 120 > IF 5 STATUS := THEN
      TICKS 3 > IF
         WAIT [ TICKS 1 - ] WAIT [ TICKS 2 - ] - ABS ERR.M < IF
            WAIT [ TICKS 2 - ] WAIT [ TICKS 3 - ] - ABS ERR.M < IF
               5 STATUS := THEN THEN THEN
      STATUS 5 <> IF TICKS 12 > IF
         0 DUP EX := EY :=
         7 1 DO
            EX WAIT [ TICKS 6 - I - ] + EX :=
            EY WAIT [ TICKS I - ] + EY :=
         LOOP
         EX 6. / EX :=
         EY 5. / EY :=
```

```
         0 DUP A0 := A1 :=
         7 1 DO
            WAIT [ TICKS 6 - I - ] EX - 2 ** A0 + A0 :=
            WAIT [ TICKS I - ] EY - 2 ** A1 + A1 :=
         LOOP
         A0 6. / SQRT A0 :=
         A1 6. / SQRT A1 :=
         EX EY - ABS A0 A1 + < IF 5 STATUS := THEN THEN THEN
      STATUS 5 = IF 1 SKIP = IF TICKS 121 < IF 3 STATUS := THEN THEN THEN
      STATUS 5 = IF
         IMPRESS ALL.UPDATE RATS
         M DATA [ I , 2 ] :=
         ERR.M DATA [ I , 3 ] :=
         B DATA [ I , 4 ] :=
         ERR.B DATA [ I , 5 ] :=
         R DATA [ I , 6 ] :=
         TICKS 2 - 10 * DATA [ I , 7 ] :=
         FILTER M SBK [ I , 2 ] :=
         S2 SQRT SBK [ I , 3 ] :=
         180 N.SBK - SBK [ I , 4 ] :=
         DATA.UPDATE 1 Z 5 STATUS :=
      ELSE 8 Z RATS THEN
      STATUS 5 =
   UNTIL
   SHOW.STATUS
;
: T.INCR
   0 5 GOTO.XY ." INCREASING TEMPERATURE"
   4000 SYNC.PERIOD
   0 7 GOTO.XY ." SAMPLE TEMPERATURE = "
   5 0 FIX.FORMAT
   SYNCHRONIZE
   BEGIN
      5 "TIME "LEFT " 23:59" "= IF CLUMSY 4000 SYNC.PERIOD SYNCHRONIZE THEN
      RATE 900. / F.SET + F.SET := T.OUT
      STP 0 = IF 21 7 GOTO.XY LEFT.T . THEN
      SYNCHRONIZE TEST
      LEFT T SINT.T >=
   UNTIL
;
: T.WAIT
   HOME 0 5 GOTO.XY 80 SPACES 0 5 GOTO.XY ." AT TEMPERATURE FOR     MIN"
   A.TIME 1 + 1 DO
      5 "TIME "LEFT " 23:59" "= IF CLUMSY THEN
      59 SEC.DELAY
      500 MSEC.DELAY
      STP 0 = IF 19 5 GOTO.XY 3 0 FIX.FORMAT I . THEN
      STP 0 = IF 21 7 GOTO.XY 5 0 FIX.FORMAT LEFT.T A0 := A0 . THEN
      A0 SINT.T - 2. > IF F.SET 1 - F.SET := T.OUT THEN
      SINT.T A0 - 2. > IF F.SET 1 + F.SET := T.OUT THEN
   LOOP
;
: TEMP
   " DATA.AST" DEFER> FILE.OPEN
   DATA FILE>ARRAY
   FILE.CLOSE
   DATA .
   " SBK.AST" DEFER> FILE.OPEN
```

```
   SBK FILE>ARRAY
   FILE.CLOSE
   CR CR SBK .
;
: RANGE
   NORMAL.DISPLAY 0 0 GOTO.XY
   ." THIS PROGRAM MEASURES AND STORES SAMPLE CONDUCTIVITY OVER A RANGE OF"
   ."  TEMPERATURE"
   CR CR ." THE SAMPLE IDENTIFIER IS : " "INPUT SAMPLE.NAME ":=
   CR ." SAMPLE DIAMETER IN CM = " #INPUT 2. / 2 ** PI * AREA :=
   CR ." VOLTAGE PROBE SEPARATION IN CM = " #INPUT LENGTH :=
   CR ." INITIAL MAXIMUM SAMPLE VOLTAGE IN V = " #INPUT V.SAMP.MAX :=
   CR ." THE HEATING (AND COOLING) RATE IN DEG/HR = " #INPUT RATE :=
   CR ." THE FURNACE SETTLING TIME IN MIN = " #INPUT S.TIME :=
   CR ." THE LOWER TEMPERATURE IN DEG C = " #INPUT LOW.T :=
   CR ." THE HIGHER TEMPERATURE IN DEG C = " #INPUT HIGH.T :=
   CR ." NUMBER OF POINTS IN ONE DIRECTION (MAX. IS 30) = " #INPUT N.PTS .=
   CR ." START AT POINT NUMBER = " #INPUT START.POINT :=
   CR ." HOURS OF ANNEALING TIME BEFORE MEASUREMENTS = " #INPUT 60 * A.TIME :=
   CR ." ANNEALING TEMPERATURE = " #INPUT SINT.T :=
   CR ." WAITING TIME AT TEMPERATURE IN MINUTES = " #INPUT W.TIME :=
   CR CR ." (DO A SCREEN DUMP AND PRESS <RETURN> TO CONTINUE.)" "INPUT
   NORMAL.DISPLAY HOME
   SAMP.T F.SET :=
   A.TIME 0 > IF T.INCR T.WAIT THEN
   0 RAT := 0 X := 0 Y := 0 DATA := 0 WAIT := 0 SBK := 0 STATUS :=
   START.POINT 1 > IF TEMP THEN
   DATA.SAVE.INIT
   LOW.T 1. / HIGH.T 1. / - N.PTS / DELTA.T :=
   SAMP.T F.SET :=
   N.PTS 2 * 2 + START.POINT DO
      0 TICKS := 1 N.SBK := IMPRESS ALL.UPDATE RATS
      I N.PTS 2 + < IF HIGH.T 1. / DELTA.T I 1 - * +
         ELSE LOW.T 1. / DELTA.T I N.PTS 1 + - * - THEN
      1. / FIX T.SET RATS
      W.TIME Z RESISTANCE
      DATA.SAVE WAIT.SAVE IV.SAVE SBK.SAVE
      0 WAIT :=
   LOOP
   25 T.SET RATS
;
: SINTER
   NORMAL.DISPLAY 0 0 GOTO.XY
   ." SINTERING TEMPERATURE = " #INPUT SINT.T :=
   CR ." SINTERING TIME IN HR = " #INPUT 60 * A.TIME :=
   CR ." THE HEATING (AND COOLING) RATE IN DEG/HR = " #INPUT RATE :=
   LEFT.T F.SET :=
   T.INCR T.WAIT
   HOME 0 5 GOTO.XY 80 SPACES 0 5 GOTO.XY ." DECREASING TEMPERATURE"
   5 0 FIX.FORMAT
   4000 SYNC.PERIOD
   SYNCHRONIZE
   BEGIN
      5 "TIME "LEFT " 23:59" "= IF CLUMSY 4000 SYNC.PERIOD THEN
      F.SET RATE 900. / - F.SET := T.OUT
      STP 0 = IF 21 7 GOTO.XY LEFT.T . THEN
      SYNCHRONIZE TEST
      F.SET 100 <=
```

```
   UNTIL
   0 F.SET := T.OUT
;
: SINGLE
   NORMAL.DISPLAY 0 0 GOTO.XY
   ." THIS PROGRAM MEASURES THE RESISTANCE AT ONE TEMPERATURE."
   CR CR ." THE SAMPLE IDENTIFIER IS : " "INPUT SAMPLE.NAME ":=
   CR ." SAMPLE DIAMETER IN CM = " #INPUT 2. / 2 ** PI * AREA :=
   CR ." VOLTAGE PROBE SEPARATION IN CM = " #INPUT LENGTH :=
   CR ." INITIAL MAXIMUM SAMPLE VOLTAGE IN V = " #INPUT V.SAMP.MAX :=
   CR ." THE HEATING (AND COOLING) RATE IN DEG/HR = " #INPUT RATE :=
   CR ." THE FURNACE SETTLING TIME IN MIN = " #INPUT S.TIME :=
   CR ." THE TEMPERATURE OF MEASUREMENT IN DEG C = " #INPUT HIGH.T :=
   CR ." HOURS OF ANNEALING TIME BEFORE MEASUREMENTS = " #INPUT 60 * A.TIME :=
   CR ." ANNEALING TEMPERATURE = " #INPUT SINT.T :=
   CR ." WAITING TIME AT TEMPERATURE IN MINUTES = " #INPUT W.TIME :=
   CR ." MEASURE RESISTANCE FOR UP TO 20 HOURS? (Y OR N) : " "INPUT X.LABEL ":=
   X.LABEL " Y" "= IF 1 SKIP := ELSE 0 SKIP := THEN
   CR CR ." (DO A SCREEN DUMP AND PRESS <RETURN> TO CONTINUE.)" "INPUT
   NORMAL.DISPLAY HOME
   SAMP.T F.SET :=
   A.TIME 0 > IF T.INCR T.WAIT THEN
   0 RAT := 0 X := 0 Y := 0 DATA := 0 WAIT :=
   0 SBK := 0 STATUS := 0 TICKS := 1 N.SBK :=
   DATA.SAVE.INIT
   2 1 DO
      IMPRESS ALL.UPDATE RATS HIGH.T T.SET RATS
      W.TIME 2 RESISTANCE DATA.SAVE WAIT.SAVE IV.SAVE SBK.SAVE
   LOOP
   25 T.SET RATS
;
: GO
   NORMAL.DISPLAY 0 0 GOTO.XY
   ." --RANGE--  MEASURES RESISTIVITY OVER A RANGE OF TEMPERATURE"
   CR CR ." --SINGLE--  MEASURES RESISTIVITY FOR A SINGLE TEMPERATURE"
   CR CR ." --SINTER--  SINTERS SAMPLE"
   CR CR ." NOTE:"
   CR ."    1) FOR SINTERING CONNECT THE THERMOCOUPLE TO CHANNEL 1 (LEFT.T)"
   CR ."    2) PRESS THE | KEY TO TURN DISPLAY ON OR OFF DURING EXECUTION"
   CR CR
   DAS.INIT
;
0 STP :=
INSTALL GO IN TURNKEY
```

III Conductivity Results

DATA FOR CRYSTAL SAMPLE Ia, TAKEN 10/31/86 TO 11/4/86, P.148A TO 149
SAMPLE GEOMETRY :
VOLTAGE PROBE LENGTH = 1.5 (cm) +/- 0.01
DIAMETER = 0.452 (cm) AREA = 0.1604 (cm)2 +/- 0.001

No.	T (deg C)	R (ohm)	ERR ON R (ohm)	B (volt)	ERR ON B (volt)	R	t (min)	(10)3/T (K)-1	COND (ohm-cm)-1	+/-
1	1507	0.09722	0.00021	-0.00015	0.00006	0.999936	130	0.56180	96.19	1.67
2	1484	0.09996	0.00018	-0.00004	0.00005	0.999956	30	0.56915	93.55	1.59
3	1473	0.10215	0.00019	-0.00003	0.00005	0.999954	70	0.57274	91.55	1.56
4	1444	0.10698	0.00025	-0.00016	0.00006	0.999921	40	0.58241	87.41	1.53
5	1423	0.11093	0.00025	-0.00013	0.00006	0.999932	50	0.58962	84.30	1.47
6	1402	0.11545	0.00027	-0.00012	0.00006	0.999924	30	0.59701	81.00	1.42
7	1381	0.1209	0.00021	-0.00018	0.00005	0.999959	150	0.60459	77.35	1.31
8	1362	0.2294	0.0004	-0.00019	0.00005	0.999958	320	0.61162	40.77	0.69
9	1342	0.32416	0.00024	-0.00024	0.00005	0.999992	500	0.61920	28.85	0.46
10	1318	0.41448	0.00039	-0.00013	0.00006	0.999987	420	0.62854	22.56	0.37
11	1300	0.53291	0.00044	-0.00021	0.00005	0.99999	90	0.63573	17.55	0.28
12	1322	0.43682	0.00045	-0.00023	0.00006	0.999986	230	0.62696	21.41	0.35
13	1340	0.33806	0.00066	-0.00022	0.00006	0.999947	80	0.61996	27.66	0.48
14	1360	0.24914	0.00053	-0.00023	0.00006	0.999938	60	0.61237	37.54	0.65
15	1382	0.15943	0.00031	-0.00014	0.00006	0.999946	180	0.60423	58.66	1.01
16	1401	0.11759	0.00021	-0.00011	0.00005	0.999956	170	0.59737	79.53	1.35
17	1422	0.1127	0.00023	-0.0001	0.00006	0.999942	40	0.58997	82.98	1.43
18	1440	0.10898	0.00023	-0.00012	0.00006	0.999938	40	0.58377	85.81	1.49
19	1462	0.10495	0.00022	-0.00019	0.00006	0.999937	80	0.57637	89.11	1.54
20	1485	0.10128	0.00022	-0.0001	0.00006	0.999935	130	0.56883	92.33	1.61
21	1505	0.09818	0.00027	-0.00006	0.00007	0.999891	120	0.56243	95.25	1.71

DATA FOR CRYSTAL SAMPLE Ib, TAKEN 11/6/86 TO 11/10/86, P.149A
SAMPLE GEOMETRY :
VOLTAGE PROBE LENGTH = 1.225 (cm) +/- 0.01
DIAMETER = 0.475 (cm) AREA = 0.177 (cm)2 +/- 0.004
CRYSTAL SAMPLE Ib, PAGE 149A

No.	T (deg C)	R (ohm)	ERR ON R (ohm)	B (volt)	ERR ON B (volt)	R	t (min)	(10)3/T (K)-1	COND (ohm-cm)-1	+/-
1	1454	0.09621	0.00025	0.00011	0.00007	0.999907	20	0.57904	71.94	2.34
2	1434	0.09894	0.00023	0.00002	0.00006	0.999922	200	0.58582	69.95	2.26
3	1412	0.10222	0.00023	0.00003	0.00006	0.999932	90	0.59347	67.71	2.18
4	1390	0.10641	0.00027	-0.00006	0.00007	0.999912	110	0.60132	65.04	2.12
5	1369	0.11024	0.00023	0.00003	0.00006	0.999937	80	0.60901	62.78	2.02
6	1348	0.11529	0.00025	-0.00009	0.00006	0.999933	100	0.61690	60.03	1.93
7	1328	0.12113	0.00026	-0.00006	0.00006	0.999937	20	0.62461	57.14	1.84
8	1306	0.1282	0.00024	-0.00011	0.00005	0.999951	40	0.63331	53.99	1.72
9	1284	0.2095	0.00046	-0.00005	0.00006	0.999932	230	0.64226	33.04	1.06
10	1263	0.24514	0.00052	-0.00001	0.00006	0.999938	120	0.65104	28.23	0.91
11	1242	0.28498	0.00064	-0.00004	0.00006	0.99993	120	0.66007	24.29	0.78
12	1223	0.34532	0.00075	-0.0001	0.00006	0.999934	290	0.66845	20.04	0.65
13	1201	0.38007	0.0008	-0.00006	0.00006	0.999939	50	0.67843	18.21	0.58
14	1221	0.36467	0.00082	-0.00014	0.00006	0.999928	90	0.66934	18.98	0.61
15	1242	0.33521	0.0007	-0.00019	0.00006	0.999938	60	0.66007	20.65	0.66
16	1264	0.28897	0.00062	-0.00018	0.00006	0.999935	160	0.65062	23.95	0.77
17	1283	0.24241	0.00049	-0.0002	0.00005	0.999942	160	0.64267	28.55	0.91
18	1305	0.18382	0.00039	-0.00013	0.00006	0.999938	200	0.63371	37.65	1.21
19	1327	0.13476	0.0003	-0.00012	0.00006	0.999932	150	0.62500	51.36	1.66
20	1349	0.11463	0.00023	-0.00006	0.00005	0.999943	240	0.61652	60.38	1.93
21	1369	0.10918	0.00024	-0.00002	0.00006	0.999934	70	0.60901	63.39	2.04
22	1392	0.10437	0.00025	-0.00004	0.00006	0.999922	110	0.60060	66.31	2.15
23	1413	0.10103	0.00016	-0.00008	0.00004	0.999963	50	0.59312	68.50	2.17
24	1435	0.09718	0.0003	-0.00001	0.00008	0.999869	20	0.58548	71.22	2.35
25	1456	0.09376	0.00025	0.00004	0.00007	0.999903	90	0.57837	73.82	2.41

DATA FOR CRYSTAL SAMPLE Ic, TAKEN 11/12/86 TO 11/17/86, P.150
SAMPLE GEOMETRY :
VOLTAGE PROBE LENGTH = 0.896 (cm) +/- 0.005
DIAMETER = 0.421 (cm) +/- 0.002 AREA = 0.1392 (cm)2 +/- 0.0013
CRYSTAL SAMPLE Ic, PAGE 150

No.	T (deg C)	R (ohm)	ERR ON R (ohm)	B (volt)	ERR ON B (volt)	R	t (min)	(10)3/T (K)-1	COND (ohm-cm)-1	+/-
1	1461	0.10286	0.00024	0.00006	0.00007	0.999922	50	0.57670	62.58	1.08
2	1446	0.10502	0.00027	0.00008	0.00007	0.99991	30	0.58173	61.29	1.07
3	1430	0.10781	0.00028	0.00004	0.00008	0.999909	90	0.58720	59.70	1.05
4	1413	0.1102	0.00024	0.00009	0.00006	0.999933	30	0.59312	58.41	1.00
5	1401	0.11294	0.00023	0.00003	0.00006	0.99994	30	0.59737	56.99	0.97
6	1387	0.11582	0.00023	0.00003	0.00006	0.999945	40	0.60241	55.57	0.94
7	1371	0.11901	0.00025	0.00003	0.00006	0.999936	90	0.60827	54.08	0.92
8	1358	0.12241	0.00024	0	0.00006	0.999944	70	0.61312	52.58	0.89
9	1340	0.12604	0.00025	0.00002	0.00006	0.999944	20	0.61996	51.07	0.86
10	1328	0.13022	0.00027	-0.00004	0.00006	0.999938	40	0.62461	49.43	0.84
11	1313	0.13463	0.00028	-0.00006	0.00006	0.99994	70	0.63052	47.81	0.81
12	1298	0.13937	0.00028	-0.00006	0.00006	0.999943	70	0.63654	46.18	0.78
13	1283	0.14413	0.00029	-0.00008	0.00006	0.999945	20	0.64267	44.66	0.75
14	1271	0.14913	0.00031	-0.00001	0.00006	0.99994	30	0.64767	43.16	0.73
15	1257	0.1554	0.00031	-0.00005	0.00006	0.999944	20	0.65359	41.42	0.70
16	1243	0.16352	0.00031	-0.00004	0.00006	0.99995	20	0.65963	39.36	0.66
17	1229	0.21144	0.00041	-0.00003	0.00006	0.999946	550	0.66578	30.44	0.51
18	1215	0.2372	0.00045	-0.00004	0.00006	0.99995	160	0.67204	27.14	0.46
19	1200	0.26563	0.00046	0	0.00005	0.999956	120	0.67889	24.23	0.40
20	1214	0.25737	0.00049	-0.00005	0.00006	0.999949	20	0.67249	25.01	0.42
21	1228	0.24312	0.00048	-0.00009	0.00006	0.999945	40	0.66622	26.47	0.45
22	1243	0.21892	0.00043	-0.00011	0.00006	0.999946	150	0.65963	29.40	0.50
23	1257	0.19653	0.00036	-0.00007	0.00005	0.999953	60	0.65359	32.75	0.55
24	1270	0.17109	0.00032	-0.00009	0.00006	0.999951	120	0.64809	37.62	0.63
25	1284	0.15419	0.0003	-0.00001	0.00006	0.999946	50	0.64226	41.74	0.70
26	1299	0.14233	0.00029	-0.00001	0.00006	0.999943	90	0.63613	45.22	0.77
27	1312	0.13791	0.00027	-0.0001	0.00006	0.999947	40	0.63091	46.67	0.79
28	1326	0.13351	0.00027	-0.00004	0.00006	0.999941	90	0.62539	48.21	0.82
29	1341	0.12935	0.00024	0.00002	0.00006	0.999951	40	0.61958	49.76	0.84
30	1356	0.12575	0.00025	0.00004	0.00006	0.999943	20	0.61387	51.19	0.87
31	1368	0.12306	0.00025	-0.00006	0.00006	0.999944	20	0.60938	52.30	0.89
32	1383	0.11951	0.00023	0.00004	0.00006	0.999949	30	0.60386	53.86	0.91
33	1396	0.11676	0.00025	-0.00002	0.00006	0.999938	50	0.59916	55.13	0.94
34	1411	0.11396	0.00023	-0.00002	0.00006	0.999944	90	0.59382	56.48	0.96
35	1425	0.11111	0.00022	-0.00005	0.00006	0.999946	30	0.58893	57.93	0.98
36	1440	0.1085	0.00022	0	0.00006	0.999941	20	0.58377	59.32	1.01
37	1453	0.10624	0.00021	-0.00001	0.00006	0.999945	50	0.57937	60.59	1.02

DATA FOR CRYSTAL SAMPLE IIa, TAKEN 12/11/86 TO 12/15/86, P.151
SAMPLE GEOMETRY : ~~*ADD ERRORS IN LENGTH AND DIA.*~~
VOLTAGE PROBE LENGTH = 1.53 (cm) +/- 0.01
DIAMETER = 0.433 (cm) +/- 0.002 AREA = 0.1473 (cm)2 +/- 0.0014
CRYSTAL SAMPLE IIa, PAGE 151

No.	T (deg C)	R (ohm)	ERR ON R (ohm)	B (volt)	ERR ON B (volt)	R	t (min)	(10)3/T (K)-1	COND (ohm-cm)-1	+/-
1	1449	0.29517	0.00056	-0.00003	0.00006	0.99995	70	0.58072	35.20	0.62
2	1430	0.30756	0.00074	-0.00009	0.00007	0.999919	30	0.58720	33.78	0.61
3	1412	0.32048	0.00071	-0.00011	0.00007	0.999932	20	0.59347	32.42	0.58
4	1395	0.33207	0.0007	-0.00005	0.00006	0.999938	20	0.59952	31.29	0.55
5	1376	0.34677	0.00077	-0.00011	0.00007	0.999931	40	0.60643	29.96	0.53
6	1358	0.36277	0.0008	-0.00013	0.00007	0.99993	80	0.61312	28.64	0.51
7	1341	0.37919	0.00077	-0.00016	0.00006	0.999943	20	0.61958	27.40	0.48
8	1322	0.39687	0.00078	-0.00027	0.00006	0.999946	20	0.62696	26.18	0.46
9	1303	0.41607	0.00078	-0.00025	0.00006	0.99995	90	0.63452	24.97	0.44
10	1286	0.43556	0.00107	-0.00025	0.00007	0.999915	170	0.64144	23.85	0.43
11	1266	0.45552	0.00065	-0.00023	0.00007	0.999971	40	0.64977	22.81	0.39
12	1249	0.47954	0.00065	-0.00015	0.00007	0.999974	20	0.65703	21.67	0.37
13	1230	0.50678	0.00083	-0.00026	0.00008	0.999963	100	0.66534	20.50	0.35
14	1212	0.53211	0.00068	-0.00024	0.00006	0.999977	90	0.67340	19.53	0.33
15	1192	0.56421	0.00084	-0.00022	0.00007	0.999969	90	0.68259	18.42	0.32
16	1175	0.59606	0.00086	-0.00027	0.00007	0.99997	40	0.69061	17.43	0.30
17	1157	0.63165	0.00085	-0.00027	0.00006	0.999974	120	0.69930	16.45	0.28
18	1139	0.67101	0.00082	-0.00034	0.00006	0.999979	30	0.70822	15.48	0.26
19	1121	0.7112	0.00088	-0.00037	0.00006	0.999978	30	0.71736	14.61	0.25
20	1101	0.75815	0.00095	-0.00048	0.00007	0.999978	50	0.72780	13.70	0.23
21	1083	0.80771	0.0009	-0.00025	0.00007	0.999983	20	0.73746	12.86	0.22
22	1065	0.86741	0.00096	-0.00035	0.00007	0.999983	90	0.74738	11.98	0.20
23	1048	0.93011	0.00091	-0.00054	0.00006	0.999986	20	0.75700	11.17	0.19
24	1027	1.01147	0.0011	-0.00048	0.00006	0.999984	40	0.76923	10.27	0.17
25	1009	1.11068	0.00127	-0.00053	0.00007	0.999982	130	0.78003	9.35	0.16
26	993	1.20687	0.00138	-0.00053	0.00007	0.999982	20	0.78989	8.61	0.14
27	974	1.31331	0.00153	-0.0007	0.00007	0.999981	20	0.80192	7.91	0.13
28	955	1.424	0.00164	-0.00065	0.00007	0.999982	40	0.81433	7.30	0.12
29	937	1.54923	0.00194	-0.00072	0.00007	0.999978	30	0.82645	6.71	0.11
30	917	1.69758	0.00202	-0.00087	0.00007	0.99998	20	0.84034	6.12	0.10
31	899	1.85119	0.00158	-0.0008	0.00005	0.999989	20	0.85324	5.61	0.09
32	919	1.68518	0.00185	-0.00077	0.00006	0.999983	20	0.83893	6.17	0.10
33	938	1.54674	0.00182	-0.00064	0.00007	0.999981	20	0.82576	6.72	0.11
34	954	1.43939	0.00165	-0.00063	0.00007	0.999982	60	0.81500	7.22	0.12
35	972	1.33615	0.00135	-0.0006	0.00006	0.999986	20	0.80321	7.78	0.13
36	992	1.24241	0.00162	-0.00057	0.00008	0.999976	150	0.79051	8.36	0.14
37	1010	1.15696	0.00141	-0.00054	0.00007	0.999979	40	0.77942	8.98	0.15
38	1027	1.0853	0.00114	-0.00044	0.00006	0.999984	30	0.76923	9.57	0.16
39	1047	1.01201	0.00105	-0.00046	0.00006	0.999986	140	0.75758	10.27	0.17
40	1065	0.94687	0.00125	-0.00033	0.00008	0.999976	20	0.74738	10.97	0.19
41	1082	0.88762	0.00093	-0.00044	0.00006	0.999985	140	0.73801	11.71	0.20
42	1102	0.81747	0.00106	-0.00038	0.00008	0.999976	60	0.72727	12.71	0.22
43	1120	0.72679	0.0009	-0.00033	0.00007	0.999978	230	0.71788	14.30	0.24
44	1139	0.66509	0.00075	-0.00044	0.00007	0.999982	80	0.70822	15.62	0.26
45	1157	0.61351	0.00061	-0.00031	0.00006	0.999986	80	0.69930	16.94	0.28
46	1175	0.57786	0.00052	-0.00036	0.00005	0.999989	50	0.69061	17.98	0.30
47	1194	0.5436	0.00066	-0.00031	0.00007	0.999979	90	0.68166	19.11	0.32

48	1212	0.51306	0.00057	-0.00023	0.00007	0.999982	140	0.67340	20.25	0.34
49	1230	0.48548	0.00062	-0.00004	0.00008	0.999977	130	0.66534	21.40	0.36
50	1247	0.46068	0.0006	-0.00006	0.00008	0.999976	40	0.65789	22.55	0.38
51	1266	0.4388	0.0005	-0.00014	0.00007	0.999982	100	0.64977	23.68	0.40
52	1284	0.41696	0.00046	-0.0001	0.00007	0.999984	40	0.64226	24.92	0.42
53	1302	0.39808	0.00039	-0.00018	0.00006	0.999987	160	0.63492	26.10	0.43
54	1321	0.37909	0.00048	-0.00004	0.00006	0.999978	180	0.62735	27.41	0.46
55	1339	0.36182	0.00059	0.00003	0.00008	0.999962	70	0.62035	28.72	0.50
56	1356	0.34638	0.00059	-0.00001	0.00008	0.999959	20	0.61387	30.00	0.52
57	1377	0.33081	0.00048	0	0.00007	0.999971	30	0.60606	31.41	0.54
58	1394	0.3177	0.00053	-0.00007	0.00008	0.99996	20	0.59988	32.70	0.57
59	1412	0.30394	0.00048	0.00019	0.00007	0.999965	20	0.59347	34.19	0.59
60	1431	0.29207	0.00047	0.0001	0.00008	0.999964	20	0.58685	35.57	0.61
61	1450	0.28046	0.00046	0.00018	0.00008	0.999963	20	0.58038	37.05	0.64

DATA FOR CRYSTAL SAMPLE IIb, TAKEN 12/20/86 TO 12/28/86, P.151A
SAMPLE GEOMETRY :
VOLTAGE PROBE LENGTH = 1.51 (cm) +/- 0.01
DIAMETER = 0.454 (cm) +/- 0.003 AREA = 0.1619 (cm)2 +/- 0.0021
CRYSTAL SAMPLE IIb, PAGE 151A

No.	T (deg C)	R (ohm)	ERR ON R (ohm)	B (volt)	ERR ON B (volt)	R	t (min)	(10)3/T (K)-1	COND (ohm-cm)-1	+/-
1	1448	0.24055	0.00041	0.00026	0.0001	0.39996	170	0.58106	38.78	0.83
2	1432	0.24801	0.00044	0.00042	0.0001	0.999956	30	0.58651	37.61	0.80
3	1412	0.25611	0.00044	0.00032	0.0001	0.999959	80	0.59347	36.42	0.78
4	1394	0.26568	0.00037	0.00031	0.00008	0.999973	20	0.59988	35.11	0.74
5	1376	0.27722	0.00031	0.00009	0.00006	0.999984	30	0.60643	33.65	0.70
6	1358	0.28828	0.00037	0.00013	0.00008	0.999977	60	0.61312	32.36	0.68
7	1340	0.30029	0.00028	0.00009	0.00005	0.999988	50	0.61996	31.06	0.64
8	1321	0.31317	0.00032	-0.00003	0.00006	0.999985	60	0.62735	29.78	0.61
9	1304	0.3267	0.00033	-0.00003	0.00006	0.999986	110	0.63412	28.55	0.59
10	1285	0.34112	0.00036	-0.00002	0.00006	0.999985	40	0.64185	27.34	0.56
11	1267	0.35788	0.00037	-0.0001	0.00006	0.999985	30	0.64935	26.06	0.54
12	1249	0.37434	0.00037	0.00005	0.00006	0.999987	260	0.65703	24.92	0.51
13	1230	0.39537	0.00036	-0.00017	0.00005	0.999989	180	0.66534	23.59	0.48
14	1212	0.41614	0.0005	-0.00017	0.00007	0.99998	120	0.67340	22.41	0.47
15	1191	0.44154	0.00041	-0.00019	0.00006	0.999988	210	0.68306	21.13	0.43
16	1174	0.4663	0.00042	-0.00019	0.00005	0.999989	50	0.69109	20.00	0.41
17	1154	0.49584	0.0005	-0.00014	0.00006	0.999986	80	0.70077	18.91	0.39
18	1137	0.52941	0.00049	-0.00012	0.00005	0.999988	130	0.70922	17.62	0.36
19	1119	0.56616	0.0005	-0.00019	0.00005	0.999989	200	0.71839	16.48	0.34
20	1105	0.60171	0.00051	-0.00017	0.00006	0.999986	60	0.72569	15.50	0.32
21	1082	0.64894	0.0007	-0.00023	0.00006	0.999984	20	0.73801	14.37	0.30
22	1066	0.731	0.00082	-0.00016	0.00007	0.999983	190	0.74683	12.76	0.26
23	1048	0.81012	0.00089	-0.00027	0.00007	0.999983	130	0.75700	11.51	0.24
24	1027	0.8863	0.00109	-0.00031	0.00007	0.999979	160	0.76923	10.52	0.22
25	1010	0.96296	0.00103	-0.00036	0.00006	0.999984	190	0.77942	9.69	0.20
26	992	1.04462	0.00108	-0.00034	0.00006	0.999985	170	0.79051	8.93	0.18
27	972	1.13887	0.00118	-0.00047	0.00006	0.999985	250	0.80321	8.19	0.17
28	954	1.23627	0.00125	-0.00051	0.00006	0.999986	90	0.81500	7.55	0.16
29	936	1.3347	0.00137	-0.00049	0.00006	0.999985	30	0.82713	6.99	0.14
30	917	1.45336	0.00209	-0.0006	0.00009	0.999971	20	0.84034	6.42	0.13
31	900	1.58064	0.00224	-0.00072	0.00008	0.999972	110	0.85251	5.90	0.12
32	916	1.46035	0.00173	-0.0006	0.00007	0.999981	40	0.84104	6.39	0.13
33	937	1.34779	0.00156	-0.00047	0.00007	0.999981	120	0.82645	6.92	0.14
34	955	1.25131	0.00148	-0.00054	0.00007	0.99998	100	0.81433	7.45	0.15
35	971	1.16553	0.00119	-0.00036	0.00006	0.999985	80	0.80386	8.00	0.17
36	992	1.07997	0.00103	-0.00031	0.00006	0.999987	70	0.79051	8.64	0.18
37	1010	1.01274	0.00114	-0.00037	0.00007	0.999983	110	0.77942	9.21	0.19
38	1028	0.94884	0.00101	-0.00031	0.00006	0.999985	20	0.76864	9.83	0.20
39	1048	0.88668	0.00103	-0.00027	0.00007	0.999981	20	0.75700	10.52	0.22
40	1065	0.83221	0.00101	-0.00034	0.00007	0.999979	40	0.74738	11.21	0.23
41	1082	0.7892	0.00096	-0.00019	0.00007	0.999979	210	0.73801	11.82	0.25
42	1103	0.73997	0.00079	-0.00027	0.00006	0.999984	190	0.72674	12.61	0.26
43	1118	0.69497	0.00066	-0.00028	0.00006	0.999988	20	0.71891	13.42	0.28
44	1135	0.64517	0.00082	-0.00017	0.00007	0.999978	40	0.71023	14.46	0.30
45	1157	0.58641	0.00057	-0.00032	0.00006	0.999985	170	0.69930	17.07	0.35
46	1174	0.47927	0.00043	-0.00022	0.00005	0.999989	520	0.69109	19.46	0.40
47	1194	0.45128	0.00032	-0.00003	0.00004	0.999993	90	0.68166	20.67	0.42

48	1211	0.42544	0.00044	-0.00013	0.00006	0.999984	320	0.67385	21.92	0.45
49	1231	0.40225	0.00033	-0.00011	0.00005	0.999991	90	0.66489	23.19	0.47
50	1248	0.38244	0.00055	-0.00016	0.00009	0.999971	30	0.65746	24.39	0.51
51	1268	0.36193	0.0003	-0.0001	0.00005	0.999991	80	0.64893	25.77	0.53
52	1286	0.34582	0.00036	-0.00013	0.00006	0.999986	30	0.64144	26.97	0.56
53	1304	0.32908	0.00033	-0.00009	0.00006	0.999985	70	0.63412	28.34	0.58
54	1321	0.31405	0.00038	-0.00002	0.00007	0.999979	20	0.62735	29.70	0.62
55	1343	0.30092	0.00027	-0.00017	0.00005	0.999988	50	0.61881	31.00	0.64
56	1357	0.28916	0.00029	0.00006	0.00006	0.999980	20	0.61350	32.26	0.66
57	1377	0.2767	0.00029	0.00001	0.00006	0.999985	230	0.60606	33.71	0.70
58	1394	0.26567	0.00033	0.00009	0.00007	0.999979	20	0.59988	35.11	0.73
59	1415	0.2551	0.00029	0.00018	0.00007	0.999982	120	0.59242	36.56	0.76
60	1432	0.2463	0.00033	0.00009	0.00008	0.999974	20	0.58651	37.87	0.79
61	1449	0.2367	0.0004	0.00026	0.0001	0.999961	30	0.58072	39.41	0.84

DATA FOR CRYSTAL SAMPLE IIc, TAKEN 1/2/87 TO 1/15/87, P.151B
SAMPLE GEOMETRY :
VOLTAGE PROBE LENGTH 1.25 (cm) +/- 0.01
DIAMETER = 0.439 (cm) +/- 0.003 AREA = 0.1514 (cm)2 +/- 0.0021
CRYSTAL SAMPLE IIc, PAGE 151B

No.	T (deg C)	R (ohm)	ERR ON R (ohm)	B (volt)	ERR ON B (volt)	R	t (min)	(10)3/T (K)-1	COND (ohm-cm)-1	+/-
1	1453	0.23521	0.00045	0.0004	0.00011	0.999948	40	0.57937	35.11	0.92
2	1434	0.24617	0.0005	0.00027	0.00012	0.999942	50	0.58582	33.55	0.79
3	1413	0.25663	0.00063	0.00047	0.00014	0.999917	20	0.59312	32.18	0.77
4	1390	0.2735	0.0003	-0.00006	0.00006	0.999983	160	0.60132	30.19	0.68
5	1378	0.28559	0.00041	0.00006	0.00009	0.999972	30	0.60569	28.92	0.66
6	1358	0.29942	0.00035	-0.00002	0.00007	0.99998	70	0.61312	27.58	0.62
7	1339	0.31398	0.00034	0	0.00006	0.999983	140	0.62035	26.30	0.59
8	1324	0.32973	0.00043	-0.00006	0.00008	0.999977	170	0.62617	25.05	0.57
9	1301	0.34716	0.00037	-0.00009	0.00006	0.999984	210	0.63532	23.79	0.53
10	1284	0.36468	0.00047	-0.00011	0.00008	0.999977	220	0.64226	22.65	0.51
11	1265	0.3838	0.00045	-0.00013	0.00007	0.999981	100	0.65020	21.52	0.49
12	1246	0.40646	0.00055	-0.00013	0.00008	0.999974	110	0.65833	20.32	0.46
13	1229	0.42807	0.00057	-0.00013	0.00008	0.999975	30	0.66578	19.29	0.44
14	1208	0.45275	0.0005	-0.00017	0.00007	0.999983	230	0.67522	18.24	0.41
15	1196	0.47914	0.00066	-0.00025	0.00008	0.999974	300	0.68074	17.24	0.39
16	1174	0.50691	0.0006	-0.00012	0.00007	0.999981	100	0.69109	16.29	0.37
17	1155	0.54074	0.00062	-0.00013	0.00007	0.999982	30	0.70028	15.27	0.34
18	1135	0.57633	0.00059	-0.00023	0.00009	0.999985	1190	0.71023	14.33	0.32
19	1122	0.61579	0.00055	-0.00023	0.00008	0.999988	40	0.71685	13.41	0.30
20	1102	0.65925	0.00049	-0.00026	0.00007	0.999992	160	0.72727	12.53	0.28
21	1080	0.70635	0.00048	-0.00005	0.00008	0.999994	1000	0.73910	11.69	0.26
22	1063	0.76036	0.00044	-0.00039	0.00007	0.999995	240	0.74850	10.96	0.24
23	1047	0.81972	0.00057	-0.00025	0.00008	0.999993	110	0.75758	10.07	0.22
24	1027	0.89124	0.00054	-0.00029	0.00007	0.999995	110	0.76923	9.27	0.20
25	1009	0.96931	0.00059	-0.00034	0.00007	0.999995	110	0.78003	8.52	0.19
26	994	1.04099	0.00064	-0.00035	0.00007	0.999994	110	0.78927	7.93	0.17
27	971	1.14762	0.00074	-0.00043	0.00008	0.999994	110	0.80386	7.20	0.15
28	955	1.26405	0.00084	-0.0006	0.00008	0.999994	120	0.81433	6.53	0.14
29	935	1.40006	0.00109	-0.00063	0.00009	0.999991	110	0.82781	5.90	0.13
30	913	1.55145	0.00077	-0.00069	0.00006	0.999997	110	0.84317	5.32	0.12
31	896	1.69881	0.00145	-0.00072	0.0001	0.99999	60	0.85543	4.86	0.11
32	920	1.55546	0.00098	-0.00067	0.00008	0.999994	80	0.83822	5.31	0.12
33	936	1.4193	0.0008	-0.00068	0.00007	0.999996	110	0.82713	5.82	0.13
34	956	1.30164	0.00082	-0.00066	0.00008	0.999994	110	0.81367	6.34	0.14
35	975	1.19379	0.00082	-0.0005	0.00008	0.999994	110	0.80128	6.92	0.15
36	992	1.10129	0.00069	-0.00047	0.00007	0.999994	110	0.79051	7.50	0.17
37	1010	1.01305	0.00067	-0.00047	0.00008	0.999994	110	0.77942	8.15	0.18
38	1028	0.94735	0.00057	-0.00048	0.00007	0.999995	110	0.76864	8.72	0.19
39	1046	0.87814	0.00051	-0.00048	0.00007	0.999995	110	0.75815	9.40	0.21
40	1065	0.80842	0.00056	-0.00024	0.00008	0.999993	110	0.74738	10.22	0.23
41	1084	0.7442	0.00042	-0.00022	0.00007	0.999995	90	0.73692	11.10	0.24
42	1102	0.67525	0.0004	-0.00029	0.00007	0.999995	130	0.72727	12.23	0.27
43	1120	0.61767	0.00039	-0.00032	0.00008	0.999994	170	0.71788	13.37	0.29
44	1139	0.57772	0.00033	-0.00019	0.00007	0.999995	110	0.70822	14.29	0.31
45	1157	0.54169	0.00036	-0.00015	0.00008	0.999993	70	0.69930	15.25	0.34
46	1171	0.5079	0.00038	-0.00015	0.00009	0.999992	110	0.69252	16.26	0.36
47	1190	0.48266	0.00039	-0.00017	0.00007	0.999991	110	0.68353	17.11	0.38

48	1210	0.45259	0.00045	-0.00005	0.00009	0.999986	110	0.67431	18.25	0.41
49	1229	0.43062	0.00035	-0.00016	0.00007	0.999991	110	0.66578	19.18	0.43
50	1266	0.38588	0.00035	-0.00004	0.00008	0.999989	50	0.64977	21.40	0.48
51	1279	0.3769	0.00024	-0.00012	0.00006	0.999994	110	0.64433	21.91	0.48
52	1282	0.36828	0.00055	-0.00019	0.00009	0.999968	110	0.64309	22.42	0.5
53	1300	0.34923	0.00044	-0.00024	0.00007	0.999978	110	0.63573	23.65	0.54
54	1322	0.33206	0.00041	0.00006	0.00007	0.999978	40	0.62696	24.87	0.56
55	1340	0.31626	0.0003	-0.00002	0.00006	0.999988	110	0.61996	26.11	0.58
56	1358	0.30193	0.00033	-0.00015	0.00007	0.999983	20	0.61312	27.35	0.62
57	1375	0.28772	0.00034	0.00001	0.00007	0.99998	70	0.60680	28.70	0.65
58	1395	0.27483	0.00045	0.00007	0.0001	0.999962	50	0.59952	30.05	0.69
59	1415	0.26287	0.00033	0.00013	0.00007	0.999977	50	0.59242	31.42	0.71
60	1435	0.25246	0.00039	0.00011	0.00009	0.999967	30	0.58548	32.71	0.75
61	1448	0.24218	0.00033	0.00012	0.00008	0.999975	40	0.58106	34.10	0.78

DATA FOR CRYSTAL SAMPLE IIIa. TAKEN 1/30/87 TO 2/3/87, P.151C
SAMPLE GEOMETRY :
VOLTAGE PROBE LENGTH = 1.47 (cm) +/- 0.01
DIAMETER = 0.447 (cm) +/- 0.003 AREA = 0.1569 (cm)2 +/- 0.0021
CRYSTAL SAMPLE IIIa, PAGE 151C

No.	T (deg C)	R (ohm)	ERR ON R (ohm)	B (volt)	ERR ON B (volt)	R	t (min)	(10)3/T (K)-1	COND (ohm-cm)-1	+/-
1	1449	0.33095	0.00067	0.00028	0.00012	0.999943	30	0.58072	28.30	0.62
2	1425	0.35299	0.00063	0.00021	0.00011	0.999956	60	0.58893	26.54	0.58
3	1404	0.37652	0.00048	0.00018	0.00007	0.999978	100	0.59630	24.88	0.53
4	1382	0.40115	0.00063	0.00012	0.00009	0.999965	30	0.60423	23.35	0.50
5	1358	0.43158	0.00047	-0.00005	0.00006	0.999984	50	0.61312	21.70	0.46
6	1335	0.46182	0.00055	-0.00009	0.00007	0.99998	40	0.62189	20.28	0.43
7	1314	0.49407	0.00065	-0.00017	0.00008	0.999976	30	0.63012	18.96	0.40
8	1290	0.53162	0.00064	-0.00014	0.00007	0.999979	20	0.63980	17.62	0.37
9	1267	0.57139	0.00056	-0.00012	0.00006	0.999986	20	0.64935	16.39	0.34
10	1244	0.6178	0.0009	-0.00034	0.00009	0.99997	40	0.65920	15.16	0.32
11	1219	0.66814	0.00074	-0.00015	0.00007	0.999983	50	0.67024	14.02	0.30
12	1198	0.72314	0.00076	-0.00026	0.00006	0.999984	40	0.67981	12.95	0.27
13	1175	0.78779	0.00087	-0.00023	0.00007	0.999983	30	0.69061	11.89	0.25
14	1152	0.85738	0.00095	-0.00039	0.00007	0.999983	20	0.70175	10.93	0.23
15	1128	0.93556	0.001	-0.0004	0.00006	0.999984	20	0.71378	10.01	0.21
16	1107	1.02106	0.00146	-0.00039	0.00009	0.999971	40	0.72464	9.17	0.20
17	1082	1.12144	0.001	-0.00041	0.00005	0.99999	20	0.73801	8.35	0.17
18	1060	1.23807	0.00134	-0.00053	0.00006	0.999984	20	0.75019	7.57	0.16
19	1037	1.36553	0.00184	-0.00057	0.00008	0.999974	20	0.76336	6.86	0.15
20	1015	1.51142	0.00226	-0.00066	0.00009	0.999969	110	0.77640	6.20	0.13
21	991	1.69133	0.00262	-0.00076	0.0001	0.999967	60	0.79114	5.54	0.12
22	968	1.88638	0.00261	-0.00091	0.00008	0.999973	90	0.80580	4.97	0.11
23	947	2.10592	0.00316	-0.00087	0.00009	0.999969	50	0.81967	4.45	0.10
24	923	2.3818	0.00344	-0.00113	0.00009	0.99997	20	0.83612	3.93	0.08
25	901	2.70383	0.00329	-0.00153	0.00008	0.999979	60	0.85179	3.46	0.07
26	923	2.39279	0.00323	-0.00121	0.00008	0.999975	20	0.83612	3.91	0.08
27	946	2.11074	0.00286	-0.00093	0.00008	0.999975	100	0.82034	4.44	0.09
28	970	1.87038	0.00243	-0.00098	0.00008	0.999976	30	0.80451	5.01	0.11
29	991	1.68029	0.00187	-0.00087	0.00007	0.999983	60	0.79114	5.57	0.12
30	1016	1.48671	0.00135	-0.00063	0.00006	0.999988	110	0.77580	6.30	0.13
31	1036	1.35533	0.00152	-0.00067	0.00007	0.999983	40	0.76394	6.91	0.15
32	1058	1.23027	0.00201	-0.00049	0.0001	0.999962	70	0.75131	7.61	0.16
33	1084	1.13026	0.00109	-0.0006	0.00006	0.999988	60	0.73692	8.29	0.17
34	1107	1.02347	0.00129	-0.00041	0.00008	0.999978	30	0.72464	9.15	0.19
35	1130	0.93505	0.00087	-0.00049	0.00006	0.999988	60	0.71276	10.02	0.21
36	1152	0.85761	0.00076	-0.00034	0.00005	0.99999	20	0.70175	10.92	0.23
37	1174	0.79019	0.00098	-0.00037	0.00008	0.999979	50	0.69109	11.85	0.25
38	1198	0.72934	0.00074	-0.00026	0.00006	0.999986	60	0.67981	12.84	0.27
39	1221	0.67082	0.00074	-0.00022	0.00007	0.999983	20	0.66934	13.96	0.29
40	1243	0.62089	0.00061	-0.00016	0.00006	0.999987	110	0.65963	15.09	0.32
41	1267	0.57666	0.00087	-0.00014	0.00009	0.999967	40	0.64935	16.24	0.35
42	1291	0.53398	0.0006	-0.00015	0.00007	0.999982	20	0.63939	17.54	0.37
43	1312	0.49976	0.00058	-0.00017	0.00007	0.999981	80	0.63091	18.74	0.40
44	1334	0.46681	0.00047	-0.00004	0.00006	0.999986	50	0.62228	20.07	0.42
45	1358	0.43495	0.00052	-0.00008	0.00007	0.99998	50	0.61312	21.54	0.46
46	1381	0.40711	0.00047	-0.00002	0.00007	0.999982	30	0.60459	23.01	0.49
47	1402	0.38408	0.00047	-0.00002	0.00007	0.999979	20	0.59701	24.39	0.52

48	1427	0.35953	0.00043	0.0001	0.00007	0.99998	20	0.59824	26.05	0.55
49	1449	0.33847	0.00044	0.00004	0.00008	0.999976	20	0.58072	27.68	0.59

DATA FOR CRYSTAL SAMPLE IIIb, TAKEN 2/10/87, P.156
SAMPLE GEOMETRY :
VOLTAGE PROBE LENGTH 1.547 (cm) +/- 0.005
DIAMETER = 0.458 (cm) +/- 0.002 AREA = 0.1647 (cm)2 +/- 0.0014
CRYSTAL SAMPLE IIIb, PAGE 156

No.	T (deg C)	R (ohm)	ERR ON R (ohm)	B (volt)	ERR ON B (volt)	R	t (min)	(10)3/T (K)-1	COND (ohm-cm)-1	+/-
1	1450	0.34924	0.00038	0.0001	0.00006	0.999983	110	0.58038	26.89	0.35
2	1424	0.37232	0.00046	-0.00006	0.00007	0.999977	60	0.58928	25.22	0.33
3	1407	0.39488	0.00044	-0.00014	0.00007	0.999983	110	0.59524	23.78	0.31
4	1390	0.41756	0.00052	-0.00006	0.00007	0.999978	20	0.60132	22.49	0.29
5	1364	0.44418	0.00058	-0.00015	0.00008	0.999976	70	0.61087	21.14	0.28
6	1343	0.46953	0.00054	-0.00008	0.00007	0.999981	80	0.61881	20.00	0.26
7	1322	0.50027	0.00051	-0.00023	0.00006	0.999985	110	0.62696	18.77	0.24
8	1302	0.53292	0.00046	-0.00027	0.00005	0.99999	110	0.63492	17.62	0.22
9	1277	0.56668	0.00066	-0.00036	0.00007	0.999981	110	0.64516	16.57	0.22

IV Electrochemical Testing Program Listing

```
INTEGER SCALAR IT
INTEGER DIM[ 1000 ] ARRAY V.A/C
INTEGER DIM[ 1000 ] ARRAY V.A/R
INTEGER DIM[ 1000 ] ARRAY I.A/C
INTEGER DIM[ 1000 ] ARRAY V.IR
INTEGER DIM[ 100 ] ARRAY VS.A/C
INTEGER DIM[ 100 ] ARRAY VS.A/R
INTEGER DIM[ 100 ] ARRAY IS.A/C
INTEGER DIM[ 100 ] ARRAY IRS
INTEGER DIM[ 100 ] ARRAY A/C.SAMP
INTEGER DIM[ 100 ] ARRAY A/R.SAMP
INTEGER DIM[ 100 ] ARRAY IR.SAMP
INTEGER DIM[ 100 ] ARRAY I.SAMP
DIM[ 100 , 2 ] DMA.ARRAY FAST
REAL DIM[ 3 , 100 ] ARRAY VAR
REAL DIM[ 100 ] ARRAY XS
REAL DIM[ 100 ] ARRAY YS
REAL DIM[ 1000 ] ARRAY XL
REAL DIM[ 1000 ] ARRAY YL
INTEGER SCALAR TICKS
REAL SCALAR TIME
REAL SCALAR I.START
REAL SCALAR I.PULSE
REAL SCALAR I.FINISH
REAL SCALAR V.START
REAL SCALAR V.PEAK
REAL SCALAR SWEEP.RATE
REAL SCALAR E.AREA
REAL SCALAR FULL.SCALE
REAL SCALAR MV
REAL SCALAR V.OUT
REAL SCALAR I.OUT
REAL SCALAR V.ZERO
REAL SCALAR TOCKS
REAL SCALAR I.SCALE
30 STRING X.LABEL
30 STRING Y.LABEL
14 STRING FILENAME.IN
14 STRING FILENAME.OUT
\
0 0 A/D.TEMPLATE COLD.JUNCTION
1 1 A/D.TEMPLATE THERMOCOUPLE
2 2 A/D.TEMPLATE VOLTAGE.A/C
3 3 A/D.TEMPLATE CURRENT.A/C
4 4 A/D.TEMPLATE VOLTAGE.A/R
5 5 A/D.TEMPLATE VOLTAGE.IR
7 7 A/D.TEMPLATE BOTH.BLIP
\
0 0 D/A.TEMPLATE V.CONTROL
1 1 D/A.TEMPLATE I.CONTROL
\
23 3 24 40 WINDOW BOTLN
GRAPHICS.DISPLAY
0.05 0.1 VUPORT.ORIG
```

```
1.3 0.85 VUPORT.SIZE
VUPORT ISEE
GRAPHICS.DISPLAY
NORMAL.DISPLAY
\
: GO
NORMAL.DISPLAY
CR ."
CR ."  COMMAND  DOES:                                #PTS   ARRAYS STORED:
CR ."  GO       Displays this summary.               none   none
CR ."  TEMP     Reads temperature.                   none   none
CR ."  ZERO     Zeros current.                       none   none
CR ."  AREA     Changes electrode area.              none   none
CR ."  RANGE    Selects current range.               none   none
CR ."  DELAY    Sets feedback delay.                 none   none
CR ."  WHAT     Displays parameters.                 none   none
CR ."  GALV     Applies current pulse.               100    i A/R A/C
CR ."  BLIP     Applies faster current pulse.        100    i A/R
CR ."  SWEEP    Applies voltage sweep.               1000   i A/C
CR ."  C.SWEEP  Applies cyclic voltage sweep.        1000   i A/C
CR ."  WHIP     Applies faster voltage sweep.        100    i A/C
CR ."  C.WHIP   Applies faster cyclic sweep.         100    i A/C
CR ."  SS       Steady - state measurements.         100    i A/C A/R IR var
CR ."  VSS      Steady - state, voltage steps.       100    i A/C A/R IR var
CR ."  I.RUN    Electrolysis, constant current.      100    A/C A/R IR
CR ."  V.RUN    Electrolysis, constant voltage.      100    i A/R IR
CR ."  OPEN     Opens *.AST data file.               none   none
CR ."
;
: SETUP
    8 3 FIX.FORMAT
    COLD.JUNCTION 3 A/D.GAIN
    THERMOCOUPLE 2 A/D.GAIN
    VOLTAGE.A/C 0 A/D.GAIN
    CURRENT.A/C 1 A/D.GAIN
    VOLTAGE.A/R 0 A/D.GAIN
    VOLTAGE.IR 0 A/D.GAIN
    BOTH.BLIP 0 A/D.GAIN
    DAS.INIT
    GO
;
: AREA
    CR ." ELECTRODE AREA IN (CM)2 IS : "
    #INPUT E.AREA :=
;
: RANGE
    CR ." ENTER CODE FOR CURRENT RANGE."
    CR ." 0 FOR 50 A, 1 FOR 5 A, 2 FOR 0.5 A, OR 3 FOR 0.1 A : "
    #INPUT IT :=
    IT 0 = IF 10. I.SCALE := ELSE
    IT 1 = IF 1. I.SCALE := ELSE
    IT 2 = IF 0.1 I.SCALE := ELSE
    IT 3 = IF 0.02 I.SCALE := ELSE
    CR ." BAD ENTRY, TRY AGAIN."
    THEN EXIT
    THEN THEN THEN
    CURRENT.A/C IT A/D.GAIN
```

```
    DAS.INIT
;
: DELAY
    CR ." DELAY TIME, IN MSEC, FOR SUPPLY CONTROL FEEDBACK IS "
       ." ( 0.2 MSEC MINIMUM ) : "
    #INPUT TOCKS :=
;
: CONVERT.TYPE.R
    1000 * MV :=
    46.674533 MV 0.11179913 * + MV MV * 2.5659255E-6 * - MV MV MV * *
    5.3473173E-11 * + TIME :=
;
: CONVERT.TYPE.K
    1000 * MV :=
     4.4041973 MV 0.025198680 * + MV MV * 9.0154824E-8 * - MV 3 **
     1.8496030E 12 * + TIME :=
;
: I.IN
    CURRENT.A/C A/D.IN I.SCALE NEG I.SCALE A/D.SCALE 0.2037 /
;
: WHAT
     NORMAL.DISPLAY
     SCREEN.CLEAR
     15 1 GOTO.XY INVERSE.ON ." STATUS" INVERSE.OFF
     0 3 GOTO.XY
     5 3 FIX.FORMAT
     ." AREA = " E.AREA . ."  (CM)2"
     6 4 FIX.FORMAT
     CR ." ZERO CURRENT VOLTAGE = " V.ZERO . ."  V"
     6 3 FIX.FORMAT
     CR ." CURRENT MEASUREMENT RANGE TO " I.SCALE 0.2037 / . ."  A/(CM)2"
     CR ." CURRENT TO " I.SCALE 0.2037 / E.AREA * . ."  A"
     4 1 FIX.FORMAT
     CR ." FEEDBACK DELAY TIME = " TOCKS . ."  MSEC"
     CR CR ." TEMPERATURE =      DEG. C"
     CR ." ROOM TEMPERATURE ="
     CR CR ." CURRENT DENSITY =        A/(CM)2"
     CR ." IR VOLTAGE =       V"
     CR ." CELL VOLTAGE =       V"
     CR ." ANODE TO REFERENCE VOLTAGE =       V"
     CR CR ." IT IS       ON"
     CR CR ." TYPE <CNTRL>+<BREAK> TO HALT."
     BEGIN
          THERMOCOUPLE A/D.IN -100. 100. A/D.SCALE CONVERT.TYPE.K
          COLD.JUNCTION A/D.IN -20. 20. A/D.SCALE .5 /
          19 10 GOTO.XY 4 1 FIX.FORMAT ?
          TIME + FIX 14 9 GOTO.XY 4 0 FIX.FORMAT .
          I.IN E.AREA / 18 12 GOTO.XY 6 3 FIX.FORMAT .
          VOLTAGE,IR A/D.IN -10. 10. A/D.SCALE 13 13 GOTO.XY 5 3 FIX.FORMAT .
          VOLTAGE.A/C A/D.IN -10. 10. A/D.SCALE 15 14 GOTO.XY .
          VOLTAGE.A/R A/D.IN -10. 10. A/D.SCALE 29 15 GOTO.XY .
          6 17 GOTO.XY "TIME "TYPE
          15 17 GOTO.XY "DATE "TYPE 29 19 GOTO.XY
          1000 MSEC.DELAY
     AGAIN
;
: PLOT.S
    GRAPHICS.DISPLAY
```

```
    ISEE
    AXIS.DEFAULTS
    WORLD.COORDS
    XS YS XY.AUTO.PLOT
    OUTLINE
    NORMAL.COORDS
    0.55 0.05 POSITION
    0 LABEL.DIR
    HORIZONTAL X.LABEL CENTERED.LABEL
    0.02 0.75 POSITION
    270 LABEL.DIR
    VERTICAL Y.LABEL CENTERED.LABEL
    0 LABEL.DIR
    WORLD.COORDS
;
: PLOT
    GRAPHICS.DISPLAY
    ISEE
    AXIS.DEFAULTS
    WORLD.COORDS
    XL YL XY.AUTO.PLOT
    OUTLINE
    NORMAL.COORDS
    0.55 0.05 POSITION
    0 LABEL.DIR
    HORIZONTAL X.LABEL CENTERED.LABEL
    0.02 0.75 POSITION
    270 LABEL.DIR
    VERTICAL Y.LABEL CENTERED.LABEL
    0 LABEL.DIR
    WORLD.COORDS
;
: FILING
    CR ." ENTER A FILE NAME LIKE A:TTPPP_##.AST : "
    "INPUT FILENAME.IN ":=
    FILENAME.IN DEFER> FILE.CREATE
    FILENAME.IN DEFER> FILE.OPEN
    CR ." FIRST COMMENT ( TYPE OF DATA, PAGE, DATE, TIME ) : " CR
    "INPUT 1 >COMMENT
    CR ." SECOND COMMENT ( ELECTRODES, ETC. ) : " CR
    "INPUT 2 >COMMENT
;
: V.SET
    V.OUT 1000. * 1.8366 / 2. + FIX V.CONTROL D/A.OUT
    800 I.CONTROL D/A.OUT
;
: ZERO
    CR ." SETTING CURRENT TO ZERO."
    18 I.CONTROL D/A.OUT
    4096 V.OUT :=
    BEGIN
         V.OUT 1 - V.OUT :=
         V.OUT V.CONTROL D/A.OUT
         TOCKS MSEC.DELAY
         I.IN 0.005 <=
    UNTIL
    VOLTAGE.A/C A/D.IN -10. 10. A/D.SCALE V.ZERO :=
    V.ZERO 0.1 + V.OUT :=
```

```
    7 4 FIX.FORMAT
    CR ." THE ZERO CURRENT VOLTAGE IS : " V.ZERO .
    8 3 FIX.FORMAT
;
: I.SET
    I.OUT 0. = IF V.ZERO V.OUT := V.SET ELSE
    I.OUT 54.6153 * 17.52 + FIX I.CONTROL D/A.OUT
    4095 V.CONTROL D/A.OUT THEN
;
: CLUMSY
    BEGIN
        4 2 "TIME "SUB " 00" "=
    UNTIL
;
: BLIP
   NORMAL.DISPLAY
   CR ." STARTING CURRENT DENSITY IS : "
   #INPUT E.AREA * I.START :=
   CR ." PULSE CURRENT DENSITY IS : "
   #INPUT E.AREA * I.PULSE :=
   CR ." FINISHING CURRENT DENSITY IS : "
   #INPUT E.AREA * I.FINISH :=
   CR ." DURATION OF PULSE IN SECONDS (0.05 SEC. MINIMUM) IS : "
   #INPUT TIME :=
   BOTH.BLIP 3 4 RESET.A/D.CHNLS
   BOTH.BLIP CLEAR.TEMPLATE.BUFFERS FAST DMA.TEMPLATE.BUFFER
   TIME 5. * CONVERSION.DELAY
   DAS.INIT
   CR ." APPLYING INITIAL CURRENT FOR 10 SECONDS."
   I.START I.OUT := I.SET
   10000 MSEC.DELAY
   CR ." APPLYING PULSE."
   I.PULSE I.OUT := I.SET
   BOTH.BLIP A/D.IN>ARRAY(DMA)
   TIME 1000 * MSEC.DELAY
   BOTH.BLIP 7 7 RESET.A/D.CHNLS
   0.3 CONVERSION.DELAY
   DAS.INIT
   I.FINISH I.OUT := I.SET
   101 1 DO
       FAST [ I , 1 ] IS.A/C [ I ] :=
       FAST [ I , 2 ] VS.A/R [ I ] :=
   LOOP
   CR ." PULSE FINISHED. PRESS <ENTER> TO PLOT."
   "INPUT
   " TIME" X.LABEL ":=
   0 TIME XS []FILL
   " A/(CM)2" Y.LABEL ":=
   IS.A/C -10. 10. A/D.SCALE 0.2037 / E.AREA / YS :=
   I.START E.AREA / YS [ 1 ] :=
   PLOT.S
   BOTLN CR ." PRESS <ENTER> FOR NEXT PLOT"
   "INPUT
   " ANODE/REF VOLTAGE" Y.LABEL ":=
   VS.A/R -10. 10. A/D.SCALE YS :=
   PLOT.S
   BOTLN CR ." PRESS <ENTER> TO CONTINUE"
   "INPUT
```

```
    GRAPHICS.DISPLAY
    NORMAL.DISPLAY
    CR ." DO YOU WANT TO SAVE THIS DATA? "
    "INPUT " N" "= IF EXIT THEN
    FILE.TEMPLATE
         5 COMMENTS
         REAL DIM[ 100 ] SUBFILE
         2 TIMES
    END
    FILING
    6 2 FIX.FORMAT
    CR ." THE CURRENT WAS PULSED FROM " I.START E.AREA / . ."  AMPS/(CM)2 TO "
         I.PULSE E.AREA / . ."  AMPS/(CM)2 FOR " TIME . ."  SECONDS."
    7 4 FIX.FORMAT
    CR ." ENTER ABOVE IN THIRD COMMENT :" CR
    "INPUT 3 >COMMENT
    " FIRST ARRAY : ANODE/REF. VOLTAGE" 4 >COMMENT
    " SECOND ARRAY : CURRENT DENSITY IN A/(CM)2" 5 >COMMENT
    1 SUBFILE VS.A/R -10. 10. A/D.SCALE ARRAY>FILE
    2 SUBFILE IS.A/C -10. 10. A/D.SCALE 0.2037 / E.AREA / ARRAY>FILE
    FILE.CLOSE
    CR ." DATA SAVED."
;
: GALV
    NORMAL.DISPLAY
    CR ." STARTING CURRENT DENSITY IS : "
    #INPUT E.AREA * I.START :=
    CR ." PULSE CURRENT DENSITY IS : "
    #INPUT E.AREA * I.PULSE :=
    CR ." FINISHING CURRENT DENSITY IS : "
    #INPUT E.AREA * I.FINISH :=
    CR ." DURATION OF PULSE IN SECONDS (0.3 SEC. MINIMUM) IS : "
    #INPUT TIME :=
    VOLTAGE.A/C CLEAR.TEMPLATE.BUFFERS VS.A/C TEMPLATE.BUFFER
    VOLTAGE.A/R CLEAR.TEMPLATE.BUFFERS VS.A/R TEMPLATE.BUFFER
    CURRENT.A/C CLEAR.TEMPLATE.BUFFERS IS.A/C TEMPLATE.BUFFER
    DAS.INIT
    CLEAR.TASKS
         VOLTAGE.A/R 1 TASK A/D.IN>ARRAY
         VOLTAGE.A/C 2 TASK A/D.IN>ARRAY
         CURRENT.A/C 3 TASK A/D.IN>ARRAY
    TIME 10. * TASK.PERIOD
         1 1 TASK.MODULO
         1 2 TASK.MODULO
         1 3 TASK.MODULO
    CR ." APPLYING INITIAL CURRENT FOR 10 SECONDS."
    I.START I.OUT := I.SET
    10000 MSEC.DELAY
    CR ." APPLYING PULSE."
    I.PULSE I.OUT := I.SET
    PRIME.TASKS
    TRIGGER.TASKS
    BEGIN
         ?BUFFER.FULL
    UNTIL
    STOP.TASKS
    I.FINISH I.OUT := I.SET
    CR ." PULSE FINISHED. PRESS <ENTER> TO PLOT."
```

```
    "INPUT
    " TIME (SEC)" X.LABEL ":=
    0 TIME XS []FILL
    " A/(CM)2" Y.LABEL ":=
    IS.A/C I.SCALE NEG I.SCALE A/D.SCALE 0.2037 / E.AREA / YS :=
    I.START E.AREA / YS [ 1 ] :=
    PLOT.S
    BOTLN CR ." PRESS <ENTER> FOR NEXT PLOT"
    "INPUT
    " CELL VOLTAGE" Y.LABEL ":=
    VS.A/C -10. 10. A/D.SCALE YS :=
    PLOT.S
    BOTLN CR ." PRESS <ENTER> FOR LAST PLOT . " "INPUT
    " ANODE/REF VOLTAGE" Y.LABEL ":=
    VS.A/R -10. 10. A/D.SCALE YS :=
    PLOT.S
    BOTLN CR ." PRESS <ENTER> TO CONTINUE"
    "INPUT
    GRAPHICS.DISPLAY
    NORMAL.DISPLAY
    CR ." DO YOU WANT TO SAVE THIS DATA? "
    "INPUT " N" "= IF EXIT THEN
    FILE.TEMPLATE
         6 COMMENTS
         REAL DIM[ 100 ] SUBFILE
         3 TIMES
    END
    FILING
    6 2 FIX.FORMAT
    CR ." THE CURRENT WAS PULSED FROM " I.START E.AREA / . ."  AMPS/(CM)2 TO "
         I.PULSE E.AREA / . ."  AMPS/(CM)2 FOR " TIME . ."  SECONDS."
    7 4 FIX.FORMAT
    CR ." ENTER ABOVE IN THIRD COMMENT :" CR
    "INPUT 3 >COMMENT
    " FIRST ARRAY : CELL VOLTAGE" 4 >COMMENT
    " SECOND ARRAY : ANODE/REF. VOLTAGE" 5 >COMMENT
    " THIRD ARRAY : CURRENT DENSITY IN A/(CM)2" 6 >COMMENT
    1 SUBFILE VS.A/C -10. 10. A/D.SCALE ARRAY>FILE
    2 SUBFILE VS.A/R -10. 10. A/D.SCALE ARRAY>FILE
    3 SUBFILE IS.A/C I.SCALE NEG I.SCALE A/D.SCALE 0.2037 / E.AREA / ARRAY>FILE
    FILE.CLOSE
    CR ." DATA SAVED."
;
: SWEEP
    NORMAL.DISPLAY
    ." THE SWEEP RATE MUST BE LESS THAN 2.0 V/SEC."
    CR ." ENTER SWEEP RATE IN V/SEC : "
    #INPUT 1000. * 1.8366 / 2. + SWEEP.RATE :=
    CR ." THE VOLTAGE MUST BE LESS THAN 10 V. "
    CR ." STARTING VOLTAGE IS : "
    #INPUT 1000. * 1.8366 / 2. + V.START :=
    CR ." PEAK VOLTAGE IS : "
    #INPUT 1000. * 1.8366 / 2. + V.PEAK :=
    V.PEAK V.START - SWEEP.RATE / 1000. * TIME :=
    V.START V.PEAK V.A/C []FILL
    V.CONTROL CLEAR.TEMPLATE.BUFFERS V.A/C TEMPLATE.BUFFER
    CURRENT.A/C CLEAR.TEMPLATE.BUFFERS I.A/C TEMPLATE.BUFFER
    VOLTAGE.A/C CLEAR.TEMPLATE.BUFFERS V.A/R TEMPLATE.BUFFER
```

```
DAS.INIT
CLEAR.TASKS
     V.CONTROL 1 TASK ARRAY>D/A.OUT
     CURRENT.A/C 2 TASK A/D.IN>ARRAY
     VOLTAGE.A/C 3 TASK A/D.IN>ARRAY
0 TICKS :=
BEGIN
     TICKS 1 + TICKS :=
     TIME 1000 / TICKS / 50 <=
UNTIL
TIME 1000 / TICKS / TASK.PERIOD
     TICKS 1 TASK.MODULO
     TICKS 2 TASK.MODULO
     TICKS 3 TASK.MODULO
PRIME.TASKS
CR ." APPLYING INITIAL CELL VOLTAGE FOR 10 SEC."
V.CONTROL 0 D/A.OUT
I.CONTROL 800 D/A.OUT
V.CONTROL V.START D/A.OUT
10000 MSEC.DELAY
CR ." APPLYING SWEEP."
TRIGGER.TASKS
BEGIN
     ?BUFFER.FULL
UNTIL
STOP.TASKS
V.ZERO V.OUT := V.SET
CR ." SWEEP FINISHED. PRESS <ENTER> TO PLOT."
"INPUT
I.A/C I.SCALE NEG I.SCALE A/D.SCALE 0.2037 / E.AREA / YL :=
V.A/R -10. 10. A/D.SCALE XL :=
" CELL VOLTAGE" X.LABEL ":=
" CURRENT DENSITY" Y.LABEL ":=
PLOT
BOTLN CR ." DO YOU WANT TO SAVE THIS DATA ? "
"INPUT " N" "= IF EXIT THEN
FILE.TEMPLATE
     5 COMMENTS
     REAL DIM[ 1000 ] SUBFILE
     2 TIMES
END
NORMAL.DISPLAY
FILING
6 2 FIX.FORMAT
CR ." THE VOLTAGE WAS SCANNED FROM " XL [ 1 ] . ."  V TO "
     XL [ 1000 ] . ."  AT A RATE OF " SWEEP.RATE 2. - 1.8366 * 1000. / .
     ."  V/SEC."
8 3 FIX.FORMAT
CR ." ENTER ABOVE AS THE THIRD COMMENT : " CR
"INPUT 3 >COMMENT
" FIRST ARRAY : CURRENT DENSITY (A/(CM)2)" 4 >COMMENT
" SECOND ARRAY : CELL VOLTAGE" 5 >COMMENT
1 SUBFILE YL ARRAY>FILE
2 SUBFILE XL ARRAY>FILE
FILE.CLOSE
CR ." DATA SAVED."

: C.SWEEP
```

```
NORMAL.DISPLAY
." THE SWEEP RATE MUST BE LESS THAN 4.0 V/SEC."
CR ." ENTER SWEEP RATE IN V/SEC : "
#INPUT 1000. * 1.8366 / 2. + SWEEP.RATE :=
CR ." THE VOLTAGE MUST BE LESS THAN 10 V. "
CR ." STARTING VOLTAGE IS : "
#INPUT 1000. * 1.8366 / 2. + V.START :=
CR ." PEAK VOLTAGE IS : "
#INPUT 1000. * 1.8366 / 2. + V.PEAK :=
V.PEAK V.START - SWEEP.RATE / 2000. * TIME :=
V.PEAK V.START - 500. / MV :=
501 1 DO
     V.START MV I * +  V.A/C [ I ] :=
     V.A/C [ I ] V.A/C [ 1001 I - ] :=
LOOP
V.CONTROL CLEAR.TEMPLATE.BUFFERS V.A/C TEMPLATE.BUFFER
CURRENT.A/C CLEAR.TEMPLATE.BUFFERS I.A/C TEMPLATE.BUFFER
VOLTAGE.A/C CLEAR.TEMPLATE.BUFFERS V.A/R TEMPLATE.BUFFER
DAS.INIT
CLEAR.TASKS
     V.CONTROL 1 TASK ARRAY>D/A.OUT
     CURRENT.A/C 2 TASK A/D.IN>ARRAY
     VOLTAGE.A/C 3 TASK A/D.IN>ARRAY
0 TICKS :=
BEGIN
     TICKS 1 + TICKS :=
     TIME 1000 / TICKS / 50 <=
UNTIL
TIME 1000 / TICKS / TASK.PERIOD
     TICKS 1 TASK.MODULO
     TICKS 2 TASK.MODULO
     TICKS 3 TASK.MODULO
PRIME.TASKS
CR ." APPLYING INITIAL CELL VOLTAGE FOR 10 SEC."
V.CONTROL 0 D/A.OUT
I.CONTROL 800 D/A.OUT
V.CONTROL V.START D/A.OUT
10000 MSEC.DELAY
CR ." APPLYING SWEEP."
TRIGGER.TASKS
BEGIN
     ?BUFFER.FULL
UNTIL
STOP.TASKS
V.ZERO V.OUT := V.SET
CR ." SWEEP FINISHED. PRESS <ENTER> TO PLOT."
"INPUT
I.A/C I.SCALE NEG I.SCALE A/D.SCALE 0.2037 / E.AREA / YL :=
V.A/R -10. 10. A/D.SCALE XL :=
" CELL VOLTAGE" X.LABEL ":=
" CURRENT DENSITY" Y.LABEL ":=
PLOT
BOTLN CR ." DO YOU WANT TO SAVE THIS DATA ? "
"INPUT " N" "= IF EXIT THEN
FILE.TEMPLATE
     5 COMMENTS
     REAL DIM[ 1000 ] SUBFILE
     2 TIMES
```

```
    END
    NORMAL.DISPLAY
    FILING
    6 2 FIX.FORMAT
    CR ." THE VOLTAGE WAS CYCLED BETWEEN " XL [ 1 ] . ."  V AND "
         XL [ 500 ] . ."  AT A RATE OF " SWEEP.RATE 2. - 1.8366 * 1000. / .
         ."  V/SEC."
    8 3 FIX.FORMAT
    CR ." ENTER ABOVE AS THE THIRD COMMENT : " CR
    "INPUT 3 >COMMENT
    " FIRST ARRAY : CURRENT DENSITY (A/(CM)2)" 4 >COMMENT
    " SECOND ARRAY : CELL VOLTAGE" 5 >COMMENT
    1 SUBFILE YL ARRAY>FILE
    2 SUBFILE XL ARRAY>FILE
    FILE.CLOSE
    CR ." DATA SAVED."
;
: WHIP
    NORMAL.DISPLAY
    ." THE SWEEP RATE MUST BE LESS THAN 20 V/SEC."
    CR ." ENTER SWEEP RATE IN V/SEC : "
    #INPUT 1000. * 1.8366 / 2. + SWEEP.RATE :=
    CR ." THE VOLTAGE MUST BE LESS THAN 10 V. "
    CR ." STARTING VOLTAGE IS : "
    #INPUT 1000. * 1.8366 / 2. + V.START :=
    CR ." PEAK VOLTAGE IS : "
    #INPUT 1000. * 1.8366 / 2. + V.PEAK :=
    V.PEAK V.START - SWEEP.RATE / 1000. * TIME :=
    V.START V.PEAK VS.A/C []FILL
    V.CONTROL CLEAR.TEMPLATE.BUFFERS VS.A/C TEMPLATE.BUFFER
    CURRENT.A/C CLEAR.TEMPLATE.BUFFERS IS.A/C TEMPLATE.BUFFER
    VOLTAGE.A/C CLEAR.TEMPLATE.BUFFERS VS.A/R TEMPLATE.BUFFER
    DAS.INIT
    CLEAR.TASKS
         V.CONTROL 1 TASK ARRAY>D/A.OUT
         CURRENT.A/C 2 TASK A/D.IN>ARRAY
         VOLTAGE.A/C 3 TASK A/D.IN>ARRAY
    TIME 100. / TASK.PERIOD
         1 1 TASK.MODULO
         1 2 TASK.MODULO
         1 3 TASK.MODULO
    PRIME.TASKS
    CR ." APPLYING INITIAL CELL VOLTAGE FOR 10 SEC."
    V.CONTROL 0 D/A.OUT
    I.CONTROL 800 D/A.OUT
    V.CONTROL V.START D/A.OUT
    10000 MSEC.DELAY
    CR ." APPLYING SWEEP."
    TRIGGER.TASKS
    BEGIN
         ?BUFFER.FULL
    UNTIL
    STOP.TASKS
    V.ZERO V.OUT := V.SET
    CR ." SWEEP FINISHED. PRESS <ENTER> TO PLOT."
    "INPUT
    IS.A/C I.SCALE NEG I.SCALE A/D.SCALE .2037 / E.AREA / YS :=
    VS.A/R -10. 10. A/D.SCALE XS :=
```

```
    " CELL VOLTAGE" X.LABEL ":=
    " CURRENT DENSITY" Y.LABEL ":=
    PLOT.S
    BOTLN CR ." DO YOU WANT TO SAVE THIS DATA ? "
    "INPUT " N" "= IF EXIT THEN
    FILE.TEMPLATE
         5 COMMENTS
         REAL DIM[ 100 ] SUBFILE
         2 TIMES
    END
    NORMAL.DISPLAY
    FILING
    5 2 FIX.FORMAT
    CR ." THE VOLTAGE WAS SCANNED FROM " XS [ 1 ] . ."  V TO "
         XS [ 100 ] . ."  AT A RATE OF " SWEEP.RATE 2. - 1.8366 * 1000. / .
         ."  V/SEC."
    7 4 FIX.FORMAT
    CR ." ENTER ABOVE AS THE THIRD COMMENT : " CR
    "INPUT 3 >COMMENT
    " FIRST ARRAY : CURRENT DENSITY (A/(CM)2)" 4 >COMMENT
    " SECOND ARRAY : CELL VOLTAGE" 5 >COMMENT
    1 SUBFILE YS ARRAY>FILE
    2 SUBFILE XS ARRAY>FILE
    FILE.CLOSE
    CR ." DATA SAVED."
;
: C.WHIP
    NORMAL.DISPLAY
    ." THE SWEEP RATE MUST BE LESS THAN 40 V/SEC."
    CR ." ENTER SWEEP RATE IN V/SEC : "
    #INPUT 1000. * 1.8366 / 2. + SWEEP.RATE :=
    CR ." THE VOLTAGE MUST BE LESS THAN 10 V. "
    CR ." STARTING VOLTAGE IS : "
    #INPUT 1000. * 1.8366 / 2. + V.START :=
    CR ." PEAK VOLTAGE IS : "
    #INPUT 1000. * 1.8366 / 2. + V.PEAK :=
    V.PEAK V.START - SWEEP.RATE / 2000. * TIME :=
    V.PEAK V.START - 50. / MV :=
    51 1 DO
         V.START MV I * + V.A/C [ I ] :=
         V.A/C [ I ] V.A/C [ 101 I - ] :=
    LOOP
    V.CONTROL CLEAR.TEMPLATE.BUFFERS VS.A/C TEMPLATE.BUFFER
    CURRENT.A/C CLEAR.TEMPLATE.BUFFERS IS.A/C TEMPLATE.BUFFER
    VOLTAGE.A/C CLEAR.TEMPLATE.BUFFERS VS.A/R TEMPLATE.BUFFER
    DAS.INIT
    CLEAR.TASKS
         V.CONTROL 1 TASK ARRAY>D/A.OUT
         CURRENT.A/C 2 TASK A/D.IN>ARRAY
         VOLTAGE.A/C 3 TASK A/D.IN>ARRAY
    TIME 100. / TASK.PERIOD
         1 1 TASK.MODULO
         1 2 TASK.MODULO
         1 3 TASK.MODULO
    PRIME.TASKS
    CR ." APPLYING INITIAL CELL VOLTAGE FOR 10 SEC."
    V.CONTROL 0 D/A.OUT
    I.CONTROL 800 D/A.OUT
```

```
    V.CONTROL V.START D/A.OUT
    10000 MSEC.DELAY
    CR ." APPLYING SWEEP."
    TRIGGER.TASKS
    BEGIN
         ?BUFFER.FULL
    UNTIL
    STOP.TASKS
    V.ZERO V.OUT := V.SET
    CR ." SWEEP FINISHED. PRESS <ENTER> TO PLOT."
    "INPUT
    IS.A/C I.SCALE NEG I.SCALE A/D.SCALE .2037 / E.AREA / YS :=
    VS.A/R -10. 10. A/D.SCALE XS :=
    " CELL VOLTAGE" X.LABEL ":=
    " CURRENT DENSITY" Y.LABEL ":=
    PLOT.S
    BOTLN CR ." DO YOU WANT TO SAVE THIS DATA ? "
    "INPUT " N" "= IF EXIT THEN
    FILE.TEMPLATE
         5 COMMENTS
         REAL DIM[ 100 ] SUBFILE
         2 TIMES
    END
    NORMAL.DISPLAY
    FILING
    6 2 FIX.FORMAT
    CR ." THE VOLTAGE WAS CYCLED BETWEEN " XS [ 1 ] . ."  V AND "
         XS [ 50 ] . ."  AT A RATE OF " SWEEP.RATE 2. - 1.8366 * 1000. / .
         ."  V/SEC."
    7 4 FIX.FORMAT
    CR ." ENTER ABOVE AS THE THIRD COMMENT : " CR
    "INPUT 3 >COMMENT
    " FIRST ARRAY : CURRENT DENSITY (A/(CM)2)" 4 >COMMENT
    " SECOND ARRAY : CELL VOLTAGE" 5 >COMMENT
    1 SUBFILE YS ARRAY>FILE
    2 SUBFILE XS ARRAY>FILE
    FILE.CLOSE
    CR ." DATA SAVED."
;
: SS
    NORMAL.DISPLAY
    CR ." SCAN FROM : "
    #INPUT E.AREA * I.START :=
    CR ." SCAN TO HOW MANY A/(CM)2 ? "
    #INPUT E.AREA * I.FINISH :=
    CR ." TIME DELAY FOR EACH POINT IN SEC (MORE THAN 1 SEC.) : "
    #INPUT TIME :=
    V.ZERO V.OUT := V.SET
    4 0 FIX.FORMAT
    CR ." THIS WILL TAKE ABOUT " TIME 10. * 6. / . ."  MINUTES."
    CR ." PRESS <ENTER> TO CONTINUE."
    "INPUT
    8 3 FIX.FORMAT
    VOLTAGE.A/C CLEAR.TEMPLATE.BUFFERS A/C.SAMP TEMPLATE.BUFFER
    VOLTAGE.A/R CLEAR.TEMPLATE.BUFFERS A/R.SAMP TEMPLATE.BUFFER
    VOLTAGE.IR CLEAR.TEMPLATE.BUFFERS IR.SAMP TEMPLATE.BUFFER
    CURRENT.A/C CLEAR.TEMPLATE.BUFFERS I.SAMP TEMPLATE.BUFFER
    DAS.INIT
```

```
CLEAR.TASKS
      VOLTAGE.A/C 1 TASK A/D.IN>ARRAY
      VOLTAGE.A/R 2 TASK A/D.IN>ARRAY
      VOLTAGE.IR 3 TASK A/D.IN>ARRAY
      CURRENT.A/C 4 TASK A/D.IN>ARRAY
10 TASK.PERIOD
      1 1 TASK.MODULO
      1 2 TASK.MODULO
      1 3 TASK.MODULO
      1 4 TASK.MODULO
TIME 1000. * SYNC.PERIOD
GRAPHICS.DISPLAY
ISEE
OUTLINE
HORIZONTAL LINEAR 0. I.FINISH E.AREA / WORLD.SET
VERTICAL LINEAR 0. 6. WORLD.SET
WORLD.COORDS
XY.AXIS.PLOT
NORMAL.COORDS
0.55 0.05 POSITION
0 LABEL.DIR
HORIZONTAL " A/(CM)2" CENTERED.LABEL
0.02 0.75 POSITION
270 LABEL.DIR
VERTICAL " CELL VOLTAGE (V)" CENTERED.LABEL
HORIZONTAL 0 LABEL.DIR
WORLD.COORDS
0 0 POSITION
7 3 FIX.FORMAT
SYNCHRONIZE
101 1 DO
       DAS.INIT
      I 100. / I.FINISH I.START - * I.START + I.OUT := I.SET
      PRIME.TASKS
      SYNCHRONIZE
      TRIGGER.TASKS
      BEGIN
         ?BUFFER.FULL
      UNTIL
      STOP.TASKS
      10 TASK.PERIOD
      A/C.SAMP MEAN VS.A/C [ I ] :=
      A/C.SAMP VARIANCE ABS SQRT VAR [ 1 , I ] :=
      A/R.SAMP MEAN VS.A/R [ I ] :=
      A/R.SAMP VARIANCE ABS SQRT VAR [ 2 , I ] :=
      IR.SAMP MEAN IRS [ I ] :=
      IR.SAMP VARIANCE ABS SQRT VAR [ 3 , I ] :=
      I.SAMP MEAN IS.A/C [ I ] :=
      IS.A/C [ I ] I.SCALE NEG I.SCALE A/D.SCALE 0.2037 / E.AREA /
      VS.A/C [ I ] -10. 10. A/D.SCALE DRAW.TO
      BOTLN CR ." C.D. =" IS.A/C [ I ] I.SCALE NEG I.SCALE A/D.SCALE
      0.2037 / E.AREA / .
      BOTLN CR ." CELL V. =" VS.A/C [ I ] -10. 10. A/D.SCALE .
LOOP
8 3 FIX.FORMAT
BOTLN V.ZERO V.OUT := V.SET
BOTLN CR ." FINISHED STEADY STATE MEASUREMENTS. PRESS <ENTER> TO PLOT."
"INPUT
```

```
    " CURRENT DENSITY A/(CM)2" X.LABEL ":=
    IS.A/C I.SCALE NEG I.SCALE A/D.SCALE 0.2037 / E.AREA / XS :=
    " ANODE/REF VOLTAGE" Y.LABEL ":=
    VS.A/R -10. 10. A/D.SCALE YS :=
    PLOT.S
    BOTLN CR ." PRESS <ENTER> FOR LAST PLOT."
    "INPUT
    " SCATTER IN A/C VOLTAGE (V)" Y.LABEL ":=
    VAR XSECT[ 1 , ! ] 0. 20. A/D.SCALE YS :=
    PLOT.S
    BOTLN CR ." DO YOU WANT TO SAVE THIS DATA ? "
    "INPUT " N" "= IF EXIT THEN
    FILE.TEMPLATE
         7 COMMENTS
         REAL DIM[ 100 ] SUBFILE
         4 TIMES
         REAL DIM[ 3 , 100 ] SUBFILE
    END
    NORMAL.DISPLAY
    FILING
    " FIRST  ARRAY : CELL CURRENT DENSITY" 3 >COMMENT
    " SECOND ARRAY : CELL VOLTAGE " 4 >COMMENT
    " THIRD ARRAY : A/R VOLTAGE" 5 >COMMENT
    " FOURTH ARRAY : IR DROP" 6 >COMMENT
    " FIFTH ARRAY : VARIANCE ON A/C, A/R, IR" 7 >COMMENT
    1 SUBFILE XS ARRAY>FILE
    2 SUBFILE VS.A/C -10. 10. A/D.SCALE ARRAY>FILE
    3 SUBFILE VS.A/R -10. 10. A/D.SCALE ARRAY>FILE
    4 SUBFILE IRS -10. 10. A/D.SCALE ARRAY>FILE
    5 SUBFILE VAR 0. 20. A/D.SCALE ARRAY>FILE
    FILE.CLOSE
    CR ." DATA SAVED."
;
: VSS
    NORMAL.DISPLAY
    CR ." SCAN FROM : "
    #INPUT V.START :=
    CR ." SCAN TO HOW MANY VOLTS ? "
    #INPUT V.PEAK :=
    CR ." TIME DELAY FOR EACH POINT IN SEC (MORE THAN 1 SEC.) : "
    #INPUT TIME :=
    V.ZERO V.OUT := V.SET
    4 0 FIX.FORMAT
    CR ." THIS WILL TAKE ABOUT " TIME 10. * 6. / . ."  MINUTES."
    CR ." PRESS <ENTER> TO CONTINUE."
    "INPUT
    8 3 FIX.FORMAT
    VOLTAGE.A/C CLEAR.TEMPLATE.BUFFERS A/C.SAMP TEMPLATE.BUFFER
    VOLTAGE.A/R CLEAR.TEMPLATE.BUFFERS A/R.SAMP TEMPLATE.BUFFER
    VOLTAGE.IR CLEAR.TEMPLATE.BUFFERS IR.SAMP TEMPLATE.BUFFER
    CURRENT.A/C CLEAR.TEMPLATE.BUFFERS I.SAMP TEMPLATE.BUFFER
    DAS.INIT
    CLEAR.TASKS
         VOLTAGE.A/C 1 TASK A/D.IN>ARRAY
         VOLTAGE.A/R 2 TASK A/D.IN>ARRAY
         VOLTAGE.IR 3 TASK A/D.IN>ARRAY
         CURRENT.A/C 4 TASK A/D.IN>ARRAY
    10 TASK.PERIOD
```

```
      1 1 TASK.MODULO
      1 2 TASK.MODULO
      1 3 TASK.MODULO
      1 4 TASK.MODULO
TIME 1000. * SYNC.PERIOD
GRAPHICS.DISPLAY
ISEE
OUTLINE
HORIZONTAL LINEAR 0. 5. WORLD.SET
VERTICAL LINEAR V.START V.PEAK WORLD.SET
WORLD.COORDS
XY.AXIS.PLOT
NORMAL.COORDS
0.55 0.05 POSITION
0 LABEL.DIR
HORIZONTAL " A/(CM)2" CENTERED.LABEL
0.02 0.75 POSITION
270 LABEL.DIR
VERTICAL " CELL VOLTAGE (V)" CENTERED.LABEL
HORIZONTAL 0 LABEL.DIR
WORLD.COORDS
0 0 POSITION
7 3 FIX.FORMAT
SYNCHRONIZE
101 1 DO
       DAS.INIT
      I 100. / V.PEAK V.START - * V.START + V.OUT := V.SET
      PRIME.TASKS
      SYNCHRONIZE
      TRIGGER.TASKS
      BEGIN
         ?BUFFER.FULL
      UNTIL
      STOP.TASKS
      10 TASK.PERIOD
      A/C.SAMP MEAN VS.A/C [ I ] :=
      A/C.SAMP VARIANCE ABS SQRT VAR [ 1 , I ] :=
      A/R.SAMP MEAN VS.A/R [ I ] :=
      A/R.SAMP VARIANCE ABS SQRT VAR [ 2 , I ] :=
      IR.SAMP MEAN IRS [ I ] :=
      IR.SAMP VARIANCE ABS SQRT VAR [ 3 , I ] :=
      I.SAMP MEAN IS.A/C [ I ] :=
      IS.A/C [ I ] I.SCALE NEG I.SCALE A/D.SCALE 0.2037 / E.AREA /
      VS.A/C [ I ] -10. 10. A/D.SCALE DRAW.TO
      BOTLN CR ." C.D. =" IS.A/C [ I ] I.SCALE NEG I.SCALE A/D.SCALE
      0.2037 / E.AREA / .
      BOTLN CR ." CELL V. =" VS.A/C [ I ] -10. 10. A/D.SCALE .
LOOP
8 3 FIX.FORMAT
BOTLN V.ZERO V.OUT := V.SET
BOTLN CR ." FINISHED STEADY STATE MEASUREMENTS. PRESS <ENTER> TO PLOT."
"INPUT
" CURRENT DENSITY A/(CM)2" X.LABEL ":=
IS.A/C I.SCALE NEG I.SCALE A/D.SCALE 0.2037 / E.AREA / XS :=
" ANODE/REF VOLTAGE" Y.LABEL ":=
VS.A/R -10. 10. A/D.SCALE YS :=
PLOT.S
BOTLN CR ." PRESS <ENTER> FOR LAST PLOT."
```

```
    "INPUT
    " SCATTER IN A/C VOLTAGE (V)" Y.LABEL ":=
    VAR XSECT[ 1 , ! ] 0. 20. A/D.SCALE YS :=
    PLOT.S
    BOTLN CR ." DO YOU WANT TO SAVE THIS DATA ? "
    "INPUT " N" "= IF EXIT THEN
    FILE.TEMPLATE
         7 COMMENTS
         REAL DIM[ 100 ] SUBFILE
         4 TIMES
         REAL DIM[ 3 , 100 ] SUBFILE
    END
    NORMAL.DISPLAY
    FILING
    " FIRST  ARRAY : CELL CURRENT DENSITY" 3 >COMMENT
    " SECOND ARRAY : CELL VOLTAGE " 4 >COMMENT
    " THIRD ARRAY : A/R VOLTAGE" 5 >COMMENT
    " FOURTH ARRAY : IR DROP" 6 >COMMENT
    " FIFTH ARRAY : VARIANCE ON A/C, A/R, IR" 7 >COMMENT
    1 SUBFILE XS ARRAY>FILE
    2 SUBFILE VS.A/C -10. 10. A/D.SCALE ARRAY>FILE
    3 SUBFILE VS.A/R -10. 10. A/D.SCALE ARRAY>FILE
    4 SUBFILE IRS -10. 10. A/D.SCALE ARRAY>FILE
    5 SUBFILE VAR 0. 20. A/D.SCALE ARRAY>FILE
    FILE.CLOSE
    CR ." DATA SAVED."
;
: I.RUN
    NORMAL.DISPLAY
    CR ." DESIRED CURRENT DENSITY IS : "
    #INPUT E.AREA * I.FINISH :=
    CR ." HOW MANY MINUTES OF ELECTROLYSIS (1 MIN. MINIMUM) ? "
    #INPUT 60 * TIME :=
    VOLTAGE.A/C CLEAR.TEMPLATE.BUFFERS CYCLIC A/C.SAMP TEMPLATE.BUFFER
    VOLTAGE.A/R CLEAR.TEMPLATE.BUFFERS CYCLIC A/R.SAMP TEMPLATE.BUFFER
    VOLTAGE.IR CLEAR.TEMPLATE.BUFFERS CYCLIC IR.SAMP TEMPLATE.BUFFER
    DAS.INIT
    CLEAR.TASKS
         VOLTAGE.A/C 1 TASK A/D.IN>ARRAY
         VOLTAGE.A/R 2 TASK A/D.IN>ARRAY
         VOLTAGE.IR 3 TASK A/D.IN>ARRAY
    5 TASK.PERIOD
         1 1 TASK.MODULO
         1 2 TASK.MODULO
         1 3 TASK.MODULO
    TIME 10 * SYNC.PERIOD
    GRAPHICS.DISPLAY
    ISEE
    OUTLINE
    HORIZONTAL LINEAR 0. TIME 60. / WORLD.SET
    VERTICAL LINEAR 0. 5. WORLD.SET
    WORLD.COORDS
    XY.AXIS.PLOT
    NORMAL.COORDS
    0.55 0.05 POSITION
    0 LABEL.DIR
    HORIZONTAL " TIME (MIN)" CENTERED.LABEL
    0.02 0.75 POSITION
```

```
270 LABEL.DIR
VERTICAL " CELL VOLTAGE (V)" CENTERED.LABEL
HORIZONTAL 0 LABEL.DIR
WORLD.COORDS
0 0 POSITION
I.FINISH I.OUT := I.SET
SYNCHRONIZE
7 3 FIX.FORMAT
101 1 DO
      4 "TIME "LEFT " 23:5" "= IF CLUMSY THEN
     5 TASK.PERIOD
     PRIME.TASKS
     SYNCHRONIZE
     TRIGGER.TASKS
     500 MSEC.DELAY
     STOP.TASKS
     A/C.SAMP MEAN VS.A/C [ I ] :=
     A/R.SAMP MEAN VS.A/R [ I ] :=
     IR.SAMP MEAN IRS [ I ] :=
     TIME I * 6000. / VS.A/C [ I ] -10. 10. A/D.SCALE DRAW.TO
     BOTLN CR ." CELL V. =" VS.A/C [ I ] -10. 10. A/D.SCALE .
LOOP
BOTLN V.ZERO V.OUT := V.SET
BOTLN CR ." DO YOU WANT TO SAVE THIS DATA AND THE A/R AND IR "
     ." VOLTAGES ? "
"INPUT " N" "= IF EXIT THEN
FILE.TEMPLATE
     6 COMMENTS
     REAL DIM[ 100 ] SUBFILE
     3 TIMES
END
NORMAL.DISPLAY
FILING
6 2 FIX.FORMAT
CR ." A CURRENT OF " I.FINISH E.AREA / .
     ."  A/(CM)2 WAS PASSED FOR " TIME 60 / . ."  MINUTES."
7 4 FIX.FORMAT
CR ." ENTER ABOVE AS THIRD COMMENT :" CR
"INPUT 3 >COMMENT
" FIRST ARRAY : CELL VOLTAGE IN V" 4 >COMMENT
" SECOND ARRAY : ANODE/REF. VOLTAGE IN V" 5 >COMMENT
" THIRD ARRAY : IR DROP IN V" 6 >COMMENT
1 SUBFILE VS.A/C -10. 10. A/D.SCALE ARRAY>FILE
2 SUBFILE VS.A/R -10. 10. A/D.SCALE ARRAY>FILE
3 SUBFILE IRS -10. 10. A/D.SCALE ARRAY>FILE
FILE.CLOSE
CR ." DATA SAVED."
;
: V.RUN
  NORMAL.DISPLAY
  CR ." DESIRED CELL VOLTAGE IS : "
  #INPUT V.OUT :=
  CR ." HOW MANY MINUTES OF ELECTROLYSIS (1 MIN. MINIMUM) ? "
  #INPUT 60 * TIME :=
  CURRENT.A/C CLEAR.TEMPLATE.BUFFERS CYCLIC I.SAMP TEMPLATE.BUFFER
  VOLTAGE.A/R CLEAR.TEMPLATE.BUFFERS CYCLIC A/R.SAMP TEMPLATE.BUFFER
  VOLTAGE.IR CLEAR.TEMPLATE.BUFFERS CYCLIC IR.SAMP TEMPLATE.BUFFER
  DAS.INIT
```

```
CLEAR.TASKS
     CURRENT.A/C 1 TASK A/D.IN>ARRAY
     VOLTAGE.A/R 2 TASK A/D.IN>ARRAY
     VOLTAGE.IR 3 TASK A/D.IN>ARRAY
5 TASK.PERIOD
     1 1 TASK.MODULO
     1 2 TASK.MODULO
     1 3 TASK.MODULO
TIME 10 * SYNC.PERIOD
GRAPHICS.DISPLAY
ISEE
OUTLINE
HORIZONTAL LINEAR 0. TIME 60. / WORLD.SET
VERTICAL LINEAR 0. 4. WORLD.SET
WORLD.COORDS
XY.AXIS.PLOT
NORMAL.COORDS
0.55 0.05 POSITION
0 LABEL.DIR
HORIZONTAL " TIME (MIN)" CENTERED.LABEL
0.02 0.75 POSITION
270 LABEL.DIR
VERTICAL " A/(CM)2" CENTERED.LABEL
HORIZONTAL 0 LABEL.DIR
WORLD.COORDS
0 0 POSITION
V.SET
SYNCHRONIZE
7 3 FIX.FORMAT
101 1 DO
      4 "TIME "LEFT " 23:5" "= IF CLUMSY THEN
     5 TASK.PERIOD
     PRIME.TASKS
     SYNCHRONIZE
     TRIGGER.TASKS
     500 MSEC.DELAY
     STOP.TASKS
     I.SAMP MEAN IS.A/C [ I ] :=
     A/R.SAMP MEAN VS.A/R [ I ] :=
     IR.SAMP MEAN IRS [ I ] :=
     TIME I * 6000 /
     IS.A/C [ I ] I.SCALE NEG I.SCALE A/D.SCALE 0.2037 / E.AREA / DRAW.TO
     BOTLN CR ." C.D. =" IS.A/C [ I ] I.SCALE NEG I.SCALE A/D.SCALE
     0.2037 / E.AREA / .
LOOP
BOTLN V.ZERO V.OUT := V.SET
BOTLN CR ." DO YOU WANT TO SAVE THIS DATA AND THE A/R AND IR "
     ." VOLTAGES ? "
"INPUT " N" "= IF EXIT THEN
FILE.TEMPLATE
     6 COMMENTS
     REAL DIM[ 100 ] SUBFILE
     3 TIMES
END
NORMAL.DISPLAY
FILING
8 3 FIX.FORMAT
CR ." A VOLTAGE OF " V.OUT . ." WAS APPLIED FOR "
```

```
        TIME 60 / . ."  MINUTES."
    7 4 FIX.FORMAT
    CR ." ENTER ABOVE AS THIRD COMMENT :" CR
    "INPUT 3 >COMMENT
    " FIRST ARRAY : CURRENT DENSITY IN A/(CM)2" 4 >COMMENT
    " SECOND ARRAY : ANODE/REF. VOLTAGE IN V" 5 >COMMENT
    " THIRD ARRAY : IR DROP IN V" 6 >COMMENT
    1 SUBFILE IS.A/C I.SCALE NEG I.SCALE A/D.SCALE 0.2037 /
        E.AREA / ARRAY>FILE
    2 SUBFILE VS.A/R -10. 10. A/D.SCALE ARRAY>FILE
    3 SUBFILE IRS -10. 10. A/D.SCALE ARRAY>FILE
    FILE.CLOSE
    CR ." DATA SAVED."
;
: TEMP
    NORMAL.DISPLAY
    5 0 FIX.FORMAT
    SCREEN.CLEAR
    ." TYPE <CNTRL>+<BREAK> TO HALT."
    CR ." TEMPERATURE IN CELCIUS ="
    BEGIN
        THERMOCOUPLE A/D.IN -100. 100. A/D.SCALE CONVERT.TYPE.K
        COLD.JUNCTION A/D.IN -20. 20. A/D.SCALE .5 / TIME + HOME CR CR .
        1000 MSEC.DELAY
    AGAIN
    7 4 FIX.FORMAT
;
```

10. References

(1) B.J. Welch, "Advances in Aluminum Smelter Technology", CEA. Chem. Eng. Aust., ChE 5(4) 26-32 (1981)

(2) N. Jarret, W.B. Frank and R. Keller, "Advances in the Smelting of Aluminum", Metall. Treatises 137-57 Ed: J. K. Tien and J. F. Elliot (1981)

(3) T.R. Beck, "New Directions in the Aluminum Industry", Electrochem. Ind., Proc. Int. Symp. 1980 331-50 (Pub. 1982)

(4) K. Billehaug and H.A. Øye, "Inert Anodes for Aluminum Electrolysis in Hall - Héroult Cells", Aluminium (Dusseldorf) 57(2) 146-50, 57(3) 228-31 (1980)

(5) A.I. Belyaev and Y.E. Studentsov, "Electrolysis of Alumina in fused Cryolite with Oxide Anodes", Legkie Metal. 6(3) 17-24 (1937)

(6) A.I. Belyaev, "Electrolysis of Alumina with Ferrite Anodes", Legkie Metal. 7(1) 7-20 (1938)

(7) K. Grjotheim, C. Krohn, M. Malinovsky, K. Matiasovsky and J. Thonstad, "Aluminum Electrolysis. Fundamentals of the Hall - Héroult Process", 2nd. Edition, Aluminum - Verlag (1982)

(8) H.J. Klein, "Anodes for Aluminum Fusion Electrolysis", G.O. 2,059,866 (1971)

(9) H. Alder, "Melt Electrolysis With Nonconsumable Anodes", G.O. 2,425,136 (1974)

(10) K. Yamada, T. Hashimoto and K. Horinouchi, "Nonconsumable Electrode for Aluminum Electrolysis", J.P. 77 153,816 (1977)

(11) J.M. Clark and D.R. Secrist, "Aluminum in a Hall - Héroult Cell", U.S. 4,430,189 (1984)

(12) K. Yamada, T. Hashimoto and K. Horinouchi, "Electrode for Aluminum Reduction Cells", G.O. 2,446,314 (1975)

(13) K. Yamada, T. Hashimoto and K. Horinouchi, "Electrode for Electrolytic Aluminum Manufacture", J.P. 77 140,411 (1977)

(14) H. Alder, "Anodes of Dimensionally Stable Oxide Ceramic Single Components", G.O. 3,003,922 (1981)

(15) D.J. Wheeler, A.Y. Sane, J.R. Duruz and J.P. Derivaz,

"Ceramic Oxide Electrodes, and a Cell and Molten Salt Electrolysis Using These Electrodes", E.P. Appl. 30,834 (1981)

(16) S.P. Ray, "Metal Composition for Inert Electrode", G.B. 2,088,902 (1981)

(17) D.R. Secrist, J.M. Clark and H.E. Grindstaff, "Anode Assembly for Molten Salt Electrolysis", U.S. 4,443,314 (1984)

(18) V. De Nora, P.M. Paziante and A. Nidola, "Yttrium Oxide Electrodes", G.O. 2,714,487 (1977)

(19) B. Marincek, "Fused - Salt Electrolysis of Alumina Using Electron - Conducting Nonconsumable Anodes That Also Conduct Oxygen Ions", F.R. 1,533,262 (1968)

(20) H.J. Klein, H. Lehmann, B. Marineck and K.J. Leers, "Contribution to the Development of a Ceramic Ion - Conductor in Aluminum - Smelting Flux Electrolysis. Parts 1 - 3 ", Tonind.-Ztg. Keram. Rundsch. 100(3) 89-96, 100(6) 225-34, 100(11) 390-8 (1976)

(21) S.P. Ray, "Inert Anodes for Hall Cells", Light Metals 1986, R.E. Miller, editor, 287-298 (1986)

(22) S. Mochizuki, "Electrical Conductivity of α-Iron(III) Oxide", Phys. Status Solidi A 41(2) 591-4 (1977)

(23) R. Dieckmann, "Point Defects in Magnetite (Fe_3O_4) and Their Mobilities", Mater. Sci. Monogr. 10 92-9 (1982)

(24) J.D. Weyand, D.H. De Young, S.R. Ray, and G.P. Tarcy, "Inert Anodes for Aluminum Smelting", DOE Report CS/40158-17 (1984)

(25) American Ceramic Society, "Phase Diagrams for Ceramists"

(26) J. Sticher and H. Schmalzried, "The Geometrical Representation of Thermodynamic State Variables in Multicomponent Systems Based on Iron", Report to Institut für Theoretische Hüttenkunde und Angewandte Physikalische Chemie der Technischen Universität Clausthal (1975)

(27) M.W. Shafer, "High Temperature Phase Relations in the Ferrite Region of the Ni-Fe-O System", J. Phys. Chem. 65 2055-62 (1961)

(28) A.E. Paladino, "Phase Equilibriums in the Ferrite Region of the System Fe-Ni-O", J. Am. Ceram. Soc 42 168-75 (1959)

(29) A.M.M. Gadalla and J. White, "Equilibrium Relationships in the System Cu-Fe-O", Trans. Brit. Ceram. Soc. 65(1) 1-17 (1966)

(30) A. Muan and S. Somiya, "The System Iron Oxide - Manganese Oxide in Air", Am. J. Sci. 260 230-40 (1962)

(31) D.G. Wickham, "The Chemical Composition of Spinels in the System Fe_3O_4 - Mn_3O_4", J. Inorg. Nucl. Chem. 31 313-20 (1969)

(32) A. Bergstein and P. Kleinert, "Partial Phase Diagram of the System $Mn_xFe_{3-x}O_y$", Collect. Czech. Chem. Commun. 29 2549-51 (1964)

(33) K. Ono, T. Ueda, T. Ozaki, Y. Ueda, A. Yamaguchi, and J. Moriyama, "Thermodynamic Study of the Iron - Manganese - Oxygen System", J. Jap. Inst. Met. 35(8) 757-63 (1971)

(34) H.P. Peloschek, "An Investigation of Reactions and Phase Transitions in the Cu - Mn - Ferrite System", Intern. Symp. Reactivity Solids, 5th. 1964 (Pub. 1965) 549-61

(35) M.A. Zinovik, A.A. Shchepetkin, and G.I. Chufarov, "Phase Relationships in the Preparation and Cooling in Air of Spinel Solid Solutions in the $CuFe_2O_4$ - Mn_3O_4 System", Zh. Neorg. Khim. 16(2) 281-2 (1971)

(36) R.S. Weisz and D.L. Brown, "Square Loop Properties of Copper - Manganese Ferrites", J. Appl. Phys. 31(5) 269S-270S (1960)

(37) M.A. Zinovik, A.A. Shchepetkin, and G.I. Chufarov, "Ferrite Material with a Square Hysteresis Loop", USSR Patent 427,401 (1974)

(38) J. Smit and H.P.J. Wijn, "Ferrites", John Wiley and Sons (1959)

(39) H.J. Van Hook, "Phase Equilibria in Magnetic Oxide Materials", in "Phase Diagrams", Ed: A.M. Alper, Academic, N.Y., p.193-232 (1976)

(40) R. Parker, "Electrical Transport Properties", in "Magnetic Oxides", Ed: D.J. Craik, John Wiley and Sons, p.421- 79 (1975)

(41) A.J. Bosman and H.J. van Daal, "Small - Polaron versus Band Conduction in Some Transition - Metal Oxides", Adv. Phys. 19(77) 1-112 (1970)

(42) G.H. Jonker, "Analysis of the Semiconducting Properties of Cobalt Ferrite", Phys. and Chem. Solids 9 165-75 (1959)

(43) D. Elwell, B.A. Griffiths and R. Parker, "Electrical Conduction in Nickel Ferrite", Brit. J. Appl. Phys. 17(5) 587-93 (1966)

(44) V. Montoro, "Miscibility of the Saline Oxides of Iron and of Manganese", Gazz. Chim. Ital. 68 728-33 (1938)

(45) G.I. Finch, A.P.B. Sinha, and K.P. Sinha, "Crystal Distortion in Ferrite - Manganites", Proc. Roy. Soc. (London) A242 28-35 (1957)

(46) H.J. van Hook and M.L. Keith, "The System Fe_3O_4 - Mn_3O_4", Am. Mineral. 43 69-83 (1958)

(47) H.A. Jahn and E. Teller, "Stability of Polyatomic Molecules in Degenerate Electronic States. I. Orbital Degeneracy", Proc. Roy. Soc. (London) A161 220-35 (1937)

(48) V.A.M. Brabers, "Cation Migration, Cation Valencies and the Cubic - Tetragonal Transition in $Mn_xFe_{3-x}O_4$", J. Phys. Chem. Solids 32 2181- 91 (1971)

(49) M.K. Hucl and F. Van der Woude, "Cation Valences in Cubic and Tetragonal $Mn_{1.9}Fe_{1.1}O_4$", Phys. Lett. 42A(1) 99-100 (1972)

(50) J.M. Hastings and L.M. Corliss, "Neutron Diffraction Study of Manganese Ferrite", Phys. Rev. 104(2) 328-331 (1956)

(51) G.D. Rieck and F.C.M. Driessens, "The Structure of Manganese - Iron - Oxygen Spinels", Acta Cryst. 20 521-5 (1966)

(52) T. Yamanaka and M. Nakahira, "Dependence of the Cation Distribution in Manganese Ferrite, $MnFe_2O_4$, on Temperature and Oxidation", Mineral J. 7(2) 202-20 (1973)

(53) A. Bergstein, "The Lattice Constant of $Mn_xFe_{3-x}O_{4+\gamma}$ Spinels", Czech. J. Phys. B 13 613-6 (1963)

(54) V.A.M. Brabers, "Infrared Spectra of Cubic and Tetragonal Manganese Ferrites", Phys. Stat. Sol. 33 563-72 (1969)

(55) P.P. Bakare, M.P. Gupta, S.K. Date, and A.P.B. Sinha, "Structural, Magnetic and Mössbauer Studies on $Mn_xFe_{3-x}O_4$ ($0 \leq x \leq 1$)", Proc. Indian Acad. Sci. 93(8)

1349-59 (1984)

(56) T. Tanaka, "Lattice Constant and Nonstoichiometry in Mn - Fe Ferrites", Jap. J. Appl. Phys. 13(8) 1235-7 (1974)

(57) A.I. Andriyevskiy, G.F. Mocharnyuk, and Yu.G. Yuskevich, "X - Ray Diffraction Study of Certain Mixed Ferrites", Fiz. Metal. Metalloved. 20(2) 216-20 (1965)

(58) M.A. Zinovik, A.A. Shchepetkin, and G.I. Chufarov, "Crystallochemical Features of Spinel Oxides in the System Cu - Mn - Fe - O", Dokl. Akad. Nauk SSSR 187(6) 1304-7 (1969)

(59) P. Muthukumarasamy, T. Nagarajan, and A. Narayanasamy, "Mössbauer Study of Copper - Nickel and Copper - Manganese Ferrites", J. Phys. C 15 2519-28 (1982)

(60) F.W. Harrison, W.P. Osmond, and R.W. Teale, "Cation Distribution and Magnetic Moment of Manganese Ferrite", Phys. Rev. 106(5) 865-6 (1957)

(61) S. Krupicka and K. Zaveta, "The Distribution of Ions and Their Valences in Manganese Ferrites. Part I", Czech. J. Phys. 9 324-31 (1959)

(62) J. Broz, S. Krupicka, K. Zaveta, "The Distribution of Ions and Their Valences in Manganese Ferrites. Part II", Czech. J. Phys. 9 481-7 (1959)

(63) A.H. Eschenfelder, "Ionic Valences in Manganese - Iron Spinels", J. Appl. Phys. 29(3) 378-80 (1958)

(64) I.I. Yamzin, N.V. Belov, and Yu.Z. Nozik, "A Neutron - Diffraction Study of Manganese Ferrites", J. Phys. Soc. Japan 17, Suppl. B-III, 55-7 (1962)

(65) S.R. Butler and W.R. Buessem, "Magnetization of Manganese Ferrites", J. Appl. Phys. 34(6) 1754-7 (1963)

(66) F.K. Lotgering, "Semiconducting and Cation Valences in Manganese Ferrites", J. Phys. Chem. Solids 25 95-103 (1964)

(67) Z. Simsa, "Note on the Distribution of Valences in Manganese Ferrites", Czech. J. Phys. B 15 435-7 (1965)

(68) Z. Simsa, "The Thermoelectrical Properties of Manganese Ferrites", Czech. J. Phys. B 16 919-28 (1966)

(69) G.A. Sawatzky, F. van der Woude, and A.H. Morrish, "Note on Cation Distribution of $MnFe_2O_4$", Phys. Lett. 25A(2) 147-8 (1967)

(70) I. Bunget, "Note on Mössbauer Effect in $MnFe_2O_4$", Phys. Stat. Sol. 28 K39-K42 (1968)

(71) G.A. Sawatzky, F. Van Der Woude, and A.H. Morrish, "Mössbauer Study of Several Ferrimagnetic Spinels", Phys. Rev. 187(2) 747-57 (1969)

(72) V.A.M. Brabers and P. Dekker, "Infrared Spectra and Cation Distribution of Manganese Ferrites", Phys. Stat. Sol. 29 K73-K76 (1968)

(73) Z. Jirak and S. Vratislav, "Temperature Dependence of Distribution of Cations in $MnFe_2O_4$", Czech. J. Phys. B 24 642-7 (1974)

(74) Z. Simsa, "Degree of Inversion and its Effect on Some Properties of Manganese Ferrite", Konf. Keram. Elektron, [Pr.], 5th., No. 24 (1974)

(75) V.A.M. Brabers and J.H. Hendriks, "Electronic Magnetic Relaxation in Manganese Ferrites", Solid State Commun. 6 795-8 (1968)

(76) A. Marais, T. Merceron, M. Porte, and L. Brossard, "Distribution of Ions and Their Valency in $Mn_xFe_{3-x}O_{4+\delta}$ ($x > 1$) by Directional Order Study", Tr. Mezhdunar. Konf. Magn. 1973, Vol. 1, Pt. 1, 127-30 (Pub. 1974)

(77) M. Rotter, B. Sedlak, Z. Simsa, and V.A.M. Brabers, "NMR Study of Valency States in $MnFe_2O_4$", Phys. Stat. Sol. A 40 K169-K171 (1977)

(78) A.D. Pelton, H. Schmalzried, and J. Sticher, "Thermodynamics of Mn_3O_4 - Co_3O_4, Fe_3O_4 - Mn_3O_4, and Fe_3O_4 - Co_3O_4 Spinels by Phase Diagram Analysis", Ber. Bunsenges Phys. Chem. 83 241-52 (1979)

(79) S.E. Dorris, "The Electrical Properties and Cation Distributions of the Iron Oxide - Manganese Oxide Solid Solution", Ph.D. Dissertation, Northwestern University (1986)

(80) H.S. O'Neill and A. Navrotsky, "Simple Spinels : Crystallographic Parameters, Cation Radii, Lattice Energies, and Cation Distribution", Am. Mineral. 68 181-94 (1983)

(81) I. Bunget, M. Rusu, M. Andreescu, and C. Nistor, "Mössbauer Effect on Various Copper - Manganese Ferrites", An. Univ. Bucaresti, Ser. Stiint. Nat. 14 9-13 (1965)

(82) L. Cervinka and Z. Simsa, "Distribution of Copper Ions in Some Copper - Manganese Ferrites", Czech. J. Phys. B

20 470-4 (1970)

(83) S.E. Tsitsenovskaya and Yu.A. Tarasyuk, "Neutron Diffraction Analysis of the Spinel $Cu_{0.5}Mn_{0.5}Fe_{2.0}O_4$", Izv. Akad. Nauk SSSR, Necrg. Mat. 8(12) 2177-9 (1972)

(84) N. Rezlescu and E. Cuciureanu, "Cation Distribution and Curie Temperature in Some Ferrites Containing Copper and Manganese", Phys. Stat. Sol. A 3 873-8 (1970)

(85) S.E. Tsirkunova, "Cation Distribution in the System of Copper - Manganese Ferrospinels", Izv. Akad. Nauk SSSR 10(4) 683-6 (1974)

(86) V.N. Belogurov, E.M. Iolin, B.V. Kuvaldin, A.E. Petrov, P.E. Sen'kov, S.E. Tsirkunova, and M.O. Shusta, "Neutron Diffraction and Mössbauer Studies of Copper - Manganese Ferrospinels", Khimi. Svyaz Krist. Ikh Fiz. Svoistava, No. 1, p. 167-71 (1976)

(87) A. Narayanasamy and L. Häggström, "Mössbauer Study of Copper - Manganese Ferrites in an External Magnetic Field", J. Phys. C 16 591-602 (1983)

(88) K.P. Belov, A.A. Popova, and E.V. Talalaeva, "Electrical and Magnetoresistance Properties of Single Crystals of Manganese Ferrite", Kristallografiya 3 733-9 (1958)

(89) K.P. Belov, E.P. Svirina, and O.A. Malikov, "The Problem of Electrical Conductivity of Manganese Ferrite Single Crystals", Fiz. Tverd. Tela 4(10) 2829-31 (1962)

(90) K. Zaveta, E. Svirina, O. Malikova, "Effect of Heat Treatment of the Electrical Properties of a Manganese Ferrite Crystal", Fiz. Tverd. Tela 4(12) 3593-5 (1962)

(91) Z. Funatogawa, N. Miyata, and S. Usami, "Electric Resistance and Cation Distribution of Fe-Mn Ferrite System", J. Phys. Soc. Japan 14 854 (1959)

(92) C. Kooy and H.J.M. Couwenberg, "Zone Melting of Oxides in a Carbon - Arc Image Furnace", Philips Tech. Rev. 23 161-6 (1962)

(93) M. Rosenberg, P. Nicolau, and I. Bunget, "Electrical Properties of the System $Mn_xFe_{3-x}O_4$", Phys. Stat. Sol. 14 K65-K69 (1966)

(94) R. Gerber, Z. Simsa, M. Vichr, "Some Physical Properties of Single Crystal Manganese Ferrites", Czech. J. Phys. B 16 913-8 (1966)

(95) V.A.M. Brabers, "The Electical Conductivity of

Manganese Ferrites", Ber. Dt. Keram. Ges. 47 648-53 (1970)

(96) N. Rezlescu, E. Cuciureanu, C. Ioan, and E. Luca, "On the Nature of the Variation with Time of the Electrical Conductivity of Ferrites", C. R. Acad. Sci., Paris 274B 380-3 (1972)

(97) Z. Simsa and J. Simsova, "Electrical Properties and Cation Migration in Manganese Ferrites. I. Temperature Dependences", Czech. J. Phys. B 24 439-48 (1974)

(98) J. Simsova and Z. Simsa, "Electrical Properties and Cation Migration in Manganese Ferrites. II. Time Effects", Czech. J. Phys. B 24 449-56 (1974)

(99) Z. Simsa, J. Simsova, and V.A.M. Brabers, "Electrical Conductivity in Manganese Ferrites", Proc., Int. Conf. Phys. Semicond., 11th, 2 1294-9 (1972)

(100) M. Rosenberg, P. Nicolau, and I. Bunget, "On the Electrical Properties of Some Iron - Copper and Manganese Ferrites", Phys. Stat. Solidi 15 521-30 (1966)

(101) Z. Simsa and N. Andrejev, "The Electrical Properties of Manganese - Copper Ferrites", Czech. J. Phys. B 19 1389-99 (1969)

(102) L. Wu, T.S. Wu, and C.C. Wei, "Effect of Various Substitutions on the DC Resistivity of Ferrites", J. Phys. D 13 259-66 (1980)

(103) S.E. Tsirkunova, "Structure and Physical Properties of Copper Manganese Ferrospinels", Radiats. Fiz. 8 201-27 (1975)

(104) H. Makram and M. Vichr, "Crystal Structures and Fabrication of Crystals", Magn. Oxides, Ed: D. J. Craik, Part 1, 97-140 (1975)

(105) E.J. Scott, "Single Crystals of the Oxides of the Transition Elements by the Flame Fusion Method", J. Chem. Phys. 23 2459 (1955)

(106) H. Burger and I. Hanke, "Incorporation of α-Fe_2O_3 in Mn - Ferrite Single Crystals and its Effect on the Density of Dislocations", Z. Angew. Phys. 14(1) 40-3 (1962)

(107) R.F. Penoyer and M.W. Shafer, "On the Magnetic Anisotropy in Manganese - Iron Spinels", J. Appl. Phys. 30 Suppl. 315S-316S (1959)

(108) M. Paulus and A. Hamelin, "Crystal Growth of Manganese Ferrite", J. Cryst. Growth, No. 3-4, 500-3 (1968)

(109) G.I. Zyryanov, "On Growing Manganese Ferrite Single Crystals in the Solid Phase", Izv. Akad. Nauk SSSR, Ser. Fiz. 34(6) 1244-5 (1970)

(110) F.R. Monforte, F.W. Swanekamp, and L.G. Van Uitert, "Radio - Frequency Technique for Pulling Oxide Crystals Without Employing a Crucible Susceptor", J. Appl. Phys. 32 959-60 (1961)

(111) K. Nassau and A.M. Broyer, "Application of Czochralski Crystal - Pulling Technique to High Melting Oxides", J. Am. Ceram. Soc. 45(10) 474-8 (1962)

(112) R.P. Poplawsky, "Ferrite Crystals Using an Arc Image Furnace", J. Appl. Phys. 33 1616-7 (1962)

(113) R.P. Poplawsky, "Arc Imaging Furnace Crystal Growth", Thermal Imaging Tech., Proc. Conf., 1st, Cambridge, Mass. 1962, p. 209-21 (Pub. 1964)

(114) V.A.M. Brabers, "The Preparation of Tetragonal Single Crystals in the $Mn_xFe_{3-x}O_4$ System", J. Cryst. Growth 8 26-8 (1971)

(115) J.S. Haggerty, "Production of Fibers by a Floating Zone Fiber Drawing Technique", NASA Report CR-120948 (1972)

(116) T. Yamaguchi and T. Kimura, "Kinetic Studies on the Precipitation of Hematite from Iron - Rich Spinel Solid Solutions", J. Am. Ceram. Soc. 59 333-5 (1976)

(117) A. Bergstein, "Manganese Magnesium Ferrites. IV Oxygen Nonstoichiometry of Spinels $Mn_xFe_{3-x}O_{4+\gamma}$", Collect. Czech. Chem. Commun. 28 2381-6 (1963)

(118) A. Bergstein, "Spinels $Cu_{0.5}Mn_xFe_{2.5-x}O_{4+\gamma}$", Reactiv. Solids, Proc. Int. Symp., 6th 1968, 219-25 (Pub 1969)

(119) N.N. Oleinikov, Yu.D. Tretyakov, and Yu.G. Saksonov, "Phase Diagram of the Mn_2O_3 - Mn_3O_4 - Fe_3O_4 - Fe_2O_3 System at 900 - 1200 C", Fiz. Khim. Ferritov. 282-90 (1973)

(120) H.L. Tuller, H.I. Yoo, W. Kehr, and R.W. Scheidecker, "Electrical Property - Phase Equilibria Correlations in Manganese - Zinc Ferrites", Adv. Ceram., 4th Int. Conf. on Ferrites, Vol. 15, Pt. 1, (1986)

(121) J. Thonstad, "Anodic Overvoltage on Platinum in Cryolite - Alumina Melts", Electrochim. Acta 13 449-56

(1968)

(122) M. Zhang and Z. Qiu, "Anodic Overvoltage on Platinum Electrode in Cryolite - Alumina Melts", Dongbei Gongxueyuan Xuebao 42 71-9 (1985)

(123) E.W. Dewing and E.Th. van der Kouwe, "Anodic Phenomena in Cryolite - Alumina Melts. II. Chronopotentiometry at Gold and Platimum Anodes", J. Electrochem. Soc. 124(1) 58-64 (1977)

(124) Y.X. Liu and J. Thonstad, "Oxygen Overvoltage on SnO_2 - Based Anodes in NaF - AlF_3 - Al_2O_3 Melts. Electrocatalytic Effects of Doping Agents", Electrochim. Acta 28(1) 113-116 (1983)

(125) P.G. Russell, "Oxygen Evolution at Platinum and Ceramic Oxide Anodes in Cryolite - Alumina Melts", Proc. IVth Int. Symp. on Molten Salts, Ed: M. Blander, 430-42 (1984).

(126) P.G. Russell, "Activity of Anodic Oxide Films on Metal and Cermet Anodes in Cryolite - Alumina Melts", J. Appl. Electrochem. 16 147-55 (1986)

(127) K. Horinouchi, N. Tachikawa, and K. Yamada, "DSA in Aluminum Reduction Cells", Proc. Int. Symp. Molten Salt Chem. Technol., 1st, 65-8 (1983)

(128) D.H. DeYoung, "Solubilities for Inert Anodes in Cryolite - Based Melts", Light Metals 1986, R.E. Miller, editor, 299-307 (1986)

(129) G.P. Tarcy, "Corrosion and Passivation of Cermet Inert Anodes in Cryolite - Type Electrolytes", Light Metals 1986, R.E. Miller, editor, 309-20 (1986)

(130) S.P. Ray, "Effect of Cell Operating Parameters on Performance of Inert Anodes in Hall - Héroult Cells", Light Metals 1987, R.D. Zabreznik, editor, 367-80 (1987)

(131) C.F. Windisch and S.C. Marschman, "Electrochemical Polarization Studies on Cu and Cu - Containing Cermet Anodes for the Aluminum Industry", Light Metals 1987, R.D. Zabreznik, editor, 351-5 (1987)

(132) D.R. Sadoway, "Aluminum Reference Electrode", U.S. Patent Application 783,776, filed Oct. 3,1985

(133) A.D. McLeod, J.S. Haggerty, and D.R. Sadoway, "Inert Anode Materials for Hall Cells", Light Metals 1986, R.E. Miller, editor, 269-73 (1986)

(134) A.D. McLeod, J.-M. Lihrmann, J.S. Haggerty, and D.R. Sadoway, "Selection and Testing of Inert Anode Materials for Hall Cells", Light Metals 1987, R.D. Zabreznik, editor, 357-65 (1987)

(135) I. Barin and O. Knacke, Thermochemical Properties of Inorganic Substances (Berlin: Springer - Verlag, 1973)

(136) I. Barin, O. Knacke and O. Kubaschevski, Thermochemical Properties of Inorganic Substances Supplement, (Berlin: Springer - Verlag, 1977)

(137) D.D. Macdonald, Transient Techniques in Electrochemistry, (Plenum Press, New York, NY, 1977)

APPENDIX 4

Summary of Float Zone, Pendant Drop Cryolite Experiments

Table 1

FLOAT-ZONE, PENDANT-DROP CRYOLITE EXPERIMENTS

Issues:

- Establishment of Stable Pendant Drop Method
  - Optical Properties re: Laser (melt?)
  - γ/ρ (drop size, shape?)
  - Evaporation Rate (maximum time)
  - Compositional Change (unstable composition)
- Temperature Uniformity
- Compositional Uniformity
- Dissolution Rate of Candidate Anodes

Table 2

FLOAT-ZONE, PENDANT-DROP CRYOLITE EXPERIMENTS

o Cryolite on Cryolite Experiments

Feed Diameter: ~ 8 mm (Greenland Cryolite)

Melt Power: ~40 watts

Melt Temperature

Visible Pyrometer:	830° C
Infrared Pyrometer:	~800° C
Thermocouple:	765° C
Phase Diagram	
Stoichiometric:	1010° C
Eutectic:	888° C
Normal Bath:	~960° C
Greenland Cryolite:	>1000° C

Melt Properties
L/D ~ 1
Transparent, No turbidity
No Color
Low ϵ
Stable for 2, 5, 15, 25 min.

Chemistry (5 min.)

	% Na	% Al	Na/Al
Stoichiometric	32.86	12.86	2.55
Feed Rod Unmelted	30.5	12.4	2.46
Feed at S/L Interface	30.65	12.45	2.46
Quenched Drop	32.25	12.95	2.49
Condensate	23.7	17.7	1.33

Conclusions:

Cryolite Absorbs Laser Radiation
Melt Geometry is Acceptable
Vaporization Rate is Acceptable
Chemical Stability is Acceptable
Temperature Measurement Subject to Error

Table 3

FLOAT-ZONE, PENDANT-DROP CRYOLITE EXPERIMENTS

o Cryolite on Al_2O_3

Al_2O_3 Diameter: ~ 8 mm.

Cryolite Diameter: ~ 8 mm.

a. 5 mm Laser Beams Directed onto Cryolite

Melt Power: 80 - 100 Watts

Melt Temperature: not determined (incandescent)

Melt Stability: Excessive Vaporization Rates

Conclusion: High Thermal Conductivity of Al_2O_3 rod required excessive superheat.

b. Unfocused Laser Beams Directed onto Cryolite

Melt Power: 150 - 200 Watts

Melt Temperature: not determined (Al_2O_3 > 1500° C)

Melt Stability: Cryolite melt used up Al_2O_3 rod, ran into hot zone and vaporized.

Conclusion: Pendant drop experiment requires thermally guarded, isothermal environment. Experiment is feasible but difficult.

APPENDIX 5

"Selection and Testing of Inert Anode Materials for Hall Cells," reprinted from Light Metals 1987

SELECTION AND TESTING OF INERT ANODE MATERIALS FOR HALL CELLS

Alan D. McLeod, Jean-Marc Lihrmann, John S. Haggerty, and Donald R. Sadoway,

Department of Materials Science and Engineering,
Massachusetts Institute of Technology,
Cambridge, Massachusetts, 02139

A new set of criteria for Hall cell anode materials is presented. Fundamental thermodynamic data are used to estimate how well a variety of oxides will satisfy these criteria in the context of the total environment of an operating industrial cell. In addition, the results of tests of candidate anode materials performed in this laboratory are presented.

INTRODUCTION

While the current efficiency in modern Hall - Héroult cells exceeds 90% the voltage efficiency is less than 30%. In large measure the latter is a consequence of the present choice of electrode materials, which imposes severe limitations on cell design, most notably the need to separate the electrodes by a spacing so great that more than 40% of the total cell voltage is associated with the so - called iR drop across the electrolyte. The discovery of materials for an inert anode, wettable cathode, and inert sidewall would pave the way for radical innovation in cell design and operation with attendant improvements in productivity. This paper will be restricted to the discussion of inert anode materials.

The search for inert anode materials has proved to be one of the most difficult challenges for modern materials science. While a variety of formulations has been proposed and numerous patents have been granted (1) no material has proven to be fully satisfactory. Indeed, it may well be that there is no material that can meet the requirements of an industrial cell. At least, this seems to be the conclusion of all previous research which was directed to find "the inert anode material". It is the opinion of the authors that a totally different approach must be adopted, i.e., not to look for "the inert anode material" but rather to consider the entire cell in the context of a dynamic materials system. The purpose of this paper is then to state clearly the criteria of selection and to pose the problem in the light of the above.

Until recently, materials used for inert anode formulations were selected from those oxides that have low solubilities in cryolite (Na_3AlF_6), for example : Fe_2O_3, SnO_2, and Cr_2O_3. Electrical conductivity is enhanced by doping with oxide additions to the host materials or by the presence of a distinct metal phase to form a cermet. The disadvantage in such cases is that the host is selected without consideration of all the criteria and on the basis of a relatively small and frequently inaccurate data base. By consideration of other fundamental materials property data, in particular thermodynamic data, it is possible to establish an improved rationale for materials selection. Laboratory testing is necessary to confirm that candidate materials behave according to expectations.

MATERIALS SELECTION

In selecting candidate anode materials one must consider as nearly as possible how that material will behave in its total environment. In an operating Hall cell this environment is not homogeneous. While the electrolyte consists of cryolite (Na_3AlF_6) - AlF_3 - CaF_2 - Al_2O_3 there are severe gradients in chemical potential across the interelectrode gap. In the vicinity of the inert anode the melt is highly oxidizing due to the evolution of pure oxygen at pressures exceeding one atmosphere. Near the cathode the melt is highly reducing due to the presence of dissolved elemental aluminum. All the while as the cell operates electrical current is passing at current densities near 1 A/cm^2. Given this complex set of conditions it should be apparent that consideration of chemical dissolution of a candidate material in pure cryolite or even cryolite containing dissolved Al_2O_3 cannot alone serve as the basis for materials selection.

For example, the interaction of the candidate material with the aluminum dissolved in the electrolyte must be considered. The aluminum may reduce the metal oxide allowing the metal to itself dissolve in the electrolyte. Alternatively, a metal oxide may dissolve by forming a metal fluoride through an exchange reaction with the electrolyte.

Since cryolite will dissolve most, if not

all, oxides to some extent, one must consider what happens to a metal oxide once it is in solution. The metal can co-deposit with aluminum by electrolytic reduction or dissolve in the molten aluminum cathode following a metallothermic - type displacement reaction. The second new criterion, then, uses the electrochemical series in the Hall cell electrolyte to predict whether or not a metal will co-deposit. The third new criterion considers whether or not elemental aluminum will displace the impurity metal from the electrolyte by chemical reaction.

The diagram shown in Figure 1 can be used as an aid in discussing the concepts behind the proposed selection criteria. Similar to a decision tree, the diagram shows the tests a metal oxide must pass in order to be deemed useful as an anode. The first test considers the exchange reaction between the candidate metal oxide and dissolved aluminum. If aluminum reduces the metal oxide the material fails this test. However, as will be discussed in more detail below, an oxide can be protected from chemical attack by dissolved aluminum by the oxygen evolving on the anode. This oxygen acts to oxidize the dissolved elemental aluminum thereby reducing its concentration in the vicinity of the anode. Thus protected, it can still pass the first test, hence, an alternate route through "function of current density" has been included.

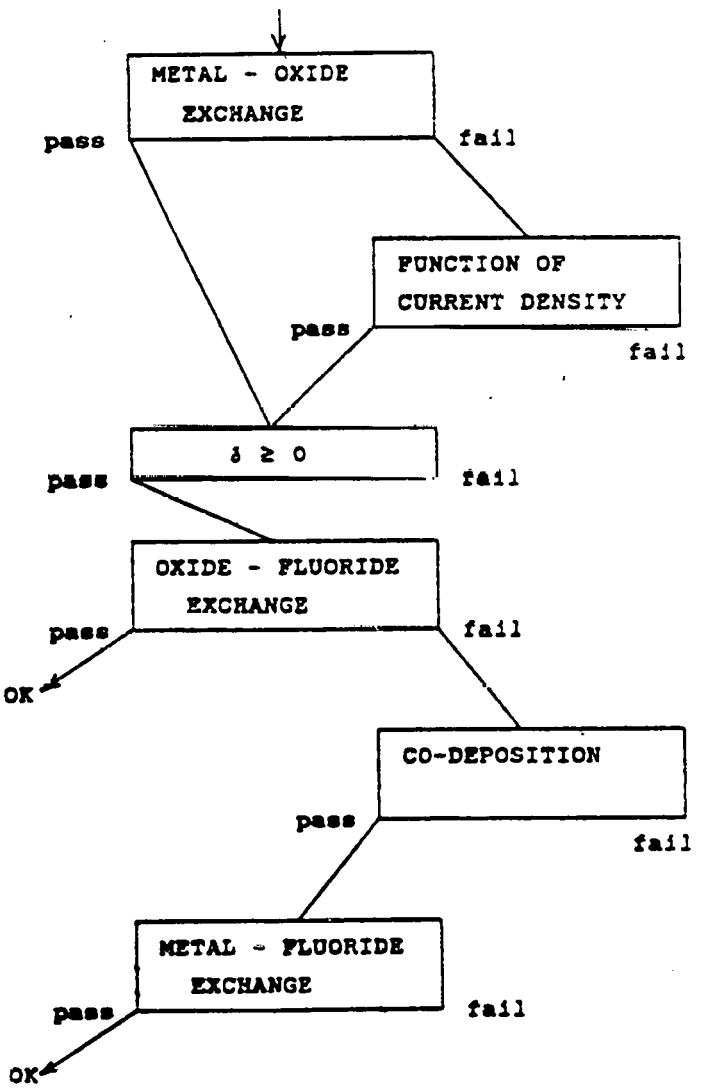

Figure 1. Stages in Materials Selection.

The third and fourth boxes determine if the oxide passes both stages of the second test. The issue here is the chemical dissolution of the metal oxide through the exchange reaction between the oxide and the molten fluorides. The first stage of this test, "$\delta \geq 0$" refers to a condition where the metal changes valence when going into solution. It will be shown that it is undesirable to have the valence of the metal increase as shown by a negative value for δ. An oxide that does not go into solution through the oxide - fluoride exchange process will pass the second stage of this test. An oxide that fails this test should not be dropped from consideration, however. The material could still be acceptable if it can pass both of the last two tests, "co-deposition" and "metal - fluoride exchange". The following discussion will consider each test in turn starting from the top of the diagram. An examination of the applicable thermodynamic data will indicate which oxides will pass which tests. The end result of this examination will be a list of oxides that are acceptable for use as anode materials on the basis of the criteria enumerated in this paper.

Both the metal - metal oxide and metal oxide - metal fluoride reactions can be thought to occur at the anode surface. The former reaction between the anode and dissolved elemental aluminum can be represented by :

$$MeO_{\frac{n}{2}} + \frac{n}{3}Al = \frac{n}{6}Al_2O_3 + Me \qquad (1)$$

This reaction is also referred to as the "crucible reaction", i.e., would a crucible made of the metal oxide under consideration be acceptable as container of molten aluminum at Hall cell operating temperatures? If aluminum oxide is stabler than the metal oxide of the crucible a reaction will occur consuming the crucible until the melt is exhausted of dissolved aluminum or is saturated with alumina. The free energy change for reaction (1) calculated per mole of metal, Me, at 1300 K is given for various oxides in Table I. All thermodynamic data for this and subsequent analyses have been taken from Barin and Knacke (2,3). Evidently a series of oxides from ZrO_2 to Y_2O_3 will satisfy the first criterion. Their positive ΔG indicates that dissolved aluminum will not reduce the oxide if it is assumed that the activities of dissolved metals are unity. Of course during electrolysis, the anode will be surrounded by a "shroud" of O_2. The

Table I. Free Energy of Reaction for Metal - Oxide Exchange at 1300 K

OXIDE	ΔG_1 (kJ)	OXIDE	ΔG_1 (kJ)	OXIDE	ΔG_1 (kJ)
PbO_2	-829	Ta_2O_5	-303	CeO_2	-30
WO_3	-733	NiO	-301	BaO	-12
Rh_2O_3	-613	CdO	-295	Li_2O	-11
SbO_2	-609	CoO	-284	TiO	-8
SnO_2	-528	FeO	-233	ZrO_2	19
Bi_2O_3	-522	Cr_2O_3	-231	UO_2	22
V_2O_5	-521	ZnO	-229	SrO	31
GeO_2	-507	Cu_2O	-184	MgO	33
WO_2	-482	V_2O_3	-181	BeO	54
Sb_2O_3	-448	K_2O	-165	CaO	72
CuO	-385	SiO_2	-150	La_2O_3	76
Fe_2O_3	-384	B_2O_3	-145	Nd_2O_3	77
Nb_2O_5	-370	MnO	-139	Sm_2O_3	82
PbO	-347	TiO_2	-130	Ce_2O_3	110
VO_2	-330	Na_2O	-124	Sc_2O_3	129
Mn_2O_3	-321	VO	-108	Y_2O_3	132
Ga_2O_3	-304	Ti_2O_3	-48		

Table II. Free Energy of Reaction for Metal Oxide - Metal Fluoride Exchange at 1300 K

OXIDE	ΔG_2 (kJ)	OXIDE	ΔG_2 (kJ)
SrO	-190	Bi_2O_3	33
PbO_2**	-186	Fe_2O_3*	59
Y_2O_3	-119	Nb_2O_5	112
Sc_2O_3	-80	V_2O_3	136
PbO	-47	Mn_2O_3	144
Ti_2O_3	-6	PbO_2	148
CoO	-1	VO_2*	174
MnO	24	VO_2	223
Mn_2O_3*	28	WO_3	285

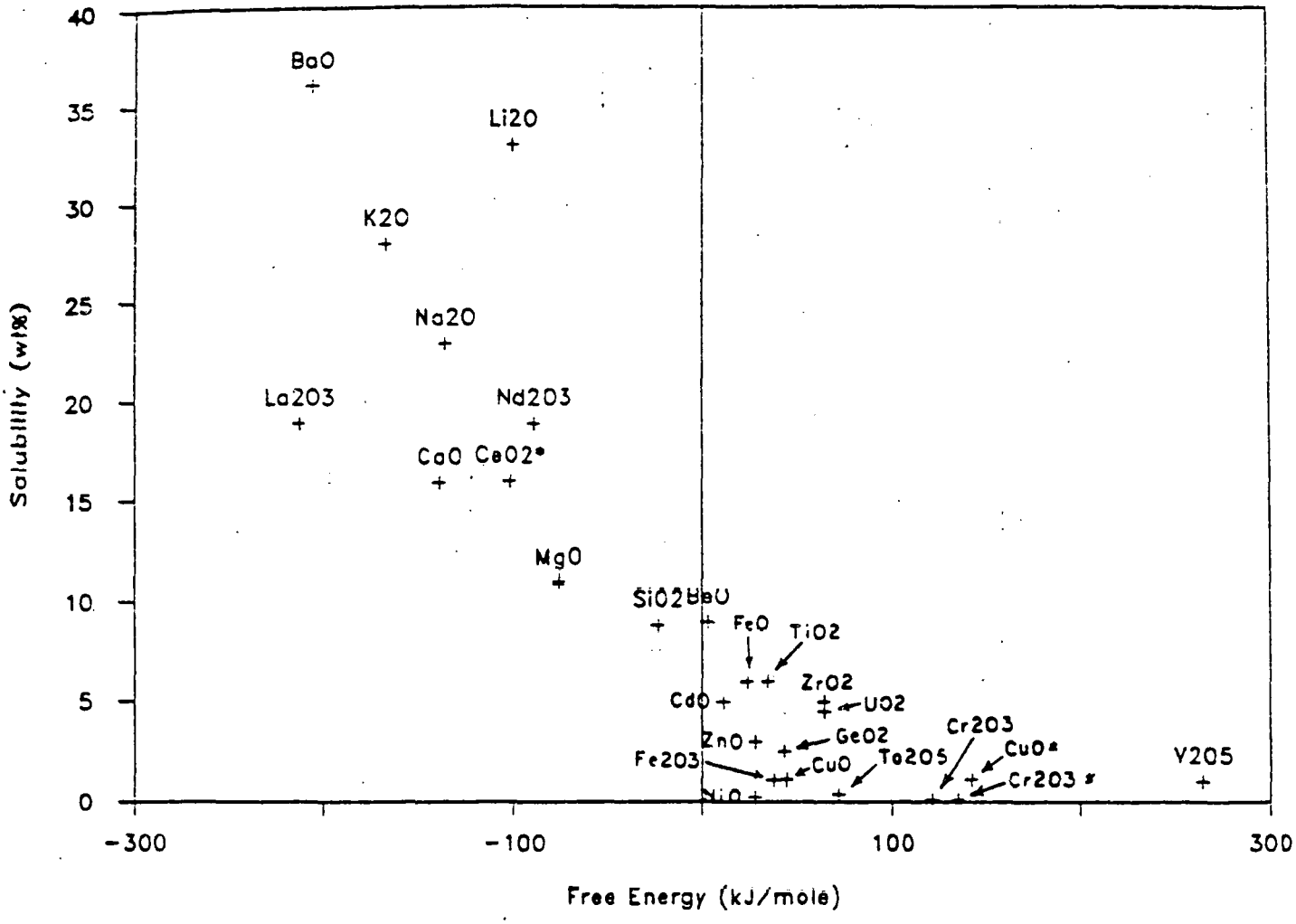

Figure 2. Metal Solublity Plotted Against ΔG_2.

resulting high oxygen pressure, P_{O_2}, will certainly lower the dissolved metal activity. This effect could move reaction (1) in either direction, depending on the metal valence, n, and the relative metal activities. For this reason some oxides may still satisfy the first criterion due to the activity shift. The importance of Table I is that it indicates that some oxides will be more susceptible to attack than others. It will be seen that the following criteria are more stringent in any case.

The metal oxide - metal fluoride exchange reaction occurring at the anode surface can be described by reaction 2 :

$$MeO_{\frac{n}{2}} + \frac{n-\delta}{3}AlF_3 = MeF_{n-\delta} + \frac{n-\delta}{6}Al_2O_3 + \frac{\delta}{4}O_2 \quad (2)$$

The value of δ is non - zero when the metal oxide changes valence state as it goes into solution. In such cases the thermodynamics of the reaction are influenced by the P_{O_2}. When $\delta < 0$, the reaction is forced to the right at higher values of the P_{O_2}, clearly not a desirable result. One can argue that ΔG_2 is related to the solubility of the metal oxide. Evidence of this can be seen in Figure 2 where solubility is plotted against ΔG_2 per mole of Me at 1300 K. The solubility data used in Figure 2 were taken from Table 10.3 in the book by Grjotheim et al. (4). This plot also shows that a positive ΔG_2 is no assurance that a metal oxide will not go into solution but rather indicates only that the metal oxide will dissolve at a reduced activity level. In fact, the values of ΔG_2 are useful primarily to rank oxides in relation to relative reactivities. The values of ΔG_2 for some oxides whose solubilities have not been measured are listed in Table II. The attached "*"'s indicate a condition where $\delta > 1$, "*" meaning $\delta = 1$, and "**" meaning $\delta = 2$. A question arises at this stage as to the importance of the second criterion in comparison with other criteria. If an oxide did not go into solution then it would certainly be acceptable as far as this criterion goes. However, it is safe to assume that all metal oxides will go into solution in varying degrees, the extent depending on the driving force, ΔG_2. Rather, it is better to consider what happens to the oxide once it has dissolved in the electrolyte. The final two criteria consider the behavior of the

dissolved metal at the cathode.

The metal Me can report to the aluminum product through two mechanisms - electrolytic co-deposition or chemical reduction by aluminum itself. Once in the metal, the impurity must either be removed or tolerated. If the metal is not returned to the cell in some form, the contamination of the aluminum product by the metal constitutes consumption of the anode material.

The co-deposition criterion can be employed using the calculated reversible decomposition potential, E_3°, at 1300 K for the reaction :

$$MeO_{\frac{n}{2}} \Longrightarrow Me + \frac{n}{4}O_2 \qquad (3)$$

This can be calculated using the equation :

$$E_3^\circ = -\frac{\Delta G_3}{zF} \qquad (4)$$

where F is the Faraday constant. The values of E_3° are given in Table III. According to these thermodynamic data those oxides whose E_3° is more negative than that of Al_2O_3 will not co-deposit with aluminum, assuming the electrolyte is saturated with the metal oxide. The metal may, however, co-deposit in the aluminum pool at an activity less than 1. However, the magnitude of the cathodic shift in E_3° is only about 0.2 V for a metal activity of 0.01 in molten aluminum. Kinetic factors are also not expected to be significant on a liquid metal cathode. Mergault (5-7), Grjotheim et al (8), and Monnier and Grandjean (9) have measured the order of deposition for some oxides using a carbon anode. The resulting series, starting from the least negative potentials is : NiO, V_2O_5, Mo_3C_4, Co_3O_4, Fe_2O_3, WO_3, TiO_2, Nb_2O_5, Cr_2O_3, Ta_2O_5, UO_2, Al_2O_3. The oxides that were more stable than Al_2O_3 were BeO, MgO, CaO, SrO, BaO, and La_2O_3. The order of the former series of oxides is in reasonable agreement with that shown in Table III. The order of the latter series was not obtained as decomposition potentials were higher than that for alumina.

The metal can also dissolve in the aluminum pool through a metallothermic type reaction :

$$MeF_n + \frac{n}{3}Al = \frac{n}{3}AlF_3 + Me \qquad (5)$$

The thermodynamic data for this exchange reaction are given in Table IV.

Tables III and IV indicate that there are a few metal oxides capable of resisting attack by electrolytic and metallothermic reduction into the product aluminum. These are MgO, SrO, La_2O_3, Nd_2O_3, CaO, Ce_2O_3, Sc_2O_3, Y_2O_3, and possibly Li_2O, BaO, UO_2, and BeO. The second criterion indicates that all

Table III. Oxide Decomposition Potentials at 1300 K

OXIDE	$-E_3^\circ$ (V)	OXIDE	$-E_3^\circ$ (V)	OXIDE	$-E_3^\circ$ (V)
PbO_2	0.043	FeO	0.987	CeO_2	2.115
Rh_2O_3	0.054	ZnO	1.052	TiO	2.158
CuO	0.206	Mn_2O_3	1.067	$^*Al_2O_3$	2.173
Cu_2O	0.380	V_2O_5	1.069	Li_2O	2.180
Bi_2O_3	0.409	Na_2O	1.117	BaO	2.202
PbO	0.466	Ga_2O_3	1.146	ZrO_2	2.213
SbO_2	0.597	VO_2	1.302	UO_2	2.234
NiO	0.640	Cr_2O_3	1.363	MgO	2.375
Sb_2O_3	0.647	Nb_2O_5	1.386	SrO	2.397
CdO	0.705	MnO	1.486	BeO	2.440
CoO	0.727	Ta_2O_5	1.529	La_2O_3	2.462
K_2O	0.748	V_2O_3	1.544	Nd_2O_3	2.484
SnO_2	0.813	B_2O_3	1.638	Sm_2O_3	2.505
Fe_2O_3	0.842	VO	1.638	CaO	2.592
GeO_2	0.846	SiO_2	1.757	Ce_2O_3	2.599
WO_3	0.879	TiO_2	1.822	Sc_2O_3	2.621
WO_2	0.911	Ti_2O_3	2.007	Y_2O_3	2.643

Table IV. Free Energy of Reaction for Metal - Fluoride Exchange at 1300 K

FLUORIDE	ΔG_5 (kJ)	FLUORIDE	ΔG_5 (kJ)	FLUORIDE	ΔG_5 (kJ)
WF_6	-989	VF_3	-317	KF	3
PbF_4	-976	CdF_2	-306	UF_3	6
VF_5	-785	PbF_2	-299	NaF	13
CoF_3	-657	CoF_2	-283	BeF_2	52
WF	-646	FeF_2	-257	LiF	90
BiF_3	-555	ZnF_2	-257	MgF_2	109
VF_4	-553	CrF_2	-180	NdF_3	167
NbF_5	-481	TiF_4	-165	ScF_3	179
MnF_3	-466	MnF_2	-163	BaF_2	195
CuF_2	-430	SiF_4	-126	CaF_2	211
FeF_3	-422	TiF_2	-78	SrF_2	221
TaF_5	-375	ZrF_4	-46	YF_3	251
CrF_3	-353	UF_4	-42	CeF_3	289
CuF	-340	TiF_3	-42	LaF_3	289
NiF_2	-329				

of these oxides have or will probably have significant solubilities in cryolite. For this reason these oxides have not been of great interest in anode formulations to date. However, the high solubility must be viewed in the light of their resistance against further decomposition. Simply stated, it is not so important that the oxide resist dissolution : it is extremely important, however, that the oxide resist exsolution.

Cerium oxide has been proposed for use as a self forming anode (s.f.a.) material (10). The desirability for the use of such a material becomes apparent from the consideration of the above criteria. The oxide will go into solution with cryolite, but only contaminates the metal pad in low concentrations. Since ΔG_5 for the material is strongly positive it can be easily removed from the metal pad and returned to the cell. Since ϕ probably equals 1 for this material it has the additional attribute of a solubility that is inversely proportional to oxygen pressure, i.e., it becomes more resistant the harder the cell is driven.

Oxides like Fe_2O_3 have been used in inert anode formulations[2](11), largely due to their low solubility in the electrolyte. Consideration of the other criteria demonstrates the weakness in using solubility as the only criterion for selecting materials. Fe_2O_3 does not satisfy the first criterion, the[2] "crucible reaction"; thus, only if the oxygen evolving on the anode completely removes dissolved aluminum form the melt can Fe_2O_3 be spared from attack by metallothermic reduction. From the standpoint of the second criterion Fe_2O_3 looks attractive; in fact, a relatively[3] low solubility has been measured. Nevertheless, this oxide still does not meet the second criterion because it does dissolve in the electrolyte as do all oxides. Fe_2O_3 does not meet the third criterion because it[3] is decomposed electrolytically, and iron reports to the molten aluminum product. As well, AlF_3 forms in preference to either of the iron fluorides. Thus, the fourth criterion is not met, and the metal can be metallothermically displaced from the melt as well. This also indicates that it would be difficult to remove the iron from the aluminum product through the addition of AlF_3. So while the solubility of Fe_2O_3 in the[3] melt appears to be low, a more complete consideration of the other criteria show that this property is insufficient to make the material acceptable as an anode. It has been suggested (12) that corrosion may be reduced by the addition of Fe_2O_3 to the cell through additions to the feed.[3] While this may slow down the "wear rate" of the anode, the iron will deposit in the aluminum and contaminate the cell product.

In addition to the above issues one must also address problems of adequate electrical conductivity along with a variety of design considerations. However, as a result of having done a materials systems analysis, a number of candidate oxides has been identified for further research.

TESTING OF CANDIDATE FERRITE ANODE MATERIALS

This laboratory has been involved with the measurement of electrical conductivity of anode materials and the testing of these materials in a bench - scale Hall cell. Ferrite materials were chosen for study because of earlier industrial interest in them (13-17). Some Hall cell testing results taken on a single crystal of cobalt ferrite have been previously reported (18). Not reported in that paper are some interesting results obtained from a subsequent SEM examination of the interface layer between the ferrite sample and the electrolyte as shown in Figure 3.

The sample was electrolyzed at 3.0 V, 1 A/cm^2, for about 1 hr in an alumina saturated bath containing 5% CaF_2 at a bath ratio of 1.11 and a temperature of 960°C. Figure 3 shows first a normal SEM micrograph with the cobalt ferrite crystal at the left and the frozen electrolyte at the right. The contrast was reversed for the other micrographs so that the elemental trace would show. The light square at the left side of each micrograph indicates the position on the sample represented in the chemical analysis trace and defines the zero concentration baseline for the profiles. This sample shows a reaction zone of about 8 μm in thickness. The reaction zone for a cobalt ferrite sample of identical composition tested in an electrolyte of the same composition for the same immersion time and electrolyzed only at 2.00 V was 25 to 30 μm thick with similarly shaped profiles. The current density for the sample electrolyzed at 2 V increased from 0.20 to 0.29 A/cm^2 during electrolysis. The profiles indicate that the reaction zone is mostly oxide with a small amount of fluoride. The concentrations of iron and cobalt show a gradual decline towards the outside of the

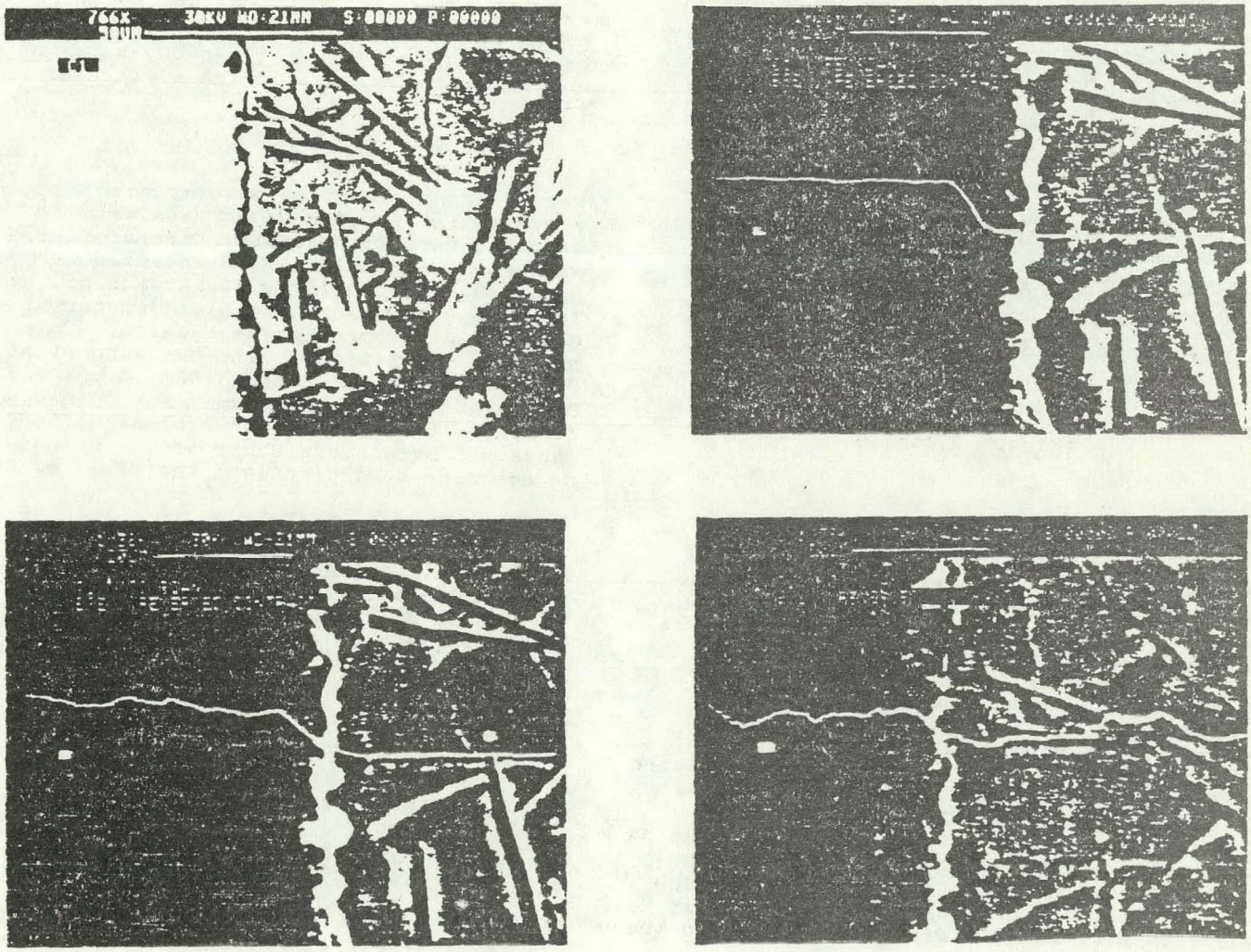

Figure 3. Scanning Electron Micrographs and Elemental Concentration Profiles of the Ferrite - Salt Interface Region for a Cobalt Ferrite Crystal Sample (25 wt% CoO in Fe_2O_3) Electrolyzed at 3.0 V, 1 A/cm^2, for 1 hr, in an Electrolyte of BR$^=$ 1.11, Containing 5% CaF_2, 11% Al_2O_3, in Greenland Cryolite, at 960°C.

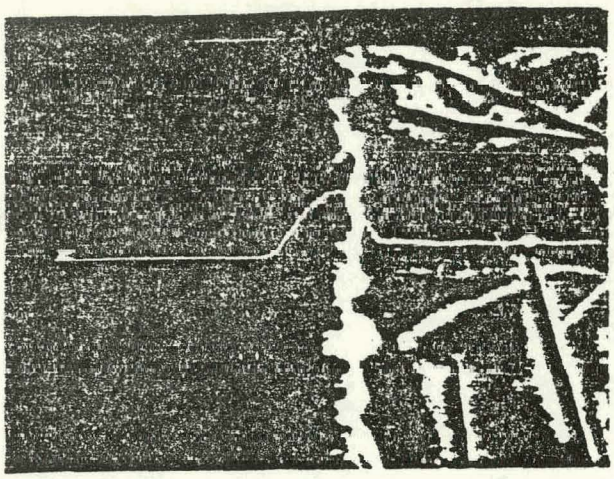

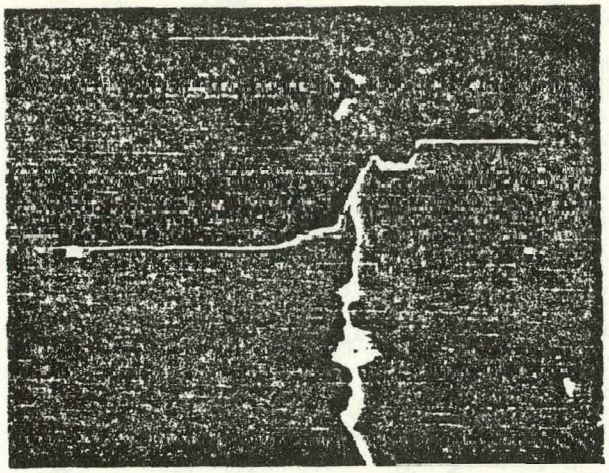

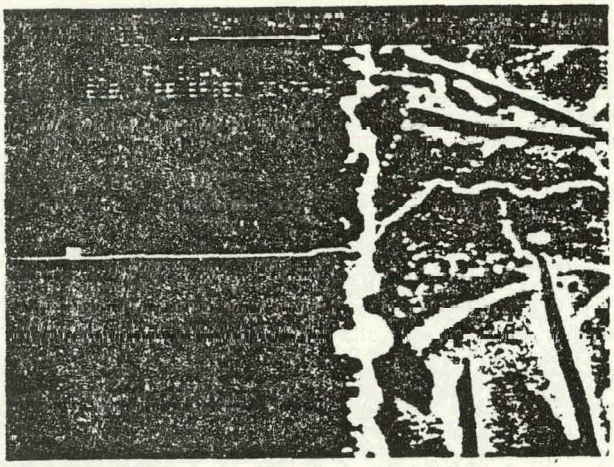

(Figure 3 cont.)

zone. The most interesting feature is the high concentration of aluminum in this zone. Microprobe analyses indicate that the aluminum concentration is higher than the concentrations of iron and cobalt combined as well as being higher than the aluminum concentration in the salt. This is reasonable in view of the fact that the activity of Al_2O_3 is one in the melt and zero in the bulk of the cobalt ferrite anode. This chemical potential gradient is the driving force for the formation of an alumina rich solid solution. For the zone to grow aluminum must diffuse from the melt through the interface to the ferrite, while cobalt and iron must diffuse from the ferrite to the melt.

The reaction zone keeps the ferrite from coming into direct contact with the electrolyte. Since iron and cobalt must diffuse through the layer the dissolution process predicted in Part 1 will be slowed down. However, the process does not stop, and any iron and cobalt that go into solution in the electrolyte will certainly co-deposit with aluminum. It may be that the "wear rate" is low enough as a result of this protection. The zone will continue to grow, however, and at longer times may cause an unacceptable increase in the electrical resistance of the anode.

ACKNOWLEDGEMENTS

Metallographic samples were mounted and prepared for subsequent SEM analysis by Battelle Pacific Northwest Laboratories, Richland, Washington. SEM analyses were prepared by Dr. Grigory Raykhtsaum of the Technology Division, Leach and Garner Company, Attleboro, Massachusetts. This material was prepared with the support of the U.S. Department of Energy (DOE) Grant No. DE-FG07-83ID12380. However, any opinions, findings, conclusions, or recommendations expressed herein are those of the authors and do not necessarily reflect the views of DOE.

REFERENCES

1) K. Billehaug and H. A. Øye, "Inert Anodes for Aluminum Electrolysis in Hall-Héroult Cells," Aluminum (Düsseldorf) 57(2)(1980), 146-150; 57(3)(1980), 228-231.

2) I. Barin and O. Knacke, Thermochemical Properties of Inorganic Substances (Berlin: Springer - Verlag, 1973).

3) I. Barin, O. Knacke and O. Kubaschevski, Thermochemical Properties of Inorganic Substances Supplement, (Berlin: Springer - Verlag, 1977).

4) K. Grjotheim, C. Krohn, M. Malinovsky, K. Matiasovsky, and J. Thonstad, Aluminum Electrolysis, Fundamentals of the Hall - Héroult Process, 2nd edition. (Düsseldorf: Aluminum - Verlag, 1982)

5) P. Mergault, "Tension de décomposition de quelques solutions d'oxydes dans la cryolithe fondue," C. R. Acad. Sci.,

Paris 240(1955), 864.

6) P. Mergault, "Tension de décomposition de solutions d'oxydes dans la cryolithe fondue," C. R. Acad. Sci., Paris 240(1955), 1568.

7) P. Mergault, "Tension de décomposition des solutions cryolithiques d'oxydes de titane, vanadium, niobium, tantale, uranium, molybdene et tungstène à 1020°C," C. R. Acad. Sci., Paris, 240(1955), 1755.

8) K. Grjotheim, "Série électrochimique des métaux dans les fluorures fondus," Revue de l'aluminum, 31(1954), 129.

9) R. Monnier and P. Grandjean, " Recherches sur l'obtention, la séparation et la purification de tantale et du niobium, notamment par voie electrochimique. II Etude d'une methode de determination des tensions effectives d'électrolyse et des tensions pratiques de décomposition: application de cette methode à des solutions cryolithiques d'oxydes," Helv. Chim. Acta, 43(1960), 2163.

10) J.-J. Duruz, J.-P. Derivaz, P.-E. Debely, I. L. Adorian, (Eltech Systems Corp.), "Molten Salt Electrowinning Method, Anode and Manufacture Thereof," Int. Pat. App. No. WO 84/02724 (1984).

11) S. P. Ray and R. A. Rapp, (Alcoa), "Composition Suitable for Inert Electrode," U.S. Pat. No. 4,455,211 (1984).

12) R. Keller, "Method to Improve the Performance of Non-consumable Anodes in the Electrolysis of Metal," U.S. Pat. No. 4,504,369 (1984).

13) F. W. Baker and R. L. Rolf, "Hall Cell Operation with Inert Anodes," Light Metals 1986, R. E. Miller, editor (Warrendale, PA: TMS-AIME, 1986), 275-286.

14) S. P. Ray, "Inert Anodes for Hall Cells," ibid., 287-298.

15) D. H. DeYoung, "Solubilities of Oxides for Inert Anodes in Cryolite-Based Melts," ibid., 299-308.

16) G. P. Tarcy, "Corrosion and Passivation of Cermet Inert Anodes in Cryolite-Type Electrolytes," ibid., 309-320.

17) J. D. Weyand, "Manufacturing Processes Used for the Production of Inert Anodes," ibid., 321-341.

18) A. D. McLeod, J. S. Haggerty and D. R. Sadoway, "Inert Anode Materials for Hall Cells," ibid., 269-273.

APPENDIX 6

"Apparatus and Method for the Electrolytic Production of Aluminum,"
U.S. Patent Application

UNITED STATES APPLICATION FOR LETTERS PATENT

Inventor(s): Donald R. Sadoway, John S. Haggerty and Alan D. McLeod

Attorney's Docket No.: MIT-4374

Title: APPARATUS AND METHOD FOR THE ELECTROLYTIC PRODUCTION OF ALUMINUM

EXPRESS MAIL Mailing Label No. B71052548

Date of Deposit January 6, 1987

I hereby certify that this paper or fee is being deposited with the United States Postal Service "Express Mail Post Office to Addressee" service under 37 C.F.R. 1.10 on the date indicated above and is addressed to the Commissioner of Patents and Trademarks, Washington, D. C. 20231.

Elizabeth Tons
(Typed or printed name of person mailing paper or fee)

Elizabeth Tons
(Signature of person mailing paper or fee)

APPARATUS AND METHOD FOR THE ELECTROLYTIC PRODUCTION OF ALUMINUM

Government Support

Work described herein was supported by a grant from the United States Department of Energy.

Background

Aluminum metal is not found naturally. Instead, aluminum is tightly combined with other elements and has to be extracted from them.

Commercially, aluminum is produced from naturally occurring aluminum compounds by the electrolytic reduction of alumina, Al_2O_3. Alumina is obtained from bauxite ore by the Bayer process which involves digesting crushed bauxite ore in strong caustic soda solution at high temperatures.

In 1886, Charles Hall in the United States and Paul Heroult in France independently developed the currently employed electrolytic process for extracting aluminum from alumina. This process, known today as the Hall-Heroult process, transformed aluminum from a precious metal into a common structural material. The process is still the most widely used commercial process for obtaining aluminum metal and is fundamentally the same as it was originally disclosed by Hall and Heroult in 1886.

In the Hall-Heroult process, electric current is passed through a bath of molten electrolyte containing alumina. An important feature of the Hall-Heroult discovery was that cryolite, a double salt of aluminum

and sodium represented by the structural formula Na_3AlF_6, would dissolve alumina at temperatures around 1000°C and that the dissolved alumina could be electrolytically reduced to form molten aluminum metal.

The electrolytic reduction is performed in heavy metal cells or pots known as Hall-Heroult cells. These cells have massive carbon cathodes at the base and carbon anodes, normally formed in the shape of large blocks, suspended above the cell and capable of being lowered into the electrolyte. Direct electric current is passed from the anodes through the electrolyte to the carbon cathodes. The carbon anodes are consumed in the chemical reaction which occurs in a Hall-Heroult cell. This reaction can be represented, as follows:

$$2Al_2O_3 + 3C \longrightarrow 4Al + 3CO_2.$$

Aluminum produced by the Hall-Heroult process is very pure, e.g., 99.0% to 99.8%. The main impurities are traces of iron and silicon.

Despite its capability to produce high purity aluminum, the Hall-Heroult process has always suffered a number of significant problems. One set of problems arises from the use of consumable carbon anodes. These anodes are expensive to produce and the costs of producing the carbon anodes adds significantly to the overall cost of aluminum produced by the Hall-Heroult process. In use, it is difficult to maintain uniform anode current loading since the anodes are consumed resulting in a continuous change in their shape. It is also difficult to maintain proper anode/cathode spacing

during operation of the cells since the anodes are consumed. Additionally, the anode/cathode spacing is typically greater than required because of the uncertainty of the consumable anode's shape and the need to maintain a deep molten aluminum pool. Such spacing results in an inordinate consumption of electrical energy for the aluminum produced.

Because of the problems caused by carbon anodes, substantial research has been conducted in an effort to find another anode material, particularly what has been referred to as an "inert" anode. An inert anode is one which would not react with oxygen formed at the anode, would not dissolve in the electrolyte and would not be consumed in the electrolytic reaction. Unfortunately, the research conducted to date has not resulted in the development of an anode material which is fully satisfactory.

Another set of problems with Hall-Heroult cells arises from the use of a carbon lining in these cells. These cells are operated under conditions which cause molten electrolyte to freeze on the side walls of cells during operation so that molten electrolyte floating on molten aluminum is contained within a shell of frozen electrolyte. This is necessary to prevent reaction between the carbon cell lining and compounds in the molten electrolyte during operation of these cells. The interface between the frozen and molten electrolyte changes, however, during operation of cells, making it difficult to operate under uniform conditions. The necessity to maintain frozen electrolyte at the side walls also results in a substantial heat loss through the side walls.

Summary of the Invention

This invention relates to the discovery that materials heretofore not considered useful in anodes and cell linings of cells for the electrolytic production of aluminum can be so employed to provide improved electrolytic cells and processes for the production of aluminum.

The improved electrolytic cells of this invention have an anode and cell lining comprising materials which, under the operating conditions of the cell: (a) have a standard potential which is more electronegative than aluminum; and (b) have a positive standard free energy for chemical displacement of metal fluoride by elemental aluminum. Additionally, the materials should be ones which can be formed into anodes and cell linings which are thermally and mechanically stable at the operating conditions of the cell, and in the case of the anode, electrically conducting.

In the method for producing aluminum employing the improved cells, the electrolyte is first saturated with the materials from which the anodes and cell lining are formed to prevent consumption of the anode and cell lining during cell operation. This can be accomplished by running the cell for a sufficient period to saturate the electrolyte with the anode and cell lining materials or, preferably, by pre-conditioning the cell by adding a sufficient amount of the materials to saturate the electrolyte with them at cell operating conditions.

The use of materials meeting the above criteria for both the anode and cell lining of an electrolytic cell results in significant advantages over the use of pre-baked carbon anodes and carbon cell linings currently

employed. For example, once the electrolyte is saturated with material meeting these criteria, the anode and cell lining become essentially non-consumable since these materials neither co-deposit with nor are chemically displaced by the aluminum product to any significant extent. Thus, the anodes retain their shape thereby facilitating the maintenance of uniform current densities in the electrolytic cell. Further, the problems encountered in maintaining proper anode/cathode spacing with consumable carbon electrodes are eliminated. In addition, anodes made from such materials obviate one of the major reasons necessitating the use of anode/cathode spacings greater than required and resulting in inordinate consumption of electrical energy. Thus, anodes made from these materials will allow greater flexibility in the choice of operating conditions for the electrolytic cells.

The use of materials as described herein will also allow significant cost reductions for the production of aluminum because the high cost of petroleum feed stock for the pre-baked carbon electrodes is eliminated as well as the expensive baking procedures required to produce these carbon electrodes. Instead, many of the materials meeting the criteria described above are readily available and can be formed by traditional forming methods, e.g., sintering and casting. In addition, of course, the anodes do not have to be replaced as frequently since they are essentially non-consumable.

The use of such materials in the cell lining eliminates the need to maintain the walls of the cell sufficiently cool to freeze molten electrolyte. Indeed, the ability to insulate the walls of the electrolytic cell so

that they are maintained in a hot condition should result in significant thermal energy savings.

Running the electrolytic cells under conditions where the electrolyte is saturated with materials satisfying the criteria described herein also provides significant advantages over traditional operating conditions. For example, the melting point of the electrolyte is reduced which will provide a number of advantages associated with the capability to run the cells at lower operating temperatures, such as a reduced heat load. It also permits operation of the cells at higher alumina concentrations thereby improving the yield of the process.

Brief Description of the Figures

Figure 1 is a schematic illustration of a Hall-Heroult cell of the type commonly employed in the commercial production of aluminum;

Figure 2 is a schematic illustration of a Hall-Heroult cell modified according to this invention;

Figure 3 is a schematic illustration of a vertical electrolytic reduction cell suitable for the production of aluminum according to this invention;

Figure 4 is a schematic illustration of an electrolytic cell, including bipolar electrodes, which cell would be suitable for the production of aluminum according to this invention.

Detailed Description of the Invention

A conventional Hall-Heroult cell 10 employing pre-baked carbon anodes is illustrated schematically in Figure 1. This cell has a steel outer shell 12 with

thermal insulation on the inside of shell 12. A carbon cathode 16 is positioned at the bottom of cell 10 and contains metallic current collector bars 18. Carbon anodes 20 are formed from prebaked carbon blocks suspended from steel anode rods 22 which serve to supply electrical current to anodes 20. Cell lining 24 is also formed from carbon blocks.

Molten electrolyte 26 contains dissolved alumina supplied by breaking alumina crust 28 and adding fresh alumina. Crust 28 forms on frozen electrolyte and helps to minimize heat loss from the top of cell 10. Cryolite, Na_3AlF_6, is commonly employed as the base material in the electrolyte since it dissolves alumina at temperatures around 1000°C. In addition, certain fluoride salts, such as aluminum fluoride, AlF_3, and calcium fluoride, CaF_2, are also traditionally present. AlF_3 and CaF_2 decrease the freezing point of electrolyte and AlF_3 also improves current efficiency in the cell.

As electric current is passed from carbon anode 20 through molten electrolyte 26 to cathode 16, dissolved alumina is reduced to form molten aluminum layer 30 at the bottom of the Hall-Heroult cell and carbon dioxide gas is generated at the anode. Carbon anode 20 is consumed during this reaction.

It is important to prevent molten electrolyte 26 from contacting carbon cell lining 24 to prevent cell lining failure caused by the formation of intercalation compounds and the dissolution of Al_4C_3. To prevent such contact, cell 10 is operated under conditions which allow a layer of frozen electrolyte 32 to form between carbon cell lining 24 and molten electrolyte 26. Thus, molten

electrolyte 26 is contained in a shell of frozen electrolyte and supported by a pad of molten aluminum 30. Unfortunately, during operation of the Hall-Heroult cell, the interface between molten and frozen electrolyte varies depending upon operating conditions. This adds to the difficulty in operating the cell under uniform conditions.

Molten aluminum 30 does not wet carbon cathode 16 which prevents the formation of aluminum carbide which would contaminate the aluminum product. It is possible, however, for disruptions in molten aluminum layer 30 to occur and to result in contact between molten electrolyte 26 and carbon cathode 16. Such contact is highly undesirable because it results in a reaction between carbon cathode 16 and dissolved alumina in molten electrolyte 26 thereby causing undesirable consumption of carbon cathode 16. To prevent this, conventional Hall-Heroult cells are operated so that a relatively deep pool of molten aluminum is always present to prevent contact between molten electrolyte and the carbon cathode. The dimensional instabilities inherent in such a deep cathode pool of aluminum through which large current densities are passed require excessive spacing between the anode and cathode with all attendant disadvantages.

As mentioned above, there has been much research directed towards finding replacement materials for the carbon anode and carbon cell lining of a conventional Hall-Heroult cell. Much of this research has been directed to finding inert anode materials. Despite the extensive research which has been conducted, a material has not been found which is entirely satisfactory.

The present invention results from the discovery that certain materials, although soluble to some extent in the molten electrolytes employed in Hall-Heroult cells, can be employed as anode and cell lining materials. The materials of this invention are carefully selected so that, despite their solubility in electrolyte, there is no net consumption of these materials and their presence in the electrolyte does not result in contamination of the aluminum product.

A first criterion for materials suitable for use as anodes and cell linings according to this invention is that the materials not co-deposit electrolytically to any significant extent with aluminum during operation of the cell.

The capability of a metal oxide to co-deposit with aluminum can be determined using the calculated reversible decomposition potential, E°, at 1300 K for the reaction,

$$MeO_{\frac{n}{2}} \longrightarrow Me + \frac{n}{4}O_2,$$

wherein Me represents the metallic element in the oxide compound under consideration and n is the valence of this metal in the oxide compound. This can be calculated using the equation:

$$E^\circ = \frac{\Delta G^\circ}{nF}$$

where F is the Faraday constant and ΔG° is the standard Gibbs free energy of the above reaction. Calculated values of E° are given in Table I.

A similar determination for the standard potential of non-oxide materials can be made in a manner similar to that described above for oxides.

Thus, the first criterion for selection of materials for molten salt electrolytic cell anodes and cell linings according to this invention is that the material have a standard potential which is more electronegative than aluminum under the operating conditions of the cell. This will normally ensure that the metal component of the material does not co-deposit with aluminum. It is possible, however, in some cases, that minor amounts of a metal from the anode material might co-deposit despite the fact that the anode material satisfies the first criterion. This could be because aluminum cells do not always operate under equilibrium conditions for which the available thermodynamic data were generated. It is also possible that the available thermodynamic data employed in calculating the standard potential is not entirely accurate. The co-deposition of minor amounts of a metal is not intolerable since all materials meeting the two criteria described herein can be readily removed from molten aluminum by conventionally practiced techniques, particularly treatment with aluminum fluoride. Such minor amounts of co-deposited metal can, upon removal, be recycled to the electrolyte to assist in maintaining saturation levels of the material in the electrolyte. In this case, there is no net loss of the material in the process.

Although the examples set forth above are all oxides, it is believed that other oxy-compounds and non-oxy-compounds meet the two criteria described above.

Examples of other oxy-compounds include multipleoxides, mixed oxides, oxyhalides and oxycarbides of metals.

The second criterion for an anode material is that it does not co-deposit by a chemical displacement with aluminum. Certain metals can dissolve in the aluminum pool following a chemical displacement represented as,

$$MeF_n + \frac{nAl}{3} = \frac{n}{3}AlF_3 + Me,$$

wherein Me represents the metal and n is the valence of the metal in the metal fluoride.

Thermodynamic data for this displacement reaction are presented in Table II.

Table II. Standard Free energy of Reaction for Chemical Displacement of Metal Fluoride by Elemental Aluminum at 1300 K

FLUORIDE	ΔG (kJ)	FLUORIDE	ΔG (kJ)	FLUORIDE	ΔG (kJ)
WF_6	-989	VF_3	-317	KF	3
PbF_4	-976	CdF_2	-306	UF_3	6
VF_5	-785	PbF_2	-299	NaF	13
CoF_3	-657	CoF_2	-283	BeF_2	52
WF	-646	FeF_2	-257	LiF	90
BiF_3	-555	ZnF_2	-257	MgF_2	109
VF_4	-553	CrF_2	-180	NdF_3	167
NbF_5	-481	TiF_4	-165	ScF_3	179
MnF_3	-466	MnF_2	-163	BaF_2	195
CuF_2	-430	SiF_4	-126	CaF_2	211
FeF_3	-422	TiF_2	-78	SrF_2	221
TaF_5	-375	ZrF_4	-46	YF_3	251
CrF_3	-353	UF_4	-42	CeF_3	259
CuF	-340	TiF_3	-42	LaF_3	289
NiF_2	-329				

Those metal oxides having a positive standard free energy for the displacement reaction described above satisfy the second criterion.

The data of Tables I and II show that there are a few metal oxides which do not co-deposit in the aluminum by electrochemical deposition or chemical displacement. Preferred metal oxides are MgO, SrO, La_2O_3, Nd_2O_3, CaO, Ce_2O_3, Sc_2O_3, Y_2O_3. Li_2O, BaO, UO_2 and BeO are examples of materials which also satisfy the criteria of this invention.

These oxides each have significant solubility in cryolite. For this reason, these oxides have not been of great interest in anode formulations to date. However, their solubility must be viewed in the light of their resistance against further decomposition. Simply stated, it is not so important that the oxide resist dissolution: it is extremely important, however, that the oxide resist exsolution.

Although the specific compounds for which data are presented above are all inorganic metallic oxides, any compound which satisfies the criteria of this invention can be employed. Additionally, anodes and cell linings can be formed from pure metals and metal alloys on which oxide films are generated, in situ, during operation of the electrolytic cells. An example of a suitable metal is lanthanum and an example of a metal alloy is a lanthanum-ytrrium alloy.

Of course, the materials employed in forming the anode and cell lining according to this invention must also be capable of being formed into solid shapes having the requisite mechanical, thermal and electrical properties. In regard to mechanical properties, the

materials should be capable of formation into self-sustaining shapes. Such shaping may be done, for example, by sintering ceramic materials with heat alone or with the simultaneous application of heat and pressure or by melt processing (e.g., casting) metals and alloys. These are art-recognized techniques for forming such materials into shaped bodies.

The materials should also be thermally stable under the conditions of operation of the electrolytic cell. This means that it must have a melting point above the temperature of the molten electrolyte and preferably undergo no phase change under working conditions of the cell.

The anode must also be inherently electrically conductive or capable of being made electrically conductive. The term "electrically conductive" is used herein to mean an anode that has an electrical conductivity under the operating conditions of a Hall-Heroult cell of at least 10% of the conductivity of a graphite anode under the same conditions. Preferably, the conductivity will be comparable to a graphite electrode.

The oxide materials disclosed herein are typically electrical insulators, i.e., high bandgap materials. Thus, their electrical conductivity must be improved considerably if they are to be used as anodes in molten salt electrolysis cells. This can be accomplished by making a composite material consisting of at least two phases: an electronically conductive phase, i.e., low bandgap, and a phase of the anode material disclosed herein. The electronically conductive phase can be chosen from the following: metal, metal alloy, electronically conductive inorganic compound or solid

solution. In the case where the conductive phase is either a metal or metal alloy, the resulting composite material is called a cermet. The electronically conductive phase typically comprises from 10 - 30 volume per cent of the material, although a broader range is possible in many cases. The metal or metal alloy selected should not react chemically with the oxide phase materials, i.e., undergo displacement reactions. Candidate metals are copper, nickel, and their alloys and a candidate compound is tin oxide.

Another approach to an electrically conductive anode is to construct the anode of monolithic metal or metal alloy upon which an oxide coating forms, in situ, upon commencement of electrolysis. For this coating to be stable, the electrolyte must remain saturated with respect to the oxide at all times. This is achieved by the addition of appropriate metal oxide to the cell bath or by constructing the cell lining of the same metal oxide or both. Such a coating would be self-healing and its thickness would be self-regulating. The choice of metal or alloy in this case is restricted to the metallic constituents of the oxides satisfying the criteria disclosed herein. Examples of suitable metals include lanthanum, yttrium and their alloys.

The material employed for the anode should also be resistant to oxidation since oxygen is generated at the anode. Thus, the material employed as the anode is preferably an oxy-compound with the particularly preferred materials being oxides.

It is not necessary that the material employed for the anode be the same material as that employed for the

cell lining as long as both materials meet the criteria described herein. If the materials are not the same, it is desirable to saturate the electrolyte with both materials so that neither is consumed during operation of the cell. It is preferred to employ the same material for the anode and cell lining in most cases.

The use of the materials satisfying the criteria described herein opens up new possibilities for the design of molten salt electrolytic cells. One such design, employing a horizontal monopolar anode, is schematically illustrated in Figure 2. Electrolytic cell 40 contains a single anode 42 at the top of cell 40. Anode 42 is connected to a supply of electric current by anode rod 44. Molten aluminum 46 is produced on top of a cathode at the bottom of the cell formed from a current collector bar 48 electrically connected to the molten aluminum 46 by connectors 50 which can be formed from electrically conducting refractory metal compounds, such as titanium boride, TiB_2. Alternatively, current could be conducted from the collector by a graphite lead encapsulated in a non-consumable material, which may be one of the materials meeting the requirements described herein for anodes and cell linings, running from the collector through the electrolyte and out of the top of the cell.

Cell 40 also has cell lining from the same material as anode 42 or from a different material satisfying the criteria discussed above. In the operation of cell 40, it is not necessary to employ cool side walls to create a frozen layer of electrolyte. Thus, molten electrolyte extends to cell lining 52 and the only layer of frozen electrolyte 54 forms on top of the cell.

Another design for a molten salt electrolytic cell employing materials meeting the criteria as described herein for the anode and cell lining is schematically illustrated in Figure 3. Cell 60 has a series of vertically oriented anodes 62 formed from a material according to this invention. Cell 60 also contains a plurality of vertically oriented cathodes 64 which can consist of carbon or an inert wettable material.

Cell lining 66, which is enclosed within a steel outer vessel 68, is formed from the same material which is employed for anodes 62 or from a different material meeting the cell lining criteria discussed herein.

In cases where the presence of saturation values of anode and cell lining material does not alter the relative density of liquid aluminum in molten electrolyte from that of present Hall-Heroult cells, oxygen gas produced at anodes 62 rises to the melt surface and liquid aluminum falls to the bottom of cell 60. In cases where the relative density of liquid aluminum and molten electrolyte is inverted from the value in a present Hall-Heroult cell, both the oxygen gas and liquid aluminum rise to the melt surface. Under these conditions, it is desirable to interpose a retaining structure or semi-wall 70 between anodes 62 and cathodes 64 to prevent the buoyant liquid aluminum from forming an electrical short between electrodes. The choice of material for semi-wall 70 is subject to the same considerations as the choice of material for lining 66. In order not to reduce the ability of the electrolyte to dissolve aluminum oxide, semi-wall 70 and lining 66 should preferably consist of the same material.

Still yet another design for a molten bath electrolytic cell is schematically illustrated in Figure 4. Cell 80 includes a horizontal bipolar electrode stack 82. In such a design, each electrode element consists of an anodic surface and a cathodic surface separated from neighboring elements by electrically insulating spaces. A positive feeder electrode 84 and negative feeder electrode 86 are placed on the top and bottom of stack 82, respectively. Electrode elements are formed from the materials described herein for anodes and a suitable cathodic material, which can be carbon or preferably an inert wettable material. Cell lining 88, enclosed in steel jacket 90, can be selected from the same material as the anode, a different material meeting cell lining criteria or from a more conventional material. If liquid aluminum 92 is denser than the molten electrolyte 94, the bipolar stack is charged to make the upper surface of each element cathodic and the lower surface anodic. By providing a central vent, enchanced circulation of the electrolyte can be achieved as a consequence of the gas lift. If the liquid aluminum is less dense in the electrolyte, a vertical bipolar arrangement is preferred. In this case, both the liquid aluminum and oxygen gas rise to the melt surface. The electrode elements also serve as semi-walls to prevent the liquid aluminum from shorting the cathode to the anode.

Although the discussion above has been limited to electrolytic cells and methods for producing aluminum metal from molten salts, the materials described herein can also be employed in such cells and methods for producing other metals. For example, the criteria

employed herein to select materials for the anodes and cell linings of aluminum cells can also be applied to select materials suitable for the production of magnesium, neodymium or other metals. In these cases, the material selected must meet the same criteria except that these criteria are made specific to the metal to be produced rather than aluminum. Thus, the first criterion is that the material have a standard potential which is more electronegative than the metal to be produced under the operating conditions of the cell. The second criterion is that the material have a positive standard free energy for the metal fluoride displacement with the metal to be produced at the operating temperature of the cell.

Equivalents

Those skilled in the art will recognize or be able to ascertain, using no more than routine experimentation, many equivalents to the specific embodiments of the invention described herein. Such equivalents are intended to be covered by the following appended claims.

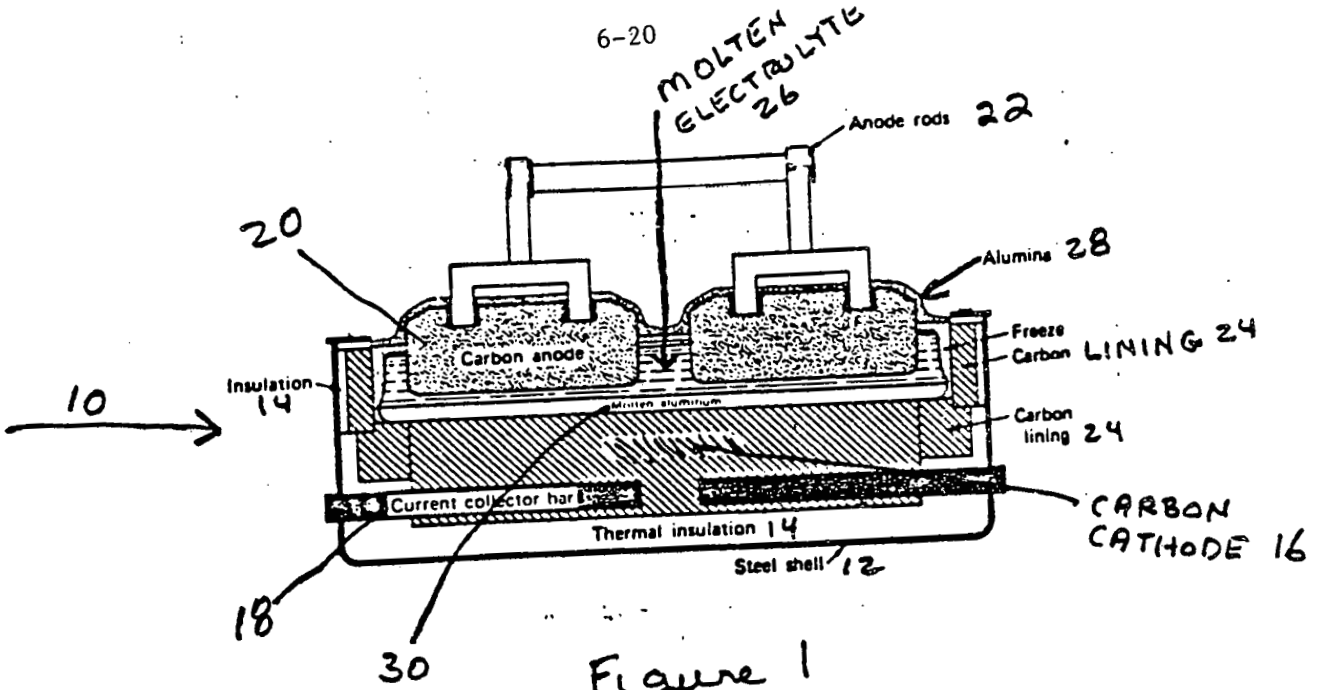

Figure 1

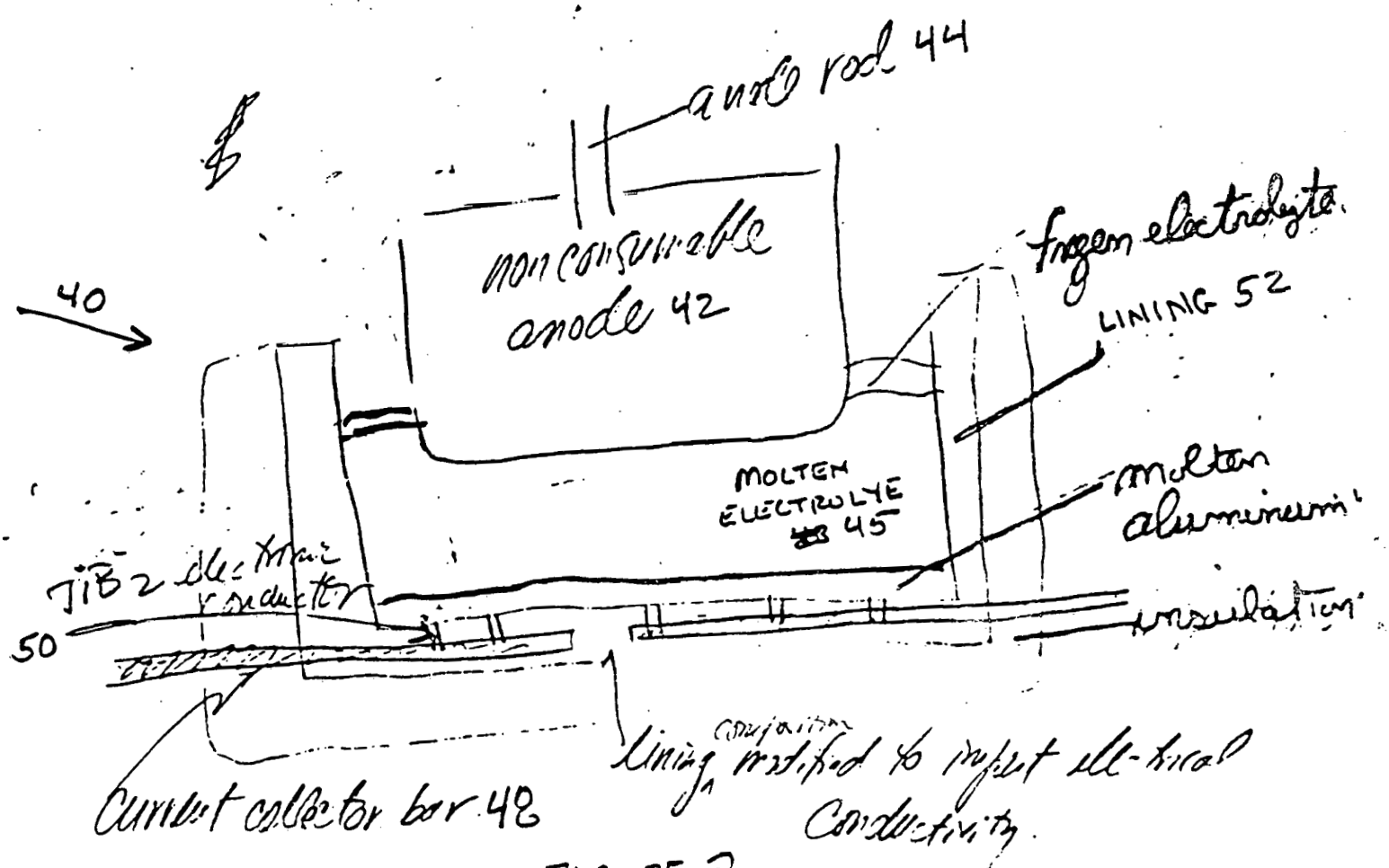

FIGURE 2

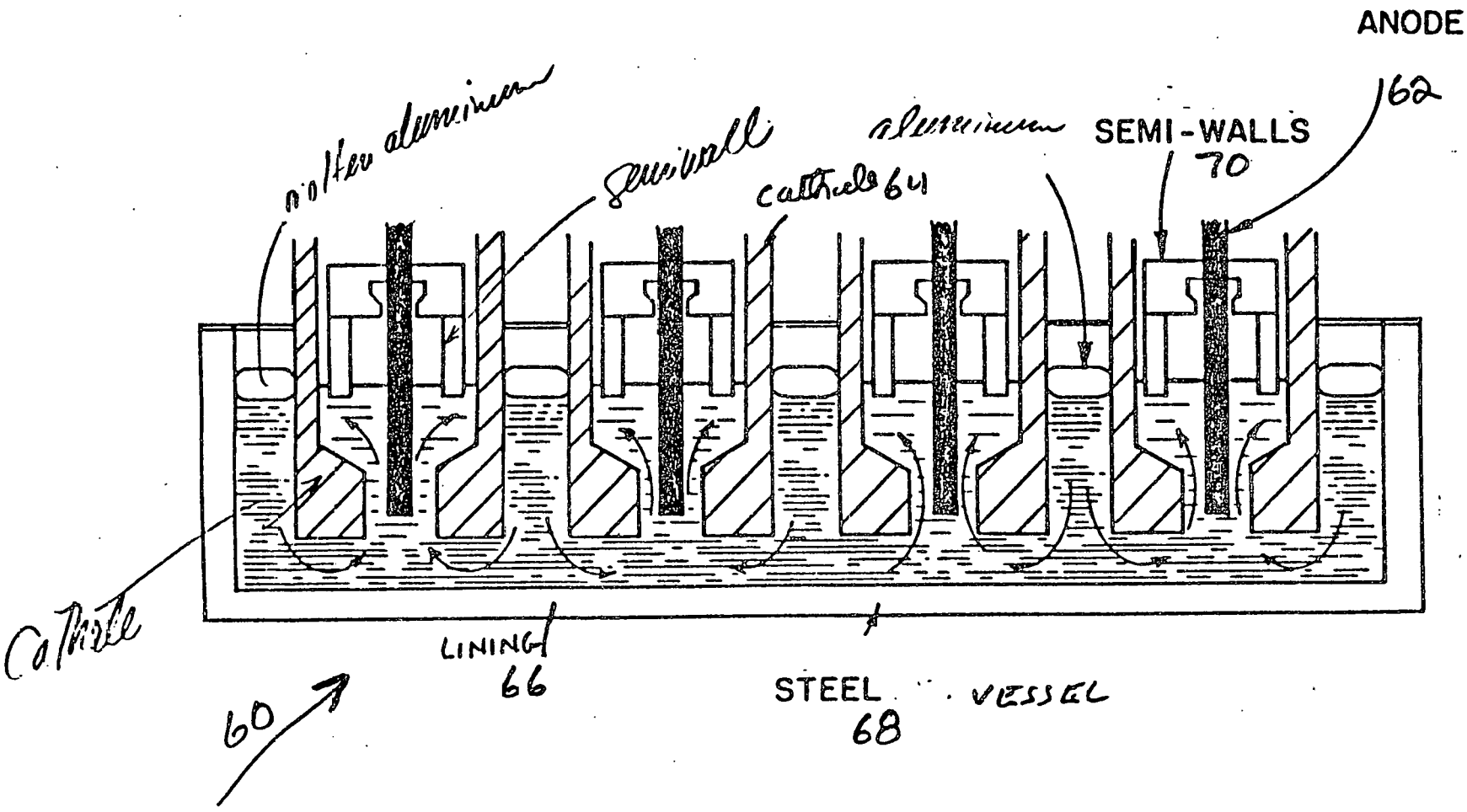
ANODE(
62
molten aluminum
sidewall
cathode 64
aluminum
SEMI-WALLS
70
Cathode
LINING
66
STEEL VESSEL
68
60

FIG. 3

Fig. 4

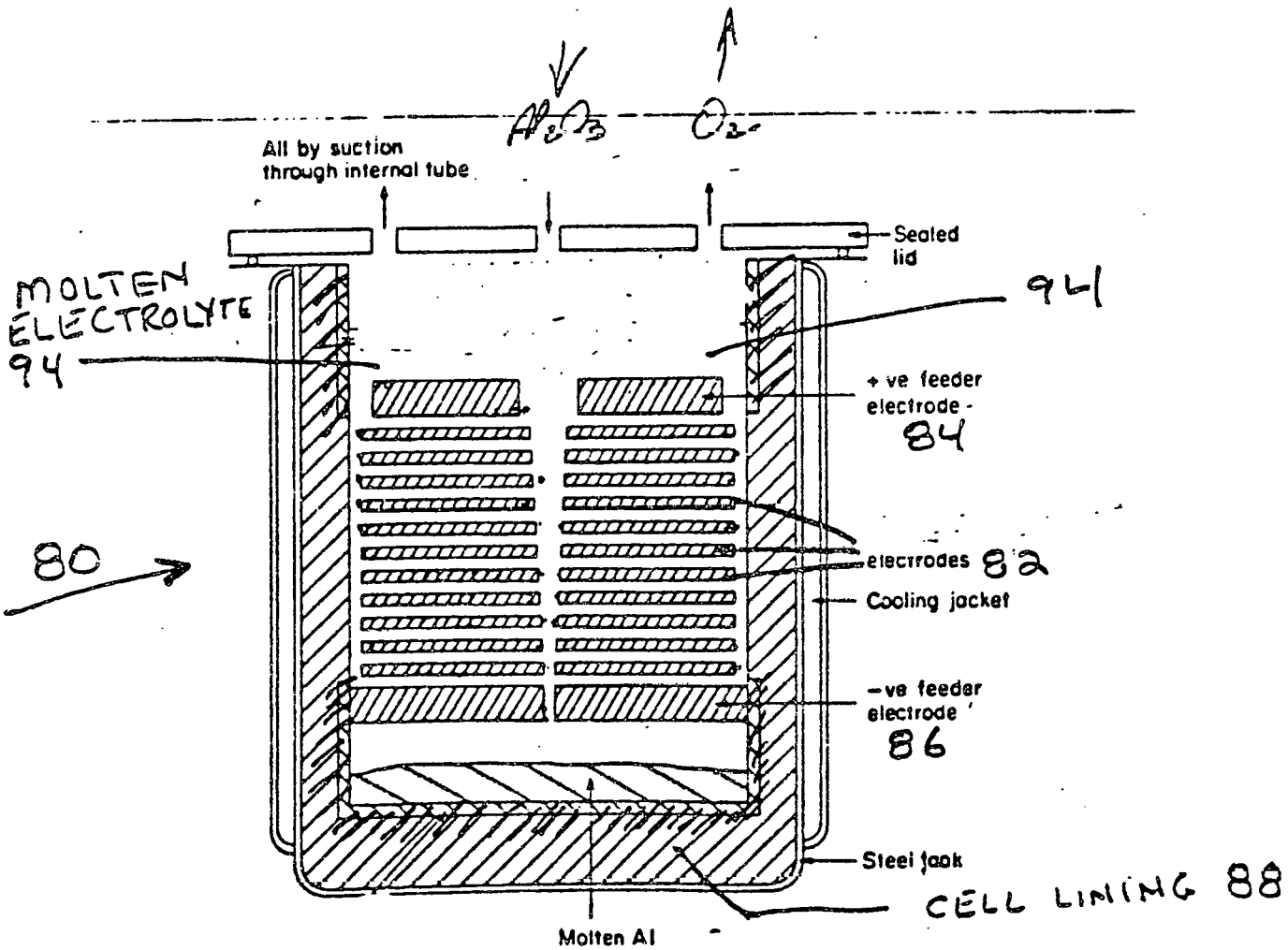
Al_2O_3
O_2
Air by suction through internal tube
Sealed lid
MOLTEN ELECTROLYTE 94
94
+ ve feeder electrode 84
80
electrodes 82
Cooling jacket
-ve feeder electrode 86
Steel jack
CELL LINING 88
Molten Al

Abstract of the Disclosure

Improved electrolytic cells and methods for producing aluminum by the electrolytic reduction of an aluminum compound dissolved in a molten fluoride electrolyte are disclosed. In the improved cells and methods, materials are employed for both the cell anode and cell lining which, at the operating conditions of the cell: (a) have a standard potential more electronegative than aluminum; and (b) have a positive free energy for a metal fluoride displacement reaction with elemental aluminum. By saturating the molten electrolyte with these materials, electrolytic cells can be run without net consumption of the cell anodes or cell linings. Use of such materials for cell anodes and cell linings produces significant advantages over the pre-baked carbon anodes and carbon cell linings presently employed in Hall-Heroult aluminum cells.

DOE/ID/12380-18

INVESTIGATION OF MATERIALS FOR INERT ELECTRODES IN ALUMINUM ELECTRODEPOSITION CELLS

DOE